ҚАЗАҚСТАН РЕСПУБЛИКАСЫ
ҒЫЛЫМ ЖӘНЕ ЖОҒАРЫ БІЛІМ МИНИСТРЛІГІ

SATBAYEV UNIVERSITY
МЕТАЛЛУРГИЯ ЖӘНЕ КЕН БАЙЫТУ ИНСТИТУТЫ

ISSN 2616-6445 (Online)
ISSN 2224-5243 (Print)
DOI 10.31643/2018/166445

Минералдық шикізаттарды кешенді пайдалану

3**(338)**

Комплексное Использование Минерального Сырья

Complex Use of Mineral Resources

ШІЛДЕ-ҚЫРКҮЙЕК 2026
JULY-SEPTEMBER 2026
ИЮЛЬ-СЕНТЯБРЬ 2026

ЖЫЛЫНА 4 РЕТ ШЫҒАДЫ
QUARTERLY JOURNAL
ВЫХОДИТ 4 РАЗА В ГОД

ЖУРНАЛ 1978 ЖЫЛДАН БАСТАП ШЫҒАДЫ
JOURNAL HAS BEEN PUBLISHING SINCE 1978
ЖУРНАЛ ИЗДАЕТСЯ С 1978 ГОДА

АЛМАТЫ - 2026

Редакция мекен жайы:
«Металлургия және кен байыту институты» АҚ
050010, Қазақстан Республикасы, Алматы қ., Шевченко к-сі, Уәлиханов к-нің қиылысы, 29/133,
Fax. +7 (727) 298-45-03, Tel. +7-(727) 298-45-02, +7 (727) 298-45-19
E mail: journal@kims-imio.kz, product-service@kims-imio.kz
http://kims-imio.com/index.php/main

«Минералдық шикізаттарды кешенді пайдалану» журналы ғылыми жұмыстардың негізгі нәтижелерін жариялау үшін Қазақстан Республикасы Білім және ғылым министірлігінің Білім және ғылым сапасын қамтамасыз ету комитеті ұсынған ғылыми басылымдар тізіміне енгізілген.
Меншік иесі: «Металлургия және кен байыту институты» АҚ

Журнал Қазақстан Республикасының Ақпарат және коммуникация министрлігінің Байланыс, ақпараттандыру және бұқаралық ақпарат құралдары саласындағы мемлекеттік бақылау комитетінде қайта тіркелген

2016 ж. 18 қазандағы № 16180-Ж Куәлігі

Address:
"Institute of Metallurgy and Ore Beneficiation" JSC
29/133 Shevchenko Street, corner of Ch. Valikhanov Street, Almaty, 050010, Kazakhstan
Fax. +7 (727) 298-45-03, Tel. +7-(727) 298-45-02, +7 (727) 298-45-19
E mail: journal@kims-imio.kz, product-service@kims-imio.kz
http://kims-imio.com/index.php/main

The Journal "Complex Use of Mineral Resources" is included in the List of publications recommended by the Committee for Control in the Sphere of Education and Science of the Ministry of Education and Science of the Republic of Kazakhstan for the publication of the main results of scientific activities.
Owner: "Institute of Metallurgy and Ore Beneficiation" JSC

The Journal was re-registered by the Committee for State Control in the Sphere of Communication, Information and Mass Media of the Ministry of Information and Communication of the Republic of Kazakhstan.

Certificate № 16180-Ж since October 18, 2016

Адрес редакции:
АО «Институт металлургии и обогащения»
050010, Республика Казахстан, г. Алматы, ул. Шевченко, уг. ул. Валиханова, 29/133,
Fax. +7 (727) 298-45-03, Tel. +7 (727) 298-45-02, +7 (727) 298-45-19
E mail: journal@kims-imio.kz, product-service@kims-imio.kz
http://kims-imio.com/index.php/main

Журнал «Комплексное использование минерального сырья» включен в Перечень изданий, рекомендуемых Комитетом по контролю в сфере образования и науки Министерства образования и науки Республики Казахстан для публикации основных результатов научной деятельности.
Собственник: АО «Институт металлургии и обогащения»

Журнал перерегистрирован в Комитете государственного контроля в области связи, информатизации и средств массовой информации
Министерства информации и коммуникации Республики Казахстан
Свидетельство № 16180-Ж от 18 октября 2016 г.

Crossref

DOI: 10.31643/2026/6445.23
Engineering and Technology

Methods for purifying table salt from the Suzak deposit

Anarbayev A.A., Kabylbekova B.N., *Smailov B.M., Ormanova G.M.

M.Auezov South Kazakhstan Research University, Shymkent, Kazakhstan

** Corresponding author email: baha_uppr@mail.ru*

Received: *January 23, 2025*
Peer-reviewed: *March 16, 2025*
Accepted: *April 7, 2025*

ABSTRACT

One of the pressing issues today is common salt purification from harmful impurities and production of salt for medical and household purposes. To obtain high-purity sodium chloride salt, it is necessary to develop more effective methods for purifying salt from impurities. The article discusses modern methods for purifying Suzak deposit common salt from harmful impurities. The main goal of the scientific work is to study the methods of purifying sodium chloride from impurities. The common salt raw material composition was studied. The content of impurities of Ca^{2+}, Mg^{2+} and $SO4^{2-}$ ions and heavy metals Pb (II), Cu (II), Cd (II), As (V) was determined. The solubility in the systems NaCl-Na_2SO_4-H'$_2$O, NaCl-$CaCl_2$-H_2O and NaCl-$MgCl_2$-H_2O at a temperature of 100-110°C was studied. The effect of temperature and time on the common salt purification degree using active reagents was studied. It was found that the highest common salt purification degree from Ca^{2+}, Mg^{2+} and $SO4^{2-}$ at 30 minutes and 90°C, respectively, is 99.8%, 99.9%, 99.93%. It was found that the use of a three-component mixture of $Mg(OH)_2$:$CaCO_3$:$CaSO_4$ in a ratio of 1:4-5:6-7 for 20 minutes during purification allows purifying the NaCl solution from trace impurities of Pb(II), Cu(II), Cd(II), As(V) by 92.0-97.7% and obtaining 99.4% NaCl. To obtain high-purity salt, effective purification methods of salt from impurities are recommended, allowing to achieve a purification level of up to 99%.

Keywords: sodium chloride, table salt, salt purification methods.

Information about authors:

Anarbayev Abibulla Abildaevich — *Doctor of Chemical Sciences, professor, Department of Technology of inorganic and Petrochemical Productions, M.Auezov South Kazakhstan University, 160000, Shymkent, Kazakhstan. E-mail: abib_28@mail.ru; ORCID ID: https://orcid.org/0000-0002-0019-4381*

Kabylbekova Balzhan Nurmanovna — *Candidate of Technical Sciences, Professor of the Department of Chemistry and Pharmaceutical Engineering, M.Auezov South Kazakhstan University, 160000, Shymkent, Kazakhstan. E-mail: balzhan.kbn@bk.ru; ORCID ID: https://orcid.org/0000-0001-8461-8008*

Smailov Bakyt Matkarimovich — *PhD doctor, Department of Scientific Research, M.Auezov South Kazakhstan University, 160000, Shymkent, Kazakhstan. E-mail: Baha_uppr@mail.ru; ORCID ID: https://orcid.org/0000-0001-7976-9776*

Ormanova Gaukhar Meyirbekovna — *PhD doctoral student of the Department of Technology of Inorganic and Petrochemical Industries, M.Auezov South Kazakhstan University, 160000, Shymkent, Kazakhstan. E-mail: ormanova_g@inbox.ru; ORCID ID: https://orcid.org/0000-0002-9625-5790*

Introduction

Kazakhstan has huge reserves of mineral raw materials – common salt, the reserves of which amount to more than 1.4 billion tons. In the chemical industry, NaCl is the main raw material for obtaining caustic ash and other inorganic sodium-containing salts. Depending on the purpose, NaCl is used in many industries [[1], [2], [3]].

The main consumer of high-purity sodium chloride is the pharmaceutical and food industries. Particular attention is paid to the methods of purifying common salt from harmful impurities of calcium, magnesium, sulfate ions and heavy metals (Pb, Cd, As, Cu). The common salt purity is considered one of the most important requirements in production. At the same time, the technogenic impact on the environment is growing, which makes a negative contribution to the deterioration of its condition [[4], [5], [6]].

The well-known lime and lime-soda methods do not always purify salts from impurities to the required quality due to the purification system complexity [[7], [8]]. To obtain high-purity salt, large expenses are required, which increase the product cost. Therefore, it is necessary to use a more effective method of purifying salt from impurities [[9], [10], [11]].

This article examines modern methods of purifying common salt [[12], [13], [14], [15], [16]]. Currently, the demand for various methods of producing and processing common salt is growing. The authors [17] found that when using the phosphate method of purifying a salt solution, the purification degree from calcium and magnesium ions increases to 95-97%.

Currently, Kazakhstan does not produce “extra” grade salt due to the lack of production and supplies it mainly from Russia and other countries.

The authors conducted research work on salt purification and the results obtained do not have full-scale application. This is due to the technology developed taking into account the physical and chemical properties of the deposits [[18], [19], [20]. [21], [22]].

For large-scale use in the pharmaceutical and food industries as an extra salt, the Suzak deposit requires chemical purification, since the salt contains many impurities.

The purpose of the scientific article is to study the physical and chemical properties of table salt and to propose modern methods of purification from harmful impurities and heavy metals using active reagents and precipitants.

To study the common salt composition, samples from Suzak deposit were used (Table 1).

Table 1 – Chemical composition of Suzak deposit common salt samples

Salt composition of common salt, %						
NaCl	KCl	$MgSO_4$	$MgCl_2$	$CaCl_2$	$CaSO_4$	Insoluble residue
93.41	0.01	0.23	0.14	0.37	2.29	3.55
97.08	0.02	0.10	0.045	0	0.16	2.67
99.07	0.019	0.11	0.046	0	0.15	0.61
98.68	0.024	0.12	0.047	0	0.17	0.95

Table 1 shows that, according to the results of chemical analysis, natural common salt contains mainly halite mineral and impurities of clay-carbonate and sulfate materials – sulfate and calcium and magnesium, magnesium chloride, calcium chloride and potassium chloride. The salt is significantly contaminated with insoluble residues (silt, sand).

Experimental part

Object of research. The purpose of the work is to purify sodium chloride from harmful impurities and obtain high-purity salt. In accordance with the logic of scientific research, a research methodology was selected for conducting the experiment. It is a complex of theoretical and experimental methods, the combination of which makes it possible to most reliably study such a complex problem of complex purification of common salt from harmful impurities and heavy metals using active reagents and precipitants.

The following research methods were used in the work: chemical, mass spectrometry, X-ray phase, scanning electron microscopy and IR spectroscopy and differential thermal analysis. The experiments were conducted on a laboratory thermostatted unit.

Experimental methodology. In the process of isotherm (Fig. 3, 4) of solubility of water-salt systems with the participation of NaCl at elevated temperatures, in the case of incomplete separation of Ca, Mg, SO_4 ions from saturated salt solutions, the remaining minor impurities contained in the liquid phase during hot filtration of solid sodium chloride pass into the filtrate.

The saturated NaCl solution separated from the sediment is evaporated at 100 - 110 °C to 1/2 of the original volume. The precipitated crystalline target product is separated from the hot solution. The mother liquor is again evaporated to 1/2 of the initial volume, the precipitated crystals are separated with NaCl and dried at 25-110 °C for 30 minutes.

The discussion of the results

The average composition of Suzak deposit salt samples No.1 and No.2 was prepared. The elemental composition of table salt is as follows,%: O-1.05, Na-36.91, Mg-0.21, S-0.30, Cl-61.72, Ca-0.11. Microstructure of Suzak deposit natural table salt are shown in Figure 1.

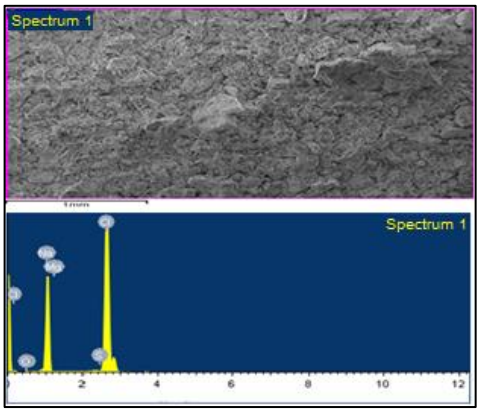

Figure 1 – Energy dispersive analysis of Suzak deposit table salt

It is evident from Figure 1 that the studied sample contains sodium, magnesium, calcium, chlorine and sulfur bound in the form of compounds NaCl, KCl, $MgS0_4$, $MgS0_4$, $MgCl_2$, $CaCl_2$ and $CaSO_4$.

Figure 2 shows the IR spectrum of Suzak deposit common salt. The IR spectrum (Figure 2) of common salt has intense absorption bands with wavelengths of 609, 612, 1091 cm^{-1}, corresponding to the Na-CI bond, other absorption frequency intensities are not observed.

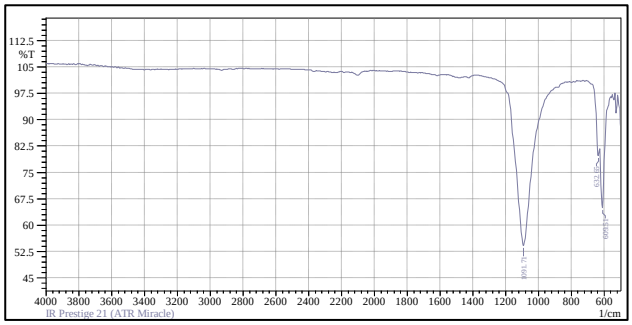

Figure 2 – IR spectrum of Suzak deposit table salt

Suzak district has large reserves of rock table salt, which is mined in an open way. There are practically no overburden rocks. Suzak steppe is rich in minerals and provides the Republic of Kazakhstan with various types of raw materials. One of the leading places in reserves is occupied by common salt with the following composition of deposits: NaCl – 90.9-98.2%; Ca – 0.45-0.69%; Mg – 0.12-0.19%; SO_4^{2-} – 1.98-2.7%; insoluble residue – 2.0-3.0%.

For deep purification and obtaining high-purity common salt, it is necessary to study the solubility diagrams of $NaCl-CaCl_2-H_2O$ and $NaCl-MgCl_2-H_2O$. To study the salt composition, salt samples were selected, the composition of which is given in Tables 2 and 3.

Table 2 – Chemical composition of Suzak deposit table salt samples

Salt composition of common salt, %						
NaCl	KCl	$MgS0_4$	$MgCl_2$	$CaCl_2$	$CaSO_4$	Insoluble residue
93.41	0.01	0.23	0.14	0.37	2.29	3.55
97.08	0.02	0.109	0.045	0	0.16	2.67

Table 2 shows that natural table salt contains mainly halite mineral and impurities of sulfate and calcium and magnesium, magnesium chloride, calcium chloride and potassium chloride.

To determine the content of other impurities and heavy metals, 2 samples of pre-prepared salt brine were analyzed using a Varian ICP-820MS inductively coupled plasma mass spectrometer. Table 3 shows the content of trace impurities (Pb, Cu, Cd, As).

Table 3 – Content of heavy metals in salt

Sample No.	Trace impurity content, μg/dm^3			
	Pb	Cu	Cd	As
1	18.21	67.53	9.00	14.01
2	16.01	60.12	7.3	12.43

The analysis results of common salt samples (Table 3) show that in addition to impurities such as calcium, magnesium, aluminum, iron, etc., the salt also contains heavy metals such as lead, copper, cadmium and arsenic, which requires purification to obtain “extra” common salt.

As can be seen, Suzak salt contains sodium, magnesium, calcium, chlorine and sulfur bound in the form of compounds NaCl, $CaCl_2$, $CaSO_4$, $MgS0_4$, $MgCl_2$, KCl and heavy metals. In this regard, it is of interest to study the solubility diagrams of saturated solutions of common salt in the presence of the above-mentioned impurities [[18], [19]].

For deep purification of salt from impurities, it is necessary to study solubility in the systems $NaCl-CaCl_2-H_2O$ and $NaC1-MgCl_2-H_2O$. The solubility isotherm in the system $NaCl-Na_2SO_4-H_2O$ was studied at the temperature of the saturated sodium chloride solution – 108.5°C. The time for establishing equilibrium was found by reaching equilibrium of sodium chloride in the solution [19].

The experimental data on the solubility in the above-mentioned systems are shown in Gibbs coordinates on Figures 3 and 4.

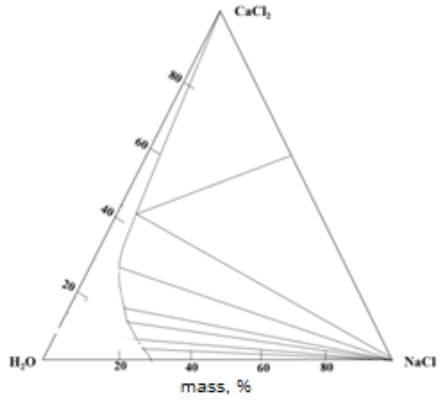

Figure 3 – Solubility isotherm in the system

NaCl-$CaCl_2$-H_2O at 100°C

From the data in Figure 3 it is evident that the solubility isotherm of the system NaCl-$CaCl_2$-H_2O at 100°C consists of two branches: the NaCl crystallization branch in the region of 6.1÷28.3 mass % NaCl and the $CaCl_2$ crystallization branch in the region of 60.3÷41.5% mass % $CaCl_2$. The eutonic point has the following composition: liquid phase 1.9% NaCl; 41.5% $CaCl_2$; solid phase 39.5% NaCl; 55.1% $CaCl_2$.

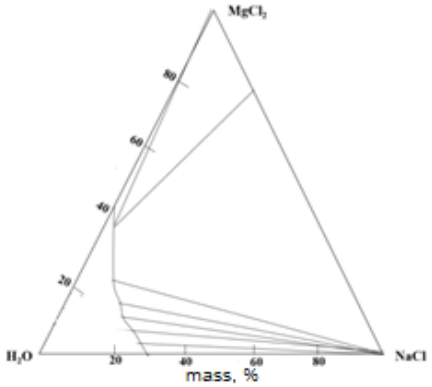

Figure 4 – Solubility isotherm in the system NaCl-$MgCl_2$-H_2O at 100°C

Similarly, from the data in Figure 4 it is evident that the solubility isotherm in the system NaC1-$MgCl_2$-H_2O at 100°C consists of two branches: the NaCl crystallization branch in the region of 28.3÷0.9 mass % NaCl and the $MgCl_2$ crystallization branch in the region of 42.2÷35.0 mass % $MgCl_2$. The eutonic point has the following composition: liquid phase 0.9% NaCl; 35.0% $MgCl_2$; solid phase 5.5% NaCl: 38.5% $MgCl_2$. As shown by the solubility isotherms of aqueous salt systems with the participation of NaCl at elevated temperatures, in the case of incomplete separation of Ca, Mg, and SO_4 ions from saturated solutions of technical salt, the remaining minor impurities contained in the liquid phase during hot filtration of solid sodium chloride pass into the filtrate.

To purify the obtained sodium chloride from trace impurities (Pb, Cu, Cd, As), studies were conducted at various concentrations of sodium chloride solution 80-140 g/l NaCl, temperature 70-90°C, contact time of the residue with the solution of 20 minutes and molar ratio of $Mg(OH)_2$:$CaCO_3$:$CaSO_4$ in the residue 1:4-5:6-7. The three-component mixture was subsequently used as a precipitant for trace impurities.

A solution of magnesium and calcium chloride, soda and alkali in an amount of 0.1-0.2% of the total mass of the solution was added to the previously obtained solution. The resulting mixture was stirred for 20 minutes, the residue was allowed to settle and the residue was filtered from the sodium chloride solution. Quantitative determination of trace impurities of lead, copper, cadmium and arsenic was carried out by the atomic adsorption method on a Contra device. The experimental results are given in Table 4.

Table 4 – Residual content of trace impurities after purification (μg/dm^3), and purification degree (%)

Elements	Concentration of sodium chloride solution, g/l				
	80	100	120	130	140
Pb	0.65	0.65	0.82	1.01	1.25
	91.2	93.4	93.1	93.3	93.1
Cu	1.81	1.80	2.20	2.10	3.37
	93.4	95.1	95.2	95.1	95.0
Cd	0.37	0.36	0.46	0.56	0.70
	89.9	92.6	92.4	92.3	92.2
As	0.13	0.43	0.71	1.32	2.78
	97.7	94.3	93.8	88.4	80.1
* numerator – content of trace impurities, μg/dm^3; denominator – purification degree, %					

From the above data of Table 6 it is evident that deep purification of the sodium chloride solution from trace impurities of Pb, Cu, and Cd is within 89.9-95.1% and from As by 80.1-97.7%. The concentration of mixtures in these solutions is more than 3 mmol/l, while the molar ratio of the mixture $Mg(OH)_2$:$CaCO_3$:$CaSO_4$ should be 1:4-5:6-7, and the contact time of the residue is not less than 20 minutes. The three-component mixture $Mg(OH)_2$:$CaCO_3$:$CaSO_4$ obtained in the process for purification of the sodium chloride solution from trace impurities of heavy metals is more effective than the known single-component coagulants based on $Fe(OH)_3$, $Mg(OH)_2$, $CaCO_3$, $CaSO_4$.

Based on the obtained data, 5 cm^3 of 0.1 M $Ca(OH)_2$ and $BaCl_2$ solutions are added to 1 dm^3 of the sodium chloride solution (100 g/dm^3) for purification. Magnesium hydroxide is precipitated, then 2 cm^3 of 1 M sodium carbonate solution and 3 M ammonia solution are added to pH 12-13.

The resulting purified sodium chloride solution has the following composition, mass %: NaCl – 13.9; Na_2SO_4 – 0.0002; $CaSO_4$ – 0.02; $MgSO_4$ – 0.001; H_2O – 86.06 and trace impurities, μg/dm^3: Pb 0.65-1.01; Cd 0.37-0.56; Cu 1.81-2.10; As 0.13-1.32. After cooling the solution to 25°C, sodium chloride

crystals containing 99.4% NaCl precipitate. Figure 5 shows the energy dispersion analysis of the obtained sodium chloride. The elemental composition of table salt is as follows,%: O-0.95, Na-37.37, Mg-0.001, S-0.000, Cl-61.46, Ca-0.002. Figure 5 shows the energy dispersion analysis of the obtained sodium chloride.

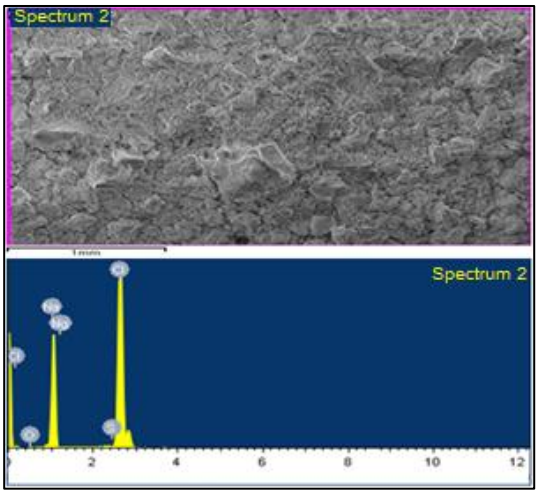

Figure 5 – Energy dispersion analysis of the purified salt

From Figure 5 it can be seen that the impurity content is Ca-0.002%, Mg-0.001%, and there is no sulfate ions.

Figure 6 shows derivatograms of purification of sodium chloride obtained using a Q-1500 Derivatograph.

Figure 6 – DTA of the residue obtained during the purification of sodium chloride

On the derivatograms of the resdiues (Figure 6) obtained during the purification of sodium chloride, the endothermic effect of dehydration of $CaSO_4 \cdot 2H_2O$ (140-160 and 120-180ºC) is visible, the endothermic effect of dehydration of $CaSO_4 \cdot 0{,}5H_2O$ (160-180^{O}C) is clearly expressed, i.e. dehydration of hemihydrate to anhydrite occurs.

X-ray phase analysis of the studied table salts was carried out on a Panalytical Empyrean X-ray diffractometer and results are shown in Figure 7.

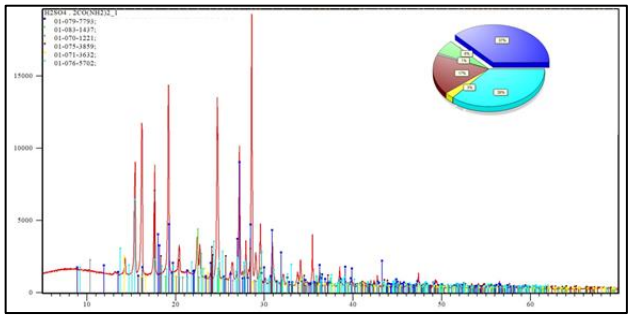

Figure 7 – Diffractogram of the purified sodium chloride

X-ray phase analysis data (Fig. 7). compounds of table salt, it can be noted that all reflections in diffraction patterns, as a rule, are characterized by their own reflection angles, a set of interplanar distances and intensities of diffraction lines. This indicates the individuality of the crystal lattices of the resulting pure compounds of table salt

Thus, the use of a three-component mixture consisting of $Mg(OH)_2$:$CaCO_3$:$CaSO_4$ in a ratio of 1:4-5:6-7 and contact of the residue with it for 20 minutes allows to purify the NaCl solution from trace impurities of Pb(II), Cu(II), Cd(II), As(V) by 92.0-97.7% and obtain 99.4% NaCl that meets the requirements of GOST P51574-2018.

Based on the work carried out, it was determined that the proposed method for purifying table salt from harmful impurities is effective, since the degree of purification is up to 99.0%. This method is aimed at the Suzak deposits, taking into account the physical and chemical properties of table salt.

A distinctive feature of this method from other methods is the study of the physicochemical properties of table salt, taking into account the composition of harmful impurities and heavy metals using active reagents and precipitants.

Conclusions

As a result of the research work, Suzak deposit common salt's raw material composition was studied and the content of impurities of Ca^{2+}, Mg^{2+} и SO_4^{2} ions and the content of heavy metals Pb (II), Cu (II), Cd (II), As (V) were determined. The solubility in the systems NaCl-Na_2SO_4-H_2O, NaCl-$CaCl_2$-H_2O and NaCl-$MgCl_2$-H_2O was studied and the isotherm of salt solubility at a temperature of 100-110°C was constructed.

The effect of temperature and time on the purification degree of common salt using barium chloride and sodium carbonate was studied, it was found that the highest purification degree of common salt from Ca^{2+}, Mg^{2+} и SO_4^{2} ions at 30 minutes and 90°C, respectively, is 99.8%, 99.9%, 99.93%. It was found that the use of a three-component mixture of $Mg(OH)_2$:$CaCO_3$:$CaSO_4$ in a ratio of 1:4-5:6-7 for 20 minutes allows purifying the NaCl solution from trace impurities of Pb(II), Cu(II), Cd(II), As(V) by 92.0-97.7% and obtaining 99.4% NaCl.

Based on the data obtained, effective methods for purifying salt from impurities were recommended, and the combined method can achieve salt purification above 99.0%.

CRediT author statement: **A. Anarbayev:** Conceptualization, formal analysis, investigation, data writing, original draft preparation, writing–review and editing; **B. Kabylbekova:** Data curation, writing draft preparation, methodology; **B. Smailov:** Resources, supervision, software, investigation; **G. Ormanova:** visualization, validation.

Conflicts of Interest. On behalf of all authors, the correspondent author declares no conflict of interest.

Funding: This research was funded by the Science Committee of the Ministry of Science and Higher Education of the Republic of Kazakhstan, Grant No. BR21882181.

Cite this article as: Anarbayev AA, Kabylbekova BN, Smailov BM, Ormanova GM. Methods for purifying table salt from the Suzak deposit. Kompleksnoe Ispolzovanie Mineralnogo Syra = Complex Use of Mineral Resources. 2026; 338(3):5-12. https://doi.org/10.31643/2026/6445.23

Созақ кен орнының ас тұзын қоспалардан тазарту әдістері

Анарбаев А.А., Кабылбекова Б.Н., *Смайлов Б.М., Орманова Г.М.

М. Әуезов атындағы Оңтүстік Қазақстан Зерттеу Университеті, Шымкент, Қазақстан

Мақала келді: *23 қаңтар 2025*
Сараптамадан өтті: *16 наурыз 2025*
Қабылданды: *7 сәуір 2025*

ТҮЙІНДЕМЕ

Бүгінгі күннің өзекті мәселелерінің бірі – ас тұзын зиянды қоспалардан тазарту және медициналық және тұрмыстық ас тұзын өндіру. Белгілі болғандай, «экстра» ас тұзына сұраныс жыл сайын артып келеді. Жоғары тазалықтағы натрий хлоридін алу үшін тұзды қоспа заттардан тазалаудың тиімді әдісін жасау қажет. Мақалада Созақ кен орнының ас тұздарын қоспалардан тазалаудың қазіргі жетілдірілген әдістері қарастырылған. Ғылыми жұмыстың негізгі мақсаты натрий хлоридін қоспа заттардан тазалау әдісін зерттеу. Ас тұзының бастапқы шикізатының құрамы зерттеліп, ол Ca^{2+}, Mg^{2+} және SO_4^{2-} иондарынан және Pb(II), Cu(II), Cd(II), As(V) ауыр металдарынан тұратыны анықталды. 100-110^{O}C температура аралығында NaCl - $CaCl_2$ - H_2O және NaCl-$MgCl_2$-H_2O жүйелеріндегі тұздардың ерігіштігі зерттелді. Белсенді заттарды қолданып ас тұзын тазалау дәрежесіне температура мен уақыттың әсері зерттеліп, ас тұзын Ca^{2+}, Mg^{2+} және SO_4^{2} иондарынан жоғары дәрежеде тазалау 30 минутта және 90^{O}C температурада болатыны және сәйкесінше тазалау дәрежесі 99,8%, 99,9%, 99,93% құрайтыны анықталды. $Mg(OH)_2$:$CaCO_3$:$CaSO_4$ үш компонентті қоспасын 1:4-5:6-7 қатынасында қолданып 20 минут ішінде NaCl ерітіндісін Pb(II), Cu(II), Cd(II), As(V) микроқоспаларынан 92,0-97,7% дейін тазартуға болады және тазалығы 99,4% NaCl алынатыны анықталды. Жоғары тазалықта тұзды алу үшін, 99% дейін тазарту деңгейін қамтамасыз ететін, қоспалардан тұзды тазартудың тиімді әдістері ұсынылады.

Түйін сөздер: натрий хлориді, ас тұзы, тұзды тазалау әдістері.

Авторлар туралы ақпарат:

Анарбаев Абибулла Абилдаұлы — *Техника ғылымдарының докторы, профессор, мұнай химиясы және бейорганикалық заттар өндірісінің технологиясы факультеті, М. Әуезов атындағы Оңтүстік Қазақстан зерттеу университеті, 160000, Шымкент, Қазақстан. E-mail: abib_28@mail.ru; ORCID ID: https://orcid.org/0000-0002-0019-4381*

Қабылбекова Балжан Нурманқызы — *Техника ғылымдарының кандидаты, профессор, химия және фармацевтикалық инженерия кафедрасы, М. Әуезов атындағы Оңтүстік Қазақстан зерттеу университеті, 160000, Шымкент, Қазақстан. E-mail: balzhan.kbn@bk.ru; ORCID ID: https://orcid.org/0000-0001-8461-8008*

Смайлов Бакыт Маткаримулы — *PhD доктор, ғылыми зерттеу департаменті, М. Әуезов атындағы Оңтүстік Қазақстан зерттеу университеті, 160000, Шымкент, Қазақстан. E-mail: Baha_uppr@mail.ru; ORCID ID: https://orcid.org/0000-0001-7976-9776*

Орманова Гаухар Мейрбекқызы — *PhD докторант, мұнай химиясы және бейорганикалық заттар өндірісінің технологиясы кафедрасы, М. Әуезов атындағы Оңтүстік Қазақстан зерттеу университеті, 160000, Шымкент, Қазақстан. E-mail: ormanova_g@inbox.ru; ORCID ID: https://orcid.org/0000-0002-9625-5790*

Способы очистки поваренной соли Сузакского месторождения от примесей

Анарбаев А.А., Кабылбекова Б.Н., *Смайлов Б.М., Орманова Г.М.

Южно-Казахстанский Исследовательский Университет имени М. Ауезова, Шымкент, Казахстан

Поступила: *23 января 2025*
Рецензирование: *16 марта 2025*
Принята в печать: *7 апреля 2025*

АННОТАЦИЯ

Одним из актуальных вопросов на сегодняшний день является очистка поваренной соли от вредных примесей и получение соли медицинского и бытового назначения. Как известно, ежегодно на потребность пищевой соли «экстра» растет. Для получения высокочистой соли хлорида натрия необходимо разработка более эффективных методов очистки соли от примесей. В статье рассмотрены современные методы очистки поваренной соли Сузакского месторождения от вредных примесей. Основная цель научной работы исследование методов очистки хлорида натрия от примесей. Исследован состав исходного сырья поваренной соли и определены содержание примесей Ca^{2+}, Mg^{2+} и SO_4^{2-}ионов и тяжелых металлов Pb(II), Cu(II), Cd(II), As(V). Изучен растворимость в системе NaCl-Na_2SO_4-H_2O, NaCl - $CaCl_2$ - H_2O и NaCl-$MgCl_2$-H_2O при температуре 100-110^OC. Исследован влияние температуры и времени на степень очистки поваренной соли с использованием активных реагентов, установлен что наивышее степень очистки поваренной соли от Ca^{2+}, Mg^{2+} и SO_4^{2} при 30 мин. и 90^OC соответственно составляет 99,8%, 99,9%, 99,93%. Установлена, что использование при очистке трехкомпонентной смеси $Mg(OH)_2$:$CaCO_3$:$CaSO_4$ в соотношении 1:4-5:6-7 в течение 20 минут позволяет очистить раствор NaCl от микропримесей Pb(II), Cu(II), Cd(II), As(V) на 92,0-97,7% и получить 99,4% NaCl. Для получения соли высокой степени чистоты рекомендованы эффективные методы очистки соли от примесей позволяющие достичь степень очистки до 99%.

Ключевые слова: хлорид натрия, поваренная соль, методы очистки соли.

Информация об авторах:

Анарбаев Абибулла Абилдаевич — *Доктор технических наук, профессор, факультет технологии производства нефтехимических и неорганических веществ, Южно-Казахстанский исследовательский университет им. М. Әуезова, 160000, Шымкент, Қазақстан. E-mail: abib_28@mail.ru; ORCID ID: https://orcid.org/0000-0002-0019-4381*

Кабылбекова Балжан Нурмановна — *Кандидат технических наук, профессор кафедры профессор кафедры химия и фармацевтическая инженерия, Южно-Казахстанский исследовательский университет им. М.Ауезова, 160000, Шымкент, Казахстан. E-mail: balzhan.kbn@bk.ru; ORCID ID: https://orcid.org/0000-0001-8461-8008*

Смайлов Бакыт Маткаримулы — *PhD доктор, департамент научных исследований, Южно-Казахстанский исследовательский университет им. М. Әуезова, 160000, Шымкент, Қазақстан. E-mail: Baha_uppr@mail.ru; ORCID ID: https://orcid.org/0000-0001-7976-9776*

Орманова Гаухар Мейрбековна — *PhD докторант кафедры технология неорганических и нефтехимических производств, Южно-Казахстанский исследовательский университет им. М.Ауезова, 160000, Шымкент, Казахстан. E-mail: ormanova_g@inbox.ru; ORCID ID: https://orcid.org/0000-0002-9625-5790*

References

[1] Bishimbayev VK, Amreev DD, Kapsalyamov BA, Gapparova KM, Sarsenov A. Analız rynka súlfata natrıa ı ıssledovanıe vozmojnostı ego polýchenıa ız súlfatnıkov mestorojdenıa Jaksykylysh [Analysis of the sodium sulfate market and study of the possibility of its production from sulfate rocks of the Zhaksykylysh deposit]. Bulletin of Science of Southern Kazakhstan. 2019; 1(5):58-65. (in Russ).

[2] Desyatov AV, Kruchinina NE, Novikov SV. Glýbokaıa pererabotka mıneralızovannyh shahtnyh vod s polýcheníem krıstalıcheskogo súlfata natrıa [Deep processing of mineralized mine water to produce crystalline sodium sulfate. Advances in chemistry and chemical technology]. 2016; 9:96-99. (in Russ).

[3] Ren Z, Wei X, Li R, Wang W, Wang Y, Zhou Z. Highly selective extraction of lithium ions from salt lake brines with sodium tetraphenylborate as co-extractant, Separation and Purification Technology. 2021; 269:118756. https://doi.org/10.1016/j.seppur.2021.118756

[4] Cipolletta G, Lancioni N, Akyol Ç, Eusebi AL, Fatone F. Brine treatment technologies towards minimum/zero liquid discharge and resource recovery: State of the art and techno-economic assessment, Journal of Environmental Management. 2021; 300:113681. https://doi.org/10.1016/j.jenvman.2021.113681

[5] Zhang X, Ren Y, Ping L, Ma H, Liu C, Wang Y, Kong L, Shen W. Solid-liquid equilibrium for the ternary systems and atmospheric pressure, J. Chem. Eng. 2014; 12:3969-3974. https://doi.org/10.1021/je500854m

[6] Shen Y, Linnow K, Steiger M. Crystallization behavior and damage potential of Na_2SO_4 –NaCl mixtures in porous building materials. Cryst. Growth Des. 2020; 20(9):5974-5985. http://dx.doi.org/10.1021/acs.cgd.0c00671

[7] Ren Z, Wei X, Li R, Wang W, Wang Y, Zhou Z. Highly selective extraction of lithium ions from salt lake brines with sodium tetraphenylborate as co-extractant. Separation and Purification Technology. 2021; 269:118756. http://dx.doi.org/10.1016/j.seppur.2021.118756

[8] Xingguo Luo, Xingbin Li, Chang Wei, Zhigan Deng, Ye Liu, Minting Li, Sanqiang Zheng, Xing Huang. Recovery of NaCl and Na2SO4 from high salinity brine by purification and evaporation. Desalination. 2022; 530:115631. http://dx.doi.org/10.1016/j.desal.2022.115631

[9] Klammer N, Engtrakul C, Zhao Y, Vidal J, Wu Y. Method to Determine MgO and MgOHCl in Chloride Molten Salts. Analytical Chemistry. 2020; 92(5):3598-3604. https://doi.org/10.1021/acs.analchem.9b04301

[10] Xu Zhao, Qi Zhang, Haihong Wu, Xiaocui Hao, Liang Wang, Xiping Huang. Extraction of Lithium from Salt Lake Brine. Progress in Chemistry. 2017; 29(7):796-808. (In Chinese). https://doi.org/10.7536/PC170313

[11] Dahmardeh H, Akhlaghi Amiri HA, Nowee SM. Evaluation of mechanical vapor recompression crystallization process for treatment of high salinity wastewater. Chemical Engineering and Processing - Process Intensification. 2019; 145:107682. http://dx.doi.org/10.1016/j.cep.2019.107682

[12] Myerson A, Erdemir D. & Lee A. (Eds.). Handbook of Industrial Crystallization (3rd ed.). Cambridge: Cambridge University Press. 2019. http://dx.doi.org/10.1017/9781139026949

[13] Rismana E, Arbianto AD, Kusumaningrum S. Development of Efficient and Scalable Production Process of Analytical Grade Sodium Chloride at Laboratory Scale. International Journal of Technology. 2024; 15(3):743-752. https://doi.org/10.14716/ijtech.v15i3.5606

[14] Kadirbayeva AA, Urazkeldiyeva DA, Tanirbergenov R, Shaimerdenova G. Purification of technical sodium chloride from the tasty tuz deposit of the Republic of Kazakhstan. Series chemistry and technology. 2022; 4(453):80-87. http://dx.doi.org/10.32014/2518-1491.136

[15] Li Zhu, YuLong Ma, ShaoYing Ge, YuYu Wang. Solid-liquid phase equilibria of the quaternary system. The Journal of Chemical Thermodynamics. 2022; 165:106658. https://doi.org/10.1016/j.jct.2021.106658

[16] GOST P 51574-2000. Common salt. Test methods. Publishing House of Standards, Moscow. (in Russ).

[17] Dahmardeh H, Akhlaghi Amiri HA, Nowee SM. Evaluation of mechanical vapor recompression crystallization process for treatment of high salinity wastewater. Chemical Engineering and Processing - Process Intensification. 2019; 145:107682. http://dx.doi.org/10.1016/j.cep.2019.107682

[18] Goetzfried F, Kondorosy E. Technologies for the production of pharmaceutical grade sodium chloride. 2018 World Salt Symposium. June 19-21, 2018; Park City, Utah, USA.

[19] Geertman RM. Sodium chloride: Crystallization. Encyclopedia of Separation Science. 2000; 61:4127-4134. https://doi.org/10.1016/B0-12-226770-2/06061-0

[20] Badrut Tamam Ibnu Ali, Hamzah, Mochammad Ismail, Imam Wahyudi, Ali Nurdin, Fausiah, Budiyono, Hens Saputra. Refining NaCl: Elevating salt's quality from coarse to industrial and pharmacy grade through innovative hydroextraction techniques. Case Studies in Chemical and Environmental Engineering. 2024; 9:100752. https://doi.org/10.1016/j.cscee.2024.100752

[21] Hussein IM, Metwally Salman AS, Ashraf MS. A Review on Extraction Processes of Salts from Different Salt Lakes and their Environmental Impact in Industry. Letters in Applied NanoBioScience. 2022; 11(4):4016-4039. https://doi.org/10.33263/LIANBS114.40164039

[22] Zhao Y, Klammer N, Vidal J. Purification strategy and effect of impurities on corrosivity of dehydrated carnallite for thermal solar applications. Royal Society of Chemistry. 2019; 9:41664-41671. https://doi.org/10.1039/C9RA09352D

Crossref
DOI: 10.31643/2026/6445.24
Engineering and Technology

Epoxy Resin Development for Anticorrosion Coatings

[1*]Negim E.-S., [2]Bekbayeva L., [3]Puzikova D.S., [3]Zhurynov M.Zh., [3] Nefedov A.N., [3]Khussurova G.M., [4] Shadin N.A.,[5]Jamal Khatib

[1]School of Materials Science and Green Technologies, Kazakh British Technical University, Almaty, Kazakhstan
[2]National Nanotechnology Open Laboratory, Al-Faraby Kazakh National University, Almaty, Kazakhstan
[3]D.V. Sokolsky Institute of Fuel, Catalysis and Electrochemistry, Kazakh British Technical University, Almaty, Kazakhstan
[4]Department of Chemistry, Institute of Natural Sciences and Geography, Abai Kazakh National Pedagogical University, Almaty, Kazakhstan
[5]Department of Civil and Environmental Engineering, Faculty of Engineering, Beirut Arab University, Beirut, Lebanon

**Corresponding author: El-Sayed Negim, elashmawi5@yahoo.com*

Received: *January 23, 2025*
Peer-reviewed: *March 4, 2025*
Accepted: *April 9, 2025*

ABSTRACT

In this study, a high molecular weight epoxy resin (ELM-NG 900Z) based on diglycidyl ether of bisphenol A was cured with different types of hardeners to examine their impact on the physical and mechanical properties of the epoxy resin. The hardeners used were G-5022X70 (140-170 mg KOH/g), G-A0533 (310-350 mg KOH/g), and G-0930 (280-320 mg KOH/g). The results indicated that the hardener G-A0533 provided the best mechanical properties for the epoxy resin compared to other hardeners. Furthermore, various additives including silica fume, talc, barium sulfate, ferric oxide, and pigments were mixed with the epoxy resin in the presence of the hardener G-A0533 to enhance its mechanical properties. It was observed that the addition of 3% silica fume, 10% ferric oxide, and 3% inorganic pigments improved the mechanical properties, while the addition of 5% talc decreased most mechanical properties and only increased hardness. The incorporation of barium sulfate into the epoxy resin enhanced adhesion and flexural strength but decreased tensile strength and hardness. The inclusion of organic pigment had no significant effect on the mechanical properties of the epoxy resin. This enhancement in mechanical properties is attributed to the type of hardener used as well as the types and amounts of additives mixed with the epoxy resin.

Keywords: Epoxy, hardener, mechanical, corrosion, additives.

Information about authors:

El-Sayed Negim — *School of Materials Science and Green Technologies, Kazakh British Technical University, St. Tole bi, 59, Almaty 050000, Kazakhstan. Email: elashmawi5@yahoo.com*

Lyazzat Bekbayeva — *National Nanotechnology Open Laboratory, Al-Faraby Kazakh National University, al-Farabi av., 050040, Almaty, Republic of Kazakhstan. Email: lyazzat_bk2019@mail.ru*

Puzikova Darya Sergeevna — *D.V. Sokolsky Institute of Fuel, Catalysis and Electrochemistry, Kazakh British Technical University. 050010, Kunaev St., 142, Almaty, Kazakhstan. Email: d.puzikova@ifce.kz*

Zhurynov Murat Zhurynovich — *D.V. Sokolsky Institute of Fuel, Catalysis and Electrochemistry, Kazakh British Technical University. 050010, Kunaev St., 142, Almaty, Kazakhstan. Email: mur.zhurinov@mail.ru*

Nefedov Alexandr Nikolayevich — *D.V. Sokolsky Institute of Fuel, Catalysis and Electrochemistry, Kazakh British Technical University. 050010, Kunaev St., 142, Almaty, Kazakhstan. Email: a.nefedov@ifce.kz*

Khussurova Gulinur Marsovna — *D.V. Sokolsky Institute of Fuel, Catalysis and Electrochemistry, Kazakh British Technical University. 050010, Kunaev St., 142, Almaty, Kazakhstan. Email: gulinur_k@bk.ru*

Shadin Nurgul Adyrbekkyzy — *Department of Chemistry, Institute of Natural Sciences and Geography, Abai Kazakh National Pedagogical University, 30 Kazybek Bi str., Almaty, Kazakhstan. Email: nugen_87@mail.ru*

Jamal Khatib — *Department of Civil and Environmental Engineering, Faculty of Engineering, Beirut Arab University, P.O. Box: 11 5020 Beirut, Lebanon. Email: j.khatib@bau.edu.lb*

Introduction

Epoxy resins are a type of polymer that contains two or more epoxy rings. Anticorrosive paints are often made from thermosetting polymers known as epoxy resins. The curing process of these resins can be done by one or two components using chemical cross-linkers such as hardeners. These epoxy resins can be cross-linked with hardeners (amines) for various industrial applications such as coatings, paints, anti-corrosion coatings, and adhesives due to their good thermal and mechanical properties [1]. They can react with various curing agents that contain active groups, including hydrogen, such as amines and anhydrides [2]. Hardener amines are categorized into primary (one hydrogen molecule),

secondary (two hydrogen molecules), and tertiary (three hydrogen molecules). Additionally, hardeners are classified as aliphatic or aromatic amines and play a key role in curing epoxy resins at room temperature. The physical and mechanical properties of epoxy resins vary depending on the type of hardeners and the ratio between epoxy resins and hardeners [3]. The combination of aliphatic hardeners with epoxy resins enhances both the bonding properties and resistance to alkalis and certain inorganic acids [4]. However, the aromatic hardeners improve the heat resistance of the epoxy resins as well as chemical resistance [[5], [6]]. Selecting an appropriate hardener requires careful consideration of the processing conditions, including pot life, viscosity, mixing ratio, and temperature, as well as the desired properties of the final product, such as strength, chemical and thermal resistance, toughness, and flexibility.

The Silica fume is a kind of filler that has active and inorganic powder [7]. Silica fume differs significantly from epoxy resin. It enhances epoxy properties by reducing shrinkage, improving stability, preventing cracking, and lowering coating costs. Research has shown that silica fume increases the strength, thermal stability, and hardness of epoxy resins [[7], [8], [9], [10], [11], [12], [13]]. On the other hand, the mixing of barium sulfate and ferric oxide has different influences on the mechanical properties of the epoxy resin. The results showed that barium sulfate increased the mechanical properties, while ferric oxide improved the adhesion of epoxy on the metal [[14], [15]]. The effect of different pigments on the properties of epoxy resins was investigated by authors [[16], [17], [18]]. Pigments are classified as organic, inorganic, etc. Most pigments enhance the properties of epoxy and others disperse problems with the epoxy resins. To solve the problem of dispersing, mixing very well by using a dissolver and followed by milling. This study aims to develop an anticorrosion coating based on epoxy for industrial applications. Various additives, such as barium sulfate, talc, ferric oxide, silica fume, and inorganic and organic pigments, are mixed with epoxy and different hardeners to enhance the coating's mechanical properties.

Experimental part

Materials

Epoxy resins ELM-NG 900Z were supplied by Elcos Marketing LLP, Almaty Kazakhstan. ELM-NG 900Z has an epoxy value of 5.25-5.5 eq/Kg, weight per epoxide of 450-525 g/eq, viscosity of 13000 mPa-s at 25 ^{o}C and density of 1.1 gm/cm^{3}. G-5022X70 has amine value 140-170 mgKOH/g and viscosity 585 mPa-s at 25 ^{o}C, G-A0533 has amine value 310-350 mg KOH/g and viscosity 935 mPa-s at 25 ^{o}C and G-0930 has amine value 280-320 mg KOH/g and viscosity 8,000 mPa-s at 25 ^{o}C were purchased from Kukdo chemical company, South Korea. Silica fume, talc, barium sulfate, Fe_2O_3 and inorganic pigment (cobalt blue) & organic pigment (carbon black) were supplied by ETC – company, Almaty, Kazakhstan.

Mixing epoxy resin with hardeners

Epoxy resin ELM-NG 900Z was mixed with different hardeners (G-5022X70, G-A0533 and G-0930) at a ratio of 1.0: 0.5 respectively. All ingredients were thoroughly mixed, both slowly and deliberately, to minimize the introduction of air bubbles. Scrape the sides and bottom of the container to ensure all components are fully mixed. Mixed was cast to specimens of dimensions of 7 mm x 7 mm x 7 mm in steel molds and allowed to dry at room temperature for 6 days and keep it for tests [19].

Mixing epoxy resin with additives

In all experiments, the epoxy resin ELM-NG 900Z was transferred to a vial and mixed for 10 minutes at a speed of 500 rpm. After adding the silica fume (3% based on the epoxy resin), talc (5% based on epoxy weight), barium sulfate (15% based on epoxy resin), ferric oxide (10% based on epoxy weight), and pigments (3% based on epoxy weight) to the epoxy separately, the mixture was stirred for 30 minutes at a speed of 1200 rpm. Hardener was then added, and the mixture was stirred at a speed of 500 rpm for 5 minutes. The mixture was cast into specimens with dimensions of 7 mm x 7 mm x 7 mm in steel molds and allowed to dry at room temperature for 6 days before being tested for mechanical properties [[19], [20]].

Tests (Physical and Mechanical properties)

Viscosity was measured at room temperature using a Brookfield viscometer, according to ISO 12058-1 (ISO 12058-1, 2018) [21] at 25 ^{o}C. The MTS 10/M tensile testing equipment was used to quantify the tensile properties of the cast films with a crosshead speed of 50 mm/min. A minimum of four values were averaged, and a 1-kN load cell was utilized A cylindrical Mandrel Tester (ASTM D522, 2001) [22] was used to assess the resistance of a coating of product to cracking and/or detachment from a metal substrate when subjected to bending around a cylindrical mandrel under standard

conditions. The tubular impact tester (ASTM D2794, 2019) [23] determined film resistance to impact, and the economic cross hatch tester (ASTM D3359, 2001) [24] was used to evaluate the adhesion of applied coatings. For adhesion strength measurements of the epoxy and diluted epoxy mixture, pull-out tests were conducted according to the EN 1542 standard (En,1542, 1999) [25].

Results and discussion

Physical properties

Table 1 shows the viscosity of epoxy resin ELM-NG 900Z mixed with different hardeners in a 1:0.5 ratio, measured at 25°C and speeds of 5 and 50 rpm. The viscosity decreased as speed increased from 5 to 50 rpm. Hardener G-0930 had the highest viscosity at both speeds, while hardener G-A0533 had the lowest. The variation is due to the influence of the hardeners on the epoxy's viscosity. Additionally, hardener G-A0533 exhibited the highest thixotropic index (6.4), and hardener G-5022X70 had the lowest (2.35).

Table 1 - Viscosity and thixotropic index of epoxy resin mixed with hardeners in ratio (1: 0.5)

Sample code	ELM-NG 900Z	ELM-NG 900Z / G-5022X70	ELM-NG 900Z / G-0930	ELM-NG 900Z / G-A0533
Viscosity at 5 rpm (mPa-s)	13000	8000	11000	4500
Viscosity at 50 rpm (mPa-s)	2500	3400	2200	700
Thixotropic index (TI)	5.2	2.35	5.0	6.4

Mechanical properties

Table 2 shows the mechanical properties of epoxy resin mixed with different hardeners at a 1:0.5 ratio. The hardener G-A0533 provided the highest values in adhesion strength (64 Kgf/cm²), tensile strength (315 Kgf/cm²), hardness (69), and flexural strength (834 Kgf/cm²). In contrast, the hardener G-5022X70 showed the lowest values in adhesion strength (100 Kgf/cm²), tensile strength (627 Kgf/cm²), hardness (84), and the same flexural strength (834 Kgf/cm²). Generally, the performance of epoxy resin depends on the type of hardeners and the crosslinking network formed during the reaction. However, all epoxy resin mixtures passed impact tests, cylindrical mandrel, and cross-hatch tests [[25], [26], [27]].

Table 2 - Mechanical properties of epoxy resin mixed with hardeners in ratio (1: 0.5)

Sample code	ELM-NG 900Z / G-5022X70	ELM-NG 900Z / G-0930	ELM-NG 900Z / G-A0533
Adhesion Strength (Kgf/cm^2)	64	80	100
Tensile Strength (Kgf/cm^2)	315	425	627
Flexural Strength (Kgf/cm^2)	834	710	460
Hardness (Shore D)	69	75	84
Impact test	Pass	Pass	Pass
Cylindrical Mandrel	Pass	Pass	Pass
Crosshatch	Pass	Pass	Pass

The effect of silica fume and talc on the mechanical properties of epoxy resin

Table 3 shows that adding 3% silica fume to epoxy resin enhances its mechanical properties when mixed with different hardeners at a 1:0.5 ratio. Silica fume increased adhesion by 21% for G-A0533, 11.25% for G-0930, and 10.9% for G-5022X70 due to hardener activity and crosslinking bonds. Tensile strength also improved by 10.04% for G-A0533, 12.2% for G-0930, and 11.11% for G-A0533. Conversely, adding 5% talc decreased adhesion by 2% for G-A0533, 16.25% for G-0930, and 14.06% for G-5022X70 as shown in Table 4, while hardness strength increased by 5.9%, 10.66%, and 7.0% respectively.

Table 3 - Mechanical properties of epoxy resin mixed with hardeners in the ratio (1: 0.5) in the presence of 3% silica fume

Sample code	ELM-NG 900Z / G-5022X70	ELM-NG 900Z / G-0930	ELM-NG 900Z / G-A0533
Adhesion Strength (Kgf/cm^2)	71	89	121
Tensile Strength (Kgf/cm^2)	350	477	690
Flexural Strength (Kgf/cm^2)	634	410	380
Hardness (Shore D)	71	78	86
Impact test	Pass	Pass	Pass
Cylindrical Mandrel	Pass	Pass	Pass
Crosshatch	Pass	Pass	Pass

Table 4 - Mechanical properties of epoxy resin mixed with hardeners in the ratio (1: 0.5) in the presence of 5% talc

Sample code	ELM-NG 900Z / G-5022X70	ELM-NG 900Z / G-0930	ELM-NG 900Z / G-A0533
Adhesion Strength (Kgf/cm^2)	55	67	98
Tensile Strength (Kgf/cm^2)	285	305	576
Flexural Strength (Kgf/cm^2)	573	369	295
Hardness (Shore D)	76	83	89
Impact test	Pass	Pass	Pass
Cylindrical Mandrel	Pass	Pass	Pass
Crosshatch	Pass	Pass	Pass

The effect of barium sulfate and ferric oxide on the mechanical properties of epoxy resin

Table 5 shows increasing in the adhesion strength and flexural strength but decreasing in the tensile strength and hardness of the epoxy resin mixed with 15% barium sulfate in the presence of different hardeners. Flexural strength increased from 834 to 1005 Kgf/cm^2 for epoxy mixed with hardener G-5022X70 and 15% barium sulfate, from 710 to 934 Kgf/cm^2 for hardener G-0930 and from 460 to 860 Kgf/cm^2 for hardener G-A0533. While adhesion of epoxy increased from 64 to 70 Kgf/cm^2, from 80 to 86 Kgf/cm^2, and from 100 to 110 Kgf/cm^2, for harnerers G-5022X70, G-0930 and G-A0533, respectively. Table 6 shows the increase in mechanical properties including tensile strength, adhesion, hardness and decreasing in the flexural strength of epoxy resin mixed with 10% ferric oxide and different hardeners. For example, 10% ferric oxide gave the highest adhesion 170 Kgf/cm^2 for hardener G-A0533, while 10% ferric oxide gave the lowest adhesion 77 Kgf/cm^2 for hardener G-5022X70. However, 10% ferric oxide increased tensile strength by 12.12 % for hardener G-A0533, 16.4% for hardener G-0930 and 28,5% for hardener G-5022X70. The increase in the mechanical properties of epoxy resin is attributed to the hydroxy group resulting from the reaction of epoxy group and hardeners. Epoxy resin's improved mechanical properties come from the reaction between the epoxy group and hardeners, forming hydroxy groups that enhance adhesion, tensile strength, and elongation at break [[15], [19], [20]].

Table 5 - Mechanical properties of epoxy resin mixed with hardeners in the ratio (1: 0.5) in the presence of barium sulphate (15%)

Sample code	ELM-NG 900Z / G-5022X70	ELM-NG 900Z / G-0930	ELM-NG 900Z / G-A0533
Adhesion Strength (Kgf/cm^2)	70	86	110
Tensile Strength (Kgf/cm^2)	300	405	610
Flexural Strength (Kgf/cm^2)	1005	934	860
Hardness (Shore D)	60	71	82
Impact test	Pass	Pass	Pass
Cylindrical Mandrel	Pass	Pass	Pass
Crosshatch	Pass	Pass	Pass

The effect of different pigments on the mechanical properties of epoxy resin

The effect of inorganic pigment (cobalt blue) & organic pigment (carbon black) on the mechanical properties of epoxy resin mixed with different hardeners are presented in Tables 7 and 8. Table 7 shows an increase in adhesion, tensile strength and hardness while a decrease in flexural strength of epoxy resin mixed with different hardneres. For example, increased adhesion strength 10%, 7.5% and 7.8 % for epoxy mixed with hardeners G-A0533, G-0930 and G-5022X70, respectively. While tensile strength of the epoxy increased by 7,3%, 2,3% and 11.11% when mixed with hardeners G-A0533, G-0930 and G-5022X70, respectively. Flexural strength of epoxy resin 15.2%, 2.1% and 15.4% mixed with hardeners G-A0533, G-0930 and G-5022X70, respectively. However, there is no significant influence of organic pigment on the mechanical properties of the epoxy mixed with different hardners as shown in Table 8.

Table 6 - Mechanical properties of epoxy resin mixed with hardeners in the ratio (1: 0.5) in the presence of ferric oxide (10%)

Sample code	ELM-NG 900Z / G-5022X70	ELM-NG 900Z / G-0930	ELM-NG 900Z / G-A0533
Adhesion Strength (Kgf/cm^2)	77	90	170
Tensile Strength (Kgf/cm^2)	405	495	703
Flexural Strength (Kgf/cm^2)	645	515	390
Hardness (Shore D)	74	80	92
Impact test	Pass	Pass	Pass
Cylindrical Mandrel	Pass	Pass	Pass
Crosshatch	Pass	Pass	Pass

Table 7 - Mechanical properties of epoxy resin mixed with hardeners in the ratio (1: 0.5) in the presence of inorganic pigment (3 %)

Sample code	ELM-NG 900Z /. G-5022X70	ELM-NG 900Z / G-0930	ELM-NG 900Z / G-A0533
Adhesion Strength (Kgf/cm^2)	69	86	110
Tensile Strength (Kgf/cm^2)	350	435	673
Flexural Strength (Kgf/cm^2)	705	695	390
Hardness (Shore D)	71	79	91
Impact test	Pass	Pass	Pass
Cylindrical Mandrel	Pass	Pass	Pass
Crosshatch	Pass	Pass	Pass

Table 8 - Mechanical properties of epoxy resin mixed with hardeners in the ratio (1: 0.5) in the presence of organic pigment (3 %)

Sample code	ELM-NG 900Z /. G-5022X70	ELM-NG 900Z / G-0930	ELM-NG 900Z / G-A0533
Adhesion Strength (Kgf/cm^2)	62	81	105
Tensile Strength (Kgf/cm^2)	320	419	630
Flexural Strength (Kgf/cm^2)	832	703	469
Hardness (Shore D)	70	74	86
Impact test	Pass	Pass	Pass
Cylindrical Mandrel	Pass	Pass	Pass
Crosshatch	Pass	Pass	Pass

Conclusion

The following results were obtained during the development of epoxy resin for anticorrosion coating.

1. The effect of different hardeners on the physical and mechanical properties of epoxy was studied. The hardener G-A0533 resulted in the highest physical and mechanical properties compared to other hardeners due to its higher activity.

2. Adding 3% silica fume to the epoxy resin mixed with hardener G-A0533 increased adhesion by 21.0%, tensile strength by 10%, and hardness by 2%.

3. Adding 5% talc to the epoxy resin mixed with G-A0533 decreased adhesion, tensile strength, and flexural strength but increased hardness by 5%.

4. Premixed barium sulfate with epoxy resin increased adhesion by 10%, flexural strength by 86%, and decreased tensile strength and hardness in the presence of hardener G-A0533.

5. The mechanical properties of the epoxy resin mixed with 10% ferric oxide and different hardeners were investigated. The hardener G-A0533 provided the highest adhesion (170 Kgf/ cm^2), tensile strength (703 Kgf/cm^2), and hardness (92 shore D) compared to the epoxy resin without ferric oxide [adhesion 100 Kgf/ cm^2, tensile strength 627 Kgf/cm^2, and hardness 84 shore D].

6. The influence of inorganic pigment on the mechanical properties of epoxy resin mixed with different hardeners at a ratio of 1:0.5 was examined. Adding 3% inorganic pigment increased the mechanical properties of the epoxy resin mixed with hardener G-A0533 more than other hardeners, such as increasing adhesion by 10%, tensile strength by 7.3%, and hardness by 8.3%.

7. The addition of organic pigment to the epoxy resin mixed with different hardeners had no significant effect and slightly increased the mechanical properties of the epoxy resin in the presence of hardener G-A0533.

Conflicts of interest. The authors declare no conflict of interest.

CRediT author statement: **E.-S. Negim:** performed the methodology and prepared the original draft; **L. Bekbayeva, D. Puzikova, M. Zhurinov,** and **A. Nefedov**: performed the data collection and part of the methodology; G. **Khussurova, N. Shadin** and **Jamal Khatib**: revised the final draft of the manuscript.

All authors agree to be accountable for the content and conclusions of the article.

Acknowledgements. This research was funded by the Committee of Science of the Ministry of Science and Higher Education of the Republic of Kazakhstan (Grant No. BR24992812Development of materials and technologies aimed at comprehensive anti-corrosion protection of process equipment in the petrochemical, machine and instrument-making industries).

Cite this article as: Negim E-S, Bekbayeva L, Puzikova DS, Zhurynov MZh, Nefedov AN, Khussurova GM, Shadin NA, Jamal Khatib. Epoxy resin development for anticorrosion coatings. Kompleksnoe Ispolzovanie Mineralnogo Syra = Complex Use of Mineral Resources. 2026; 338(3):13-20. https://doi.org/10.31643/2026/6445.24

Коррозияға қарсы жабындар үшін эпоксидті шайырды әзірлеу

[1*]Negim E.-S., [2] Бекбаева Л.К., [3]Пузикова Д.С., [3]Жұрынов М.Ж., [3]Нефедов А.Н., [3]Хусурова Г.М., [4]Шадин Н.А., [5]Jamal Khatib

[1]Материалтану және жасыл технологиялар мектебі, Қазақстан-Британ техникалық университеті, Алматы, Қазақстан
[2]Ашық түрдегі нанотехнологиялық зертхана, әл-Фараби атындағы Қаз¥У, Алматы, Қазақстан
[3]Д.В. Сокольский атындағы жанармай, катализ және электрохимия институты, Қазақстан-Британ техникалық университеті, Алматы, Қазақстан
[4] Жаратылыстану және география институты, Абай атындағы Қазақ Ұлттық педагогикалық университеті, Алматы, Қазақстан
[5]Бейрут араб университетінің инженерлік факультетінің азаматтық және қоршаған ортаны қорғау кафедрасы, Бейрут, Ливан

Мақала келді: *23 қаңтар 2025*
Сараптамадан өтті: *4 наурыз 2025*
Қабылданды: *9 сәуір 2025*

ТҮЙІНДЕМЕ

Бұл зерттеуде эпоксидті шайырдың физикалық және механикалық қасиеттеріне әсерін зерттеу үшін бисфенол А диглицидил эфирің негізіндегі жоғары молекулалы эпоксидті шайыр (ELM-NG 900Z) әр түрлі қатайтқыштармен қатайтылды. G-5022X70 (140-170 мг KOH/г), G- A0533 (310-350 мг KOH/г) және G-0930 (280-320 мг KOH/г) қатайтқыштар қолданылды. Нәтижелер қатайтқыш G-A0533 басқа қатайтқыштармен салыстырғанда эпоксидті шайырдың ең жақсы механикалық қасиеттерін қамтамасыз ететінін көрсетті. Сонымен қатар, механикалық қасиеттерін жақсарту үшін G-A0533 қатайтқыштың қатысуында кремний диоксиді, тальк, барий сульфаты, темір оксиді және пигменттер сияқты әртүрлі қоспалар эпоксидті шайырмен араластырылды. 3% кремний оксиді, 10% темір оксиді және 3% бейорганикалық пигменттерді қосқанда механикалық қасиеттер жақсарса, 5% тальк қосылғанда механикалық қасиеттердің көпшілігі төмендеп, тек қаттылық жоғарылағаны байқалды. Эпоксидті шайырға барий сульфаты қосылғанда адгезия мен иілу беріктігі артты, бірақ созылу беріктігі мен қаттылығы төмендеді. Органикалық пигментті қосу эпоксидті шайырдың механикалық қасиеттеріне айтарлықтай әсер еткен жоқ. Бұл механикалық қасиеттердің жақсаруы қолданылатын қатайтқыштың түріне, сондай-ақ эпоксидті шайырмен араласқан қоспалардың түрлері мен мөлшеріне байланысты.

Түйін сөздер: Эпоксидті шайыр, қатайтқыш, механикалық, коррозия, қоспалар.

Авторлар туралы ақпарат:

El-Sayed Negim — *Материалтану және жасыл технологиялар мектебі, Қазақстан-Британ техникалық университеті, 050000, Төле би көшесі, 59, Алматы,Қазақстан. Email: elashmawi5@yahoo.com*

Бекбаева Ляззат Кайратовна — *Ашық түрдегі нанотехнологиялық зертхана, әл-Фараби атындағы Қаз¥У 71, әл-Фараби даңғылы, 050040, Алматы, Қазақстан. Email: lyazzat_bk2019@mail.ru*

Пузикова Дарья Сергеевна — *Д.В. Сокольский атындағы жанармай, катализ және электрохимия институты, Қазақстан-Британ техникалық университеті, 050010, Кунаев көшесі, 142, Алматы, Қазақстан. Email: d.puzikova@ifce.kz*

Жұрынов Мұрат Жұрынұлы — *Д.В. Сокольский атындағы жанармай, катализ және электрохимия институты, Қазақстан-Британ техникалық университеті, 050010, Кунаев көшесі, 142, Алматы, Қазақстан. Email: mur.zhurinov@mail.ru*

Нефедов Александр Николаевич — *Д.В. Сокольский атындағы жанармай, катализ және электрохимия институты, Қазақстан-Британ техникалық университеті, 050010, Кунаев көшесі, 142, Алматы, Қазақстан. Email: a.nefedov@ifce.kz*

Хусурова Гулинур Марсовна — *Д.В. Сокольский атындағы жанармай, катализ және электрохимия институты, Қазақстан-Британ техникалық университеті, 050010, Кунаев көшесі, 142, Алматы, Қазақстан. Email: gulinur_k@bk.ru*

Шадин Нұргүл Адырбекқызы — *Химия кафедрасы, жаратылыстану және география институты, Абай атындағы Қазақ Ұлттық педагогикалық университеті, Қазыбек би көшесі, Алматы, Қазақстан. Email: nugen_87@mail.ru*

Jamal Khatib — *Бейрут араб университетінің инженерлік факультетінің азаматтық және қоршаған ортаны қорғау кафедрасы, П.О. Жәшік: 11 5020 Бейрут, Ливан. Email: j.khatib@bau.edu.lb*

Разработка эпоксидной смолы для антикоррозионных покрытий

[1*]Negim E.-S., [2] Бекбаева Л.К., [3]Пузикова Д.С., [3]Журинов М.Ж., [3]Нефедов А.Н., [3]Хусурова Г.М., [4]Шадин Н.А., [5]Jamal Khatib

[1] Факультет материаловедения и зеленых технологий, Казахстанско-Британский технический университет, Алматы, Казахстан
[2]Открытая нанотехнологическая лаборатория КазНУ им. Аль-Фараби, Алматы, Казахстан
[3]АО Институт топлива, катализа и электрохимии им. Д.В. Сокольского, Казахстанско-Британский технический университет, Алматы, Казахстан
[4]Институт естественных наук и географии, Казахский национальный педагогический университет имени Абая, Алматы, Казахстан
[5]Кафедра гражданской защиты и защиты окружающей среды, Бейрутско-арабский университет, Бейрут, Ливан

Поступила: *23 января 2025*
Рецензирование: *4 марта 2025*
Принята в печать: *9 апреля 2025*

Аннотация
В этом исследовании высокомолекулярная эпоксидная смола (ELM-NG 900Z) на основе диглицидилового эфира бисфенола А была отверждена с различными типами отвердителей для изучения их влияния на физические и механические свойства эпоксидной смолы. Были использованы отвердители: G-5022X70 (140-170 мг KOH/г), G-A0533 (310-350 мг KOH/г) и G-0930 (280-320 мг KOH/г). Результаты показали, что отвердитель G-A0533 обеспечил наилучшие механические свойства эпоксидной смолы по сравнению с другими отвердителями. Кроме того, различные добавки, включая кремнеземную пыль, тальк, сульфат бария, оксид железа и пигменты, были смешаны с эпоксидной смолой в присутствии отвердителя G-A0533 для улучшения ее механических свойств. Было отмечено, что добавление 3% микрокремнезема, 10% оксида железа и 3% неорганических пигментов улучшило механические свойства, в то время как добавление 5% талька ухудшило большинство механических свойств и увеличило только твердость. Включение сульфата бария в эпоксидную смолу улучшило адгезию и прочность на изгиб, но снизило прочность на растяжение и твердость. Включение органического пигмента не оказало существенного влияния на механические свойства эпоксидной смолы. Это улучшение механических свойств объясняется типом используемого отвердителя, а также типами и количеством добавок, смешанных с эпоксидной смолой.

Ключевые слова: Эпоксидная смола, отвердитель, механический, коррозия, добавки.

Сведения об авторах:

El-Sayed Negim *Факультет материаловедения и зеленых технологий, Казахстанско-Британский технический университет, 050000, Толе би, 59, Алматы, Казахстан. Email: elashmawi5@yahoo.com*

Ляззат Бекбаева *Открытая нанотехнологическая лаборатория, КазНУ им. Аль-Фараби 71, проспект Аль-Фараби, 050040, Алматы, Казахстан. Email: lyazzat_bk2019@mail.ru*

Дарья Пузикова *Институт топлива, катализа и электрохимии им. Д.В. Сокольского, Казахстанско-Британский технический университет, 050010, ул. Кунаева, 142, Алматы, Казахстан. Email: d.puzikova@ifce.kz*

Журинов Мурат Журинович *Институт топлива, катализа и электрохимии им. Д.В. Сокольского, Казахстанско-Британский технический университет. 050010, ул. Кунаева, 142, Алматы, Казахстан. Email:* mur.zhurinov@mail.ru

Нефедов Александр Николаевич *Институт топлива, катализа и электрохимии им. Д.В. Сокольского, Казахстанско-Британский технический университет. 050010, ул. Кунаева, 142, Алматы, Казахстан. Email: a.nefedov@ifce.kz*

Хусурова Гулинур Марсовна *Институт топлива, катализа и электрохимии им. Д.В. Сокольского, Казахстанско-Британский технический университет, 050010, ул. Кунаева, 142, Алматы, Казахстан. Email: gulinur_k@bk.ru*

Шадин Нургуль Адырбековна *Кафедра химии, Институт естественных наук и географии, Казахский национальный педагогический университет имени Абая, улица Казыбек би, Алматы, Казахстан. Email: nugen_87@mail.ru*

Jamal Khatib *Кафедра гражданской защиты и охраны окружающей среды инженерного факультета Бейрутско-арабского университета, почтовый ящик: 11 5020 Бейрут, Ливан. Email: j.khatib@bau.edu.lb*

References

[1] Bhavith K, Prashanth Pai M, Sudheer M, Ramachandra CG, Maruthi Prashanth BH, Kiran Kumar B. The Effect of Metal Filler on the Mechanical Performance of Epoxy Resin Composites. Engineering Proceedings. 2023; 59(1):200. https://doi.org/10.18517/ijaseit.7.4.2480

[2] Najat J S, Adnan A A, Manal A T, Mariam E. A study on mechanical properties of epoxy resin cured at constant curing time and temperature with different hardeners. Engg. & Tech. Journal. 2011; 29:1804. https://doi.org/10.30684/etj.29.9.15

[3] Sudheer M, Subbaya KM, Jawali D, Bhat T. Mechanical Properties of Potasium Titanate Whisker Reinforced Epoxy Resin Composites. J. Miner. Mater. Charact. Eng. 2012; 11:193. https://doi.org/10.4236/jmmce.2012.112016

[4] Dheeraj KG, Gujjala R, Syam PP, Ojha S. Enhanced mechanical properties of glass fibre epoxy composites by 2D exfoliated graphene oxide filler. Ceramics International. 2021; 47(24):34860-34868. https://doi.org/10.1016/j.ceramint.2021.09.027 .

[5] Kowshik S, Shettar M, Rangaswamy N, Chate G, Somdee P. Effect of nanoclay on mechanical, flammability, and water absorption properties of glass fiber-epoxy composite. Cogent Eng. 2022; 9:2069070. https://10.1080/23311916.2022.2069070

[6] Ramkumar Y, Mayank S, Deepika S, Seul-Yi L, Soo-Jin P. The role of fillers to enhance the mechanical, thermal, and wear characteristics of polymer composite materials: A review. Composites Part A: Applied Science and Manufacturing. 2023; 175:107775. https://10.1016/j.compositesa.2023.107775

[7] Baroncini E, Kumar S, Palmese G, and Stanzione J. Recent Advances in Bio-based Epoxy Resins and Bio-based Epoxy Curing Agents. Journal of Applied Polymer Science. 2016; 44103:1. https://doi.org/10.1002/app.44103

[8] Allahverdi A, Ehsani M, Janpour H, Ahmadi S. The effect of nanosilica on mechanical, thermal and morphological properties of epoxy coating. Progress in Organic Coatings. 2012; 75(4):543-548. https://doi.org/10.1016/j.porgcoat.2012.05.013

[9] Avilés M, Perugachi R. Rigail-Cedeño A. Bio-Based Silica Reinforced Aliphatic Bio-Epoxy Composites. Global Partnerships for Development and Engineering Education. Proceedings of the 15th LACCEI International Multi-Conference for Engineering, Education and Technology. 2017; 1. http://dx.doi.org/10.18687/LACCEI2017.1.1.299

[10] Jin F-L, Park S-J. Thermal properties of epoxy resin/filler hybrid composites. Polymer Degradation and Stability. 2012; 97(11):2148-2153. https://doi.org/10.1016/j.polymdegradstab.2012.08.015

[11] Negim E, Shalash M, Al Azzam KM, Sagatbekovna MZ, Kairatovna BA, Konstantinovich AT, Adlikhanovna NA, Ermekovna KA, Ravindran B. Synthesis, Characterization, and Application of Polyurethane-Acrylic Hybrids as Anticorrosion Coatings. International Journal of Technology. 2024;15(6):009-2023. https://doi.org/10.14716/ijtech.v15i6.7044

[12] Rigail-Cedeño A, Schmidt DF. Bio-based epoxy clay nanocomposites. AIP Conference Proceedings. 2017; 1914:030023. https://doi.org/10.1063/1.5016710

[13] Sienkiewicz A, Czub P. Modification of Epoxy Compositions by the Application of Various Fillers of Natural Origin. Materials. 2023; 16(8):3149. https://doi.org/10.3390/ma16083149

[14] Abd El-Ghaffar MA, Abdelwahab NA, Amany M Fekry, Sanad MA, Sabaa MW, Soliman SMA. Polyester-epoxy resin/conducting polymer/barium sulfate hybrid composite as a smart eco-friendly anti-corrosive powder coating. Progress in Organic Coatings. 2020; 144:105664. https://doi.org/10.1016/j.porgcoat.2020.105664

[15] Neha KR, Sharif A. Synergistic effect of nanosize and irradiation on epoxy/conducting poly(o-phenyldiamine) nanospheres composite coatings: Synthesis, characterization and corrosion protective performance. Materials Chemistry and Physics. 2018; 204: 282-293. https://doi.org/10.1016/j.matchemphys.2017.10.044

[16] Bekbayeva L, Negim E-S, Zhanibekov R, Sharipov R, Maldybayev G, Puzikova D, Kenzin N, Maridan A. Epoxy coatings for anticorrosion applications: a review. Kompleksnoe Ispolzovanie Mineralnogo Syra = Complex Use of Mineral Resources. 2026; 337(2): 35. https://doi.org/10.31643/2026/6445.15

[17] Sally C. The Munsell Color System: A scientific compromise from the world of art. Studies in History and Philosophy of Science Part A. 2014; 47:26-41. https://doi.org/10.1016/j.shpsa.2014.03.004

[18] Gatis V, Irina A, Yukako H, Ilvars I. Colour Extraction and Analysis Solution for Design of Cross-cultural Websites. Procedia Computer Science. 2015; 77:215-220. https://doi.org/10.1016/j.procs.2015.12.374

[19] Dong WK, Ki B N, Sung CH. Influence of tungsten on the activity of a Mn/Ce/W/Ti catalyst for the selective catalytic reduction of NO with NH_3 at low temperatures. Applied Catalysis A: General. 2015; 497:160-166. https://doi.org/10.1016/j.apcata.2015.01.013

[20] Negim SM, Bahruddin S, Mahyuddin R, & Idiris MS. Effects of TDI and FA-703 on physico-mechanical properties of polyurethane dispersion. Journal of Applied Polymer Science. 2011; 121(1):8-13. https://doi.org/10.1002/app.33569

[21] ISO 12058-1. International standard: Determination of viscosity using a falling-ball viscometer. 2018. ISO 12058-1:2018(E)

[22] American Society for Testing and Materials (ASTM). ASTM D3359. Standard Test Methods for Rating Adhesion by Tap Test – 2001.

[23] American Society for Testing and Materials (ASTM). ASTM D2794. Standard Test Methods for Resistance of Organic Coatings to The Effects of Rapid Deformation (Impact) – 2019.

[24] American Society for Testing and Materials (ASTM). ASTM D1652. Standard Test Method for Epoxy Content of Epoxy Resins – 2019.

[25] En, B., 1542. Products and systems for the protection and repair of concrete structures. Test methods Measurement of bond strength by pull-off – 1999.

[26] Syrmanova K, Negim E**,** Kaldybekoekova J, Tuleuov AM. Epoxylitane compositions modification with using thermoplastic polyurethane. Oriental Journal of Chemistry. 2016; 32(1). http://dx.doi.org/10.13005/ojc/320101

[27] Sabergaliyev M, Yeligbayeva G, Khassanov D, Muradova S, Orazalin Z, Ainakulova D, Sharipov R, & Negim E-S. Modified bitumen-polymer mastic to protect metal coatings from corrosion. Kompleksnoe Ispolzovanie Mineralnogo Syra = Complex Use of Mineral Resources. 2024; 331(4); 12. https://doi.org/10.31643/2024/6445.35

Crossref
DOI: 10.31643/2026/6445.25
Engineering and Technology

Study of Steam Condensation on Vertical Finned Tubes

[1]Toshov J.B., [1]Eshkuvatov L.M., [2]Smagulova K.K., [2]Zheldikbayeva A.T., [2*]Rabatuly M., [1]Tashbayev N.N., [3]Madaminova G.

[1]Islam Karim Tashkent State Technical University, Tashkent, Uzbekistan
[2]Abylkas Saginov Karaganda Technical University, Karaganda, Kazakhstan
[3]Fergana State University, Fergana, Uzbekistan

** Corresponding author email: mukhammedrakhym@mail.ru*

Received: *January 29, 2025*
Peer-reviewed: *January 30, 2025*
Accepted: *April 10, 2025*

ABSTRACT

The article is devoted to the methodology of conducting and processing the results of an experimental study of the process of condensation of water vapour on vertical pipes with specially profiled fins of a heat exchanger. Based on the analysis of heat transfer during laminar condensation of water vapour in the form of a layer of flowing liquid both inside and on the outer surface of vertical pipes with a stationary steam flow, a laboratory installation was developed on which experimental studies were carried out. One of the ways to intensify heat transfer is to optimize the geometry of the heat exchange surface on the condensation side, which reduces the thermal resistance of the wall layers of the resulting condensate. This method is based on increasing the heat exchange area by using specially shaped fins on the surface of the heat exchanger tubes. As a result, an important scientific problem is being solved – disruption of the continuous flow of laminar condensate, which contributes to the direct contact of steam with the cooled surface of the pipe and increases heat transfer. The article describes the methodology of conducting experiments, describes the methods of processing the results obtained, as well as provides calculated data and graphical dependencies illustrating the experimental results.

Keywords: heat exchangers, heat transfer, condensation, condensate, fins, steam.

Information about authors:

Toshov Javokhir Buriewicz — *Doctor of Technical Sciences, Professor of Islam Karim Tashkent State Technical University, 100095 Republic of Uzbekistan, Tashkent, Almazar district, Universitetskaya Street 2. E-mail: j.toshov@tdtu.uz; ORCID ID: https://orcid.org/0000-0003-4278-1557*

Eshkuvatov Lutfulla Muradullayevich — *Doctor of Philosophy, associate professor, Head of the Department, Tashkent State Technical University named after Islam Karimov, 100095, Republic of Uzbekistan, Tashkent, Olmazor district, University str. 2. E-mail: l.eshkuvatov@tdtu.uz; ORCID ID: https://orcid.org/0000-0001-7442-5018*

Smagulova Karshiga Kanatovna — *Ph.D., Acting Associate Professor of the Department of Automation of Manufacturing Processes of Abylkas Saginov Karaganda Technical University, 100027, The Republic of Kazakhstan, Karaganda, Ave. Nursultan Nazarbayev, 56. E-mail: smagulovakk@mail.ru; ORCID ID: https://orcid.org/0000-0001-6834-8490*

Zheldikbayeva Aisaule Takenovna — *PhD student of the department of the Department of Automation of Manufacturing Processes of Abylkas Saginov Karaganda Technical University, 100027, The Republic of Kazakhstan, Karaganda, Ave. Nursultan Nazarbayev, 56. E-mail: aisaule89@mail.ru; ORCID ID: https://orcid.org/0009-0005-1325-5576*

Rabatuly Mukhammedrakhym — *Ph.D., Acting Associate Professor of the Department of Development of Mineral Deposits of Abylkas Saginov Karaganda Technical University, 100027, The Republic of Kazakhstan, Karaganda, Ave. Nursultan Nazarbayev, 56. E-mail: mukhammedrakhym@mail.ru; ORCID ID: https://orcid.org/0000-0002-7558-128X*

Tashbayev Nazim Tulayevich — *Candidate of Technical Sciences, Associate Professor of the Department, Tashkent State Technical University named after Islam Karimov, 100095, Republic of Uzbekistan, Tashkent, Olmazor district, University str. 2. E-mail: n.tashbayev@tdtu.uz; ORCID ID: https://orcid.org/0000-0003-0121-4660*

Gulsora Madaminova — *Senior lecturer of the Department, Ferghana State University, 150100, Republic of Uzbekistan, Fergana region, Fergana, st. Murabbiylar, 19. E-mail: gulsora.madaminova@fdu.uz; ORCID ID: https://orcid.org/0009-0005-4026-0119*

Introduction

One of the key challenges in heat transfer intensification is the simultaneous increase in thermal power, which contributes to a reduction in both the size and weight of heat exchangers. Numerous studies have proposed various methods to enhance heat transfer efficiency during the condensation of heating steam in tubular devices.

During the condensation of heating steam inside a vertical tube, a liquid condensate film forms, progressively increasing in thickness as it moves downward. This alters the thermal resistance, consequently affecting the overall heat transfer process [[1], [2], [3]].

Research on the condensation performance of pure water outside integral-fin and pin-fin tubes has shown that, under identical conditions, pin-fin tubes retain less condensate than integral-fin tubes, leading to improved heat transfer efficiency [[4], [5], [6]].

Heat exchangers are fundamental components of process systems, with tubular heat exchangers being among the most commonly used in industrial applications. The most efficient designs leverage phase transitions, such as evaporation and condensation, to optimize heat transfer. The thermal design of tubular heat exchangers, particularly those operating on condensation principles, requires a thorough understanding of phase transition processes within tubes. This study focuses on the experimental analysis of steam condensation in both smooth and specially profiled small-diameter vertical tubes [7].

The development and optimization of high-performance heat transfer surfaces play a crucial role in improving heat exchange equipment, particularly heat exchangers with vertical tubes. Heat transfer characteristics during the condensation of water vapour on vertical tube surfaces are of particular significance [[8], [9]].

In studies of steam condensation on vertical tubes, the primary research focus is on film flow dynamics. Single vertical tubes with specially profiled fins have been developed to enhance heat transfer efficiency. Experimental investigations were conducted using the setup described in [[10], [11], [12], [13]]. To ensure the reliability of results, tests were performed on both finned and smooth tubes. Before experimentation, the setup was calibrated, measuring instruments were tested, and data processing methodologies were verified. Comparing condensation performance between smooth tubes and tubes with specially profiled fins helps validate the experimental approach while minimizing external influences on the results.

For each experiment, the steam and cooling water parameters were maintained at consistent levels for both smooth and finned tubes, ensuring accurate comparisons of their heat transfer performance.

The experimental part

In the conducted research, the investigated parameters varied within the following ranges: water mass flow rate G_{water} = 0,01133 to 0,025 kg/s, steam mass flow rate D_{steam} = 0,0000833 ÷ 0,000115 kg/s, and pressure P = 0,05 to 0,13 MPa. The velocity of the cooling liquid was in the range of W_{water} = 0,14 to 0,32 m/s, while the Reynolds number for cooling water varied from Re_{water} = 1500 to 3300. The steam velocity was measured within W_{steam} = 0,07 to 0,09 m/s, with the corresponding Reynolds number ranging between Re_{steam} = 125 and 170, The steam temperature was recorded between t_{steam} = 94 and 105 ^{0}C.

The geometric parameters of an edge with an improved surface (EIS) are assumed in Table 1 [14].

Boundary conditions were established for different tubes used in the experiments. The velocity of steam entering the experimental flask was within the range of Re_{steam} = 0,07 to 0,09 m/s corresponding to Reynolds numbers between W_{steam} = 125 and 170. The power output of the steam generator was increased to Q = 300 to 630 W.

When a heat carrier undergoes a phase transition, such as steam condensation due to cooling with water, the heat transfer process is described by the equation:

$$Q_v = G_v(h_v - h_c) = G_w c_w(t_{out} - t_{in}) \quad (1)$$

where G_v, G_w - mass flow rates of steam and cooling water, kg/sec; h_v, h_c - enthalpy of steam entering the heat exchanger and condensate exiting, kJ/kg; c_w - specific heat capacity of cooling water, $kJ/(kg^0C)$; t_{in}, t_{out} - temperatures of cooling water at the inlet and outlet of the heat exchanger, ^0C.

To determine the heat balance, the temperatures of the cooling water entering and exiting the heat exchanger were measured using a DS18B20 temperature sensor. The heat balance equation for water is given by:

$$Q_w = G_w c_w(t_{out} - t_{in}) \quad (2)$$

The heat balance accuracy between water and steam was assessed using the discrepancy formula [15]:

$$\bar{\delta} = \frac{2|Q_v - Q_w|}{Q_v + Q_w} \cdot 100\ \%$$

Table 1 - Geometric Parameters of a Vertical Tube with an Enhanced Surface (EIS)

Geometric parameters	**A**	**B**	**C**	**D**	**E**	**F**	**G**
The outer diameter of the EIS d_{EIS}, mm	18 – 22	18 – 22	18 – 22	18 – 22	18 – 22	18 – 22	18 – 22
Diameter of smooth tube d_{out}/d_{in}, mm	12/10	12/10	12/10	12/10	12/10	12/10	12/10
The radius of curvature of the edge end r, mm	3 – 4	3 – 4	3 – 4	3 – 4	3 – 4	3 – 4	3 – 4
The angle between the smooth tube and the fin φ, degree	30 - 35	30 - 35	30 - 35	30 - 35	30 - 35	30 - 35	30 - 35
Distance between fins S_2, mm	150	100	50	43	25	20	16.6
Fin sheet thickness δ, мм	0.001	0,001	0.001	0,001	0.001	0.001	0.001
Tube Length, ℓ, mm	300	300	300	300	300	300	300
Forming height of the EIS, a, mm	5-7	5-7	5-7	5-7	5-7	5-7	5-7
EIS surface area, $f_{EIS} = 10^{-4}$, m^2	4.396	8.792	21.98	28.4	48.4	61.54	79.9
Distance between the base of the generatrix and the smooth tube, b, mm.	3 - 5	3 - 5	3 - 5	3 - 5	3 - 5	3 - 5	3 - 5
Smooth tube surface area, $f_0 = 10^{-4}$, $м^2$	1.13	1.13	1.13	1.13	1.13	1.13	1.13
The total surface area of the vertical tube with EIS, $f = f_{EIS} + f_0$, m^2	0.0117	0.0121	0.0139	0.015	0.0164	0.0181	0.02
Finning ratio f / f_0	1.04	1.07	1.23	1.34	1.45	1.6	1.76

The measurement error was considered acceptable if the heat balance discrepancy did not exceed 5%.

The heat transfer coefficient for condensation, α_v, measured in [Wt / ($m^2 \cdot {}^0C$] can be predicted theoretically or experimentally. The classical theoretical model for condensation heat transfer was proposed [16], expressed as:

$$\alpha_v = 0.9428 \cdot \left[\frac{g \cdot \rho_c \cdot r \cdot \lambda_c^3}{v_c \cdot (t_v - t_{wal}) h}\right]^{0.25} \quad (3)$$

However, analysis of this formula equation (4) indicates that it applies primarily to stationary steam. The presence of vapour flow induces wave formation on the condensate surface, which enhances heat transfer by approximately 20.6%. The authors [17] proposed the following modified equation to account for this effect:

$$\alpha_v = 1.137 \cdot \left[\frac{g \cdot \rho_c \cdot r \cdot \lambda_c^3}{v_c \cdot (t_v - t_{wal}) h}\right]^{0.25} \quad (4)$$

Further refinements led to the development of a theoretical equation for the heat transfer coefficient, incorporating wave effects. Hobler's equation [17] (Equation 5) is widely applied in engineering calculations and is valid for various liquids under pressure conditions $0.07<p_v$ [MPa]<17 and specific heat flux values $1.0< q_v$ [kWt / m^2] < 1000.

$$б_v = 0.00252 \cdot \left(\frac{c_v \cdot r}{c_c - c_v} \cdot \frac{c_c}{д_c}\right)^{0.33} \cdot \frac{л_c^{0.8} \cdot q_v^{0.7}}{м_c^{0.5} \cdot c_c^{0.167} \cdot t_v^{0.37}} \cdot p_v^{\frac{10}{t_v}} \quad (5)$$

The heat transfer coefficient function follows the relation $= C \cdot q^n$, where the specific heat flux q_v, [kWt / m^2] is considered. The constant C depends on the surface type and liquid properties, often taken as $C = 1.537$.

For vertical tubes with fine fins, the average heat transfer coefficient during steam condensation is determined using the following equation [[18], [19]].

$$Nu_v = 0{,}34 \frac{a^{0,15} \cdot h^{1,1} \cdot \theta^{-0,667}}{H^{0,25} \cdot S \cdot \cos\varphi} \cdot We^{0,21} \cdot (Ga \cdot Pr \cdot K)^{0,37} \quad 6)$$

where $\bar{\theta} = 0.7n^{-0.4}We^{-0.1}$ at $\beta < 1, nWe^{0.25} \geq 1$; $\bar{\theta} = 0.7\beta^{-0.07}(nWe^{0.25})^m$ at $\beta \geq$

$1, nWe^{0.25} \geq 1$; $m = -0.4\beta^{-0.15}$; $\bar{\theta} = 1 - 0.23\beta^{-0.36}(nWe^{0.25})^{1.2}$ at $\beta \geq 1, nWe^{0.25} < 1$;

$$n = \left[\frac{\rho'^2 \cdot g \cdot r \cdot \lambda'^3 \cdot h^7 \cdot \cos\varphi}{4 \cdot \mu' \cdot b^4 \cdot \lambda_{wal}^4 \Delta t_0}\right]^{0,25};$$

$We = \frac{\sigma \cdot \cos\varphi}{g \cdot \rho' \cdot b \cdot h \cdot (1 + tan\,\varphi)}$; $\beta = \frac{h \cdot tan\,\varphi}{b}$; $Ga = \frac{g d_{eq}^3}{\nu'^2}$; $K = \frac{r}{c_v \Delta t_0}$;

where a - half the width of the intercostal groove, *m*; b - half the thickness of the fin at the end, *m*; h - fin height, *m*; H - tube length, *m*; *s* - fin spacing, *m*; φ - acute angle between the fin's lateral surface and axial plane; ρ' - density along the saturation line, *kg/m*^{3}; ρ'' - density of dry saturated steam, *kg/m*^{3}; λ_{metal} - metal thermal conductivity, *Wt/(m·*^{0}*C)*; λ - thermal conductivity along the saturation line, *Wt/(m·*^{0}*C)*; *r* - heat of vaporization, *J/kg*; We - Weber number; Δt_0 - temperature difference at the fin base, ^0C; σ - surface tension, N/m; K - phase transition criterion; μ' - dynamic viscosity at the saturation line, *Pa·s*; ν' - kinematic viscosity at the saturation line, m^2/s; Ga - Galileo number; c_v - specific heat capacity of steam, *J/(kg·*^{0}*C)*; Pr - Prandtl number.

Subscripts: v - vapour; c - condensate; w - water; *eq* – equivalent; $aver$ – average; in - inlet; out - outlet; wal - tube wall.

In all conducted experiments, a turbulent flow of cooling water was maintained ($Re_в > 10^4$). Therefore, the heat transfer coefficient on the water side was determined using the following equation [20]:

$$\alpha_w = 0.021 Re_w^{0.8} Pr_w^{0.43} \left(\frac{Pr_w}{Pr_{wal}}\right)^{0.25} \frac{\lambda_w}{d_{in}}. \quad (7)$$

The temperature difference between the inlet and outlet cooling water remained within10 ^{0}C. Consequently, the logarithmic mean temperature difference (LMTD) between the heat exchange media was calculated using the formula:

$$\Delta\bar{t} = \frac{(t_v - t_{out}) - (t_c - t_{in})}{ln\left(\frac{t_v - t_{out}}{t_c - t_{in}}\right)} \quad (8)$$

For the inner tube, the overall heat transfer coefficient was determined based on heat transfer through a flat wall, incorporating the effect of finning in specially profiled finned tubes:

$$k = \frac{1}{\frac{1}{\alpha_v \frac{f_{fins}}{f_{smooth}}} + \frac{\delta}{\lambda_{metal}} + \frac{1}{\alpha_w} + R_{ther}} \quad (9)$$

where $\frac{f_{fins}}{f_{smooth}}$- is the finning coefficient, accounting for the increased heat exchange area; f_{fins} - represents the finned area, while f_{smooth} corresponds to a smooth tube surface; R_{ther} - denotes thermal resistance due to fouling, expressed in, *(m*^{2} *·K)/Wt*.

Discussion of the results

Generalized results from experimental studies are presented in Figures 1 and 2. The empirical equation describing the relationship between thermal resistance R_{ther} and film thickness (δ) is given as:

$$R_{ther} = 14{,}7409 \ln(\delta) + 49{,}9661 \quad (10)$$

Additionally, the heat transfer coefficient α dependence on film thickness was determined empirically as:

$$\alpha = 731{,}1334\delta^{-0{,}95936} \quad (11)$$

The relative errors associated with equations (10) and (11) were 2.9% and 0.14%, respectively. The Fisher criterion was used to validate equation (10), yielding Fr = 5.3033 with a reliability probability of P = 0.95, while the tabulated value was Ft = 10.13. Similarly, equation (11) produced Fp= 5.1884 confirming its adequacy against the same tabulated value.

Experiments were conducted on a 300 mm-long test tube, where fin spacing (S_2) was optimized using the Nusselt criterion. The study revealed that maximum relative heat transfer coefficient values$\alpha/\alpha_0 = 1{,}6 \div 1{,}8$ corresponded to optimal fin spacing $S_2 = 50 \div 35$ mm. Alternatively, this range aligns with finning coefficient values of $f/f_0 = 1{,}23 \div 1{,}35$ as shown in Figure 2.

The finning coefficient (f/f_0) represents the ratio of the total finned surface area (f) to that of a smooth tube (f_0). The dependency of the relative heat transfer coefficient on the finning coefficient was determined through the least squares method, yielding the empirical equation:

$$\alpha/\alpha_0 = 8{,}1029(f/f_0)^3 - 37{,}42(f/f_0)^2 + 56{,}194(f/f_0) - 25{,}914 \quad (12)$$

A comparative analysis of experimental data and mathematical modelling results demonstrated their consistency. Adequacy was verified using the Fisher criterion, with an average relative error ranging between 2.03% and 3.8%.

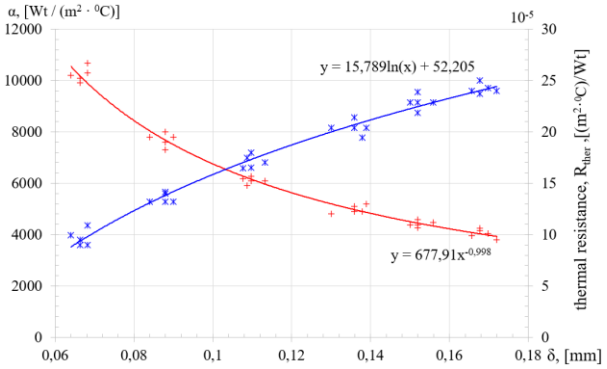

Figure 1 - Dependence of α heat transfer coefficient and R_{ther} thermal resistance on film thickness

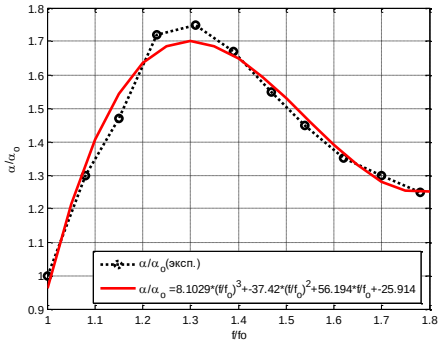

Figure 2 - Dependence of the relative change in the heat transfer coefficient on the finning coefficient

Conclusion

Based on the experimental results, it was determined that the average heat transfer coefficient for smooth tubes is 7258 $Wt/(m^2 \cdot ℃)$, while for vertical tubes with an enhanced finned surface, it reaches 8911 $Wt/(m^2 \cdot ℃)$. This indicates that the heat transfer efficiency of the improved surface is 23% higher compared to a smooth tube. Additionally, the condensate yield of a relatively smooth tube is 57% greater, and in comparison to surfaces shaped as truncated cones proposed by Mikheev and Mikheeva, it is 27% higher.

For vertical tubes, both theoretical and experimental data were used to determine and validate the optimal geometric parameters that enhance the efficiency of installations with finned surfaces. These include:

- The outer diameter of the rib relative to the perpendicular to the surface: (d_{EIS} =18÷20 mm);
- The rib inclination angle: (φ = 30 ÷ 35°);
- The finning coefficient: (ƒ / ƒ₀ =1,23÷1,35);
- The optimal vertical rib spacing: (S_2 = 35 ÷ 50 mm).

Conflict of interest. On behalf of all the authors, the correspondent author declares that there is no conflict of interest.

CRediT author statement: **J. Toshov**, **M. Rabatuly**: Conceptualization, Methodology, Software; **K. Smagulova, A. Zheldikbayeva**: Data curation, Writing-Original draft preparation; L. **Eshkuvatov**, **N. Tashbayev**: Visualization, Investigation; **G. Madaminova**: Software, Validation.

Cite this article as: Toshov JB, Eshkuvatov LM, Smagulova KK, Zheldikbayeva AT, Rabatuly M, Tashbayev NN, Madaminova G. Study of Steam Condensation on Vertical Finned Tubes. Kompleksnoe Ispolzovanie Mineralnogo Syra = Complex Use of Mineral Resources. 2026; 338(3):21-28. https://doi.org/10.31643/2026/6445.25

Қатайту қабырғалары бар тік түтіктердегі бу конденсациясын зерттеу

[1]Тошов Ж.Б., [1]Эшкуватов Л.М.,[2]Смагулова К.К., [2]Желдикбаева А.Т., [2*]Рабатұлы М., [1]Ташбаев Н.Н., [3]Мадаминова Г.

[1]Ислам Кәрім атындағы Ташкент Мемлекеттік Техникалық Университеті, Ташкент, Өзбекстан
[2]Ә. Сағынов атындағы Қарағанды техникалық университеті, Қарағанды, Қазақстан
[3]Ферғана Мемлекеттік Университеті, Ферғана, Өзбекстан

Мақала келді: *29 қаңтар 2025*
Сараптамадан өтті: *30 қаңтар 2025*
Қабылданды: *10 сәуір 2025*

ТҮЙІНДЕМЕ

Мақала жылу алмастырғыштың арнайы профильді қабырғалары бар тік құбырлардағы су буының конденсация процесіне эксперименттік зерттеу жүргізуге және оның нәтижелерін өңдеу әдістемесіне арналған. Стационарлық бу ағынында тік құбырлардың ішінде де, сыртқы бетінде де ағып жатқан сұйықтық қабаты түріндегі су буының ламинарлы конденсациясындағы жылу алмасуды талдау негізінде зертханалық қондырғы жасалды, онда эксперименттік зерттеулер жүргізілді. Жылу алмасуды күшейту әдістерінің бірі конденсация жағындағы жылу алмасу бетінің геометриясын оңтайландыру болып табылады, бұл алынған конденсаттың қабырға қабаттарының жылу кедергісін азайтуға

мүмкіндік береді. Бұл әдіс жылу алмастырғыш құбырларының бетіне арнайы профильді жиектерді қолдану арқылы жылу алмасу аймағын ұлғайтуға негізделген. Нәтижесінде маңызды ғылыми міндет шешіледі – ламинарлы ағып жатқан конденсаттың үздіксіз ағыны бұзылады, бұл будың құбырдың салқындатылған бетімен тікелей жанасуына және жылу беруді арттыруға ықпал етеді. Мақалада эксперименттерді жүргізу әдістемесі берілген, алынған нәтижелерді өңдеу әдістері сипатталған, сонымен қатар эксперименттік нәтижелерді бейнелейтін есептелген мәліметтер мен графикалық тәуелділіктер келтірілген.

Түйін сөздер: жылу алмастырғыштар, жылу беру, конденсация, конденсат, қатайту қабырғалар, бу.

Авторлар туралы ақпарат:

Тошов Жавохир Буриевич
Техника ғылымдарының докторы, Ислам Каримов атындағы Ташкент мемлекеттік техникалық университетінің профессоры, 100095, Алмазар ауданы Университетская көшесі 2, Ташкент, Өзбекстан. E-mail: j.toshov@tdtu.uz; ORCID ID: https://orcid.org/0000-0003-4278-1557

Эшкуватов Лутфулла Мурадуллаевич
PhD докторы, доцент, Ислам Каримов атындағы Ташкент мемлекеттік техникалық университетінің кафедра меңгерушісі, 100095, Алмазар ауданы, Университетская көшесі 2, Ташкент, Өзбекстан. E-mail: l.eshkuvatov@tdtu.uz; ORCID ID: https://orcid.org/0000-0001-7442-5018

Смагулова Каршыга Канатовна
PhD докторы, Әбілқас Сағынов атындағы Қарағанды техникалық университетінің өндірістік процестерді автоматтандыру кафедрасының доценті, 100027, Нұрсұлтан Назарбаев даңғ. 56, Қарағанды, Қазақстан. E-mail: smagulovakk@mail.ru; ORCID ID: https://orcid.org/0000-0001-6834-8490

Желдикбаева Айсауле Такеновна
Әбілқас Сағынов атындағы Қарағанды техникалық университетінің өндірістік процестерді автоматтандыру кафедрасының PhD докторанты, 100027, Нұрсұлтан Назарбаев даңғ. 56, Қарағанды, Қазақстан. E-mail: aisaule89@mail.ru; ORCID ID: https://orcid.org/0009-0005-1325-5576

Рабатұлы Мұхаммедрахым
PhD докторы, Әбілқас Сағынов атындағы Қарағанды техникалық университетінің пайдалы қазбалар кенорындарын өндіру кафедрасы доцентінің м.а., 100027, Нұрсұлтан Назарбаев даңғ. 56, Қарағанды, Қазақстан. E-mail: mukhammedrakhym@mail.ru; ORCID ID: https://orcid.org/0000-0002-7558-128X

Ташбаев Назим Тулаевич
Техника ғылымдарының кандидаты, Ислам Каримов атындағы Ташкент мемлекеттік техникалық университетінің доценті, 100095, Алмазор ауданы, Университетская көшесі 2, Ташкент, Өзбекстан. E-mail: n.tashbayev@tdtu.uz; ORCID ID: https://orcid.org/0000-0003-0121-4660

Гульсора Мадаминова
Ферғана мемлекеттік университетінің аға оқытушысы, 150100, Мураббийлар көшесі, 19, Ферғана, Өзбекстан. E-mail: gulsora.madaminova@fdu.uz; ORCID ID: https://orcid.org/0009-0005-4026-0119

Изучение конденсации пара на вертикальных трубах с ребрами жесткости

[1]Тошов Ж.Б., [1]Эшкуватов Л.М.,[2]Смагулова К.К., [2]Желдикбаева А.Т., [2*]Рабатулы М., [1]Ташбаев Н.Н., [3]Мадаминова Г.

[1]Ташкентский государственный технический университет имени Ислама Карима, Ташкент, Узбекистан
[2]Карагандинский технический университет имени А. Сагинова, Караганда, Казахстан
[3]Ферганский государственный университет, Фергана, Узбекистан

Поступила: *29 января 2025*
Рецензирование: *30 января 2025*
Принята в печать: *10 апреля 2025*

АННОТАЦИЯ

Статья посвящена методологии проведения и обработки результатов экспериментального исследования процесса конденсации водяного пара на вертикальных трубах с специально профилированными рёбрами теплообменника. На основе анализа теплообмена при ламинарной конденсации водяного пара в виде слоя стекающей жидкости как внутри, так и на внешней поверхности вертикальных труб при стационарном паровом потоке была разработана лабораторная установка, на которой проведены экспериментальные исследования. Одним из способов интенсификации теплообмена является оптимизация геометрии теплообменной поверхности на стороне конденсации, что позволяет снизить термическое сопротивление пристенных слоев образующегося конденсата. Этот метод основан на увеличении площади теплообмена за счёт применения специально профилированных рёбер на поверхности труб теплообменника. В результате решается важная научная задача – нарушение сплошного потока ламинарно стекающего конденсата, что способствует непосредственному контакту пара с охлажденной поверхностью трубы и увеличению теплопередачи. В статье изложена методика проведения экспериментов, описаны способы обработки полученных результатов, а также приведены расчётные данные и графические зависимости, иллюстрирующие экспериментальные результаты.

Ключевые слова: теплообменники, теплопередача, конденсация, конденсат, ребра жесткости, пар.

Тошов Жавохир Буриевич	***Информация об авторах:*** *Доктор технических наук, профессор Ташкентского государственного технического университета имени Ислама Карима, 100095, улица Университетская 2, Ташкент, Узбекистан. E-mail: j.toshov@tdtu.uz; ORCID ID: https://orcid.org/0000-0003-4278-1557*
Эшкуватов Лутфулла Мурадуллаевич	*Доктор PhD, доцент, заведующий кафедрой Ташкентского государственного технического университета имени Ислама Каримова, 100095, Алмазарский район, ул. Университетская, 2, Ташкент, Узбекистан. E-mail: l.eshkuvatov@tdtu.uz; ORCID ID: https://orcid.org/0000-0001-7442-5018*
Смагулова Каршыга Канатовна	*Доктор PhD, доцент кафедры автоматизации производственных процессов Карагандинского технического университета имени Абылкаса Сагинова, 100027, пр. Нурсултана Назарбаева, 56, Караганда, Казахстан. E-mail: smagulovakk@mail.ru; ORCID ID: https://orcid.org/0000-0001-6834-8490*
Желдикбаева Айсауле Такеновна	*PhD докторант кафедры автоматизации производственных процессов Карагандинского технического университета имени Абылкаса Сагинова, 100027, пр. Нурсултана Назарбаева, 56, Караганда, Казахстан. E-mail: aisaule89@mail.ru; ORCID ID: https://orcid.org/0009-0005-1325-5576*
Рабатулы Мухаммедрахым	*Доктор PhD, и.о. доцента кафедры разработки месторождений полезных ископаемых Карагандинского технического университета имени Абылкаса Сагинова, 100027, пр. Нурсултана Назарбаева, 56, Караганда, Казахстан. E-mail: mukhammedrakhym@mail.ru; ORCID ID: https://orcid.org/0000-0002-7558-128X*
Ташбаев Назим Тулаевич	*Кандидат технических наук, доцент Ташкентского государственного технического университета имени Ислама Каримова, 100095, Алмазорский район, ул. Университетская, 2, Ташкент, Узбекистан. E-mail: n.tashbayev@tdtu.uz; ORCID ID: https://orcid.org/0000-0003-0121-4660*
Гульсора Мадаминова	*Старший преподаватель Ферганского государственного университета, 150100, ул. Мураббийлар, 19, Фергана, Узбекистан. E-mail: gulsora.madaminova@fdu.uz; ORCID ID: https://orcid.org/0009-0005-4026-0119*

References

[1] Eshkuvatov L, Babakhodjaev R., Tashbaev N. Intensification of heat transfer during condensation of water vapor on a vertical tube. E3S Web of Conferences. 4th International Conference on Energetics, Civil and Agricultural Engineering, (ICECAE 2023). Tashkent. 2023; 434:01012. https://doi.org/10.1051/e3sconf/202343401012

[2] Roberta M, Benjamin Z, Vikrant A, Wiebke BM, and Brian EW. Performance of Heat Pumps Using Pure and Mixed Refrigerants with Maldistribution Effects in Plate Heat Exchanger Evaporators, Int. J. Refrig. 2019; 104:390-403.

[3] Tong P, Fan G, Sun Z, Ding M. Experimental study of steam–air condensation over a vertically longitudinal finned tube. International Journal of Heat and Mass Transfer. 2015; 89:1230-1238. https://doi.org/10.1016/j.ijheatmasstransfer.2015.06.036

[4] Yue C, Tong L, Zhang S. Thermal and economic analysis on vehicle energy supplying system based on waste heat recovery organic Rankine cycle. Applied Energy. 2019; 248:241-255. https://doi.org/10.1016/j.apenergy.2019.04.081

[5] Damiani L, Repetto M, Prato A. Improvement of powertrain efficiency through energy breakdown analysis. Applied Energy. 2014; 121:252-263. https://doi.org/10.1016/j.apenergy.2013.12.067

[6] Rabatuly M, Myrzathan SA, Toshov JB, Nasimov J, Khamzaev A. Views on drilling effectiveness and sampling estimation for solid ore minerals. Kompleksnoe Ispolzovanie Mineralnogo Syra = Complex Use of Mineral Resources. 2026; 336(1):5-14. https://doi.org/10.31643/2026/6445.01

[7] Tian JJ, Wu MP, Zhang Z, Wang SQ, Lang YL, Mehendale S, Wu QY, Wang XX, Wang JY, and Liou HF. Effects of Header Configuration on Flow Maldistribution in Plate-Fin Heat Exchangers, *J. Eng. Therm.* 2023; 32:321-339; https://doi.org/10.1134/S1810232823020091

[8] El Achkar G, Septet C, Le Metayer O, and Hugo JM. Experimental Thermohydraulic Characterisation of Flow Boiling and Condensation in Additive Manufactured Plate-Fin Heat Exchanger, *Int. J. Heat Mass Transfer.* 2022; 199:123465. https://doi.org/10.1016/j.ijheatmasstransfer.2022.123465

[9] Gu LD, and Min JC. Airside Thermal-Hydraulic Characteristics for Tube Bank Heat Exchangers Used to Cool Compressor Bleed Air in an Aero Engine—ScienceDirect, Appl. Thermal Engin. 2018; 141:939-947.

[10] Toshov ZhB, Rahutin MG, Toshov BR, Baratov BN. The method of constructing the scans of the toroidal belts of the faces during drilling wells. Eurasian Mining. 2024; 1:62-66. https://doi.org/10.17580/em.2024.01.15

[11] Volodin V, Tuleushev Y, Kenzhaliyev B, & Trebukhov S. Thermal degradation of hard alloys of the niobiumcadmium system at low pressure. Kompleksnoe Ispolzovanie Mineralnogo Syra = Complex Use of Mineral Resources. 2020; 312(1):41-47. https://doi.org/10.31643/2020/6445.05

[12] Seban RA, Hodgson JA. Laminar film condensation in a tube with upward vapor flow, Int. J. Heat Mass Transfer. 1982; 25(9):1291-1300. http://dx.doi.org/10.1016/0017-9310(82)90123-5

[13] Kallath H, Kholi FK, Jin Q, Ha MY, Park SH, Kim H, Chetwynd-Chatwin J, and Min JK. Numerical Study of the Flow Uniformity Inside the High-Pressure Side Manifolds of a Cooled Cooling Air Heat Exchanger, Appl. Thermal Engin. 2021; 189. https://doi.org/10.1016/j.applthermaleng.2021.116645

[14] Eshkuvatov LM, Babakhodjaev RP, Ismailov BR, Tashbaev NT, Ismailov XB, Mirzaev JA, Kuchinov XA, Kurbanbaeva M. Finned tube. RepUz. Intellectual property agency. Patent for utility model FAP 02024, 27.06.2022.

[15] Ji-H Hwang, H Kim, D-W Jerng. Effect of wall subcooling on condensation in a steam-air mixture on a vertical tube, International Communications in Heat and Mass Transfer. 2023; 143:106665. https://doi.org/10.1016/j.icheatmasstransfer.2023.106665

[16] Kubín M, Hirš J, Plášek J. Experimental analysis of steam condensation in vertical tube with small diameter, Int. J. Heat Mass Transfer. 2016; 94:403-410. https://doi.org/10.1016/j.ijheatmasstransfer.2015.11.022

[17] Toshov JB, Rabatuly M, Bogzhanova ZhK, Zheldikbayeva AT, Malikov ShR, Toshov BR, Ergashev OS. Influence of Radiation and Magnetic Pulse Treatment on The Wear Resistance of Carbide Tools. Kompleksnoe Ispolzovanie Mineralnogo Syra = Complex Use of Mineral Resources. 2026; 337(2):47-54. https://doi.org/10.31643/2026/6445.16

[18] Bukhmirov VV, Rakutina DV. Reference materials for solving problems in the course Heat and mass transfer. Ivanovo State Power Engineering University named after V.I. Lenin. Ivanovo. 2017, 99-106.

[19] Ivanov AN, Belousov VN, Smorodin SN. Heat exchange equipment of industrial enterprises: Tutorial. 2016, 41-46.

[20] W-X Chu et al. Numerical study on a novel hyperbolic inlet header in straight-channel printed circuit heat exchanger. Applied Thermal Engineering. 2019; 146:805-814. https://doi.org/10.1016/j.applthermaleng.2018.10.027

Crossref

DOI: 10.31643/2026/6445.26
Engineering and Technology

Development of Hybrid Coatings for Anti-Corrosion Applications in Oil and Gas sector

[1*]Ainakulova D.T., [1]Yessenova M.D., [1]Zhanibekov R.B., [2]Kusherova P.T., [3]Mukatayeva Zh.S., [4]Baidullayeva A.K., [5]Moshera Samy, [1]Dosymbek A.D.

[1] School of Materials Science and Green Technologies, Kazakh-British Technical University, Almaty, Kazakhstan
[2] Physico-Technical Institute in Alatau, Almaty, Kazakhstan
[3] Institute of Natural Science and Geography, Abal Kazakh National Pedagogical University, Almaty, Kazakhstan
[4] School of Pharmacy, S.D. Asfendiyarov Kazakh National University, Almaty, Kazakhstan
[5] Polymers and Pigments Department, National Research Centre, Dokki, Giza, Egypt

** Corresponding author email: dana.ainakulova@gmail.com*

Received: *March 24, 2025*
Peer-reviewed: *March 28, 2025*
Accepted: *April 11, 2025*

ABSTRACT

The physical, and mechanical properties as well as chemical and corrosion resistance of hybrid coatings comprising polyurethane/acrylic hybrids (PUA/AC) and acrylic polymers (AK) were investigated. Polyurethane (PUA) was synthesized through polyaddition polymerization of isocyanates [Isophorone diisocyanate (IPDI) and hexamethylene diisocyanate (HDI)] with polyols (GP 2000 and GP 4000) at an NCO/OH ratio of 0.85 and a temperature of 100°C. The acrylic copolymer (AC), based on methyl methacrylate (MMA) and butyl methacrylate (BuMA), was produced via bulk polymerization with benzoyl peroxide as a catalyst. The acrylic copolymer (AK) was prepared by grafting xanthan gum with styrene in various ratios (XG: St = 1:1.6, 1:5, and 1:8 w/w%). The results revealed that hybrid coatings demonstrated optimal chemical and corrosion resistance when PUA/AC hybrids were combined with AK. Enhancing both mechanical properties and corrosion resistance was achieved by integrating PUA/AC-10 with AK containing 8% styrene, resulting in superior anticorrosion performance including chemical and solvent resistances for the hybrid coating.

Keywords: polyurethane, acrylic, hybrid, coating, anti-corrosion

Information about authors:

Ainakulova Dana Tulegenkyzy — *PhD candidate of Materials Science and Technology of New Materials, Researcher at the Laboratory of Advanced Materials and Technologies, School of Materials Science and Green Technologies, Kazakh-British Technical University, st. Tole bi 59, 050000, Almaty, Kazakhstan. Email: dana.ainakulova@gmail.com; ORCID ID: https://orcid.org/0000-0002-5335-6102*

Yessenova Maral Duisenbaevna — *Candidate of Chemical Sciences, Researcher at the Laboratory of Advanced Materials and Technologies, School of Materials Science and Green Technologies, Kazakh-British Technical University, st. Tole bi 59, 050000, Almaty, Kazakhstan. Email: maral2375@mail.ru; ORCID ID: https://orcid.org/0009-0000-6223-3131*

Zhanibekov Rinat Bakytnurovich — *PhD candidate of Chemical Engineering, Researcher at the Laboratory of Advanced Materials and Technologies, School of Materials Science and Green Technologies, Kazakh-British Technical University, st. Tole bi 59, 050000, Almaty, Kazakhstan. Email: rin_zhanibeko@kbtu.kz; ORCID ID: https://orcid.org/0009-0004-2453-4768*

Kusherova Parassat Tulegenovna — *PhD candidate, Physico-Technical Institute in Alatau, Ibragimov str. 11, 050032, Almaty, Kazakhstan. Email: partykush@mail.ru; ORCID ID: https://orcid.org/0000-0001-9412-3818*

Mukatayeva Zhazira Sagatbekovna — *Candidate of Chemical Sciences, Associate Professor of the Institute of Natural Sciences and Geography of Abai KazNPU. Email: jazira-1974@mail.ru; ORCID ID: https://orcid.org/0000-0002-1584-5810*

Baidullayeva Ainash Kairatovna — *Department of Engineering Disciplines and Good Practices, School of Pharmacy, S.D. Asfendiyarov Kazakh National Medical University, Almaty, Kazakhstan. Email: ainasha.kz@list.ru; ORCID ID: https://orcid.org/0000-0002-6918-6320*

Moshera Samy — *Polymers and Pigments Department, National Research Centre, 33 El Buhouth St., Dokki, Giza 12622, Egypt. Email: moshera_samy1984@yahoo.com; ORCID ID: https://orcid.org/0000-0002-7272-4134*

Dosymbek Akniyet Dosymbekuli — *Engineer at the Laboratory of Advanced Materials and Technologies, School of Materials Science and Green Technologies, Kazakh-British Technical University, st. Tole bi 59, 050000, Almaty, Kazakhstan. Email: akont1@icloud.com*

Introduction

Metal corrosion in the oil and gas industry shortens equipment lifespan, causing financial losses and safety risks [[1], [2], [3], [4], [5]]. Polyurethane polymers (PUs), known for their renewable and versatile nature, are widely used in coatings to protect metals from corrosion, maintaining their critical role in this application [[6], [7], [8], [9], [10], [11], [12], [13], [13]]. Polyurethane polymers (PUs) are synthesized through the polymerization reaction between isocyanates and polyols [14].

Polyurethanes (PUs) have found immense success in the coating industry due to their enhanced mechanical and physical properties [10]. However, the emergence of new water-based polymers with lower volatile organic compounds (VOCs) has lessened the prominence of polyurethane resins in coatings, primarily for environmental reasons. Despite their eco-friendly nature, water-based coatings often suffer from high surfactant concentrations, which negatively impact surface characteristics [[1], [8], [15], [16], [17], [18]]. Additionally, both water-based and solvent-based polyurethanes exhibit low mechanical and physical performance. To address these limitations, modified polyurethane resins are developed by integrating modifiers into the polyurethane fiber structure through a hybrid process. Combining acrylics with PUs is expected to deliver significant performance enhancements in the resulting materials [[19], [20], [21], [22], [23]].

Acrylics and polyurethanes (PUs) offer notable advantages, such as excellent mechanical properties and strong chemical resistance [24]. Styrene and (meth)acrylates are commonly utilized to create hybrid materials with PUs, aiming to merge the benefits of different polymers for enhanced functionality. Polyurethane-acrylic latex has emerged as a promising alternative to PU-based coatings. By combining the unique features of PUs and polyacrylates, the resulting copolymer can exhibit desirable traits like rapid drying, strong substrate adhesion, high gloss associated with PUs, oxidative drying capabilities, efficient film formation, and the chemical resilience characteristic of acrylic latexes. However, the incompatibility between hydrophobic PU polymer units and the aqueous dispersions of acrylic polymers poses a challenge, limiting their effectiveness as blends in certain applications.

PU-acrylate hybrids often lead to reduced gloss and haze formation in films. To address this, polyurethane and acrylates are chemically bonded to produce PU-acrylic copolymer latexes. Negim et al. (2024) [25], however, explored an alternative approach by hybrid PU with 2-hydroxy ethyl acrylate to develop polyurethane-acrylic hybrids featuring an NCO/OH ratio of 2.2. Their findings revealed that, compared to pure PU, these hybrids' physical and mechanical properties improved as the proportion of 2-hydroxy ethyl methacrylate increased. The integration of acrylic components into the hybrids significantly altered the structure of the pure polyurethane and enhanced its final characteristics. PUA-acrylic hybrids were formulated by hybrid PUA with varying amounts of acrylic polymer to examine the impact of acrylic content on the hybrid films' mechanical and physical properties, as well as their chemical and corrosion resistance [26]. As a result, the hybrids demonstrated enhanced tensile strength, adhesion, hardness, and contact angle compared to the pure PUA and acrylic monomers. However, increased acrylic polymer content in the hybrid further elevated tensile strength, adhesion, hardness, and contact angle while reducing elongation at break. This was primarily attributed to the polymeric network formed by the cross-linking between PUA and acrylic polymer. Interestingly, hybrids with a PUA/acrylic hybrid composition containing 10% acrylic polymer displayed optimal chemical and corrosion resistance, making them particularly effective as coating materials [26]. The hybrid coating demonstrates an environmentally friendly profile, exceptional durability, and robust resistance to solvents and chemicals, along with superior mechanical properties. Additionally, the coating can be produced effortlessly without the need for specialized equipment. The work was further extended to include the application of the obtained acrylic copolymer based on xanthan and styrene compositions (XG: St - 1:1.6, 1:5, and 1:8 w/w%) to modify physicomechanical and anti-corrosion properties of the hybrid coating.

Experiments

Materials

Polypropylene glycol variants—GP-2000 (Mw = 2000 g/mol, OH number = 56 mg KOH/g), GP-4000 (Mw = 4000 g/mol, OH number = 29.5 mg KOH/g), GP-3000 (Mw = 3000 g/mol, OH number = 37 mg KOH/g), and GP - 2100 (Mw = 3000 g/mol, OH

Table 1 – Fee composition of polyurethane polymer (PUA)

	Wt (g)		Wt (%)
Polyols, OH			
GP 2000	168.5		82.2
GP 4000	21.6		10.5
Total	190.1		92.7
Mole of OH (gm/ mole)		0.0896	
Isocyanate, NCO			
IPDI	8.5		4.1
HDI	6.4		3.1
Total	14.9		7.3
Mole of NCO (gm/mole)		0.0762	
NCO/OH		0.85	

number = 56 mg KOH/g)—were sourced from Korea PTG, Korea. These were dried at 80°C and 1–2 mm Hg for 2 hours before use. Dibutyltin dilaurate (DBTDL), isophorone diisocyanate (IPDI), and hexamethylene diisocyanate (HDI) were procured from Bayer AG, Germany. Methyl methacrylate (MMA), butyl methacrylate (BuMA), Styrene (St), potassium persulfate($K_2S_2O_8$), and biopolymer xanthan gum (XG) were purchased from Sigma-Aldrich Chemical Co. (USA). Various solvents were utilized, including xylene, methyl ethyl ketone (MEK, purity > 99.9%), hydrochloric acid (ACS reagent, 37%), sulfuric acid (ACS reagent, 37%), ethanol (ACS reagent, 20%), and sodium chloride (ACS reagent, 10%), all obtained from Sigma Aldrich, USA. MOCA, a curing agent from TPUCO, Taiwan, was employed alongside ESOL N100 plasticizer from VISTALINE, Russia, and BYK-054, a defoamer from BYK, USA. Fillers such as calcium carbonate and pigments like TiO_2-R-996 were acquired from Elementis, Malaysia, and utilized without further purification.

Polyurethane polymer (PUA) Synthesis

The polyurethane (PUA) based on isophorone diisocyanate (IPDI), hexamethylene diisocyanate (HDI), and polyols (GP 2000 and GP 4000) were added to the reactor, and the mixture was heated at 100°C for 3 hours until the theoretical NCO value was attained, as evaluated by the di-n-butylamine titration technique (ASTM D 2572-19, 2019) [27]. The preparation of PUA and the methods of analysis have been previously described in a previous investigation [26]. Table 1 displays the samples that were made. The resulting PUA was clear and liquid, with viscosities of 120 mPa-s and 464.4 mPa-s at 5 and 50 rpm, respectively.

Synthesis of poly (methyl methacrylate-co-butyl methacrylate) (AC)

The preparation of copolymer based on methyl methacrylate (MMA) and butyl methacrylate (BuMA) in feed (5/5) and the methods of analysis have been previously described [26]. The MMA-co BuMA was liquid and transparent in appearance with viscosities of 432 mPa-s and 600 mPa-s at 5 and 50 rpm, respectively.

Synthesis of poly (xanthan gum -g- styrene) (AK)

The preparation of grafted copolymer based on xanthan (XG) and different ratios of styrene (St) (1:1.6 AK1, 1: 5 AK2, and 1: 8 AK3 w/w, %) respectively and the methods of analysis have been previously described [28].

Preparation of polyurethane/acrylic hybrids (PUA/AC)

PUA/AC hybrid was prepared by mixing process 90 % PUA and 10% AC at temperatures 60 °C and 600 rpm and labeled as PUAC-10.

Preparation of polyurethane/acrylic hybrids (PUACK)

Polyurethane/acrylic hybrids (PUACK) were prepared by mixing PUA/AC-10 and AK process at temperatures 60 °C and 600 rpm. Further details about the PUA/AK1 hybrids are given in Table 2.

Table 2 – Fee composition of the PUACK hybrids

Samples	PUAC-10 Wt., (gm)	PolyXG-g-St (AK) Wt., (gm)
PUACK1	90	10 (AK1)
PUACK2	90	10 (AK2)
PUACK3	90	10 (AK3)

Preparation of PUACK hybrid films

PUACK films were prepared by casting the solution onto a flat surface, followed by a curing process that lasted five days at room temperature. The cured films were then stored in a desiccator at ambient conditions to ensure proper preservation before undergoing characterization and measurement

Preparation of the PUACC and PUACK coatings

The preparation of PUACC (based on PUAC-10) and PUACK coatings followed specific formulations, with the weight percentages of the components detailed in Table 3. Across all formulations, the solid content of PUA or PUA/AC accounted for 27% of the total composition. Xylene and polyols (GP-3000 and GP-2100) were first combined in a vial and mixed for 10 minutes at 500 rpm. The plasticizer ESOL N100 and the defoamer BYK-054 were then incorporated into the mixture, followed by five minutes of stirring. Next, calcium carbonate (filler) and TiO_2-R-996 (pigment) were added, and the blending process continued for 30 minutes at a higher speed of 1200 rpm. Finally, the catalyst DBTL was introduced during the application of the coating onto the metal surface.

Table 3 – Anti-corrosion polyurethane/acrylic hybrid coatings (PUACC) and (PUACKC) formulations

Raw materials	Weight percent
PUAC-10 or PUACK	27
Xylene	6.45
GP-3000	9.24
GP-2100	4.5
ESOL N100	4.5
BYK-054	0.35
Calcium carbonate	40.16
TiO_2-R-996	4
DBTDL	0.4
Total	100

Application of the PUACC and PUACKC as coatings

Before coating application, metal samples measuring 9.0 cm × 0.9 cm × 15 cm were abrasively blasted and thoroughly cleaned. The PUACC and PUACKC-based coatings were applied using a film applicator, ensuring a wet film thickness of 75 µm. The coated samples were then left to cure at room temperature for 6 days.

Tests

The viscosity (η) of PUA/AC-10 and PUACK hybrids was determined using a Brookfield viscometer (Spindle 2) at rotational speeds of 5 and 50 rpm, maintained at a temperature of 25°C. The thixotropy index was calculated based on Equation 1.

$$\text{Thixotropy index (TI)} = \eta 5/\eta 50 \quad (1)$$

The contact angle between water droplets and the sample surface was measured using a CAHN DCA-322 contact angle measuring device. The measurement was conducted at 25°C with a water droplet applied at a velocity of 100 lm/s. A small syringe was utilized to deposit the water droplet onto the surface being analyzed, and the contact angle was determined by observing the droplet formation on the monitor. The findings were derived by averaging three measurements conducted on distinct portions of the film. The tensile properties of the cast films were assessed using an MTS 10/M tensile testing system, operating at a crosshead speed of 50 mm/min with a 1-kN load cell. At least four values were averaged for accuracy. Additionally, the hardness of the films was determined using an indentation Barcol hardness tester by ASTM B648-10 [29]. Adhesion between the metal and hybrid polymers was evaluated using pull-off testing, as outlined in ASTM D4541-22 [30]. Corrosion resistance tests were performed on coated panels under various conditions, including exposure to salt (10% NaCl), base (10% NaOH), acid (37% HCl and H_2SO_4), and solvents (xylene, MEK, and ethanol), following ASTM D5402-93 [31] standards. Water resistance was assessed in compliance with ASTM D1647-89 [32]. Dry times were recorded at a stable temperature of 25°C.

Results and discussion

To enhance the mechanical properties of polyurethane/acrylic hybrid (PUA/AC-10) and improve their anticorrosion coating capabilities, copolymers derived from xanthan gum and styrene were prepared through grafting polymerization.

Viscosity and thixotropic index (TI) of PUA/AC-10 and PUACK

Figure 1 illustrates the effect of acrylic copolymer (AK), derived from xanthan gum (XG) and styrene (St), on the viscosity of polyurethane/acrylic hybrids (PUA/AC-10). The viscosity of PUA/AC-10 increases when combined with copolymer AK. As the content of styrene in AK increases, the viscosity of PUA/AC-10 increases from 476 mPa·s to 1105 mPa·s at 5 rpm and increases from 135 mPa·s to 290 mPa·s at 50 rpm which is attributed to the behavior of XG as a fluid [33]. Factors such as particle deformation, orientation of non-spherical particles, polymer chain alignment in the flow direction, and chain deformation contribute to this increase in viscosity [34]. Consequently, polyurethane/acrylic hybrids (PUACK) incorporating (XG-g-St) exhibit higher

viscosity than PU/AC-10, due to the branched, cross-linked, and three-dimensional network structure of XG-g-St [35]. PUACK3, with 8% styrene, demonstrates the highest viscosities at 5 and 50 rpm, exceeding those of other polyurethane-acrylic hybrids [26]. The thixotropic index (TI) of polymer solutions is influenced by several factors, such as the type of copolymer, composition ratios, and polymer concentration [36]. Figure 2 shows the TI of PUACK across different ratios of St content. The results indicate that PUACK3, containing 8% of St, exhibited the highest TI value of 3.8, whereas PUACK2, with 5% of St, had the lowest TI value of 3.5. Thixotropy plays a significant role in shaping the formulations and preparation processes of coatings, which in turn affects their rheological properties [36]. These results are lower compared to those of polyurethane hybrids with acrylic polymers formulated using a 5:5 feed ratio of methyl and butyl methacrylate [26].

Adhesion

The adhesion of polyurethane to metal results from adsorbate layers and chemical bonds formed between isocyanate groups and the metal surface. Several factors influence polyurethane adhesion, including isocyanate content, polyol composition, and acrylic polymer properties [[37], [38]]. Figure 3 demonstrates the effect of AK on the adhesion of the PUA/AC-10 hybrid to metal. Results show that incorporating AK into the PUA/AC-10 hybrid enhances adhesion. While the adhesion strength of PUA/AC-10 is 6.9 MPa, the PUACK hybrid, formed by combining AK with PUA/AC-10, exhibits increased adhesion from 6.9 to 10.7.

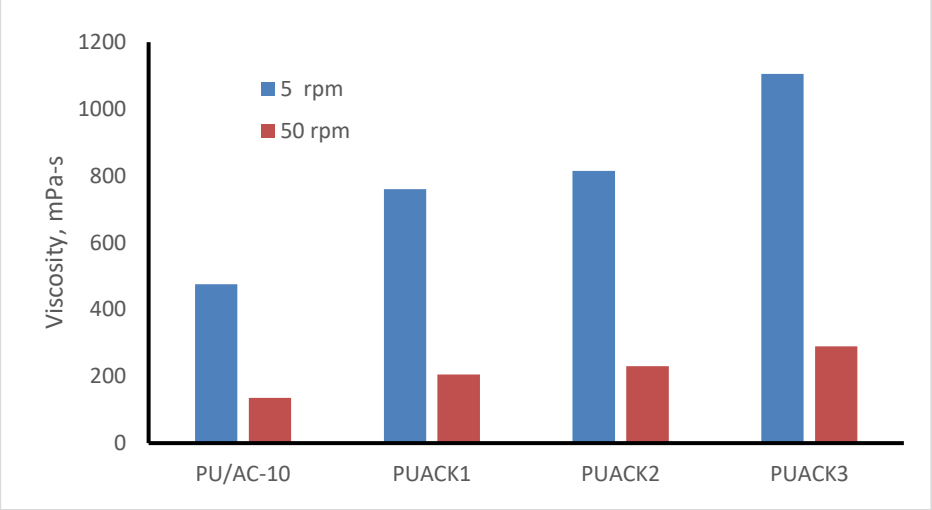

Figure 1 – The viscosity of PUA/AC-10 and PUACK hybrids

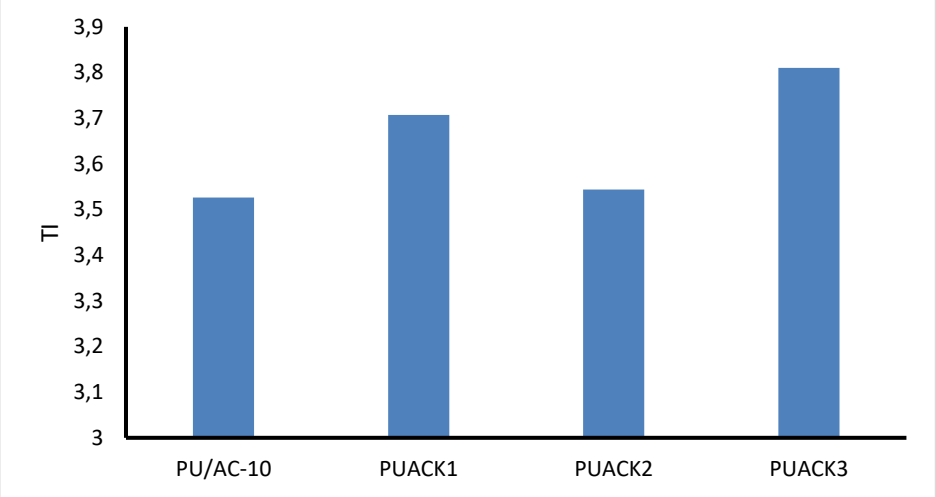

Figure 2 – TI of PUA/AC-10 and PUACK hybrids

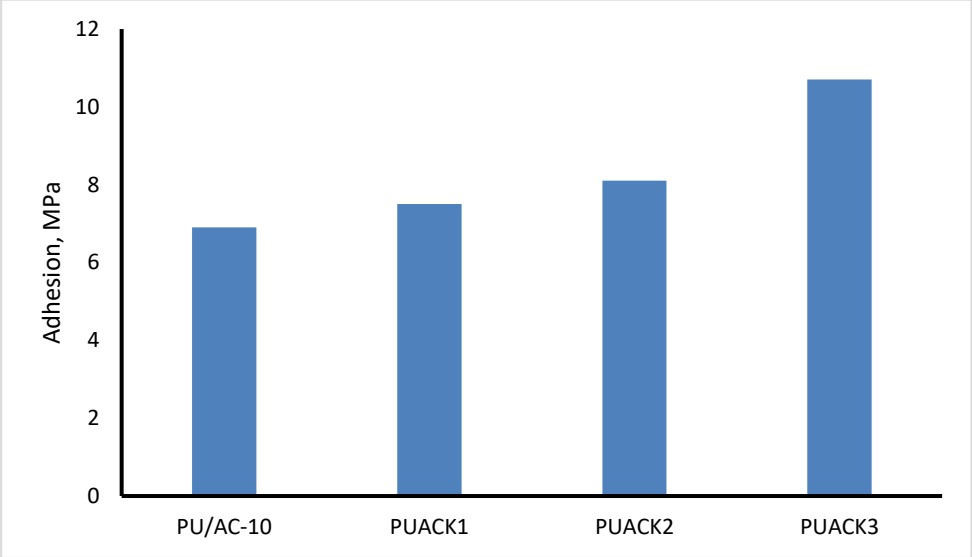

Figure 3 – Adhesion of PUACK hybrids on the metal

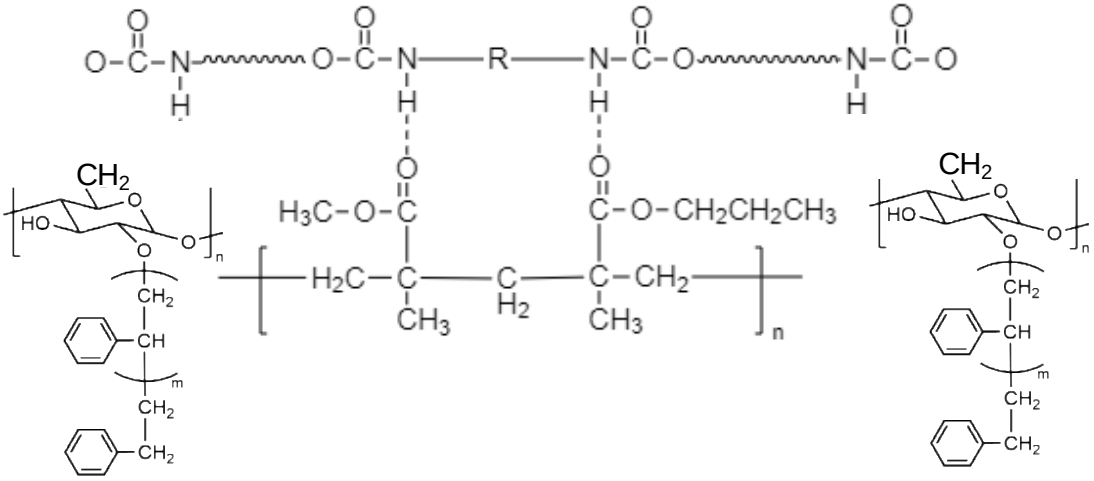

Figure 4 – The cross-linking between PUA, AC and AK in the PUACK hybrids

However, increasing the styrene (St) concentration in AK from 1.6% to 8.0% boosts adhesion strength from 7.5 MPa to 10.7 MPa. This improvement is attributed to crosslinking between PUA, AC, and AK, as depicted in Figure 4, which highlights the crosslinking between PUA and AK and the functional (NCO) groups on the substrate responsible for enhanced adhesion [[39], [40], [41]]. These results are lower compared to those of polyurethane hybrids with acrylic polymers formulated using a 5:5 feed ratio of methyl and butyl methacrylate [26].

Mechanical Properties

Table 4 shows the effect of acrylic copolymer AK with varying St compositions on the mechanical properties of the PUA/AC-10 hybrid. The results reveal that mixing AK with PUA/AC-10 significantly enhances the mechanical properties of PUACK, driven by crosslinking among PUA, AC, and AK and influenced by the side chain lengths forming hydrogen bonds between PUA, AC, and AK, as depicted in Figure 4. Increasing the St concentration in AK further boosts the mechanical properties of PUACK hybrids. For instance, the tensile strength of PU/AC-10 was 164 MPa, whereas PUACK improved tensile strength to 187.5 MPa for PUACK1 (St, 1.6%) and 245.1 MPa for PUACK3 (St, 8.0%). Additionally, hardness (shore D) increased from 53 for PU/AC-10 to 83.6 for PUACK3. All samples passed the impact test and crosshatch test, with PUACK displaying superior mechanical properties compared to PUA/AC-10 due to its dual crosslinking mechanism. Among PUACK hybrids, PUACK3 exhibited the best mechanical properties. Studies have consistently demonstrated that crosslinking the polymer backbone is an effective strategy for improving the mechanical properties of polymer films [42], [43], [44], [45]].

Table 4 – Mechanical properties of the PUA/AC-10 and PUA/AK hybrids

	Tensile strength, MPa	Elongation, %	Hardness, shore D	Contact angle	Impact test	Cross Hatch
PU/AC-10	164	125	53	132	Pass	Pass
PUACK1	187.5	105	65	135	Pass	Pass
PUACK2	195.9	91.8	71	149	Pass	Pass
PUACK3	245.1	88.2	83.6	151	Pass	Pass

Table 5 – The effectiveness of the hybrid coating against corrosion and chemical resistances reduced when the amount of St in AK in the hybrids increased.

Contact angle	PUACC-10	PUACKC1	PUACKC2	PUACKC3
Corrosion resistance				
NaCl (10%)	O	O	O	O
NaOH (10%)	O	O	O	O
HCl (37%)	O	O	O	O
H_2SO_4 (37%)	Δ	Δ	O	O
Water	O	O	O	O
Chemical resistance				
MEK	Δ	Δ	O	O
Xylene	O	O	O	O
Ethanol (20%)	O	O	O	O
Ethylene glycol	O	O	O	O
Wine	Δ	Δ	O	O
Acetone	Δ	Δ	Δ	O
Butyl alcohol	Δ	Δ	Δ	O

O: Suitable
Δ: Slight Suitable

Chemical and corrosion resistance

Table 5 demonstrates the chemical and corrosion resistance of hybrid coatings formulated with PU/AC-10 and AK to create anti-corrosion coatings (PUACKC). The chemical resistance of all coating samples was evaluated using MEK, xylene, ethanol (20%), ethylene glycol, wine, acetone, and butyl alcohol. Additionally, their corrosion resistance was assessed against NaCl (10%), NaOH (10%), HCl (37%), H_2SO_4 (37%), and water. The results indicate that hybrid coatings (PUACKC) based on AK exhibit superior chemical and corrosion resistance compared to hybrid coatings (PUACC-10) based on AC. Notably, PUACKC3, derived from AK3 with 8.0% St content, displayed the best anti-corrosion properties among the tested samples, attributed to the influence of the styrene ring on the mechanical properties of the polyurethane hybrid (PUACK).

Conclusions

Anti-corrosion coating hybrids were developed by combining PUA/AC-10 with AK to produce polyurethane/acrylic hybrids (PUACK) and examine how the AK content influenced the hybrid films' mechanical and physical properties, as well as their resistance to chemicals and corrosion. The inclusion of AK and PUA/AC-10 improved the mechanical and physical properties of the coating hybrids due to the functional groups present in PUA, AC, and AK, such as NCO, NH, carbonyl, styrene, and ester groups, which facilitate cross-linking among PUA, AC, and AK. The PUACK hybrids exhibited enhanced tensile strength, adhesion, hardness, and contact angle compared to PUA/AC-10. However, as the styrene (St) concentration increased, properties such as tensile strength, adhesion, contact angle, and hardness improved, while elongation at break decreased. This is attributed to the polymeric

network formed through cross-linking among PUA, AC, and AK in the hybrid structure. Incorporating AK3 (St, 8.0%) into PUA/AC-10 further enhanced chemical and corrosion resistance compared to coatings based on PUA/AC-10.

CRediT author statement: Writing-original draft Ainakulova D.T. and Yessenova M.D.; Writing review Zh. S. Mukatayeva; Methodology A.K. Baidullayeva; Formal analysis Kusherova P.T. and Moshera Samy. All authors have read and agreed to the published version of the manuscript.

Acknowledgements. The work was financially supported by the Ministry of Science and Education of the Republic of Kazakhstan, program-targeted financing out of competitive procedures for 2023-2025. Project No. (BR21882301) entitled "Comprehensive solution to current issues related to geology, production and processing of mineral and hydrocarbon raw materials."

Conflicts of interest. The authors declare no conflict of interest.

Cite this article as: Ainakulova DT, Yessenova MD, Zhanibekov RB, Kusherova PT, Mukatayeva ZhS, Baidullayeva AK, Moshera Samy, Dosymbek AD. Development of Hybrid Coatings for Anti-Corrosion Applications in Oil and Gas sector. Kompleksnoe Ispolzovanie Mineralnogo Syra = Complex Use of Mineral Resources. 2026; 338(3):29-39. https://doi.org/10.31643/2026/6445.26

Мұнай-газ секторында коррозияға қарсы қолдануға арналған гибридті жабындарды әзірлеу

[1]Айнакулова Д.Т., [1] Есенова М.Д., [1] Жанибеков Р.Б., [2] Кушерова П.Т., [3]Мукатаева Ж.С., [4]Байдуллаева А.К., [5]Мошера Сами, [1]Досымбек А.Д.

[1] Материалтану және жасыл технологиялар мектебі, Қазақ-Британ техникалық университеті, Алматы, Қазақстан
[2] Физико-техникалық институт Алатау, Алматы, Казахстан
[3] Жаратылыстану және география институты, Абай атындағы ҚазҰПУ, Алматы, Қазақстан
[4] С. Д. Асфендияров атындағы Қазақ ұлттық медицина университеті, Алматы, Қазақстан
[5] Ұлттық зерттеу орталығы, Докки, Гиза, Египет

Мақала келді: *24 наурыз 2025*
Сараптамадан өтті: *28 наурыз 2025*
Қабылданды: *11 сәуір 2025*

ТҮЙІНДЕМЕ

Гибридті жабындардың физикалық және механикалық қасиеттері зерттелді. Олардың құрамында полиуретан/акрил гибридтері (PUA/AC) және акрил полимерлері (АК) бар. Полиуретан (PUA) изоцианаттардың [изофорондицианат (IPDI) және гексаметилендиизоцианат (HDI)] полиолдармен (GP 2000 және GP 4000) 0,85 NCO/OH қатынасында және 100°C температурада поли біріктіретін полимерлеу арқылы синтезделді. Метилметакрилат (MMA) және бутилметакрилат (BuMA) негіздегі акрил сополимері (AC) бензой пероксиді катализатор ретінде қолданылған көлемді полимерлеу әдісімен алынды. Акрил сополимері (АК) ксантан сағызы мен стиролды әртүрлі қатынаста (XG:St = 1:1,6, 1:5 және 1:8 мас.%) араластыру арқылы алынды. Нәтижелер көрсеткендей, PU/AC гибридтері мен АК үйлескен кезде гибридті жабындар оңтайлы химиялық және коррозияға төзімділік көрсетті. Механикалық қасиеттер мен коррозияға төзімділіктің жоғарылауына PU/AC-10-ды құрамында 8% стирол бар АК-мен біріктіру арқылы қол жеткізілді, бұл гибридті жабынның антикоррозиялық қасиеттерінің жоғары болуына әкелді.

Түйін сөздер: полиуретан, акрил, гибридті, коррозияға қарсы жабын.

Авторлар туралы ақпарат:

Айнакулова Дана Тулегенқызы
PhD докторант, Материалтану және жаңа материалдар технологиясы, Перспективті материалдар және технологиялар зертханасының ғылыми қызметкері, Материалтану және жасыл технологиялар мектебі, Қазақ-Британ Техникалық Университеті, Төле би көш., 59, 050000, Алматы, Қазақстан. Email: dana.ainakulova@gmail.com; ORCID ID: https://orcid.org/0000-0002-5335-6102

Есенова Марал Дуйсенбайқызы
Химия ғылымдарының кандидаты, Перспективті материалдар және технологиялар зертханасының ғылыми қызметкері, Материалтану және жасыл технологиялар мектебі, Қазақ-Британ Техникалық Университеті, Төле би көш., 59, 050000, Алматы, Қазақстан. Email: maral2375@mail.ru; ORCID ID: https://orcid.org/0009-0000-6223-3131

Жанибеков Ринат Бакытнурович
PhD докторант, Химиялық инженерия, Перспективті материалдар және технологиялар зертханасының ғылыми қызметкері, Материалтану және жасыл технологиялар мектебі, Қазақ-Британ Техникалық Университеті, Төле би көш., 59, 050000, Алматы, Қазақстан. Email: rin_zhanibeko@kbtu.kz; ORCID ID: https://orcid.org/0009-0004-2453-4768

Кушерова Парасат Тулегеновна	*PhD докторант, Химиялық инженерия, Физико-техникалық институт Алатау, Ибрагимов көш. 11, 050032, Алматы, Казахстан. Email: partykush@mail.ru; ORCID ID: https://orcid.org/0000-0001-9412-3818*
Мукатаева Жазира Сагатбековна	*Химия ғылымдарының кандидаты, Жаратылыстану және география институтының қауымдастырылған профессоры, Абай атындағы Қаз¥ПУ, Алматы, Қазақстан. Email: jazira-1974@mail.ru; ORCID ID: https://orcid.org/0000-0002-1584-5810*
Байдуллаева Айнаш Кайратовна	*Инженерлік пәндер және озық практика кафедрасы, С. Д. Асфендияров атындағы Қазақ ұлттық медицина университетінің фармацевтика факультеті, Алматы, Қазақстан. Email: ainasha.kz@list.ru; ORCID ID: https://orcid.org/0000-0002-6918-6320*
Мошера Сами	*Полимерлер мен пигменттер кафедрасы, Ұлттық зерттеу орталығы, Әл-Бухут көшесі, 33, Докки, Гиза, 12622, Египет. Email: moshera_samy1984@yahoo.com; ORCID ID: https://orcid.org/0000-0002-7272-4134*
Досымбек Акниет Досымбекулы	*Инженер, Перспективті материалдар және технологиялар зертханасы, Материалтану және жасыл технологиялар мектебі, Қазақ-Британ Техникалық Университеті, Төле би көш., 59, 050000, Алматы, Қазақстан. Email: akont1@icloud.com*

Разработка гибридных покрытий для антикоррозийного применения в нефтегазовом секторе

[1]Айнакулова Д.Т., [1] Есенова М.Д., [1] Жанибеков Р.Б., [2] Кушерова П.Т., [3]Мукатаева Ж.С., [4]Байдуллаева А.К., [5]Мошера Сами, [1]Досымбек А.Д.

[1] Школа материаловедения и зеленых технологий, Казахстанско-Британский Технический Университет, Алматы, Казахстан
[2] Физико- технический институт Алатау, Алматы, Казахстан
[3] Институт естествознания и географии КазНПУ имени Абая, Алматы, Казахстан
[4] Казахский национальный медицинский университет имени С.Д. Асфендиярова, Алматы, Казахстан
[5] Национальный исследовательский центр, Гиза, Египет

Поступила: *24 марта 2025*
Рецензирование: *28 марта 2025*
Принята в печать: *11 апреля 2025*

АННОТАЦИЯ

Исследованы физические и механические свойства гибридных покрытий, содержащих полиуретановые/акриловые гибриды (PUA/AC) и акриловые полимеры (АК). Полиуретан (PUA) синтезирован путем полиприсоединительной полимеризации изоцианатов [изофорондиизоцианата (IPDI) и гексаметилендиизоцианата (HDI)] с полиолами (GP 2000 и GP 4000) при соотношении NCO/OH, равном 0,85, и температуре 100°C. Акриловый сополимер (АС) на основе метилметакрилата (MMA) и бутилметакрилата (BuMA) получен методом объемной полимеризации с использованием пероксида бензоила в качестве катализатора. Акриловый сополимер (АК) получен путем смешивания ксантановой камеди со стиролом в различных соотношениях (XG:St = 1:1,6, 1:5 и 1:8 мас.%). Результаты показали, что гибридные покрытия продемонстрировали оптимальную химическую и коррозионную стойкость при сочетании гибридов PU/AC с АК. Повышение механических свойств и коррозионной стойкости было достигнуто за счет сочетания PU/AC-10 с АК, содержащим 8% стирола, что привело к превосходным антикоррозийным свойствам гибридного покрытия.

Ключевые слова: полиуретановое, акриловое, гибридное, антикоррозийное покрытие.

Информация об авторах:

Айнакулова Дана Тулегенқызы	*PhD докторант, Материаловедения и технологии новых материалов, научный сотрудник лаборатории перспективных материалов и технологий, Школа материаловедения и зеленых технологий, Казахстанско-Британский технический университет, ул. Толе би, 59, 050000, Алматы, Казахстан. Email: dana.ainakulova@gmail.com; ORCID ID: https://orcid.org/0000-0002-5335-6102*
Есенова Марал Дуйсенбайкызы	*Кандидат химических наук, научный сотрудник лаборатории перспективных материалов и технологий, Школа материаловедения и зеленых технологий, Казахстанско-Британский технический университет, ул. Толе би, 59, 050000, Алматы, Казахстан. Email: maral2375@mail.ru; ORCID ID: https://orcid.org/0009-0000-6223-3131*
Жанибеков Ринат Бакытнурович	*PhD докторант химической инженерии, научный сотрудник лаборатории перспективных материалов и технологий, Школа материаловедения и зеленых технологий, Казахстанско-Британский технический университет, ул. Толе би, 59, 050000, Алматы, Казахстан. Email: rin_zhanibeko@kbtu.kz; ORCID ID: https://orcid.org/0009-0004-2453-4768*
Кушерова Парасат Тулегеновна	*PhD докторант химической инженерии, Физико-технический институт Алатау, ул. Ибрагимов 11, 050032, Алматы, Казахстан. Email: partykush@mail.ru; ORCID ID: https://orcid.org/0000-0001-9412-3818*
Мукатаева Жазира Сагатбековна	*Кандидат химических наук, Ассоциированный профессор института естествознания и географии КазНПУ имени Абая, Алматы, Казахстан. Email: jazira-1974@mail.ru; ORCID ID https://orcid.org/0000-0002-1584-5810*
Байдуллаева Айнаш Кайратовна	*Кафедра инженерных дисциплин и передовой практики, Фармацевтический факультет Казахского национального медицинского университета имени С.Д. Асфендияров, Алматы, Казахстан. Email: ainasha.kz@list.ru; ORCID ID: https://orcid.org/0000-0002-6918-6320*

Мошера Сами	*Кафедра полимеров и пигментов, Национальный исследовательский центр, ул. Эль-Бохут, 33, Докки, Гиза, 12622, Египет. Email: moshera_samy1984@yahoo.com; ORCID ID: https://orcid.org/0000-0002-7272-4134*
Досымбек Акниет Досымбекулы	*Инженер лаборатории перспективных материалов и технологий, Школа материаловедения и зеленых технологий, Казахстанско-Британский технический университет, ул. Толе би, 59, 050000, Алматы, Казахстан. Email: akont1@icloud.com*

References

[1] Marathe RJ, & Gite V V. Encapsulation of 8-HQ as a corrosion inhibitor in PF and UF shells for enhanced anticorrosive properties of renewable source based smart PU coatings. RSC Advances. 2016; 6(115):114436–114446. https://doi.org/10.1039/C6RA21684F

[2] Bender R, Féron D, Mills D, Ritter S, Bäßler R, Bettge D, De Graeve I, Dugstad A, Grassini S, Hack T, Halama M, Han E, Harder T, Hinds G, Kittel J, Krieg R, Leygraf C, Martinelli L, Mol A, … Zheludkevich M. Corrosion challenges towards a sustainable society. Materials and Corrosion. 2022; 73(11):1730-1751. https://doi.org/10.1002/maco.202213140

[3] Lawal SL, Afolalu SA, & Ogedengbe TS. Overview of Corrosion and its Consequences in the Oil and Gas Industry. In 2023 2nd International Conference on Multidisciplinary Engineering and Applied Science (ICMEAS). 2023 2nd International Conference on Multidisciplinary Engineering and Applied Science (ICMEAS). 2023. https://doi.org/10.1109/ICMEAS58693.2023.10429890

[4] Solovyeva VA, Almuhammadi KH, & Badeghaish WO. Current Downhole Corrosion Control Solutions and Trends in the Oil and Gas Industry: A Review. Materials. 2023; 16(5):1795. https://doi.org/10.3390/ma16051795

[5] Vakili M, Koutník P, & Kohout J. Addressing Hydrogen Sulfide Corrosion in Oil and Gas Industries: A Sustainable Perspective. In Sustainability. 2024; 16(4):1661. https://doi.org/10.3390/su16041661

[6] Jiang F, Zhao W, Wu Y, Dong J, Zhou K, Lu G, & Pu J. Anti-corrosion behaviors of epoxy composite coatings enhanced via graphene oxide with different aspect ratios. Progress in Organic Coatings. 2019; 127:70-79. https://doi.org/10.1016/j.porgcoat.2018.11.008

[7] Kenzhaliyev BK, Surkova TYu. Azlan MN, Yulusov SB, Sukurov BM, Yessimova DM. Black shale ore of Big Karatau is a raw material source of rare and rare earth elements. Hydrometallurgy. 2021; 205:105733. https://doi.org/10.1016/j.hydromet.2021.105733

[8] Negim E-S, Omurbekova K, Bekbayeva L, & Abdelhafiz A. Effect of NCO/OH ratio on the physico-mechanical properties of polyurethane-polyurea hybrid spray coatings. Egyptian Journal of Chemistry. 2020; 63(11):4503-4508.

[9] Deng Y, Bai W, Chen J, Zhang X, Wang S, Lin J, & Xu Y. Bio-inspired electrochemical corrosion coatings derived from graphene/natural lacquer composites. RSC Advances. 2017; 7(71):45034-45044. https://doi.org/10.1039/C7RA08536B

[10] Cao Y, Liu Z, Zheng B, Ou R, Fan Q, Li L, Guo C, Liu T, & Wang Q. Synthesis of lignin-based polyols via thiol-ene chemistry for high-performance polyurethane anticorrosive coating. Composites Part B: Engineering. 2020; 200:108295.

[11] Maurya AK, de Souza F M, & Gupta RK. Polyurethane and Its Composites: Synthesis to Application. Polyurethanes: Preparation, Properties, and Applications. 2023; 1:1–20. http://doi.org/10.1021/bk-2023-1452.x001

[12] Patil CK, Jung DW, Jirimali HD, Baik JH, Gite VV, & Hong SC. Nonedible Vegetable Oil-Based Polyols in Anticorrosive and Antimicrobial Polyurethane Coatings. Polymers. 2021; 13(18):3149. https://doi.org/10.3390/polym13183149

[13] Alshabebi AS, Alrashed MM, El Blidi L, & Haider S. Preparation of Bio-Based Polyurethane Coating from Citrullus colocynthis Seed Oil: Characterization and Corrosion Performance. Polymers. 2024; 16(2):214. https://doi.org/10.3390/polym16020214

[14] Ramezanzadeh B, Ghasemi E, Mahdavian M, Changizi E, & Mohamadzadeh Moghadam MH. Characterization of covalently-grafted polyisocyanate chains onto graphene oxide for polyurethane composites with improved mechanical properties. Chemical Engineering Journal. 2015; 281:869-883. https://doi.org/10.1016/j.cej.2015.07.027

[15] Negim ES, et al. Effect of polyol on physico-mechanical properties of polyurea film. AIP Conference Proceedings. AIP Publishing. 2019; 2124:020051. https://doi.org/10.1063/1.5117111

[16] Zhang J, Ge D, Wang X, Wang W, Cui D, Yuan G, Wang K, & Zhang W. Influence of Surfactant and Weak-Alkali Concentrations on the Stability of O/W Emulsion in an Alkali-Surfactant–Polymer Compound System. ACS Omega. 2021; 6(7):5001-5008. https://doi.org/10.1021/acsomega.0c06142

[17] Kurpanik R, Lechowska-Liszka A, Mastalska-Popławska J, Nocuń M, Rapacz-Kmita A, Ścisłowska-Czarnecka A, & Stodolak-Zych E. Effect of Ionic and Non-Ionic Surfactant on Bovine Serum Albumin Encapsulation and Biological Properties of Emulsion-Electrospun Fibers. Molecules. 2022; 27(10):3232. https://doi.org/10.3390/molecules27103232

[18] Bartman M, Balicki S, Hołysz L, & Wilk KA. Surface Properties of Graffiti Coatings on Sensitive Surfaces Concerning Their Removal with Formulations Based on the Amino-Acid-Type Surfactants. In Molecules. 2023; 28(4):1986. https://doi.org/10.3390/molecules28041986

[19] Zhang X, Kim Y, Kim D, Liu M, Erramuspe IBV, Kaya GB, Wang X, Kim T, Via BK, & Cho H. Shape-Stabilized Phase Change Material by a Synthetic/Natural Hybrid Composite Foam with Cell-Wall Pores. ACS Applied Energy Materials. 2020; 4(1):416-424. https://doi.org/10.1021/acsaem.0c02341

[20] Wang G, Zhou Z, Chen M, Wang J, & Yu Y. UV-Curable Polyurethane Acrylate Pressure-Sensitive Adhesives with High Optical Clarity for Full Lamination of TFT-LCD. ACS Applied Polymer Materials. 2023; 5(3):2051-2061. https://doi.org/10.1021/acsapm.2c02092

[21] Lovato MJ, del Valle LJ, Puiggalí J, & Franco L. Performance-Enhancing Materials in Medical Gloves. Journal of Functional Biomaterials. 2023; 14(7):349. https://doi.org/10.3390/jfb14070349

[22] Bichu Y M, Alwafi A, Liu X, Andrews J, Ludwig B, Bichu A Y, & Zou B. Advances in orthodontic clear aligner materials. Bioactive Materials. 2023; 22:384-403. https://doi.org/10.1016/j.bioactmat.2022.10.006

[23] Yan T, Balzer AH, Herbert KM, Epps TH, & Korley LTJ. Circularity in polymers: addressing performance and sustainability

challenges using dynamic covalent chemistries. Chemical Science. 2023; 14(20):5243-5265. https://doi.org/10.1039/D3SC00551H

[24] Bui TMA, Nguyen TV, Nguyen TM, Hoang TH, Nguyen TTH, Lai TH, Tran TN, Hoang VH, Le TL, Dang TC, et al. Investigation of crosslinking, mechanical properties and weathering stability of acrylic polyurethane coating reinforced by SiO2 nanoparticles issued from rice husk ash. Mater. Chem. Phys. 2020; 241:122445. https://doi.org/10.1016/j.matchemphys.2019.122445

[25] Negim E, Yeligbayeva G, Al Azzam KM, et al. Synthesis, characterization, and application of polyurethane/2-hydoxyethyl methacrylate hybrids as additives to unsaturated polyester resins. Polym. Bull. 2024; 81:4459-4475.

[26] Negim E, Shalash M, Al Azzam KM, Sagatbekovna MZ, Kairatovna BA, Konstantinovich AT, Adlikhanovna NA, Ermekovna KA, Ravindran B. Synthesis, Characterization, and Application of Polyurethane-Acrylic Hybrids as Anticorrosion Coatings. International Journal of Technology. 2024; 15(6):2009-2023. https://doi.org/10.14716/ijtech.v15i6.7044

[27] ASTM D 2572-19, Standard method of test for isocyanate group in urethane materials or prepolymer, 2019.

[28] Kusherova PT, Negim El-Sayed, Al Azzamd Khaldun M, Mukatayevae Zh S, Baidullayevaf A K, Moshera Samy. Modification of Xanthan Gum with Styrene and Investigation of its Rheological Properties, Egyptian Journal of Chemistry. 2024; 67(4):1-6.

[29] ASTM B648-10, Standard Test Method for Indentation Hardness of Aluminum Alloys by Means of a Barcol Impressor. 2015.

[30] ASTM D4541-22, Standard Test Method for Pull-Off Strength of Coatings Using Portable Adhesion Testers. 2022.

[31] ASTM D5402-93, Standard Practice for Assessing the Solvent Resistance of Organic Coatings Using Solvent Rubs. 1999.

[32] ASTM D1647-89, Standard Test Methods for Resistance of Dried Films of Varnishes to Water and Alkali. 2017.

[33] Madbouly SA, & Otaigbe JU. Rheokinetics of Thermal-Induced Gelation of Waterborne Polyurethane Dispersions. In Macromolecules. 2005; 38(24):10178-10184.

[34] Kozakiewicz J. Developments in aqueous polyurethane and polyurethane-acrylic dispersion technology. Part I. Polyurethane dispersions. Polimery. 2015; 60(09):525-535. http://dx.doi.org/10.14314/polimery.2015.525

[35] Wang X, Xu Q, Yu H, & Xu J. Synthesis of high-solid, low-viscosity hydroxy acrylic resin modified with TBCHA. In Journal of Saudi Chemical Society. 2019; 23(7):992-998. https://doi.org/10.1016/j.jscs.2019.04.005

[36] Sinha D. Structural modifications of gamma irradiated polymers: An FT-IR study. Adv. Appl. Sci. Res. 2012; 3(3):1365.

[37] Sahoo S, Chakraborti CK, Behera PK, Mishra SC. FTIR and raman spectroscopic investigations of a norfloxacin/carbopol 934 polymeric suspension. J. Young Pharm. 2012; 4(3):138.

[38] Chhabra RP, Richardson JF. Non-Newtonian flow and applied rheology, 2nd Edition. Butterworth Heinemann, Oxford. 2008.

[39] Patel J, Maji B, Moorthy NSHN, Maiti S. Xanthan gum derivatives: review of synthesis, properties and diverse applications. RSC Advances. 2020; 10(45):27103. https://doi.org/10.1039/D0RA04366D

[40] Wang W, Hu Y, Li L, Zeng J, & Yao Y. Effect of various polymer additives on the rheology and thixotropy of organic vehicles. Journal of Materials Science: Materials in Electronics. 2022; 33(15):12002-12015.

[41] Nacas AM, Ito NM, De Sousa RR, Spinacé MA, and Dos Santos DJ. Effects of NCO:OH Ratio on the Mechanical Properties and Chemical Structure of Kraft Lignin–Based Polyurethane Adhesive. The Journal of Adhesion. 2017; 93(1-2):18-29. https://doi.org/10.1080/00218464.2016.1177793

[42] Nathalie MI, Julia RG, Suel EV, Mathilde JGCF, Demetrio JS. Interplay of polyurethane mechanical properties and practical adhesion of flexible multi-layer laminates. The Journal of Adhesion. 2020; 96(14):1219-1232. https://doi.org/10.1080/00218464.2019.1580580

[43] Lei L, Xia Z, Ou C, Zhang L, & Zhong L. Effects of crosslinking on adhesion behavior of waterborne polyurethane ink binder. In Progress in Organic Coatings. 2015; 88:155-163.

[44] Gomez-Lopez A, Panchireddy S, Grignard B, Calvo I, Jerome C, Detrembleur C, & Sardon H. Poly(hydroxyurethane) Adhesives and Coatings: State-of-the-Art and Future Directions. ACS Sustainable Chemistry & Engineering. 2021; 9(29):9541-9562. https://doi.org/10.1021/acssuschemeng.1c02558

[45] Negim E-S, Yeligbayeva G, Al Azzam K M, Irmukhametova G, Bekbayeva L, Kalugin S N, & Uskenbayeva S. Synthesis, characterization, and application of polyurethane/2-hydoxyethyl methacrylate hybrids as additives to unsaturated polyester resins. In Polymer Bulletin. 2024; 81(5):4459-4475.

Crossref
DOI: 10.31643/2026/6445.27
Engineering and Technology

Utilization of Natural Silicate Rocks to Reduce the Carbon Footprint in the Cement Industry

[1]Iskandarova M.I., [1]Atabaev F.B., [2*]Khadzhiev A.Sh.

[1] Institute of General and Inorganic Chemistry of the Academy of Sciences of Uzbekistan, Tashkent
[2] Urgench State University named after Abu Rayhon Beruni, Urgench, Uzbekistan

** Corresponding author email: azamat.x@urdu.uz*

Received: *March 15, 2025*
Peer-reviewed: *March 19, 2025*
Accepted: *April 17, 2025*

ABSTRACT
Portland cement production is associated with high energy consumption and CO_2 emissions, highlighting the need for alternative raw materials to improve environmental sustainability. Research findings indicate that porphyrite, a natural silicate rock, exhibits pozzolanic and hydraulic activity, making it a promising additive in composite cement production. In this study, the physicochemical properties and hydration processes of porphyrite-modified Portland cement were analyzed using X-ray diffraction (XRD), differential thermal analysis (DSC), and Fourier-transform infrared spectroscopy (FTIR). The compressive strength and setting time of cement samples were tested according to GOST 30744-2001 and GOST 310-91 standards. The results showed that porphyrite addition slightly slowed the hydration process, reducing C_3S content while promoting the formation of calcium hydroxide ($Ca(OH)_2$). Cement containing 20% porphyrite met the 32.5N strength class requirements and demonstrated stable mechanical properties. Water absorption tests confirmed a gradual hydration process, with no sudden crystallohydrate formation observed. This study confirms that porphyrite is an effective mineral additive, contributing to cement durability, reduced clinker consumption, and lower energy demand. Future research should focus on the long-term stability of porphyrite-based cement using advanced thermal analysis techniques.

Keywords: Pozzolanic activity, hydration process, calcium hydroxide ($Ca(OH)_2$), physicochemical properties, X-ray diffraction (XRD), differential thermal analysis (DSC).

Information about authors:

Iskandarova Mastura Iskandarovna
Doctor of Technical Sciences, Professor, Chief Scientific Researcher at the STROM Research Laboratory and Testing Center of the Institute of General and Inorganic Chemistry of the Academy of Sciences of Uzbekistan, 77 Mirzo Ulugbek Street, 100170, Tashkent, Uzbekistan. Email: mastura.iskandarova@mail.ru; ORCID ID: https://orcid.org/0000-0003-1152-8938

Atabaev Farrukh Bakhtiyarovich
Doctor of Technical Sciences, Professor, Chief Scientific Researcher at the STROM Research Laboratory and Testing Center of the Institute of General and Inorganic Chemistry of the Academy of Sciences of Uzbekistan, 77 Mirzo Ulugbek Street, 100170, Tashkent, Uzbekistan. Email: atabaev_farruh@mail.ru; ORCID ID: https://orcid.org/0009-0004-4941-5060

Khadzhiev Azamat Shamuratovich
Doctor of Philosophy in Technical Sciences, Associate Professor at the Faculty of Chemical Technology, Urgench State University named after Abu Rayhon Beruni, Urgench, H. Olimjon Street 14, 220100, Uzbekistan. Email: xadjiyev2019@mail.ru; ORCID ID: https://orcid.org/0000-0003-2131-8256

Introduction

In modern construction materials manufacturing, one of the pressing tasks is to improve the Portland cement production process and reduce its environmental impact. In traditional cement manufacturing, a significant amount of natural resources is consumed for clinker production, and during the thermal decomposition of carbonate raw materials, a large volume of CO_2 is released into the atmosphere. Studies show that CO_2 emissions from cement production account for approximately 7-8% of total industrial emissions [[1], [2]]. In this regard, extensive scientific research is being conducted to enhance the environmental sustainability of the cement industry and reduce its carbon footprint [[3], [4]].

The prospects for producing composite Portland cement using alternative mineral components are attracting the attention of researchers. In particular, it has been proven that the incorporation of natural and industrial mineral additives—such as silicate rocks, volcanic ash-based materials, and industrial by-products—improves the physical and mechanical properties of cement [[5], [6]]. For instance, studies conducted by Gartner et al. demonstrated that

adding silicon oxide-rich components to the cement composition not only preserves strength but also significantly reduces CO_2 emissions by decreasing the clinker content [[7], [8], [9], [10]].

Scrivener and co-authors studied technological solutions for the production of low-carbon cement and analyzed the effect of mineral additives on the hydration process [11]. The results of the study show that the addition of silicon oxide-rich mineral components to the cement composition increases their hydraulic activity while maintaining the strength of cement composites during long-term operation [12].

Moreover, according to the research conducted by Wang et al., additives in OPC (Ordinary Portland Cement) can significantly affect the cement hydration process. Experimental results showed a strength reduction of more than 30%, which was attributed to the retardation of the hydration process [[13], [14]]. These findings are crucial for studying the impact of porphyrite additives on cement hydration and its strength characteristics.

Studies indicate that the incorporation of natural silicate rocks, such as porphyrite, into construction materials can significantly enhance their physical, mechanical, and chemical properties. Porphyrite is a volcanic-origin rock, with silicon dioxide (SiO_2), aluminum oxide (Al_2O_3), and iron oxide (Fe_2O_3) as its main components. Due to its chemical composition, porphyrite exhibits pozzolanic and hydraulic activity, making it suitable for use in combination with various binding materials [[15], [16], [17], [18], [19]].

The production of composite cement with the addition of porphyrite has been recognized in recent years as one of the key innovative directions in the construction materials industry. This method enhances the overall energy efficiency of the cement manufacturing process and reduces its environmental impact. In traditional cement production, clinker is used as the main component; however, its calcination requires high temperatures (approximately 1450°C). This process consumes a significant amount of thermal energy and releases a large volume of CO_2 into the atmosphere due to the thermal decomposition of carbonate raw materials [[20], [21], [22]].

The incorporation of natural additives, such as porphyrite, into the cement composition allows for a reduction in clinker content, which, in turn, decreases the overall energy consumption during production. Additionally, due to the natural composition and chemical properties of porphyrite, its pozzolanic and hydraulic activity contributes to improving the physical and mechanical properties of cement. For example, silicon dioxide (SiO_2) and aluminum oxide (Al_2O_3) present in porphyrite actively participate in the hydration process, promoting the formation of additional binding phases, which positively affects the strength and durability of the material [23].

Reducing clinker content lowers emission levels, thereby contributing to the reduction of the carbon footprint in the construction materials industry. For this reason, cement production with porphyrite additives is not only economically beneficial but also highly relevant in terms of environmental sustainability.

Moreover, various studies show that the strength and durability of porphyrite-based types of cement can exceed that of traditional cement. Particularly under long-term operation, such cements demonstrate high resistance to moisture, sulfate ions, and other aggressive external factors. This expands the potential applications of porphyrite types of cement in road construction, marine infrastructure, and other structures exposed to harsh environments.

Silicon dioxide (SiO_2) present in porphyrite reacts with calcium hydroxide ($Ca(OH)_2$) when combined with cement or other hydraulic binders, forming additional calcium silicate hydrates (C-S-H) [[24], [25]]. This process enhances the density and strength of the material. As a result, the compressive and flexural strength of materials with porphyrite additives increases. Furthermore, aluminum oxide (Al_2O_3) and iron oxide (Fe_2O_3) in porphyrite improve the chemical stability of the material and its resistance to external influences.

In addition, due to its pozzolanic activity, porphyrite influences the hydration process of cement and other binding materials. During this process, the reactive ions of SiO_2 and Al_2O_3 present in porphyrite interact with the hydration products, strengthening the material's microstructure. For this reason, porphyrite additives are considered a promising component for the production of concrete and other high-strength construction materials.

Another important feature of porphyrite is its environmental efficiency. The production of traditional clinker-based binding materials requires significant energy consumption and is accompanied by carbon dioxide (CO_2) emissions into the atmosphere. The use of natural additives, such as porphyrite, helps reduce the carbon footprint of the production process. In this regard, in recent years, many researchers have been exploring the potential of porphyrite for the production of environmentally friendly binding materials.

This article presents a scientific analysis of the potential for producing composite Portland cement based on the clinker of Karakalpak Cement LLC and porphyrites from the Karatau deposit, as well as the changes in mineralogical composition, microstructure, and the increase in hydraulic activity as a result of mechanical activation of mineral additives.

The study aims to investigate the hydration kinetics, microstructure changes, and mechanical properties of composite cement based on porphyrite, as well as to assess its potential for industrial production.

In addition, this article provides a detailed examination of the possibilities of using porphyrites from the Karatau deposit in cement production, their impact on the hydration processes, and the physico-chemical properties of Portland cement.

Experimental part

As the research material, porphyrite from the "Karatau-1" section of the Karatau deposit was selected. The primary matrix for forming the compositions of composite Portland types of cement (CPC) was ordinary Portland cement clinker (Cl) from LLC "Karakalpak Cement." Gypsum stone (GS) from the Kogon deposit was used to regulate the setting time.

Standard methods corresponding to the following regulatory documents were used for conducting physico-chemical studies and physico-mechanical tests. The chemical analysis of Portland cement clinker from LLC "Karakalpak Cement," gypsum stone from the Kogon deposit, and porphyrite from the "Karatau-1" section of the Karatau deposit was carried out by GOST 5382-91 (“Cements and materials for cement production. Methods of chemical analysis”).

The hydraulic activity of porphyrite was determined according to O‘z DSt 336:2024 “Active mineral additives for cements. Technical requirements.” The results were evaluated according to the requirements of GOST 31108-2003 based on the Student's t-test criterion. The physico-mechanical properties of cement samples with porphyrite additives (PC) were studied according to GOST 310.4-81 “Types of cement. Methods for determining the strength limit in bending and compression.” The evaluation of the results was carried out according to the requirements of GOST 31108-2020 “Cements for general construction. Technical requirements.”

The physico-chemical properties of "green" cement composites were studied using the following analytical methods: X-ray phase analysis (X-ray diffractometer XRO–6100, Shimadzu), DTA – thermal analysis (Netzsch Simultaneous Analyzer STA 409 PG), IR spectroscopy (Fourier spectrometer “IRTracer-100,” SHIMADZU CORP), and electron microscopic analysis (scanning electron microscope JSM-6490LV with INCA Energy energy-dispersive microanalysis systems and HKL-Basic structural analysis).

Results and Discussion

The chemical and mineralogical composition of clinker during the cement production process directly affects its strength, hardening kinetics, and hydraulic activity. The composition of the portland cement clinker (PC) produced by "Karakalpak Cement" LLC meets the requirements of O‘z DSt 2801. This clinker contains the main oxides: CaO (58.93%), SiO_2 (18.03%), Al_2O_3 (6.22%), and Fe_2O_3 (3.94%), whose ratio determines the hydraulic activity of the clinker. A high sulfate content can affect the clinker hardening process; therefore, to enhance its hydraulic activity and stability, the use of mineral additives is advisable. The high content of alite (C_3S – 55.04%) and belite (C_2S – 17.81%) in the clinker ensures rapid hardening and positively influences the mechanical properties of the final product.

Porphyrite, being one of the natural silicate rocks, exhibits pozzolanic activity due to its high content of silica (SiO_2 – 51.42%) and aluminum oxide (Al_2O_3 – 18.51%). The mineralogical composition of porphyrite from the Karatau deposit allows it to be used as a pozzolanic additive in the production of Portland cement.

SiO_2 and Al_2O_3 contained in porphyrite react with $Ca(OH)_2$ during the hydration process, forming additional calcium silicate hydrate (C-S-H), which enhances the strength of concrete and other construction materials. Moreover, the presence of Fe_2O_3 (7.53%) and MgO (0.98%) in porphyrite ensures its chemical stability and increases the material's resistance to environmental impacts.

Gypsum stone is used in cement production as the primary setting regulator. When mixed with clinker, it prevents the excessive reaction of C_3A (tricalcium aluminate) with SO_3, thereby limiting the rapid setting of cement and providing the necessary time for its processing. In this study, the gypsum used contains 92.02% $CaSO_4 \cdot 2H_2O$, which indicates its high quality as an additive (Table 1).

Table 1 - Chemical composition of raw materials

Material name	Oxide content, mass %								
	k.m.y	SiO_2	$A1_2O_3$	Fe_2O_3	SaO	MgO	SO_3	Pr.	∑
Clinker PC	0.32	18.01	6.25	3.92	58.91	1.99	5.56	5.05	100.0
	Mineralogical composition of Clinker, mass %								
	C_3S-55.04; C_2S-17.81; C_3A-5.15; C_4AF-15.47; CS-1.65								
Porphyrite	5.71	51.43	18.52	7.52	5.27	3.9	0.92	6.82	100.0
Gypsum stone	20.31	2.79	0.48	сл.	30.99	сл.	42.81	2.62	100.0
	$CaSO_4.2N_2O$ = 42.80x2.15 = 92.02%								

The Karatau-1 deposit is located in the Karauzyak district of the Republic of Karakalpakstan, 80 km southeast of the Kegeyli settlement, with total reserves exceeding 63 million tons. The porphyritic rocks of this deposit consist of fine particles, have a light gray color, and may acquire a brownish tint due to the presence of iron oxides. Due to the high silicon dioxide content (SiO_2 – 51.42%), these rocks belong to the group of pyroxene porphyrites.

Research results confirm that the porphyrite composition includes quartz (SiO_2), feldspars ($KAlSi_3O_8$ – $NaAlSi_3O_8$ – $CaAl_2Si_2O_8$), micas (biotite and muscovite), as well as amphiboles and pyroxenes. These components provide porphyrite with high mechanical strength and chemical resistance. Infrared (IR) spectroscopy of the porphyrite sample revealed absorption peaks in the 400–1100 cm^{-1} range (Figure 1).

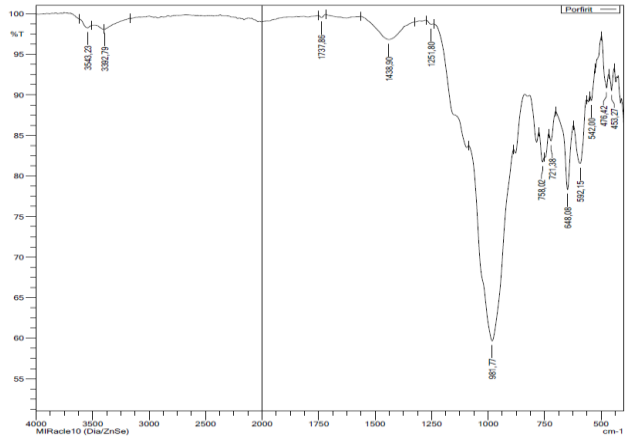

Figure 1 - Infrared (IR) spectroscopic analysis of porphyrite

The main recorded peaks are distributed as follows:

- 453.27 cm^{-1} and 470.42 cm^{-1} – Si-O-Al bonds typical for feldspars and amphiboles;
- 592.15 cm^{-1} and 648.08 cm^{-1} – stretching vibrations of pyroxenes and amphiboles;
- 721.38 cm^{-1} and 758.02 cm^{-1} – Si-O-Si bonds, indicating the presence of quartz and feldspars;
- 981.77 cm^{-1} – a pronounced absorption maximum associated with quartz stretching vibrations.

The physical and chemical properties of porphyrite allow its wide application in the construction industry. The high compressive strength and chemical resistance are associated with the following factors:

- High density and mechanical strength – due to the presence of hard minerals (quartz, feldspars, pyroxenes).
- Chemical resistance – the presence of silicates and oxide minerals makes porphyrite resistant to acidic and alkaline environments.
- Thermal stability – the content of silicon dioxide (SiO_2) and aluminosilicate minerals ensures the stability of the rock at high temperatures.

The results of the study show that porphyrite, due to its composition, can be used as a mineral additive in cement production. In particular, it has the potential to enhance the strength of cement and improve its hydraulic activity. Moreover, the use of porphyrite in road pavements and the production of durable construction materials is also considered feasible.

The mineralogical composition of porphyrite was determined based on the results of X-ray diffraction analysis (XRD). The most intense peaks on the diffractogram correspond to various minerals. A detailed analysis of the obtained data is provided below:

- Quartz (SiO_2) – d/n values (0.424; 0.333; 0.244; 0.228; 0.212; 0.182).
- Feldspars – d/n values (0.631; 0.495; 0.468; 0.400; 0.375; 0.365; 0.318; 0.291; 0.282; 0.182; 0.178).
- Calcite ($CaCO_3$) – d/n values (0.303; 0.249; 0.228; 0.209; 0.200; 0.188).

- Hydromicas (muscovite, biotite, etc.) – d/n values (0.495; 0.365; 0.352; 0.333; 0.303; 0.291; 0.282; 0.254).
- Chlorite minerals – d/n values (0.700; 0.631; 0.495; 0.468; 0.385; 0.375; 0.365; 0.291; 0.259; 0.244; 0.228; 0.212; 0.188; 0.182; 0.178; 0.156) (Figure 2).

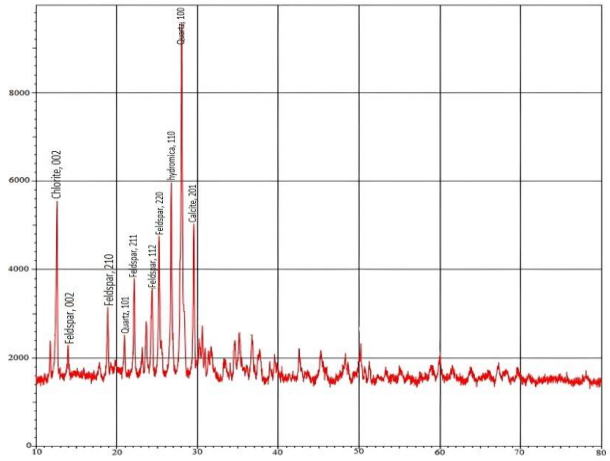

Figure 2 - X-ray diffraction (XRD) spectrum of porphyrite from the "Karatau-1" deposit

The presented image shows the XRD spectrum of porphyrite rock, containing various peaks. The most intense peaks on the diffractogram confirm the presence of quartz, feldspars, and hydromicas. Specifically, the peaks with d/n = 0.375 and 0.365 correspond to feldspars, indicating the predominance of silicate minerals in the composition of porphyrite. Additionally, the peaks with d/n = 0.424 and 0.333 indicate the dominant content of quartz.

The presence of hydromicas and chlorites in the composition of porphyrite affects its mechanical properties, allowing its use as an active mineral additive in cement compositions. Hydromicas and chlorites exhibit pozzolanic activity and contribute to the formation of calcium silicate hydrate (C-S-H), which provides additional strength during hydration.

To study the thermal properties of porphyrite, differential scanning calorimetry (DSC) analysis was conducted. According to the research results, a two-step water loss process is observed when heating porphyrite samples (Figure 3).

At the first stage (in the range of 25–140°C) at Tmax = 60°C, a pronounced endothermic effect was observed, associated with the release of water molecules adsorbed on the surface of porphyrite. The enthalpy of this reaction was -138.5 J/g, indicating a high content of free or weakly bound water in the porphyrite structure.

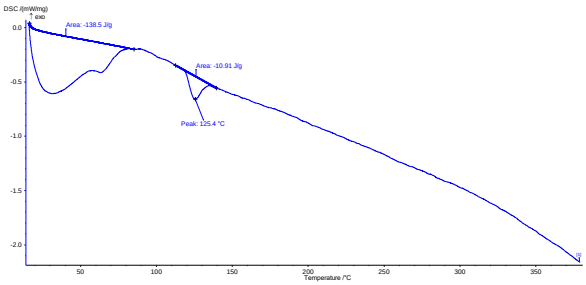

Figure 3 - Differential scanning calorimetry (DSC) analysis of porphyrite

In the second stage (Tmax = 125.4°C), the release of chemically bound water from the crystal lattice of the mineralogical composition of porphyrite occurred. This process is due to the thermal decomposition of hydrated minerals (e.g., hydromicas or chlorites), with the reaction enthalpy being -10.91 J/g. The obtained results are crucial for understanding the hydration properties of porphyrite in the cement production process. They serve as the basis for assessing the feasibility of using porphyrite as an active mineral additive in composite types of cement.

According to the study results, the hydraulic activity of porphyrite based on the Student's t-criterion was t = 24.47. This indicator significantly exceeds the threshold value of t = 2.07 established by the O‘z DSt 336:2024 standard. This proves that porphyrite possesses sufficient hydraulic activity and can be used as an active mineral additive in Portland cement.

Silicon dioxide (SiO_2) and other oxides present in porphyrite play a vital role in the hydraulic binding processes, contributing to the increased strength of cement. The conducted research has scientifically justified the potential of using porphyrite and sandstone as mineral additives in Portland cement production.

The production of composite cement based on porphyrite can not only improve product quality but also be economically efficient. The use of natural mineral additives reduces clinker consumption and helps decrease energy costs.

The addition of porphyrite to Portland cement clinker significantly affects the grinding process. According to the data presented in Table 2 and Figure 4, the research results show that as the amount of porphyrite increases, the fineness of the cement powder decreases. Sieve analysis through sieve №. 008 (4900 openings/cm²) revealed that the difference in fineness between pure Portland cement and types of cement with 10–25% porphyrite addition ranges from 0.5% to 2.0%.

Table 2 - The influence of porphyrite addition on the grindability of Portland cement clinker

№ p/p	Cement Designation	Component Ratio, wt. %		Grinding Time, min	Residue on Sieve № 008, wt. %
		Clinker + Gypsum stone	Porphyrite		
1	PC-D0	100	-	40	9.5
2	PC -D10	90	10	40	10
3	PC -D15	85	15	40	11
4	PC -D20	80	20	40	11.5
5	PC -D25	75	25	40	11.5

This process is explained by the fact that the physico-mechanical properties of porphyrite affect the grinding of clinker. Specifically, when milling the raw mix with the addition of porphyrite, the adhesion forces between particles and their density change, leading to a reduction in the number of fine fractions. This, in turn, influences the final particle size distribution of the cement and determines its rheological (flow) properties.

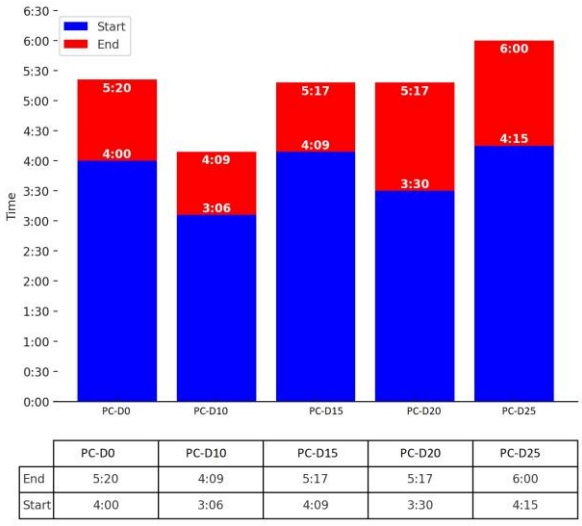

	PC-D0	PC-D10	PC-D15	PC-D20	PC-D25
End	5:20	4:09	5:17	5:17	6:00
Start	4:00	3:06	4:09	3:30	4:15

Figure 4 - The change in the setting time of portland cement produced by "Karakalpakcement" LLC depending on the porphyrite additive content (mass %): 1 - PC-D0 (0% porphyrite); 2 - PC-D10 (10% porphyrite); 3 - PC-D15 (15% porphyrite); 4 - PC-D20 (20% porphyrite); 5 - PC-D25 (25% porphyrite).

From the provided table and diagram, it is evident that increasing the porphyrite content reduces the cement setting time. Without additives, Portland cement (PC-D0) began its initial setting after 4 hours, while the final setting lasted 5 hours and 35 minutes. With the addition of 10% porphyrite (PC-D10), the initial setting time decreased to 3 hours and 15 minutes, while the final setting was completed within 4 hours and 15 minutes. As the porphyrite content increased, the initial setting time was further reduced, and with 25% porphyrite (PC-D25), it dropped to 3 hours and 5 minutes, with the final setting occurring in 4 hours and 10 minutes.

These results show that porphyrite reacts with clinker, accelerating the cement hydration process. This reduces the time required to achieve initial strength, making the cement more convenient for use in construction processes within shorter periods.

To determine the actual hydraulic activity of the cement, a technological batch was prepared, containing 80% clinker and 20% porphyrite, in accordance with the requirements of GOST 30744-2001. The resulting cement was tested following the methodology of GOST 310-91 using standard prismatic samples with dimensions of 4×4×16 cm (Table 3).

According to the table, increasing the porphyrite content significantly affects the compressive strength of the cement.

Cement with 100% clinker showed the highest strength:

- 2 days – 34.1 MPa
- 7 days – 36.0 MPa
- 28 days – 48.0 MPa

With the addition of 10% porphyrite, the strength slightly decreased:

- 2 days – 27.0 MPa
- 7 days – 31.0 MPa
- 28 days – 36.5 MPa

With 15–25% porphyrite content, the strength decreased even further. For cement with 25% porphyrite, the strength after 28 days was 31.8 MPa.

Table 3 - Physical and mechanical properties of types of cement with porphyrite additive

№	Mass percentage of component ratio		Compressive strength of 2×2×2 cm cube samples, MPa		
	Clinker	Porphyrite	2 days	7 days	28 days
1	100	-	34.1	36.0	48.0
2	90	10	27.0	31.0	36.5
3	85	15	25.1	29.0	35.0
4	80	20	20.5	28.8	34.5
5	75	25	20.0	28.0	31.8
Flexural/compressive strength of standard sanded Portland cement specimens measuring 4×4×16 cm, MPa					
			2 days	7 days	28 days
1	Clinker 100%	-	-	-	7.2/38.6
2	Clinker 80%	20%	4.9/24.2	5.8/32.5	6.9/34.6

Table 4 - Changes in the hydration activity of portland cement with porphyrite additives

№	**Cement type**	**Amount of chemically bound water (%) at the following time intervals:**			
		2 days	7 days	28 days	90 days
1	PC-D0	11.89	13.4	19.54	17.56
2	PC with Porphyrite additive	11.61	11.47	13.63	15.26

The analysis shows that the porphyrite additive affects the cement strength (Table 4). However, cement with 20% porphyrite meets the requirements of grade PC-D20 (32.5N). Such cement reached a strength of 32.5 MPa after 7 days, which complies with the requirements of GOST 30744-2001. Cement with 80% clinker and 20% porphyrite demonstrates optimal strength characteristics. Based on the results of 28-day tests, cement with 20% porphyrite achieved a cement strength subclass of 32.5N, confirming its suitability for construction use (Figure 5).

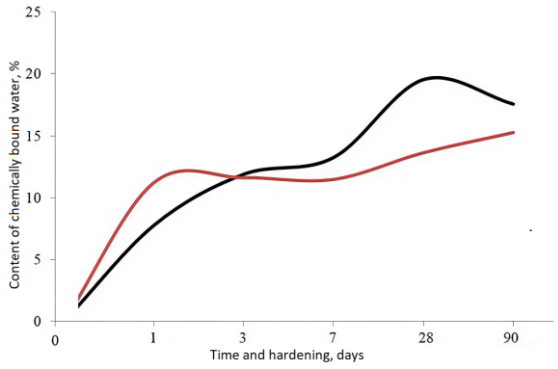

Figure 5 - The change in the content of chemically bound water during the hardening process of blended types of cement depending on the porphyrite content: №1 (————) PC-D0 (pure portland cement); №2 (————) PC-D20-PO (portland cement with 20% porphyrite addition).

These results validate the stability of the mechanical properties of types of cement with porphyrite additives and their potential application as building materials.

The hydration results of Portland cement with porphyrite additives indicate that porphyrite extracted from the "Koratov-1" site of the Koratov deposit modifies the hydration process of Portland cement. In such cement, water absorption decreased to 0.28–1.77% within 2–7 days, and by the 28th day, the amount of bound water became nearly identical (18.63% and 19.54%).

The introduction of porphyrite led to a 20% reduction in C_3S content, causing a slight slowdown in the hydration process. However, the resulting cement stone demonstrated high strength, meeting the strength class 32.5N requirements.

After three months of observation, the amount of bound water reached 15%, which is 2.3% lower compared to conventional cement. This indicates a gradual hydration process and the absence of rapid crystallohydrate formation, which contributes to enhanced durability and strength of the cement.

On the diffractograms of cement with the addition of porphyrite, prominent lines of calcium hydroxide and calcium carbonate were observed within the first day, with their intensity remaining almost unchanged for up to three days (Figure 6).

The study results demonstrate that the addition of porphyrite significantly affects the hydration

process of Portland cement. The data on the change in the amount of chemically bound water correspond to the XRD results. Although, at the initial stage (within the first day), the amount of chemically bound water in cement with porphyrite is higher, at the 28-day and 90-day intervals, this indicator is lower compared to traditional Portland cement (PC-D0), indicating a slight deceleration of the hydration process.

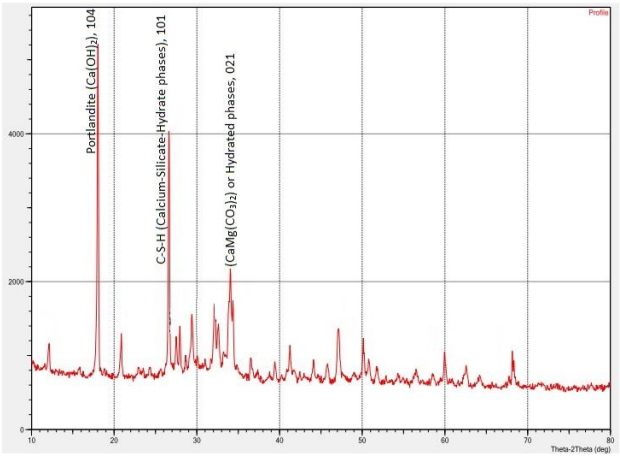

Figure 6 - X-ray Diffraction Pattern of Portland Cement with 20% Porphyrite Addition, Hydrated in Water for 28 Days

The diffractogram clearly shows distinct lines corresponding to calcium hydroxide ($Ca(OH)_2$) and calcium carbonate ($CaCO_3$), indicating the parallel progression of hydration and carbonation processes.

During hydration, the presence of hydrated calcium silicate phases (C-S-H) was also detected, which form as a result of the decomposition of C_3S (alite) and C_2S (belite). However, the addition of porphyrite slightly slows down this process, which may reduce the early strength development rate of the cement but does not affect its final strength.

Conclusions

In the course of the conducted research, the hydration processes of Portland cement with the addition of porphyrite, as well as its physico-chemical properties, were studied. The obtained results showed the following:

• Hydration process – the addition of porphyrite slightly slowed down the cement hydration rate; however, the final degree of hydration did not significantly affect the cement strength. This is mainly due to the reduction in C_3S content and the formation of calcium hydroxide ($Ca(OH)_2$) in the cement system.

• Chemically bound water content – an increase in the amount of bound water was observed during the first day, but at the 28- and 90-day intervals, this indicator was lower than that of traditional Portland cement (PC-D0), indicating a gradual hydration process.

• X-ray phase analysis (XRD) – distinct lines of calcium hydroxide and calcium carbonate were clearly recorded in the cement with porphyrite addition, with their intensity remaining unchanged during the first three days. This confirms the slower hydration of minerals in the cement system.

• Mechanical properties – the strength indicators of cement stone with porphyrite addition meet the requirements of strength subclass 32.5N cement, ensuring its stability.

These results confirm that the use of porphyrite as an additive can be an effective solution in cement production, offering an alternative raw material. Further, more detailed studies on the long-term stability of cement with porphyrite addition, using thermal analysis and other physico-chemical methods, are necessary.

Conflicts of interest. On behalf of all authors, the corresponding author states that there is no conflict of interest.

CRediT author statement: **M. Iskandarova**: Conceptualization, Methodology, Software; **F. Atabaev**: Data curation, writing draft preparation; A. **Khadzhiev**: Visualization, Investigation; A. **Khadzhiev**: Supervision; A. **Khadzhiev**: Software, Validation; **A. Khadzhiev**: Reviewing and Editing.

Acknowledgements. We express our deep gratitude to **Atabaev Farrukh Bakhtiyarovich**, Chief Scientific Researcher at the "STROM" Research Laboratory and Testing Center of the Institute of General and Inorganic Chemistry of the Academy of Sciences of Uzbekistan, for his practical assistance in conducting the experiments for this research. We also extend our sincere appreciation to **Jumaniyazov Arslon G'anibek o'g'li** for his translation support and language-related matters, as well as to the co-authors for their contributions to the writing and editing of the article.

Formatting of funding sources. This research did not receive any specific grant from funding agencies in the public, commercial, or not-for-profit sectors.

Cite this article as: Iskandarova MI, Atabaev FB, Khadzhiev ASh. Utilization of Natural Silicate Rocks to Reduce the Carbon Footprint in the Cement Industry. Kompleksnoe Ispolzovanie Mineralnogo Syra = Complex Use of Mineral Resources. 2026; 338(3):40-50. https://doi.org/10.31643/2026/6445.27

Цемент өнеркәсібіндегі көміртегі мөлшерін азайту үшін табиғи силикат жыныстарын пайдалану

[1] Искандарова М.И., [1] Атабаев Ф.Б., [2*]Хаджиев А.Ш.

[1] Өзбекстан ҒА Жалпы және бейорганикалық химия институты, Ташкент
[2] Әбу Райхан Беруни атындағы Үргеніш мемлекеттік университеті, Үргеніш, Өзбекстан

Мақала келді: *15 наурыз 2025*
Сараптамадан өтті: *19 наурыз 2025*
Қабылданды: *17 сәуір 2025*

ТҮЙІНДЕМЕ

Портландцемент өндірісі көп энергияны тұтынады және CO_2-ның шығарындылары бар. Бұл экологиялық тұрақтылықты жақсарту үшін балама шикізат қажет болатынын көрсетеді. Зерттеу нәтижелері табиғи силикат жынысы порфириттің пуццоландық және гидравликалық белсенділігін көрсетті, бұл оны композиттік цемент өндірісінде перспективалы қоспаға айналдырады. Бұл зерттеуде порфиритпен модификацияланған портландцементтің физика-химиялық қасиеттері мен гидратация процестері рентгендік дифракция (XRD), дифференциалды термиялық талдау (DSC) және Фурье-трансформациялық инфрақызыл спектроскопия (FTIR) көмегімен талданды. Цемент үлгілерінің қысу күші мен қату уақыты МемСТ 30744-2001 және МемСТ 310-91 стандарттары бойынша тексерілді. Нәтижелер көрсеткендей, порфирит қосылғанда гидратация процесі аздап баяулайды, C_3S мөлшері азаяды, бұл кальций гидроксидінің ($Ca(OH)_2$) түзілуіне ықпал етеді. Құрамында 20% порфирит бар цемент 32,5N беріктік класының талаптарына сай болды және тұрақты механикалық қасиеттерді көрсетті. Суды сіңіру сынақтары кристаллогидрат кенеттен түзілмейтінін, гидратация процесі біртіндеп жүретінін растады. Бұл зерттеу порфирит цементтің беріктігіне, клинкерді тұтынуды азайтуға және энергияға сұранысты төмендетуге ықпал ететін тиімді минералды қоспа екенін дәлелдеді. Болашақ зерттеулерде озық термиялық талдау әдістерін қолдана отырып, порфирит негізіндегі цементтің ұзақ мерзімді тұрақтылығына назар аудару керек болады.

Түйін сөздер: Поцзоландық белсенділік, гидратация процесі, кальций гидроксиді ($Ca(OH)_2$), физика-химиялық қасиеттері, рентген сәулелерінің дифракциясы (XRD), дифференциалды термиялық талдау (DSC).

Авторлар туралы ақпарат:

Искандарова Мастура Искандаровна
Техника ғылымдарының докторы, профессор, Өзбекстан Ғылым академиясы Жалпы және бейорганикалық химия институтының STROM ғылыми-зерттеу зертханасы және сынақ орталығының бас ғылыми қызметкері, Мирзо Улугбек көш., 77, 100170, Ташкент, Өзбекстан. Email: mastura.iskandarova@mail.ru; ORCID ID: https://orcid.org/0000-0003-1152-8938

Атабаев Фаррух Бахтиярович
Техника ғылымдарының докторы, профессор, Өзбекстан Ғылым академиясы Жалпы және бейорганикалық химия институтының STROM ғылыми-зерттеу зертханасы және сынақ орталығының бас ғылыми қызметкері, Мирзо Улугбек көш., 77, 100170, Ташкент, Өзбекстан. Email: atabaev_farruh@mail.ru; ORCID ID: https://orcid.org/0009-0004-4941-5060

Хаджиев Азамат Шамуратович
Техника ғылымдары бойынша философия докторы, Әбу Райхон Беруни атындағы Үргеніш мемлекеттік университетінің химия-технология факультетінің доценті, Үргеніш қ. Х.Олимжон, 14, 220100, Өзбекстан. Email: xadjiyev2019@mail.ru; ORCID ID: https://orcid.org/0000-0003-2131-8256

Использование природных силикатных пород для снижения углеродного следа в цементной промышленности

[1] Искандарова М.И., [1] Атабаев Ф.Б., [2*]Хаджиев А.Ш.

[1] Институт общей и неорганической химии Академии наук Узбекистана, Ташкент
[2] Ургенчский государственный университет имени Абу Райхона Беруни, Ургенч, Узбекистан

АННОТАЦИЯ

Производство портландцемента сопровождается высоким энергопотреблением и выбросами CO_2, что подчеркивает необходимость использования альтернативного сырья для повышения экологической устойчивости. Результаты исследований показывают, что порфирит, являющийся природной силикатной породой, обладает пуццоланической и

Поступила: *15 марта 2025*
Рецензирование: *19 марта 2025*
Принята в печать: *17 апреля 2025*

гидравлической активностью, что делает его перспективной добавкой при производстве композитного цемента. В данном исследовании были проанализированы физико-химические свойства и процессы гидратации портландцемента, модифицированного порфиритом, с использованием рентгеновской дифракции (XRD), дифференциального термического анализа (DSC) и инфракрасной спектроскопии с преобразованием Фурье (FTIR). Прочность на сжатие и время схватывания цементных образцов определяли в соответствии со стандартами ГОСТ 30744-2001 и ГОСТ 310-91. Результаты показали, что добавление порфирита несколько замедляет процесс гидратации, снижая содержание C_3S, но способствует образованию гидроксида кальция ($Ca(OH)_2$). Цемент с 20% содержанием порфирита соответствовал требованиям прочностного класса 32.5N и демонстрировал стабильные механические свойства. Испытания на водопоглощение подтвердили постепенный процесс гидратации без резкого образования кристаллогидратов. Данное исследование подтверждает, что порфирит является эффективной минеральной добавкой, способствующей повышению долговечности цемента, снижению потребления клинкера и уменьшению энергозатрат. В дальнейшем рекомендуется изучить долгосрочную стабильность цемента с добавлением порфирита с применением передовых методов термического анализа.

Ключевые слова: Пуццолановая активность, процесс гидратации, гидроксид кальция ($Ca(OH)_2$), физико-химические свойства, рентгеновская дифракция (XRD), дифференциальный термический анализ (DSC).

Информация об авторах:

Искандарова Мастура Искандаровна
Доктор технических наук, профессор, главный научный сотрудник научно-исследовательской лаборатории и испытательного центра STROM Института общей и неорганической химии Академии наук Узбекистана, улица Мирзо Улугбека, 77, 100170, Ташкент. Email: mastura.iskandarova@mail.ru; ORCID ID: https://orcid.org/0000-0003-1152-8938

Атабаев Фаррух Бахтиярович
Доктор технических наук, профессор, главный научный сотрудник научно-исследовательской лаборатории и испытательного центра STROM Института общей и неорганической химии Академии наук Узбекистана, улица Мирзо Улугбека, 77, 100170, Ташкент. Email: atabaev_farruh@mail.ru; ORCID ID: https://orcid.org/0009-0004-4941-5060

Хаджиев Азамат Шамуратович
Доктор философии в области технических наук, доцент факультета химической технологии Ургенчского государственного университета имени Абу Райхона Беруни, Ургенч, улица Х. Олимжона, 14, 220100, Узбекистан. Email: xadjiyev2019@mail.ru; ORCID ID: https://orcid.org/0000-0003-2131-8256

References

[1] Gartner E. Industrially interesting approaches to low-CO_2 cements. Cement and Concrete Research. 2011; 41(7):736-749. https://doi.org/10.1016/j.cemconres.2011.03.019

[2] Licht S. Co-production of cement and carbon nanotubes with a carbon negative footprint. Journal of CO_2 Utilization. 2017; 18:378-389. https://doi.org/10.1016/j.jcou.2017.02.011

[3] Mohammad M, & Ehsani M. A quantitative investigation of CO_2 sequestration by mineral carbonation. Physics-Geophysics. 2015. https://doi.org/10.48550/arXiv.1512.05189

[4] Scrivener KL. Options for the future of cement." Indian Concrete Journal. 2018; 92(7):11-21.

[5] Juenger MCG, & Siddique R. Recent advances in understanding the role of supplementary cementitious materials in concrete. Cement and Concrete Research. 2010; 41(12):1232-1243. https://doi.org/10.1016/j.cemconres.2010.09.011

[6] Mehta PK. Reducing the environmental impact of concrete. Concrete International. 2001; 23(10):61-66.

[7] Snellings R, Mertens G, & Elsen J. Supplementary cementitious materials." Reviews in Mineralogy and Geochemistry. 2012; 74(1):211-278. https://doi.org/10.2138/rmg.2012.74.6

[8] Shi C, & Qian J. High performance cementing materials from industrial slags—a review. Resources, Conservation and Recycling. 2000; 29(3):195-207. https://doi.org/10.1016/S0921-3449(99)00060-9

[9] Gartner E, & Hirao H. A review of alternative approaches to the reduction of CO_2 emissions associated with the manufacture of the binder phase in concrete. Cement and Concrete Research. 2015; 78:126-142. https://doi.org/10.1016/j.cemconres.2015.04.012

[10] Juenger MCG, Snellings R, & Bernal SA. Supplementary cementitious materials: New sources, characterization, and performance insights. Cement and Concrete Research. 2019; 122:257-273. https://doi.org/10.1016/j.cemconres.2019.05.008

[11] Scrivener K L, John VM, & Gartner EM. Eco-efficient cements: Potential economically viable solutions for a low-CO_2 cement-based materials industry. United Nations Environment Program Report. 2018.

[12] Dhandapani Y, Santhanam M, & Gettu R. Performance of blended cements with supplementary cementitious materials: A review. Construction and Building Materials. 2021; 293:123524. https://doi.org/10.1016/j.conbuildmat.2021.123524

[13] Wang L, Wang D, Zhang Y, & Gao Y. Hydration and strength evolution of Portland cement blended with chemically modified mineral additives. Construction and Building Materials. 2018; 171:531-539. https://doi.org/10.1016/j.conbuildmat.2018.03.170

[14] Smith J, & Brown R. Pozzolanic properties of natural silicate rocks in cement production. Construction Materials Journal. 2021.

[15] Yang Y, Lepech MD, Yang EH, & Li VC. Autogenous healing of engineered cementitious composites under wet–dry cycles. Cement and Concrete Research. 2009; 39(5):382-390. https://doi.org/10.1016/j.cemconres.2009.01.013

[16] Li VC, & Herbert E. Robust Self-Healing Concrete for Sustainable Infrastructure. Journal of Advanced Concrete Technology. 2012; 10(6):207-218. https://doi.org/10.3151/jact.10.207

[17] Ataíde A, & Liborio J B L. Use of volcanic rock powder in concrete as a partial substitute of cement. Construction and Building Materials. 2016; 121:1-8. https://doi.org/10.1016/j.conbuildmat.2016.05.146

[18] Kramar S, & Mladenovič A. The influence of natural pozzolan addition on the properties of lime–cement pastes. Construction and Building Materials. 2013; 47:354-361. https://doi.org/10.1016/j.conbuildmat.2013.05.066

[19] Massazza F. Pozzolana and Pozzolanic Cements. In: P. Hewlett, Ed., Lea's Chemistry of Cement and Concrete, Arnold, London. 1998, 471-631.

[20] Habert G, d'Espinose de Lacaillerie J B, & Roussel N. An environmental evaluation of geopolymer based concrete production: reviewing current research trends. Journal of Cleaner Production. 2011; 19(11):1229-1238. https://doi.org/10.1016/j.jclepro.2011.03.01

[21] Müller CJ, & Harnisch J. A blueprint for a climate friendly cement industry. Cement and Concrete Research. 2008; 38(5): 712-715. https://doi.org/10.1016/j.cemconres.2008.02.002

[22] Damtoft JS, Lukasik J, Herfort D, Sorrentino D, & Gartner EM. Sustainable development and climate change initiatives. Cement and Concrete Research. 2008; 38(2):115-127. https://doi.org/10.1016/j.cemconres.2007.09.008Scrivener

[23] Scrivener KL, & Gartner E. Eco-friendly cementitious materials: Challenges and opportunities. Cement and Concrete Research. 2018.

[24] Turayev X X, Mukimov AS, Tojiyev PJ, & Karimov MU. Physical and chemical properties of micro-silica cement composite. Uzbekistan Chemistry Journal. 2023; (4):20-30.

[25] Adilhodzhaev AI, Shipacheva E, Shaumarov S, & Umarov K. On the method of assessing the structure of cellular concretes. Railway Transport: Current Tasks and Innovations. 2019; 1(3):18-26.

Crossref

DOI: 10.31643/2026/6445.28
Engineering and Technology

Effect of Rice Straw on the Mechanical and Biodegradability Properties of the Poly (Polyethylene-G-Acrylic Acid)

[1,2*]Yeligbayeva G., [3]Orazalin Zh.K., [4]Abdassalam A. Alfergani, [5]Omirzakova K.K., [5]Milissova N.B., [6]Eny Kusrini

[1]Institute of Organic Synthesis and Carbon Chemistry of the Republic of Kazakhstan, Karaganda
[2] Satbayev University, Almaty, Kazakhstan
[3] Kazakh-British Technical University, Almaty, Kazakhstan
[4]Sirte University, Sirte, Libya
[5]S.D. Asfendiyarov Kazakh National Medical University, Almaty, Kazakhstan
[6]Universitas Indonesia, Kampus Baru UI, Depok 16424, Indonesia

**Corresponding author: Yeligbayeva G.Zh, gulzhakh@yandex.ru*

Received: *March 25, 2025*
Peer-reviewed: *March 28, 2025*
Accepted: *April 21, 2025*

ABSTRACT

A polyethylene/acrylic copolymer was synthesized using a grafting technique with benzoyl peroxide as a catalyst and xylene as a solvent. Acrylic acid (AA) was grafted onto polyethylene (PE) in a 1:5 ratio. The resulting grafted copolymer, characterized by FTIR, was blended with rice straw at varying percentages of 3%, 5%, and 7% to produce biodegradable films. The properties of these films in water were evaluated through analyses of viscosity, tensile strength, elongation at break, water contact angle, and solubility. Incorporating rice straw enhanced the grafted copolymer's biodegradability, resulting in increased viscosity, tensile strength, and elongation at break of the films, while reducing the water contact angle and solubility. However, incorporating 7% rice straw in the grafted copolymer-based on PE (1.0%) and AA (5.0%) resulted in increases in viscosity, tensile strength, and elongation at break by 29.5%, 46.1%, and 9.6%, respectively, while reducing the contact angle and biodegradability solubility time at 45°C by 25.8%.

Keywords: Polyethylene, acrylic acid, rice straw, biodegradable, mechanical, sustainability.

Information about authors:

Yeligbayeva Gulzhakhan Zhakparovna — *Professor at the School of Petroleum Engineering, Satbayev University, 22 Satpayev Street, 050013, Almaty; Institute of Organic Synthesis and Carbon Chemistry of the Republic of Kazakhstan, Karaganda, Kazakhstan. Email: g.yeligbayeva@satbayev.university; ORCID ID: https://orcid.org/0000-0002-7098-5437*

Orazalin Zhandos Kairatuly — *PhD student at the School of Materials Science and Green Technologies, Kazakh-British Technical University, 59 Tole bi Street, 050000, Almaty, Kazakhstan. Email: zhandos1403@bk.ru; ORCID ID: https://orcid.org/0009-0002-0835-8392*

Abdassalam A. Alfergani — *Professor at Chemistry Department, Faculty of Education, Sirte University, Sirte, Libya. Email: abdassalamtameem@yahoo.com; ORCID ID: https://orcid.org/0009-0009-6632-2380*

Omirzakova Kulshat — *Candidate at the Department of Biochemistry, School of General Medicine-1, S.D. Asfendiyarov Kazakh National Medical University, 151 Bogenbay Str., Almaty 480012, Kazakhstan. Email: omirzakova.k@kaznmu.kz*

Milissova Nazerke — *Master's in Department of Engineering disciplines and Proper Practices, School of Pharmacy, S.D. Asfendiyarov Kazakh National Medical University, 151 Bogenbay Str., Almaty 480012, Kazakhstan. Email: milisova.n@kaznmu.kz; ORCID ID: https://orcid.org/0000-0001-7833-6258*

Eny Kusrini — *Professor at Department of Chemical Engineering, Universitas Indonesia, Kampus Baru UI, Depok 16424, Indonesia. Email: eny.k@ui.ac.id; ORCID ID: https://orcid.org/0000-0002-7919-0083*

Introduction

Synthetic polymers, such as polyethylene and polypropylene, have become widely used as packing materials due to their advantageous physico-mechanical properties and cost-effectiveness [1]. However, polyethylene and polypropylene, non-biodegradable polymers contribute to the growing challenge of plastic waste management, with their quantities increasing each year [[2], [3], [4]]. Recent studies highlight the importance of pinpointing plastic waste sources and differentiating polymers by structural traits, including their crystalline and amorphous forms [5]. Such distinctions are vital for understanding how these materials affect aquatic ecosystems and organisms [6]. Beyond being highly toxic, the key chemicals used in manufacturing plastic bags, such as polyethylene, polypropylene, benzene and vinyl chloride, are known carcinogens [[6], [7]]. These, along with gaseous and liquid

hydrocarbons, not only pose serious health risks but also contribute significantly to environmental degradation. Numerous methods, including blending, derivation, and graft copolymerization, have been extensively studied to improve the characteristics of synthetic polymers using starch; this is attributed to its complete biodegradability [[8], [9], [10]]. Modified polyethylene using grafting polymerization with starch in the presence of benzoyl peroxide as a catalyst and xylene as a solvene. The ratio between PE and starch was 1: 5 w/w%. The grafted copolymer was combined with rice straw, wheat straw, and calcium carbonate ($CaCO_3$) as a filler to produce biodegradable films. Starch, calcium carbonate ($CaCO_3$), and rice and wheat straws enhanced the biodegradability of the grafted copolymer. The inclusion of $CaCO_3$, alongside rice and wheat straws, increased the viscosity and tensile properties [11]. Rice straw fiber-reinforced high-density polyethylene (HDPE) composites were developed to explore how rice straw fiber morphology and varying concentrations of maleic anhydride polyethylene (MAPE) influence their mechanical and thermal properties. The result showed that higher aspect ratio rice straw fibers were utilized to enhance tensile strength, while lower aspect ratio fibers were applied to improve the flexural strength of the composites. An increase in rice straw fiber content from 20 to 40 wt% within the HDPE matrix slightly boosted flexural strength; however, impact strength dropped significantly due to the fiber's stiffness. The addition of MAPE to the system improved tensile, flexural, and impact strength for composites containing 20 wt% rice straw fiber, although it led to a marginal reduction in tensile elongation at break [12]. This study investigates the modification of polyethylene via graft polymerization, using acrylic acid as the grafting monomer and benzoyl peroxide as the catalytic initiator. The modified polymer is subsequently blended with rice straw to enhance its mechanical properties.

Materials and Methods

Low density polyethylene (PE), xylene, benzoyl peroxide, and acrylic acid (AA) were purchased from Sigma-Aldrich Company (USA). Rice straw was gathered from the fields and allowed air to dry. The dried straw was subsequently cut into pieces measuring 2–5 mm in length and milled into a fine powder.

Synthesis of polyethylene-g-acrylic acid P(PE-g-AA)

Graft polymerization was conducted in a three-necked flask equipped with a mechanical stirrer under a nitrogen atmosphere. Polyethylene (1.0 g) was dissolved in xylene (50 g) by stirring in a water bath maintained at 80°C. Once dissolved, benzoyl peroxide (0.1 g) was introduced as a catalytic initiator. After 5 minutes, acrylic acid (5 g) was added as the grafting monomer. The reaction mixture was maintained at 80°C for 3 hours under constant stirring in a nitrogen environment. The resulting product was precipitated using 2-propanol, air-dried at room temperature, and subsequently oven-dried at 60°C to achieve a constant weight.

Film formation

For the first film, polyethylene-g-acrylic acid P(PE-g-AA) was incorporated into glycerol at 50°C and stirred for 30 minutes until achieving homogeneity. The resulting material was cast onto a levelled surface and designated as PEA. For the second film, the fully grafted copolymer was dissolved in glycerol, followed by the addition of rice straw in varying proportions (3, 5, and 7 w/w%). The mixture was then milled for 40 minutes, cast onto a leveled surface, and labeled as PEAS. All films were left to dry at room temperature for 10 days before being stored in a desiccator at ambient conditions for subsequent characterization and analysis.

Measurements

FTIR absorbance spectra were acquired using a Bruker Tensor 37 FTIR spectrometer, with spectral data collected in the range of 4000–400 cm^{-1}. The viscosity (η) of the dispersions was measured with a Brookfield viscometer (Model LVTDV-II) at a shear rate of 100 s^{-1} and a temperature of 25°C. The contact angle between water droplets and the sample surface was determined using a CAHN DCA-322 contact angle analyzer at 25°C, operating at a velocity of 100 µm/s. A microsyringe was used to deposit water droplets onto the sample surface, and contact angles were measured via monitor observation, with three measurements taken at different locations on the film. Mechanical properties, including tensile strength and elongation at break, were evaluated following ASTM D882-91 [13] standards using an MTS 10/M tensile testing machine at a crosshead speed of 50 mm/min. A minimum of three readings was averaged, with a 1-kN load cell employed during the testing process. Thermogravimetric analysis (TGA) was performed using METTLER TOLEDO's TGA/SDTA851e system

with aluminum-crimped pans under a nitrogen flow of 20 mL/min. The analysis covered a temperature range of 100–500°C at a heating rate of 10°C/min, allowing for the determination of degradation temperature and thermal stability.

Results and discussion of FTIR analysis

Figure 1 presents the FTIR spectra of polyethylene (PE), highlighting key characteristic peaks. The peaks observed at 2914 cm^{-1} and 2847 cm^{-1} correspond to the asymmetric stretching vibrations of CH_2 groups. Additionally, the peak at 1463 cm^{-1} indicates bending deformation, while the peak at 719 cm^{-1} is attributed to rocking deformation [14]. Figure 2 illustrates the FTIR absorbance spectra of PE-g-AA, revealing new characteristic peaks. A peak at 2848 cm^{-1} corresponds to C-H stretching, while peaks at 1370 cm^{-1} and 738 cm^{-1} are attributed to the C-H vibrations of ethylene groups. Additionally, a peak at 1179 cm^{-1} signifies C-O-C stretching, 1462 cm^{-1} related to CH2 scissor, 980 cm^{-1} to CH_2 twist, 809 cm^{-1} to CH bend and the presence of a peak at 1722 cm^{-1} indicates the carbonyl group, which confirms the successful grafting of polyethylene with acrylic acid (AA) [[15], [16], [17]].

Viscosity

Table 1 demonstrates the viscosity enhancement of the P(PE-g-AA) when blended with rice straw. For instance, incorporating 3% rice straw into P(PE-g-AA) increased its viscosity from 475 mPa·s to 560 mPa·s. With a further increase in rice straw content to 5%, the mixture's viscosity rose to 573 mPa·s, while 7% rice straw achieved the highest viscosity of 615 mPa·s. This viscosity increase can be attributed to the more polar nature and larger surface area of rice straw, which significantly improves the interaction and viscosity relative to the grafted copolymer [[18], [19]]. Consistent with the findings previously reported by the authors [11], the viscosity of polyethylene/starch films increases with the incorporation of rice straw

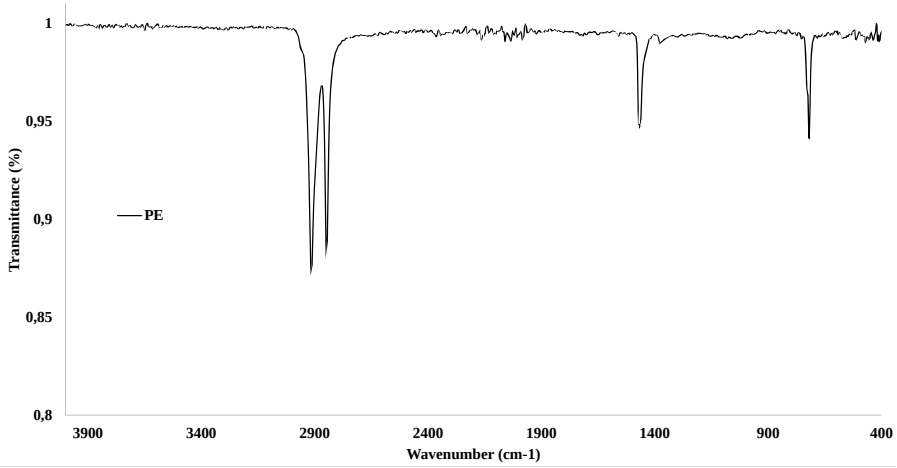

Figure 1 - FTIR spectra of polyethylene (PE)

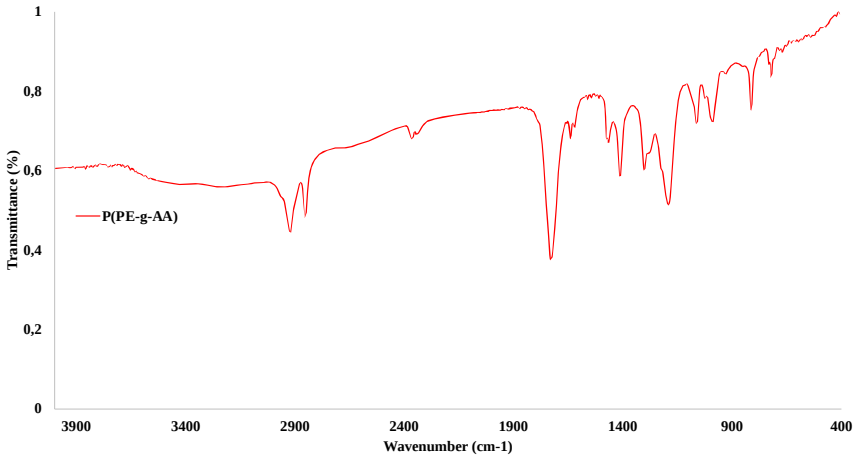

Figure 2 - FTIR spectra of the P(PE-g-AA)

Table 1 - Viscosity values for the P(PE-g-AA) and its mixture with glycerol, rice straw

Samples	Composition	Viscosity (mPa-s)
PEA	P(PE-g-AA), glycerol	475
PEAS1	P(PE-g-AA), glycerol, and rice straw 3%	560
PEAS2	P(PE-g-AA), glycerol, and rice straw 5%	573
PEAS3	P(PE-g-AA), glycerol, and rice straw 7%	615

Table 2 - Water contact angles of P(PE-g-AA) and the grafted copolymer mixed with rice straw

Sample Number	Contact angle (deg)
PEA	102
PEAS1	98
PEAS2	95
PEAS3	89

Table 3 - Mechanical properties of P(PE-g-AA) and the grafted copolymer mixed with rice straw

Samples	Tensile strength (MPa)	Elongation (%)
PEA	25.2	114
PEAS1	27.6	119
PEAS2	32.5	122
PEAS3	36.8	125

Water contact angle

The water contact angle serves as a critical parameter for assessing the hydrophilicity of dried polymer films. As shown in Table 2, incorporating rice straw into P(PE-g-AA) resulted in a progressive decrease in the water contact angle, with the addition of rice straw yielding the lowest values. Specifically, the integration of 3% rice straw reduced the water contact angle of the grafted copolymer by 3.6%, while 5% rice straw further decreased it by 6.8%. The addition of 7% rice straw exhibited the greatest impact, enhancing hydrophilicity by 12.7%. The hydrophilicity of these polymers is influenced by various factors, including the type of polymer matrix, additives, ingredients, fillers and rice straw utilized [[20], [21]]. The same behavior was observed by Irmukhametova et al. [8], who reported on the biodegradability of polymer blends composed of polyvinyl alcohol, starch, and chitosan, enhanced by the addition of rice straw.

Mechanical properties

The influence of rice straw on tensile strength and elongation at break is illustrated in Table 3. Incorporating rice straw into the grafted copolymer resulted in an increase in tensile strength from 25.2 MPa to 27.6 MPa, a change attributed to the higher SiO_2 content in the rice straw, as in the study reported in Ref. [[3], [4], [22], [23]]. Further enhancement in tensile strength, from 27.6 MPa to 36.8 MPa, was observed with a rice straw concentration increase from 3% to 7%. The highest tensile strength of 36.8 MPa was achieved at 7% rice straw. Additionally, the elongation at break improved significantly, rising from 4.3% to 9.6% with the addition of rice straw to the grafted copolymer.

Biodegradability properties of P(PE-g-AA) films

The effect of rice straw on the swelling behavior of grafted copolymer films, as influenced by time and temperature, is presented in Figure 3. Swelling time was observed to decrease with increasing temperatures from 30°C to 45°C. Additionally, incorporating rice straw into the grafted copolymer reduced swelling time compared to the grafted PEA copolymer. Swelling time further decreased with higher rice straw content in the grafted copolymer. For instance, at 45°C, the swelling time decreased by 5.8% with 3% rice straw, 15% with 5% rice straw, and 25.8% with 7% rice straw. This reduction in swelling time is attributed to the role of rice straw in enhancing the water solubility of the blend films.

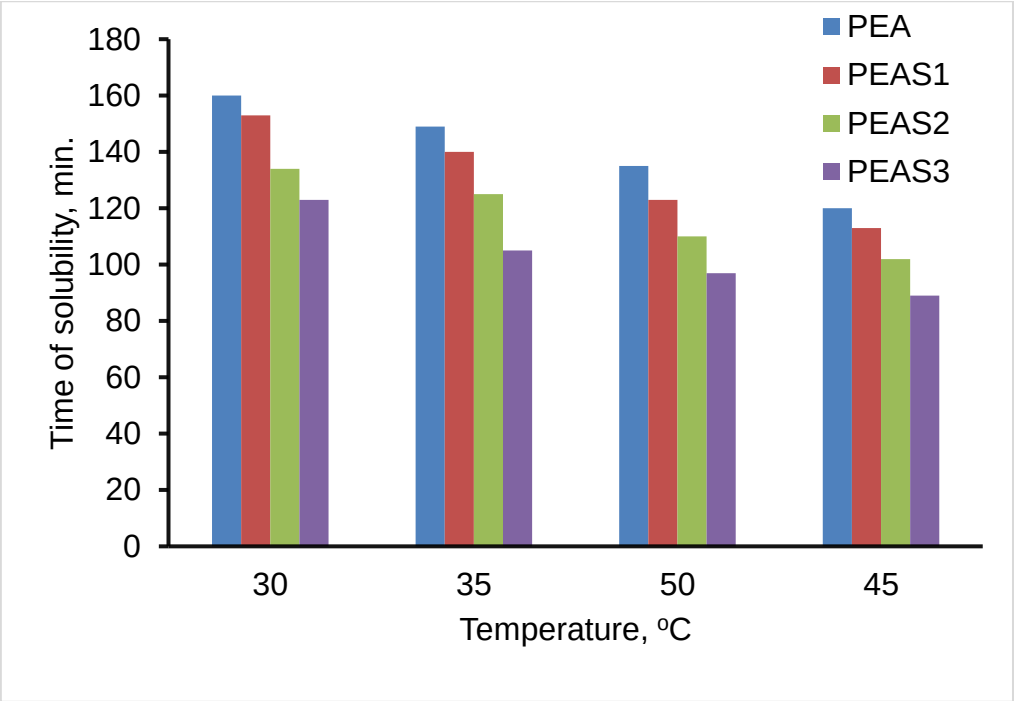

Figure 3 - The effect of water on the biodegradability of films

Conclusions

A polyethylene (PE)-based copolymer grafted with acrylic acid (AA) in a 1:5 ratio was synthesized using a grafting polymerization technique. Rice straw was incorporated into the grafted copolymer at varying concentrations (3%, 5%, and 7%) to enhance its biodegradability. The findings demonstrated that the addition of rice straw improved both the mechanical properties and biodegradability of the copolymer. The grafted copolymer containing 5% rice straw exhibited the best mechanical performance and a shorter swelling time compared to the grafted copolymer without rice straw. We explored the potential of utilizing the prepared grafted films, incorporating 5% rice straw (based on grafted polymer weight), for packaging applications. Furthermore, we evaluated alternative approaches to developing eco-friendly packaging films, alongside the essential role of petroleum in polymer production.

CRediT author statement: **G. Yeligbayeva:** Writing-original draft**; Zh. Orazalin, A. Abdassalam:** Writing review**; K. Omirzakova:** Methodology**; N. Milissova** and **Eny Kusrini:** Formal analysis.

All authors have read and agreed to the published version of the manuscript.

Acknowledgments. The work was financially supported by the Ministry of Science and Education of the Republic of Kazakhstan, competition for grant funding for scientific and technical projects 2023–2025. Project No. (AP19676789), entitled “Production of biodegradable plastic bags based on ethylene and cornstarch, Republic of Kazakhstan”.

Conflicts of interest. Authors declare no conflict of interest, financial or otherwise.

Cite this article as: Yeligbayeva G, Orazalin ZhK, Abdassalam A. Alfergani, Omirzakova KK, Milissova NB, Eny Kusrini. Effect of Rice Straw on the Mechanical and Biodegradability Properties of the Poly (Polyethylene-G-Acrylic Acid). Kompleksnoe Ispolzovanie Mineralnogo Syra = Complex Use of Mineral Resources. 2026; 338(3):51-58. https://doi.org/10.31643/2026/6445.28

Күріш сабанының полиэтилен-г-акрил қышқылының механикалық және биологиялық ыдырайтын қасиеттеріне әсері

[1,2*]Елигбаева Г.Ж., [3]Оразалин Ж. К., [4]Abdassalam A. Alfergani, [5]Омирзакова К.К., [5]Милисова Н. Б., [6]Eny Kusrini

[1]Органикалық синтез және көміртек химиясы институты, Қарағанды, Қазақстан
[2]Сәтбаев университеті, Алматы, Қазақстан
[3] Қазақ-Британ техникалық университеті, Алматы, Қазақстан
[4]Сирт университеті, Сирт, Ливия
[5] С.Д. Асфендияров атындағы Қаз¥МУ, Алматы, Қазахстан
[6] Индонезия университеті, UI New Campus, Индонезия

Мақала келді: *25 наурыз 2025*
Сараптамадан өтті: *28 наурыз 2025*
Қабылданды: *21 сәуір 2025*

ТҮЙІНДЕМЕ

Полиэтилен/акрил сополимері катализатор ретінде бензоил пероксиді және еріткіш ретінде ксилолмен егу әдісін қолдану арқылы синтезделді. Акрил қышқылы (АА) 1:5 қатынасында полиэтиленге (ПЭ) егілді. FTIR арқылы сипатталатын егілу арқылы алынған сополимер биологиялық ыдырайтын қабықшаларды алу үшін әртүрлі 3%, 5% және 7% арақатынаста күріш сабанымен араластырылды. Бұл қабықтардың судағы қасиеттері тұтқырлық, созылу беріктігі, үзілу кезіндегі ұзару, сумен жанасу бұрышы және ерігіштік талдаулары арқылы бағаланды. Күріш сабанын қосу арқылы егілген сополимердің биологиялық ыдырағыштығы артты, нәтижесінде тұтқырлық, созылу беріктігі және пленкалардың үзілуі кезінде созылу артады, сонымен бірге сумен жанасу бұрышы мен ерігіштігі төмендеді. Дегенмен, ПЭ (1,0%) және АА (5,0%) негізіндегі егілген сополимерге 7% күріш сабанын қосу тұтқырлықты, созылу беріктігін және үзілу кезіндегі ұзаруды тиісінше 29,5%, 46,1% және 9,6% арттыруға әкелді, бұл сәйкес жанасу бұрышы мен биоградация уақытын 45°C-да 54 25,8%-ға төмендетеді.

Түйін сөздер: Полиэтилен, акрил қышқылы, күріш сабаны, биологиялық ыдырайтын, механикалық.

Авторлар туралы ақпарат:

Елигбаева Гульжахан Жакпаровна *Химия ғылымдарының докторы, профессор, Мұнай инженериясы кафедрасы, Сәтбаев университеті, 050013, Сәтбаев көшесі, 22, Алматы; Органикалық синтез және көміртек химиясы институты, Қарағанды, Қазақстан. Email: g.yeligbayeva@satbayev.university; ORCID ID: https://orcid.org/0000-0002-7098-5437*

Оразалин Жандос Кайратулы *PhD студент, Материалтану және жасыл технологиялар мектебі, Қазақстан-Британ техникалық университеті, Төле би көшесі, 59, 050000, Алматы, Қазақстан. Email: zhandos1403@bk.ru; ORCID ID: https://orcid.org/0009-0002-0835-8392*

Abdassalam A. Alfergani *Профессор, Химия бөлімі, білім беру факультеті, Сирт университеті, Сирт, Ливия. Email: abdassalamtameem@yahoo.com; ORCID ID: https://orcid.org/0009-0009-6632-2380*

Омирзакова Кульшат Калибековна *Химия ғылымдарының кандидаты, Биохимия факультеті, Жалпы медицина мектебі-1, С.Д. Асфендияров атындағы Қаз¥МУ, Богенбай батыр көшесі 151, 480012, Алматы, Қазахстан. Email: omirzakova.k@kaznmu.kz*

Милисова Назерке Бакыткызы *Магистр, Инженерлік пәндер және тиісті практикалар кафедрасы, Фармация мектебі, С.Д. Асфендияров атындағы Каз¥МУ, Богенбай батыр көшесі 151, 480012, Алматы, Қазахстан. Email: milisova.n@kaznmu.kz; ORCID ID: https://orcid.org/0000-0001-7833-6258*

Eny Kusrini *Профессор, Химиялық инженерия кафедрасы, Индонезия университеті, UI New Campus, Depok 16424, Индонезия. Email: eny.k@ui.ac.id; ORCID ID: https://orcid.org/0000-0002-7919-0083*

Влияние рисовой соломы на механические и биоразлагаемые свойства полиэтилен-г-акриловой кислоты

[1,2*]Елигбаева Г.Ж., [3]Оразалин Ж. К., [4]Abdassalam A. Alfergani, [5]Омирзакова К. К., [5]Милисова Н. Б., [6]Eny Kusrini

[1]Институт органического синтеза и химии углерода Республики Казахстан, Караганда
[2]Сатбаев Университет, Алматы, Казахстан
[3]Казахстанско-Британский Университет, Алматы, Казахстан
[4]Сиртский университет, Сирт, Ливия
[5]КазНМУ им. С.Д. Асфендиярова, Алматы, Казахстан
[6]Университет Индонезии, Новый кампус UI, Индонезия

Поступила: *25 марта 2025*
Рецензирование: *28 марта 2025*
Принята в печать: *21 апреля 2025*

Аннотация
Полиэтилен/акриловый сополимер был синтезирован с использованием техники прививки с бензоилпероксидом в качестве катализатора и ксиленом в качестве растворителя. Акриловая кислота (АК) была привита к полиэтилену (ПЭ) в соотношении 1:5. Полученный привитой сополимер, охарактеризованный FTIR, был смешан с рисовой соломой в различных соотношениях 3%, 5% и 7% для получения биоразлагаемых пленок. Свойства этих пленок в воде были оценены с помощью анализа вязкости, прочности на разрыв, удлинения при разрыве, угла контакта с водой и растворимости. Включение рисовой соломы повысило биоразлагаемость привитого сополимера, что привело к повышению вязкости, прочности на разрыв и удлинения при разрыве пленок, при этом уменьшив угол контакта с водой и растворимость. Однако включение 7% рисовой соломы в привитой сополимер на основе ПЭ (1,0%) и АА (5,0%) привело к увеличению вязкости, прочности на разрыв и удлинения при разрыве на 29,5%, 46,1% и 9,6% соответственно, при одновременном снижении угла контакта и времени растворимости при биоразлагаемости при 45°C на 25,8%.

Ключевые слова: Полиэтилен, акриловая кислота, рисовая солома, биоразлагаемый, механический.

Информация об авторах:

Елигбаева Гульжахан Жакпаровна — *Доктор химических наук, профессор, Кафедра нефтяной инженерии, Сатбаев университет, ул. Сатбаева, 22, 050013, Алматы*; *Институт органического синтеза и химии углерода Республики Казахстан, Караганда, Казахстан. Email: g.yeligbayeva@satbayev.university; ORCID ID: https://orcid.org/0000-0002-7098-5437*

Оразалин Жандос Кайратулы — *PhD студент, Школа материаловедения и зеленых технологий, Казахстанско-Британский технический университет, ул. Толе би, 59, 050000, Алматы, Казахстан. Email: zhandos1403@bk.ru; ORCID ID: https://orcid.org/0009-0002-0835-8392*

Abdassalam A. Alfergani — *Профессор, Химический факультет, педагогический факультет, Сиртский университет, Сирт, Ливия. Email: abdassalamtameem@yahoo.com; ORCID ID: https://orcid.org/0009-0009-6632-2380*

Омирзакова Кулшат Калибековна — *Кандидат химических наук, Факультет биохимии, Школа общей медицины-1, КазНМУ им. С.Д. Асфендиярова, ул. Богенбай батыра, 151, 480012, Алматы, Казахстан. Email: omirzakova.k@kaznmu.kz*

Милисова Назерке Бакытқызы — *Магистр, Школа фармации, кафедра инженерных дисциплин и надлежащих практик, КазНМУ им. С.Д. Асфендиярова, ул. Богенбай батыра, 151, 480012, Алматы, Казахстан. Email: milisova.n@kaznmu.kz; ORCID ID: https://orcid.org/0000-0001-7833-6258*

Eny Kusrini — *Профессор факультета химической инженерии, университет Индонезии, Новый кампус UI, Депок 16424, Индонезия. Email: eny.k@ui.ac.id; ORCID ID: https://orcid.org/0000-0002-7919-0083*

References

[1] Ghatge S, Yang Y, Ahn JH, et al. Biodegradation of polyethylene: a brief review. Appl Biol Chem. 2020; 63(27):1-14. https://doi.org/10.1186/s13765-020-00511-3

[2] Amzan Alsabri, Furqan Tahir, Sami G. Al-Ghamdi. Environmental impacts of polypropylene (PP) production and prospects of its recycling in the GCC region, Materials Today: Proceedings. 2022; 56(4):2245-2251. https://doi.org/10.1016/j.matpr.2021.11.574

[3] Samy M, Bekbayeva L, Mohammed A, Irmukhametova G, Zhetpisbay D, Majeed N, Yermukhambetova B, & Mun G. Overview of biodegradable polymers: synthesis, modification and application. Kompleksnoe Ispolzovanie Mineralnogo Syra = Complex Use of Mineral Resources. 2024; 332(1):19-31. https://doi.org/10.31643/2025/6445.02

[4] Iskalieva A, Orazalin Z, Yeligbayeva G, Irmukhametova G, Taburova S, & Toktar T. Synthesis of Biodegradable Polymer-Based on Starch for Packaging Films: A Review. Kompleksnoe Ispolzovanie Mineralnogo Syra = Complex Use of Mineral Resources. 2023; 329(2);110-130. https://doi.org/10.31643/2024/6445.22

[5] Kim R, Laurens D, Kevin VG, Mechanical and chemical recycling of solid plastic waste. Waste Management. 2017; 69:24-58. https://doi.org/10.1016/j.wasman.2017.07.044

[6] Amzan A, Sami GA. Carbon footprint and embodied energy of PVC, PE, and PP piping: Perspective on environmental performance, Energy Reports. 2020; 6(8):364-370. https://doi.org/10.1016/j.egyr.2020.11.173

[7] Bornali B, Heena K, Sachin RG. Bioremediation strategies for xenobiotic degradation in petroleum-impacted industrial ecosystems: Practical challenges and future directions. Journal of Water Process Engineering. 2025; 70:106877. https://doi.org/10.1016/j.jwpe.2024.106877

[8] Irmukhametova G, Al Azzam KM, Mun GA, Bekbayeva L, Dinara Z, Yermukhambetova BB, Nechipurenko SV, Efremov SA, Negim E-S, Samy M. Obtaining and Characterization of Biodegradable Polymer Blends Based on Polyvinyl Alcohol, Starch, and Chitosan. Polymers. 2025; 17;479. https://doi.org/10.3390/polym17040479

[9] Jyothi AN. Starch Graft Copolymers: Novel Applications in Industry. Composite Interfaces. 2010; 17(2-3):165-174. https://doi.org/10.1163/092764410X490581

[10] Das A, Ringu T, Ghosh S, et al. A comprehensive review on recent advances in preparation, physicochemical characterization, and bioengineering applications of biopolymers. Polym. Bull. 2023; 80:7247-7312. https://doi.org/10.1007/s00289-022-04443-4

[11] Gulzhakhan Y, Khaldun M A, Galiya I, Lyazzat B, Orazalin ZK, Asylzat I, El-Sayed Negim, Bounoua N. The Effect of Calcium Carbonate, Rice, and Wheat Straw on the Biodegradability of Polyethylene/Starch Films. Polymer Crystallization. 2024, 8674988.

[12] Pan M-Z, Mei C-T, Zhou X-B, Pu Y-L. Effects of Rice Straw Fiber Morphology and Content on the Mechanical and Thermal Properties of Rice Straw Fiber-High Density Polyethylene Composites. Journal of Applied Polymer Science. 2011; 121:2900-2907. https://doi.org/10.1002/app.33913

[13] ASTM D882; Standard Test Method for Tensile Properties of Thin Plastic Sheeting. ASTM International (ASTM): West Conshohocken, PA, USA, 2018.

[14] Brian CS. The infrared spectra of polymers II: Polyethylene. Spectroscopy. 2021; 36(9):24-29.

[15] Alfuhaid L, Al-Abbad E, Alshammari S, Alotaibi A, Malek N, Al-Ghamdi A. Preparation and Characterization of a Renewable Starch-g-(MA-DETA) Copolymer and Its Adjustment for Dye Removal Applications. Polymers (Basel). 2023; 15(5):1197.

[16] Skalieva A, Yesmurat M, Al Azzam KM, Ainakulova D, Yerbolat Y, Negim E-S, Ibrahim MNM, Gulzhakhan Y. Effect of Polyethylene Glycol Methyl Ether Methacrylate on the Biodegradability of Polyvinyl Alcohol/Starch Blend Films. *Polymers.* 2023; 15:3165. https://doi.org/10.3390/polym15153165

[17] Mieles M, Harper S, Ji H-F. Bulk Polymerization of Acrylic Acid Using Dielectric-Barrier Discharge Plasma in a Mesoporous Material. Polymers. 2023; 15:2965. https://doi.org/10.3390/polym15132965

[18] Nho Y-C, Park J-S, Lim Y-M. Preparation of Poly(acrylic acid) Hydrogel by Radiation Crosslinking and Its Application for Mucoadhesives. Polymers. 2014; 6:890-898. https://doi.org/10.3390/polym6030890

[19] Elleithy RH, Ali I, Ali MA, et al. High density polyethylene/micro calcium carbonate composites: A study of the morphological, thermal, and viscoelastic properties. Journal of Applied Polymer Science. 2010; 117(4):2413-21.

[20] Junjun L, Chanjuan J, Chunxia H. Rice Straw and Cornstarch Biodegradable Composites. AASRI Procedia. 2012; 3:83-88, https://doi.org/10.1016/j.aasri.2012.11.015

[21] Olzhabay AT, Urkimayeva PI, Kenessova ZA, Yespenbetova ShO, El-Sayed Negim. Development of a Technology for Processing Waste Plastic Bottles and Bags to Obtain Various Types of Biodegradable Polymer Films. International Journal of Biology and Chemistry. 2022; 15(1):107-116. https://doi.org/10.26577/ijbch.2022.v15.i1.012

[22] Aldas M, Pavon C, De La Rosa-Ramírez H, et al. The Impact of Biodegradable Plastics in the Properties of Recycled Polyethylene Terephthalate. Journal of Polymers and the Environment. 2021; 29(8):2686-2700.

[23] Liu J, Jia C, He C. Rice Straw and Cornstarch Biodegradable Composites. AASRI Procedia. 2012; 3:83-88.

Crossref

DOI: 10.31643/2026/6445.29
Earth sciences

Coastal Geomorphological Dynamics and Tsunami Hazard Zones (5–12 m ASL) in Padang City, West Sumatra, Indonesia

[1*] Suci F.R.Z., [2]Teuku Y.W.M.I., [3]Cipta E.

[1] Mining Engineering, College of Industrial Technology (STTIND) Padang, Padang City, West Sumatra 25586
[2,3]Geological Engineering, Padjadjaran University, Bandung 40132, Indonesia

** Corresponding author email: sucifitria1228@gmail.com*

Received: *January 2, 2025*
Peer-reviewed: *January 6, 2025*
Accepted: *April 24, 2025*

ABSTRACT

Padang City is one of the capital cities in the western part of the island of Sumatra, with a total coastline length of approximately 68,126 km and directly adjacent to the Indian Ocean. The last time the province of West Sumatra was hit by a tsunami was in 2009 and 2010, which caused tsunamis with heights of <1 metre to >12 metres caused by an earthquake with a magnitude of 7.9. Experts estimate the potential for earthquake disasters originating from megathrust plate faults along the Mentawai Islands. Early and optimal mitigation efforts can minimise the impact caused by tsunami disasters. This study aims to provide an overview of the influence of shoreline changes on the tsunami distribution zones of 5 and 12 metres above sea level. This research uses the coastline parameters of Padang city from 2005 to 2021, obtained from Google Earth, administration, slope and land cover, which will be processed by utilising the Geographic Information System in ArcGIS software. The method used in the research is Tsunami Inundation by dividing the height of tsunami inundation into three scales, including low, medium and high. Observations were made at 122 observation points spread along 18,520 metres of coastline of the study area. The results show that there are five to six sub-districts in Padang city that are affected by tsunami disasters of 5 and 12 metres above sea level, including the sub-districts of South Padang, East Padang, West Padang, North Padang, Nanggalo, and Koto Tangah. The difference in coastline from 2005 to 2021 shows a change in the area of the tsunami disaster distribution zone of around 78.69 to 91.51 hectares at each water level caused by accretion events that occur along the coastline of the observation area.

Keywords: Coastline, Earthquake, Tsunami, Disaster Mitigation.

Information about authors:

Suci Fitria Rahmadhani Z — *Master of Geological Engineering, concentration in Geological Mitigation and Disaster at Padjadjaran University; Lecturer in Mining Engineering, College of Industrial Technology (STTIND) Padang, West Sumatra, Indonesia. Email: sucifitria1228@gmail.com; ORCID ID: https://orcid.org/0000-0003-0714-3672*

Teuku Yan W M Iskandarsyah — *Doctor of Geological Engineering at Padjadjaran University, Bandung, West Java, Indonesia Email: yan@unpad.ac.id; ORCID ID: https://orcid.org/0000-0002-7583-9244*

Cipta Endyana — *Doctor of Geological Engineering at Padjadjaran University, Bandung, West Java, Indonesia Email: cipta.endyana@unpad.ac.id; ORCID ID: https://orcid.org/0000-0001-9448-1789*

Introduction

Dynamic coastlines cause the shape and space of coastal areas to change rapidly as a result of natural processes and human activities around the coast. Through coastal abrasion and accretion events, the coastline changes endlessly due to sediment movement, changes in currents, wave activity and land use [1]. Abrasion can occur in coastal areas due to wave action, changes in currents, tidal variations and climate change [2]. Abrasion causes a decrease and inundation of the land surface by water, so that the coastline can change [3].

Meanwhile, accretion is an event of changing the coastline towards the open sea due to the process of sedimentation on land areas, the process of sediment transport from river bodies to the sea and human activities in managing land. Accretion can cause siltation in the sea area. Accretion usually occurs on beaches that have many river mouths [4]. Surveillance of coastal areas is a form of protection for a country and the environment. Surveillance of the coastline is something that can be utilised in managing coastal areas and developing coastal areas [5].

It is recorded that 90 per cent of tsunami events are caused by tectonic earthquakes, and tsunami

waves cause the displacement of water in the middle of the sea to rise towards land. This causes damage and loss of life. Tsunamis are disasters whose impact can be reduced by managing disaster risk [6]. The mitigation process is very important in planning the development of an area, especially for Indonesia, which is vulnerable to natural disasters [7]. Experts predict the earthquake potential in the Mentawai segment of West Sumatra province to be around 8.8 SR [8].

This is based on historical records of West Sumatra province in 1797, which was hit by an earthquake with a magnitude of 8.4 SR, which caused tsunami waves estimated at a height of 5-10 metres or about 1 km inland. Then, in 1833, the rupture of the 1000 km long Sumatra trough caused by an earthquake with a magnitude of 9.0 SR caused a tsunami with a water height of 2-3 metres [9]. It was reported that an earthquake on 30 September 2009 with a magnitude of 7.6 occurred in the city of Pariaman, about 1,117 people were killed and 181,665 buildings were destroyed by the earthquake, there was a run up of tsunami waves < 1 metre including in the eastern part of the Mentawai islands [10].

The latest earthquake with a magnitude of 7.7 shook the Mentawai Islands. Researchers made observations and obtained run-up height values on the island of Cypora around 1 to 4 metres, Pagai island 2.4 to 8 metres and South Pagai island 2.5 to 12.4 metres. The highest run-up was found in the Sibigou area with a height of about 12.4 metres [10]. Padang City is one of the provincial capitals located on the western edge of Sumatra Island. Due to the geographical condition of the lowlands, many community activities are centred around the coast. Many vital objects that encourage all community activities are in the area around the coast of Padang city [11].

Coastal Geology and Geomorphology. The geology of Padang city consists of surface deposits, intrusions, volcanic rocks, sedimentary rocks and metamorphic rocks (Figure 1). The Padang City area is composed of 4 rock layers consisting of Jurassic age sedimentary rocks, Quaternary age sedimentary rocks and volcanic rocks. The coast of Padang City consists of surface deposits, intrusions, volcanic rocks, sedimentary rocks and metamorphic rocks [11].

Padang City is one of the developing areas on the western coast of Sumatra Island. This area has 11 sub-districts with 104 villages in it. Padang City is the provincial capital of West Sumatra. This area has an area of around 694.96 km^2 with geographical conditions bordering the Indian Ocean. In the north, the area is bordered by Padang Pariaman district, in the south by Pesisir Selatan district and in the east by Solok district. In the western part of the Padang city area lies lowland, while in the eastern part of the Padang city area lies a row of hills and the Padang city area is traversed by 21 rivers [13].

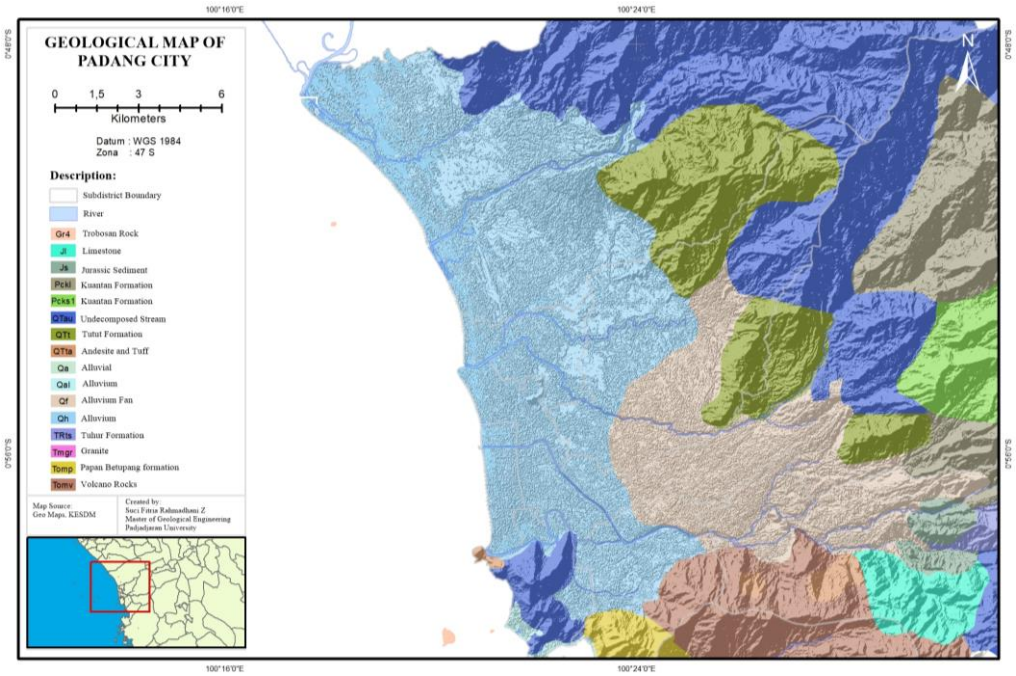

Figure 1 - Coastal geological map of Padang city

There is andesite and tuff that can be exposed around the Pengambiran area and cold water hills, in the form of greyish black and white volcanic rocks. In the west, there are andesite rock fragments in the form of chunks of volcanic origin with a blackish grey colour, scattered at the bottom of the slopes of Nago and Limau Manis hills. In the western part of the lowlands of the observation area, deposits of silt, clay, gravel and loamy sand and finally undecomposed volcanic-derived rocks generally consist of conglomerate, breccia and sandstone. These deposits are scattered around Bukit Barisan, Gunung Padang and Bukit Air Manis [12].

The land area of Padang city has an altitude between 0 to >1000 masl. The coast of Padang city forms a straight beach with alluvium lowlands. The shape of the beach around the mouth of the river is in the form of sand spits. The beach sediments that make up the coastal area mostly consist of sand. Around the mouth of the river estuary, there is active sedimentation. The coast of Padang city is classified as a type of high-energy beach that is >2 metres, which usually occurs during the west wind season [14].

The youngest rocks in the Padang City area are alluvium deposits consisting of layers of sand, silt, gravel and swamp deposits. Older sedimentary rocks consist of metamorphic rocks and limestone. In the eastern and southern hilly areas, there are volcanic rocks consisting of basaltic lava, breccia and andesitic tuff [15]. The shape of the beach around the mouth of the river in the Padang City area is in the form of sand spits. The sediments that make up the beach area consist mostly of sand. Around the mouth of the river, there is also active sedimentation.

The mainland of Padang City has an altitude between 0 to >1000 metres above sea level. On the coast of Padang City, it forms a straight beach with a landscape of alluvium lowlands as shown in Figure 2. Land cover is any appearance of physical material that exists on the Earth's surface. Land cover can illustrate the relationship between natural processes and social processes. Land cover provides information that can be used to understand natural events or phenomena on the Earth's surface [16].

Land use is any form of human interference with natural resources, whether temporary or permanent. Aiming to fulfil all needs in the form of material or spiritual [17]. In the Padang City area, Figures 2 and 3 show the land cover and land use around the coast in the form of vacant land, shrubs, settlements and water bodies. There are 6 river estuaries along the observation area in Padang City, which can be seen in Figure 2.

Ocean Waves. Ocean waves are a perpendicular movement of the rise and fall of sea water with the surface of the sea water and form a curvilinear tidal [18]. Sea waves occur due to generating forces, these forces arise from wind, tides and earthquakes [19]. Data on the average wave height in coastal areas obtained from satellite image recordings on Copernicus show that in 2005 and 2021, as shown in Figures 4 and 5.

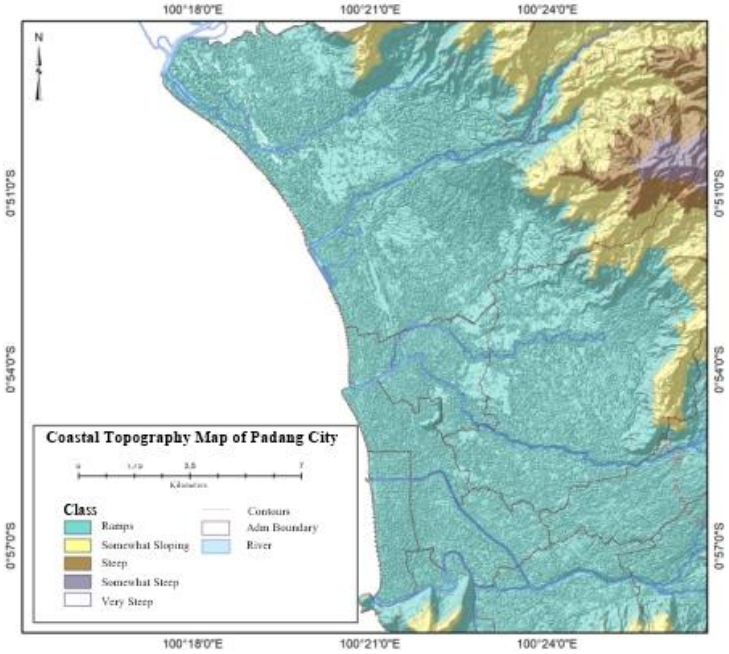

Figure 2 - Coastal Topography Map of Padang City

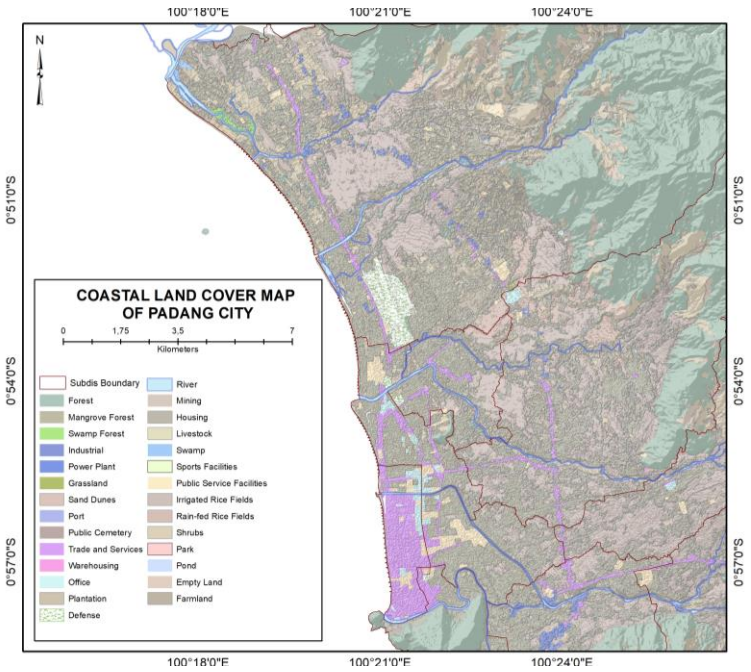

Figure 3 - Coastal Land Cover Map of Padang City

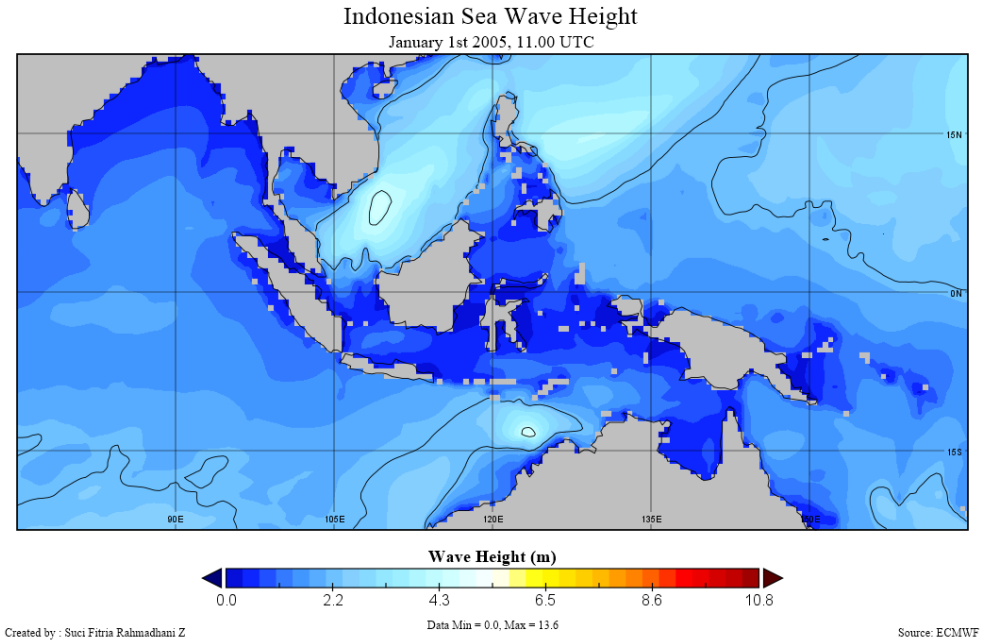

Figure 4 - Indonesian Sea Wave Height in 2005

In 2005, the area around the west coast of Sumatra Island had wave heights in the range of 0.4 - 0.6 metres. In Figure 4 above, it can be seen that Padang City, which is located in the western part of Sumatra Island, also has wave height values in the range of 0.4 - 0.6 metres. The average wave direction ranges from 180 - 216 degrees South Southwest.

Satellite image data on Copernicus in 2021 shows that the wave height around the west coast of Sumatra Island is in the range of 0.1 - 0.2 metres. In Figure 5 above, it can be seen that Padang City, which is in the western part of Sumatra Island, also has a wave height value in the range of 0.1 - 0.2 metres. The average wave direction ranges from 216-252 degrees Southwest. The wave height in the coastal area of Padang City is classified as low waves with rippling water, and there is no foam at the peak of the wave [20].

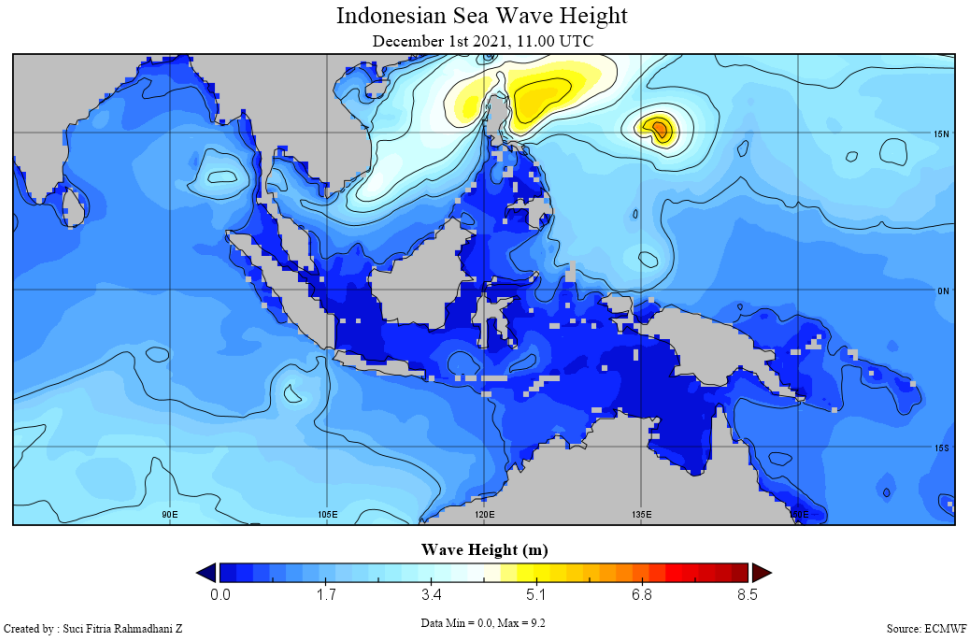

Figure 5 - Indonesian Sea Wave Height in 2021

Methods and Materials

This research was carried out only in the coastal area of the city of Padang, which has quite dense human activities, covering an observation area with a coastline length of around 18,520 metres. The method used is tsunami inundation in ArcGIS by processing variables such as coastline, administration, land cover and use and slope slope which then produces a tsunami rise model starting from the coastline in the observation area. The formula that will be processed has been determined [21] as follows;

Surface roughness is the value that each land cover and land use has when inhibiting seawater travelling inland during a tsunami. Surface roughness values have different values. The surface roughness value of each cover and land use can be seen in Table 1.

High resolution imagery on the Google Earth platform was used to extract the coastline from 2005 to 2021 to estimate variations and changes in the coastline. Estimated resolution up to 2 metres, the shoreline reference boundary used is the last area exposed to tidal waves clearly recorded on Google Earth images, which are then interpreted and digitised on the image screen with an eye rate of about 40 metres. This study aims to determine the effect of changes in coastal morphology on changes in tsunami disaster distribution zones at 122 observation points in Padang city.

Table 1 - Surface roughness coefficient values

Type of Land Cover and Use	Hardness Coefficient Value
Water body	0.007
Shrubs	0.040
Forest	0.070
Agriculture	0.035
Farmland	0.025
Vacant Land	0.015
Settlements	0.045
Mangrove Forest	0.025
Pond	0.010

Source: Berryman, 2006 [28]

Results

Through the USGS website, earthquakes with large to small magnitudes have hit the province of West Sumatra. The largest magnitude recorded by the USGS was 7.9 on the high seas [22].

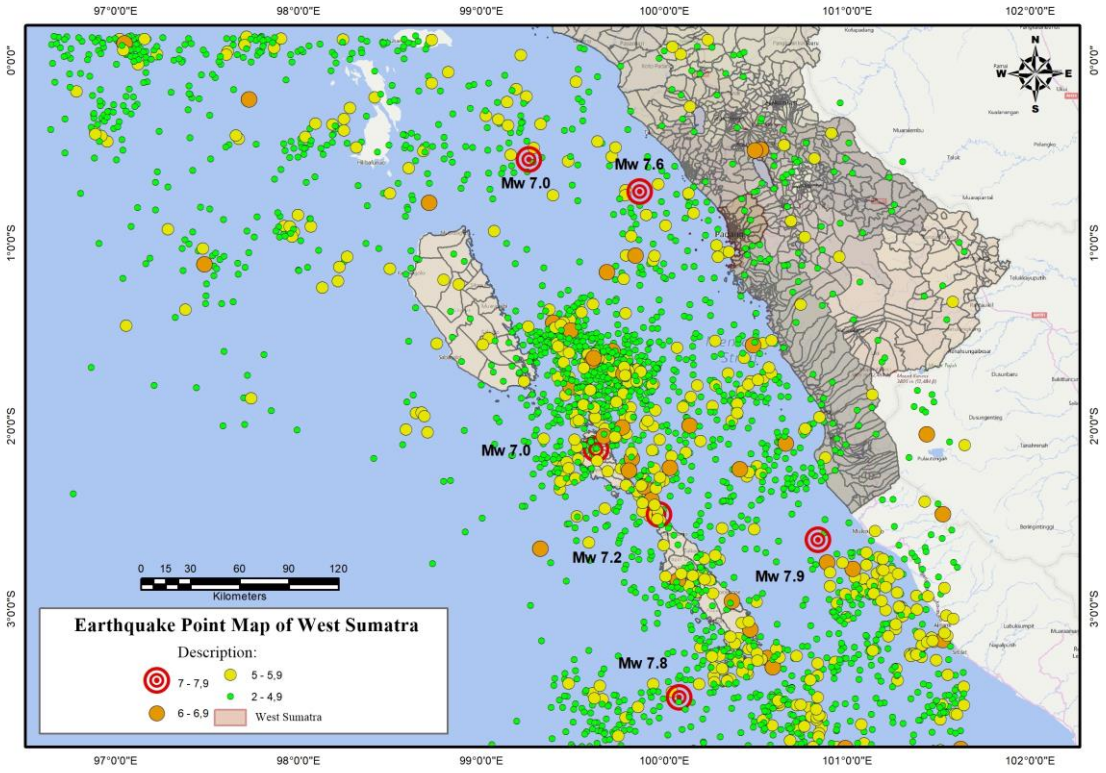

Figure 6 - Earthquake Point Map of West Sumatra Province (source: USGS, 2022)

The reported earthquake on 30 September 2009 with a magnitude of Mw 7.6 occurred 25 km northwest of Pariaman city. At least 1,117 people were killed and 181,665 buildings were destroyed, about 451,000 people were displaced, and tsunami wave run-ups at heights below 1 metre included the eastern part of the Mentawai islands [23].

Then on 25 October 2010, an earthquake with Mw 7.7 shook the Mentawai islands, West Sumatra. The earthquake was centred off the southwest coast of Pagai Island. Researchers conducted observations on the 2010 tsunami, and obtained run-up height values on Sipora island of 1 - 4 metres, on North Pagai island of 2.4 - 8 metres and South Pagai island of 2.5 - 12.4 metres. The highest run-up height is found on Sibigou island with a run-up height of about 12.4 metres [10]. Research conducted by the Indonesian Institute of Sciences in 2010 on the western Mentawai segment on Siberut island was predicted to hold the potential for an earthquake of around 8.8 SR [8].

Statistical analysis was conducted based on the data of earthquake release energy and storage energy in the Mentawai segment area, which annually produces a total energy of 1.025 x 1022 erg or equivalent to 6.8 SR. Meanwhile, the potential energy of the earthquake on the Mentawai segment is 3.59 x 1022 erg, equivalent to 7.2 SR [24].

Tsunami Rise Model 5 Metres Above Sea Level. There are three scales of tsunami distribution zones 5 metres above sea level, including low, medium and high scales. Inundation of < 1 metre is a low scale, inundation of 1-3 metres is a medium scale and > 3 metres is a high scale tsunami distribution. An overview of the tsunami forecast 5 metres above sea level from the coastline in 2005 and 2021 can be seen in Figure 7.

Five sub-districts in Padang city were estimated to be affected by the tsunami distribution of 5 metres above sea level on the coastline in 2005, with different areas affected, including Padang Selatan, Padang Barat, Padang Utara, Nanggalo and Koto Tangah sub-districts. The estimated tsunami travel distance is between 145 metres and 1,743 metres towards the mainland of Padang city, with the largest total area affected in Koto Tangah sub-district, which is about 470 hectares of affected land, and the least affected area is in East Padang sub-district, which is about 9 hectares of affected land.

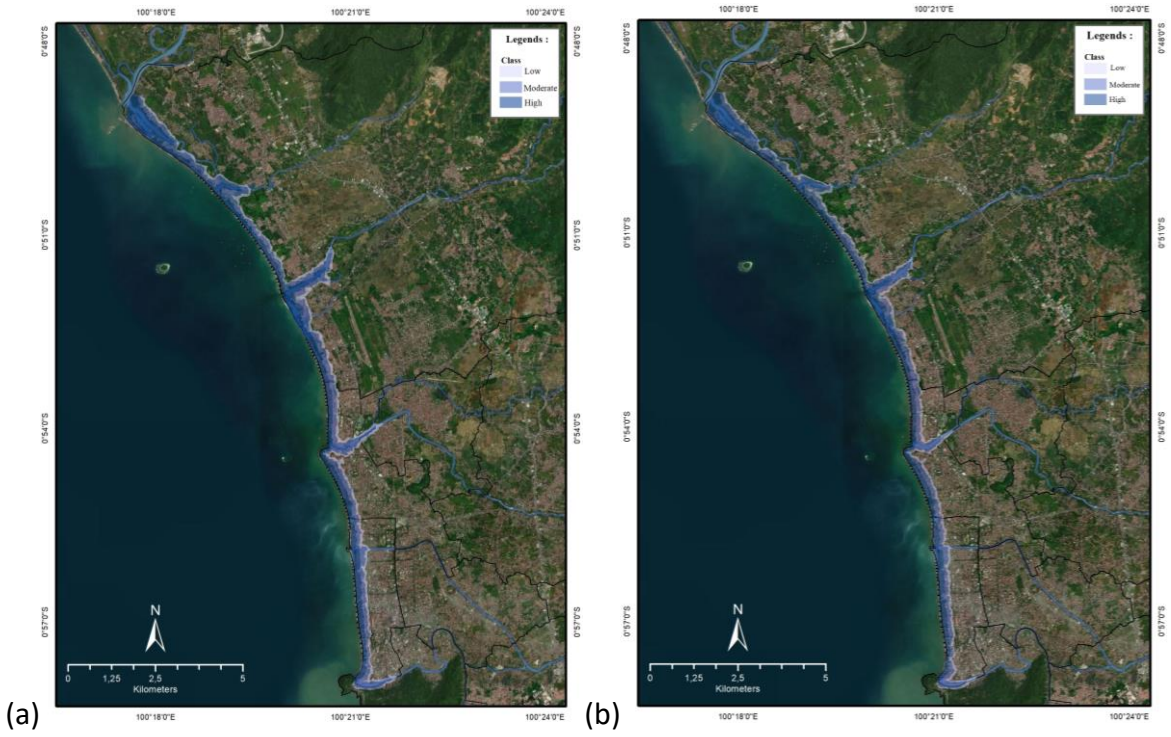

Figure 7 - Tsunami landfall zone 5 metres above sea level from the shoreline
(a) Shoreline in 2005 (b) Shoreline in 2021

Table 2 - Tsunami Disaster Land Area 5 metres above Sea Level at the Coastline in 2005 by Subdistrict

District	Low Area (hectares)	Medium Area (hectares)	Height Area (hectares)
Padang Selatan	4.972885	5.642311	0.38253
Padang Barat	31.463059	65.79509	67.133943
Padang Utara	40.069975	68.759694	59.292087
Nanggalo	7.17243	2.00828	0
Koto Tengah	86.738585	175.389818	208.19173

Five sub-districts in Padang city are predicted to be affected by a tsunami rise of 5 metres above sea level on the coastline in 2021, with different areas affected, including Padang Selatan, Nanggalo, Padang Barat, Padang Utara and Koto Tangah sub-districts. The estimated tsunami travel distance is about 173 metres to 1,595 metres towards the mainland of Padang city, with the largest total distribution hitting Koto Tangah sub-district, which is about 425 hectares of affected land and the least affected area of tsunami distribution is in East Padang sub-district, which is about 2 hectares of affected land.

Table 3 - Tsunami Disaster Land Area 5 metres above Sea Level on the Coastline in 2021 by Sub-district

District	Low Area (hectares)	Medium Area (hectares)	Height Area (hectares)
Padang Selatan	5.365604	4.047737	0.188267
Padang Barat	30.969892	60.527783	67.399522
Padang Utara	33.040827	62.881119	52.99711
Koto Tengah	83.496336	161.627067	180.830283
Nanggalo	2.447469	0	0

Tsunami Rise Model 12 Metres Above Sea Level. There are three scales of tsunami distribution zones 12 metres above sea level, including low, medium and high scales. At < 1 metre the distribution scale is low, inundation with a height of 1-3 metres is medium, and > 3 metres is a high tsunami distribution scale. An overview of the tsunami forecast 5 metres above sea level from the coastline in 2005 and 2021 can be seen in Figure 8.

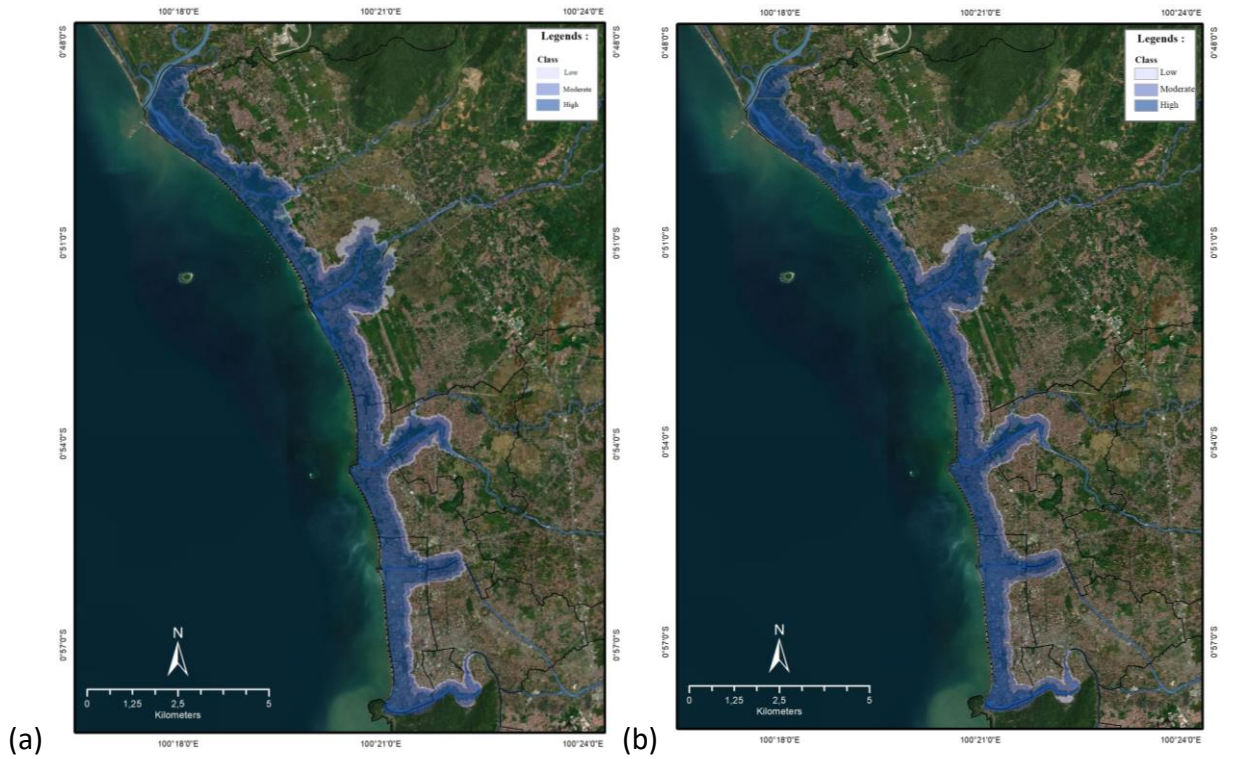

Figure 8 - Tsunami landfall zone 12 metres above sea level from the shoreline
(a)Shoreline in 2005 (b) Shoreline in 2021

Table 4 - Tsunami Disaster Land Area 12 metres above Sea Level at the Coastline in 2005 by Subdistrict

District	Low Area (hectares)	Medium Area (hectares)	Height Area (hectares)
Padang Selatan	16.587256	32.095666	46.794942
Padang Timur	9.979325	15.238699	20.632928
Padang Barat	26.431725	56.504556	310.707628
Padang Utara	34.118503	69.450707	280.365086
Nanggalo	28.859129	51.91946	62.573064
Koto Tengah	141.059106	221.433127	841.904394

The six sub-districts in Padang city that were estimated to be affected by the tsunami of 12 metres above sea level at the 2005 coastline, with different areas affected include Padang Selatan, Padang Timur, Padang Barat, Padang Utara, Nanggalo and Koto Tangah sub-districts. The estimated tsunami distance is between 527 metres and 2,703 metres towards the mainland of Padang city, with the largest total area affected in Koto Tangah sub-district, which is about 1,204 hectares of affected land, and the least affected area is in East Padang sub-district, which is about 45 hectares of affected land.

Table 5 - Tsunami Disaster Land Area 12 metres above Sea Level on the Coastline in 2021 by Sub-districts

District	Low Area (hectares)	Medium Area (hectares)	Height Area (hectares)
Padang Selatan	14.055675	26.746722	44.623357
Padang Timur	8.324235	14.874452	16.784932
Padang Barat	27.15611	57.314404	305.676819
Padang Utara	25.24563	57.041478	246.042547
Nanggalo	17.740173	28.657202	36.026197
Koto Tengah	118.040379	212.745608	355.895154

Six sub-districts in Padang city are predicted to be affected by a tsunami of 12 metres above sea level on the coastline in 2021, with different areas affected, including Padang Selatan, Padang Timur, Padang Barat, Padang Utara, Nanggalo and Koto Tangah sub-districts. The estimated tsunami travel distance is about 525 metres to 2,693 metres towards the mainland of Padang city, with the

largest total distribution hitting Koto Tangah sub-district, which is about 686 hectares of affected land and the least affected area of tsunami distribution is in East Padang sub-district, which is about 39 hectares of affected land.

Discussion

Shoreline change is a result of abrasion and accretion events on the coast [25]. Abrasion is a process of coastal erosion caused by destructive wave power and ocean currents [26]. Abrasion can occur in marine areas due to wave action, changes in current patterns, tidal variations, and climate change [2]. Abrasion causes a decrease and inundation of the land surface by water, so that the coastline can change [3].

Accretion is an event that changes the coastline towards the open sea due to the process of sedimentation from the land area caused by freshwater runoff with a large enough volume due to prolonged rain, and the process of sediment transport from river bodies to the sea, and due to human activities in managing land. Accretion can cause siltation evenly towards the sea, which will form a plain in the form of a delta or raised land. Coastal accretion usually occurs in coastal waters that have many river mouths and coastal waves with small energy and areas that rarely experience storms [4].

The research area in Figure 8 is divided into 4 stations or sections to review shoreline changes more accurately. Using images on Google Earth with a spatial resolution of up to 2 metres. The coastline along 18,520 metres obtained from the results of Google Earth digitisation with an eye of 70 m, then the coastline in KML format is inputted and processed using ArcGIS. The observation line was taken by measuring the observation distance of 150 metres between points on the 2005 coastline, as the first coastline observed.

Based on observations at 122 points of shoreline change from 2005 to 2007, there are 67 abrasion points with an average value of -8.16 and 55 accretion points with an average value of +7.73 metres. While on the coastline from 2007 to 2014, there are 49 abrasion points with an average value of -12.18 and 73 accretion points with an average value of +12.22 metres.

On the coastline from 2015 to 2017, there were 63 abrasion points with an average value of -5.15 metres and 59 accretion points with an average value of +5.33 metres. The 2017 to 2021 coastline has 78 abrasion points with an average value of -9.96 metres and 44 accretion points with an average value of +4.55 metres. Overall on the 2005 to 2021 coastline, 58 abrasion points with an average value of -17.60 metres were calculated, while there were 64 accretion event points with an average value of +13.06 metres. With a maximum value of abrasion events on the 2005 to 2021 coastline of around -68.25 metres and accretion of around +122.22 metres.

The Effect of Abrasion and Accretion on Changes in the Tsunami Landfall Zone 5 Metres Above Sea Level. At a tsunami landfall of 5 metres above sea level on the coastline from 2005 to 2021, there were 19 observation points that experienced abrasion with an average value of 23.38 metres, which caused a change in tsunami landfall distance of around 16.64 metres towards the mainland of Padang city.

The points that affect the change in the landfall zone are located at 11 points in Koto Tangah sub-district, 5 points in North Padang sub-district and 3 points in West Padang sub-district. While the accretion event on the coastline of Padang city occurred at 48 observation points with an average accretion of about 15.74 metres, and caused a change in the tsunami landfall distance of about 25.08 metres towards the sea. The difference in the area affected by the tsunami at 5 metres above sea level can be seen in Figure 9.

The area in red is the difference in the area affected on the coastline in 2005 and 2021, calculated and analysed using multivariate regression on coastline variables in the form of abrasion and accretion events on coastline changes at a tsunami landfall of 5 metres above sea level. Based on the R Square value of 0.095, it indicates that the effect of variables X1 and X2 together on variable Y is 9.5%. This explains that the geology of the observation area only significantly influences the tsunami coverage zone of 5 metres above sea level by only 9.5%. There is a change in the overall land area in the form of a reduction in the tsunami land area of 78.69 hectares from 2005 to 2021 due to accretion events.

The Effect of Abrasion and Accretion on Changes in the Tsunami Landfall Zone 12 Metres Above Sea Level. At a tsunami landfall of 12 metres above sea level, with the coastline from 2005 to 2021, 23 observation points experienced abrasion of around 23.41 metres, which caused a change in the tsunami landfall distance of around 23.87 metres towards the mainland of Padang city. The points that affect the change in the landfall zone are 18 points in Koto Tangah sub-district, 3 points in North Padang sub-district and 2 points in West Padang sub-district. The landfall points depicted in each region can be seen in Figure 10.

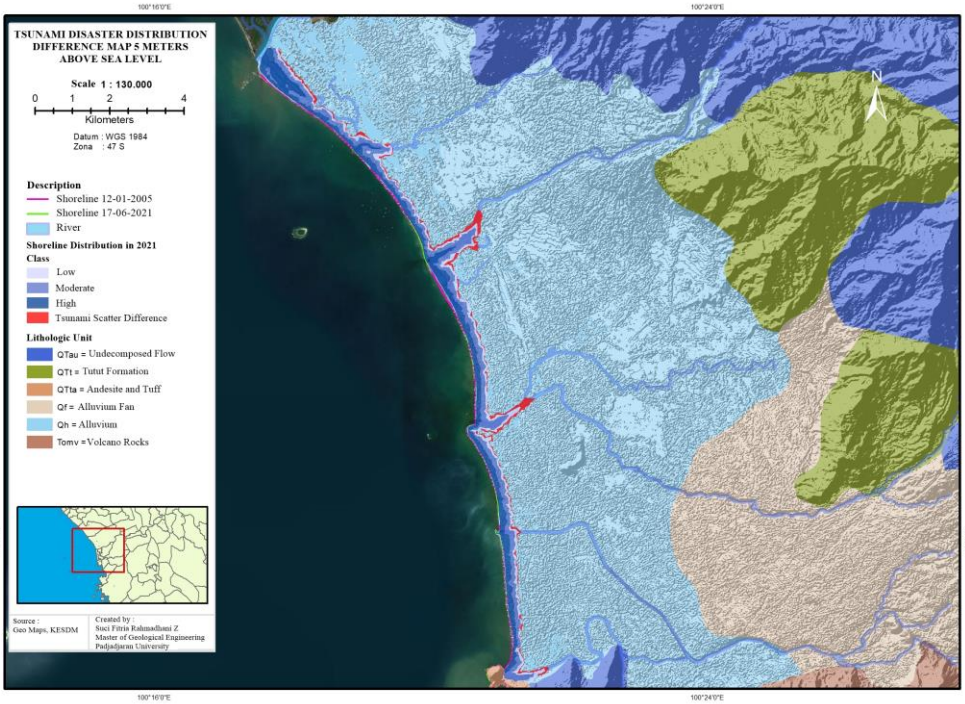

Figure 9 - Difference in Tsunami landfall zones of 5 metres above sea level at 2005 and 2021 coastlines

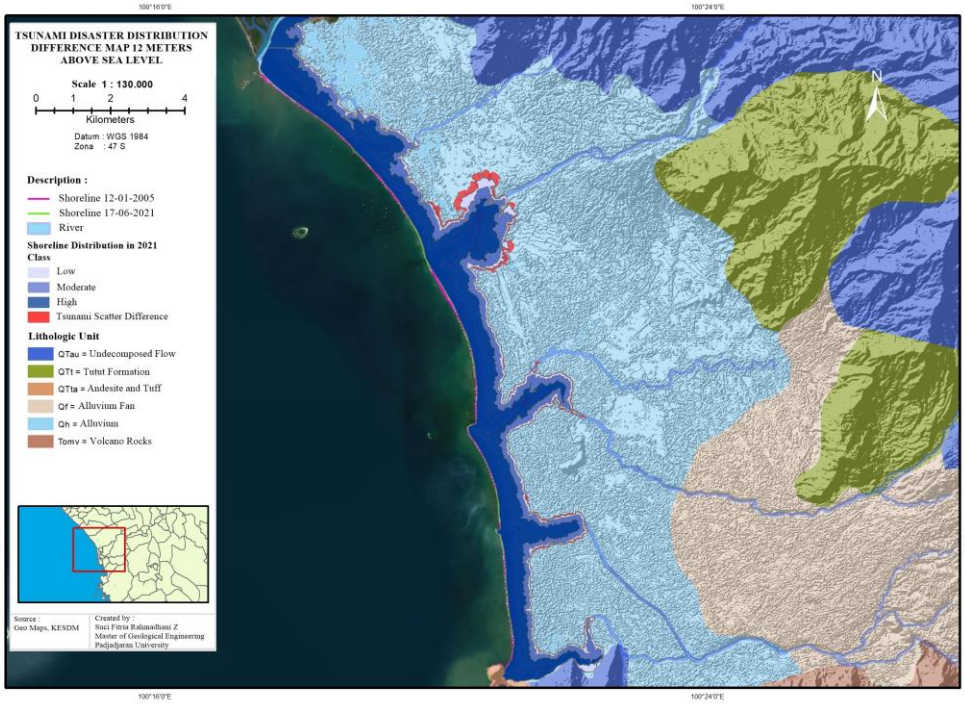

Figure 10 - Difference in Tsunami Landfall Zones of 12 meters above sea level at 2005 and 2021 coastlines

While the accretion event on the coastline of Padang city caused 48 observation points with an average of about 14.81 metres causing a tsunami landfall change of 12 metres about 22.91 metres back towards the sea. Points that affect the change in the landfall zone are 18 points in Koto Tangah sub-district, 12 points in North Padang sub-district and 18 points in West Padang sub-district.

The area in red is the difference in the area affected by the coastline in 2005 and 2021, by calculating and analysing using multivariate regression on the coastline variables in the form of abrasion and accretion events on coastline changes at a tsunami landfall of 12 metres above sea level.

Based on the R Square value of 0.122, it indicates that the effect of variables X1 and X2 together on variable Y is 12.2%. This explains that the geology of the observation area has a significant effect on the tsunami landfall zone of 12 metres above sea level by only about 12.2%. There is a change in the overall

land area, namely a reduction in the tsunami disaster land area of 91.51995 hectares from 2005 to 2021 due to accretion events.

Conclusions

Changes in the coastline over time prove that the coastline changes and is always dynamic. This is evidenced by abrasion and accretion events occurring on the coast of Padang City from 2005 to 2021, with a total of 64 accretion events with an average distance of +13.06 metres and 58 points of abrasion events with an average distance of -17.06 metres at the measurement point. Changes in distance due to abrasion and accretion events that occur on the coast of Padang City are caused by natural factors such as waves, tides, currents, climate, river mouths and human activities around the coastal area.

The calculation of tsunami landfall zones using the coastline from 2005 to 2021 with tsunami modelling of 5 and 12 metres above sea level resulted in the following areas; the prediction of tsunami landfall zones of 5 metres above sea level is expected to hit five sub-districts including South Padang, West Padang, North Padang, Nanggalo and Koto Tangah. With an estimated tsunami wave travel distance of 145 to 1,743 metres inland.

The tsunami landfall zone of 12 metres above sea level is expected to hit five sub-districts, including South Padang, East Padang, West Padang, North Padang, Nanggalo and Koto Tangah. With an estimated tsunami wave travel distance of 525 to 2,703 metres inland. This indicates that there is a reduction or shrinkage of the tsunami landfall area of 5 metres above sea level, which is approximately 78.69 hectares, due to accretion events. Previous calculations also show that there is a reduction or shrinkage of the tsunami land area 12 metres above sea level, which is approximately 91.52 hectares due to accretion.

Conflicts of interest. On behalf of all authors, the corresponding author states that there is no conflict of interest.

CRediT author statement: **F. Suci**: Conceptualization, Methodology, Software Data curation, Writing draft preparation Visualization, Investigation; **Y. Teuku, E. Cipta:** Supervision.

Acknowledgements. Our appreciation goes to Dr Ir Dicky Muslim, M.Sc, Dr Ir Zufialdi Zakaria, MT and Dr R Irvan Sophian, ST, MT who have provided constructive criticism and suggestions in the research process until completion. Our sincere thanks also go to the Geological Agency and Geospatial Information Agency for providing all supporting data in this research. This research did not receive any specific grant from funding agencies in the public, commercial, or not-for-profit sectors.

Cite this article as: Suci FRZ, Teuku YWMI, Cipta E. Coastal Geomorphological Dynamics and Tsunami Hazard Zones (5–12 m ASL) in Padang City, West Sumatra, Indonesia. Kompleksnoe Ispolzovanie Mineralnogo Syra = Complex Use of Mineral Resources. 2026; 338(3):59-71. https://doi.org/10.31643/2026/6445.29

Паданг қаласы, Батыс Суматра, Индонезия: жағалаулық геоморфологиялық динамика және цунами қаупі бар аймақтар (теңіз деңгейінен 5–12 м жоғары)

[1] Suci F.R.Z., [2]Teuku Y.W.M.I., [3]Cipta E.

[1] Тау-кен инженериясы, өнеркәсіптік технологиялар колледжі (STTIND) Паданг, Паданг қаласы, Батыс Суматра 25586
[2,3] Геологиялық инженерия, Паджаджаран университеті, Бандунг 40132, Индонезия

Мақала келді: *2 қаңтар 2025*
Сараптамадан өтті: *6 қаңтар 2025*
Қабылданды: *24 сәуір 2025*

ТҮЙІНДЕМЕ

Паданг қаласы - Суматра аралының батыс бөлігіндегі астаналық қалалардың бірі, жалпы жағалау сызығының ұзындығы шамамен 68 126 км және Үнді мұхитына тікелей іргелес. Соңғы рет Батыс Суматра провинциясы 2009 және 2010 жылдары цунамиге ұшырады, ол 7,9 баллдық жер сілкінісі салдарынан биіктігі <1 метрден >12 метрге дейінгі цунамиді тудырды. Сарапшылар Ментавай аралдарының бойындағы мегатруст плиталарының жарылуынан туындаған жер сілкінісі апаттарының ықтималдығын бағалайды. Ерте және оңтайлы жұмсарту әрекеттері цунами апаттарын барынша азайтуға мүмкіндік береді. Бұл зерттеудің мақсаты теңіз деңгейінен 5 және 12 м биіктіктегі цунами таралу аймақтарына жағалау сызығының өзгеру әсеріне шолу жасау болып табылады. Бұл зерттеуде ArcGIS бағдарламалық жасақтамасындағы Географиялық ақпараттық жүйе арқылы өңделетін

	Google Earth, әкімшілік, еңіс және жер жамылғысы туралы алынған 2005-2021 жылдардағы Паданг қаласының жағалау сызығының параметрлері пайдаланылады. Зерттеуде қолданылатын әдіс цунами тасқынының биіктігін төмен, орташа және жоғары деп үш шкалаға бөлу арқылы алынатын цунами тасқыны болып табылады. Зерттелетін аумақтың жағалау сызығының 18520 метрі бойында орналасқан 122 бақылау пунктінде бақылау жүргізілді. Нәтижелер Паданг қаласында теңіз деңгейінен 5 және 12 метр биіктіктегі цунами апаттарынан зардап шеккен бес-алты шағын аудан бар екенін көрсетеді, соның ішінде Оңтүстік Паданг, Шығыс Паданг, Батыс Паданг, Солтүстік Паданг, Нанггало, Кото Тангах. 2005 жылдан 2021 жылға дейінгі жағалау сызығының айырмашылығы бақылау аймағының жағалау сызығында болып жатқан аккрециялық құбылыстардан туындаған әрбір су деңгейінде шамамен 78,69-дан 91,51 гектарға дейін цунами таралу аймағының өзгеретінін көрсетеді.
	Түйін сөздер: Жағалау сызығы, жер сілкінісі, цунами, апат салдарын азайту.
Suci Fitria Rahmadhani Z	***Авторлар туралы ақпарат:*** *Паджаджаран университетінің геологиялық апаттар мен табиғи қауіптерді азайтуға маманданған геотехникалық инженерия саласындағы ғылым магистрі; Паданг өнеркәсіптік технологиялар колледжінің (STTIND) тау-кен инженериясы бойынша оқытушысы, Батыс Суматра, Индонезия. Email: sucifitria1228@gmail.com; ORCID ID: https://orcid.org/0000-0003-0714-3672*
Teuku Yan W M Iskandarsyah	*Паджаджаран университетінің геология ғылымдарының докторы, Бандунг, Батыс Ява, Индонезия. Email: yan@unpad.ac.id; ORCID ID: https://orcid.org/0000-0002-7583-9244*
Cipta Endyana	*Паджажаран университетінің геология ғылымдарының докторы, Бандунг, Батыс Ява, Индонезия. Email: cipta.endyana@unpad.ac.id; ORCID ID: https://orcid.org/0000-0001-9448-1789*

Геоморфологическая динамика побережья и зоны риска цунами (5–12 м над уровнем моря) в городе Паданг, Западная Суматра, Индонезия

[1] Suci F.R.Z., [2]Teuku Y.W.M.I., [3]Cipta E.

[1]Горное дело, Колледж промышленных технологий (STTIND) Паданг, Паданг-Сити, Западная Суматра 25586
[2,3] Геологическая инженерия, Университет Паджаджаран, Бандунг 40132, Индонезия

Поступила: *2 января 2025*
Рецензирование: *6 января 2025*
Принята в печать: *24 апреля 2025*

АННОТАЦИЯ
Город Паданг — одна из столиц в западной части острова Суматра с общей протяженностью береговой линии около 68 126 км, непосредственно прилегающая к Индийскому океану. В последний раз провинция Западная Суматра пострадала от цунами в 2009 и 2010 годах, что вызвало цунами высотой от <1 метра до >12 метров, вызванное землетрясением магнитудой 7,9. Эксперты оценивают потенциальные катастрофы от землетрясений, возникающих из-за мега-разрывов плит вдоль островов Ментавай. Ранние и оптимальные усилия по смягчению последствий способны минимизировать последствия, вызванные катастрофами, вызванными цунами. Целью данного исследования является предоставление обзора влияния изменений береговой линии на зоны распространения цунами высотой 5 и 12 метров над уровнем моря. В этом исследовании используются параметры береговой линии города Паданг в 2005-2021 годах, полученные из Google Earth, администрации, уклона и земельного покрова, которые будут обработаны с использованием Географической информационной системы в программном обеспечении ArcGIS. Метод, используемый в исследовании, - затопление цунами путем деления высоты затопления цунами на три шкалы, включая низкую, среднюю и высокую. Наблюдения проводились в 122 точках наблюдения, разбросанных вдоль 18 520 метров береговой линии исследуемой области. Результаты показывают, что в городе Паданг есть от пяти до шести подрайонов, которые пострадали от цунами высотой 5 и 12 метров над уровнем моря, включая подрайоны Южный Паданг, Восточный Паданг, Западный Паданг, Северный Паданг, Нанггало, Кото Тангах. Разница в береговой линии с 2005 по 2021 год показывает изменение площади зоны распространения цунами примерно на 78,69–91,51 гектара на каждом уровне воды, вызванное аккреционными явлениями, происходящими вдоль береговой линии зоны наблюдения.

Ключевые слова: Береговая линия, землетрясение, цунами, ликвидация последствий стихийных бедствий.

Suci Fitria Rahmadhani Z

Информация об авторах:
Магистр инженерно-геологической инженерии, специализирующийся на смягчении последствий геологических катастроф и стихийных бедствий в университете Паджаджаран; Преподаватель горного дела, Колледж промышленных технологий (СТТИНД) Паданг, Западная Суматра, Индонезия. Email: sucifitria1228@gmail.com; ORCID ID: https://orcid.org/0000-0003-0714-3672

Teuku Yan W M Iskandarsyah	*Доктор инженерно-геологических наук университета Паджаджаран, Бандунг, Западная Ява, Индонезия. Email: yan@unpad.ac.id; ORCID ID: https://orcid.org/0000-0002-7583-9244*
Cipta Endyana	*Доктор инженерно-геологических наук университета Паджаджаран, Бандунг, Западная Ява, Индонезия. Email: cipta.endyana@unpad.ac.id; ORCID ID: https://orcid.org/0000-0001-9448-1789*

References

[1] Arief M, Winarso G, Prayogo T. Assessment of Shoreline Changes Using Landsat Satellite Data in Kendal Regency. Journal of Remote Sensing. 2011; 8:71-80.

[2] Halim, Halili, & Afu L. Study of Shoreline Change with Remote Sensing Approach in the Coastal Area of Soropia District. Journal of Sapa Laut. 2016; 1:24-31.

[3] Nur MT. Coastal abrasion and migration process. Dissertation of Population and Environmental Education Study Program (PKLH). Postgraduate Program, State University of Jakarta. 2004.

[4] Istiqomah F, Sasmito S, Ammarohman F. Monitoring Shoreline Changes Using Digital Shoreline Analysis System (DSAS) Application Case Study: Coastal Demak Regency. Geo Undip Journal. 2016; 5:78-89. https://doi.org/10.14710/jgundip.2016.10559

[5] Kasim F. Multiple Method Approach in Monitoring Shoreline Change Using Landsat Remote Sensing Dataset and GIS. Journal of Tropical Agrosciences. 2012; 6:180-188.

[6] Didi S. Engineering Geology. Yogyakarta: ANDI Publisher. 2019.

[7] National Coordinating Board for DMP. Policy Direction for Urban Disaster Mitigation in Indonesia. Jakarta: Secretariat of BAKORNAS PBP. 2002.

[8] Indonesian Science Institute. Mentawai Earthquake Recovery Process. 2010. http://lipi.go.id/berita/gempa-mentawai-proses-pemulihan/4640 (accessed on February 26, 2023).

[9] Wiko S. The Padang Earthquake of September 30, 2009 and its Tsunami Potential. Research and Development BMKG. 2013; 7(3):163-171.

[10] Yudhicara, Widjo K, Velly A, Suranto, Sapto N, Andrian I, Widodo S, Nils B, Knut F, Krämer, and Oliver K. Traces of the October 25, 2010 Tsunami in the Mentawai Islands based on Earth Research and Interviews. Journal of Environment and Geological Disasters. 2010; 1(3):165-181. https://doi.org/10.34126/jlbg.v1i3.19

[11] Dian O, Sudomo M. Geospatial Model of Tsunami Vulnerability Potential of Padang City. Journal of Meteorology and Geophysics. 2010; 11:140-146. https://doi.org/10.31172/jmg.v11i2.73

[12] Kastowo. Geological Map of Padang Sheet, Sumatra 1:250,000. Bandung: Geological Research and Development Center. 1996.

[13] Central Bureau of Statistics. Padang City in Figures 2022. Padang City: Adyta. 2022.

[14] Darlan Y. Integrated Study of Environment and Mineral Resources of Coastal Padang and Its Surroundings - West Sumatra. Marine Geology Research and Development Center: Bandung. 2004.

[15] Adrin T, Arifan JS, Nugroho AS, Eko S. Characteristics of Passive Soil Liquefaction in Padang City Based on Microtremor Method. Proceedings of Puslit Geoteknologi LIPI. 2013, 95-106.

[16] Bounoua L, DeFries R, Collatz GJ, Sellers P, Khan H. Effects of land cover conversion on surface climate. Climatic Change. 2002; 52:29-64. https://doi.org/10.1023/A:1013051420309

[17] Vink APA. Development of Land Use in Advancing Agriculture. In Land Use in Advancing Agriculture. Springer, Berlin, Heidelberg. 1975, 327-369.

[18] Holthuijsen L H. Waves in Oceanic and Coastal Waters. New York, Cambridge University Press. 2007. https://doi.org/10.1017/CBO9780511618536

[19] Nichols CR, Williams RG. Encyclopedia of Marine Science. New York. 2009.

[20] Sastrawan B, Tanjung A, Ghalib M. Patterns of Tidal Currents and Waves in the Waters of Teluk Bayur, Padang City, West Sumatra Province. Doctoral Dissertation, University of Riau. 2017.

[21] National Disaster Management Agency. Indonesia Disaster Risk. Jakarta. 2016.

[22] United States Geological Survey. 2022. https://www.usgs.gov/programs/earthquake-hazards (accessed on Apr 17, 2022).

[23] Wiko S. The Padang Earthquake of September 30, 2009 and its Tsunami Potential. BMKG Research and Development. 2013; 7(3):163-171.

[24] Sabar S. Earthquake Potential Energy in the Mentawai-West Sumatra Segment Area (0.5o N-S-4.0o N-S and 100o E-104o E). Physics Student Journal. 2014; 2(1).

[25] Mukhopadhyay A, Mukherjee S, Mukherjee S, Ghosh S, Hazra S, & Mitra D. Automatic shoreline detection and future prediction: A case study on Puri Coast, Bay of Begal, India. European Journal of Remote Sensing. ISSN:(PRINT) 2279-7254. 2012; 45(1): 201-213.

[26] Setiyono H. Dictionary of Oceanography. First Printing. Gadjah Mada, University Press. Yogyakarta. 1996.

[27] Nur M T. Coastal abrasion and migration process. Dissertation of Population and Environment Education Study Program (PKLH). Postgraduate Program, State University of Jakarta. 2004.

[28] Berryman K. Review of Tsunami hazard and risk in New Zealand, report by the Institute of Geological and Nuclear Sciences. New Zealand. 2006.

Crossref
DOI: 10.31643/2026/6445.30
Earth sciences

Study of rock mass structural features based on laser scanning results

[*]Yartseva V.F., Ozhigin D.S., Dolgonosov V.N., Ozhigina S.B., Ozhigin S.G.

Abylkas Saginov Karaganda Technical University, Karaganda, Kazakhstan

** Corresponding author email: v.yartseva@ktu.edu*

Received: *January 22, 2025*
Peer-reviewed: *February 21, 2025*
Accepted: *April 29, 2025*

ABSTRACT

Monitoring of pit slopes benches stability and pit walls plays the important role in the safety of mining operations. Slope stability assessment and risk management are mandatory to ensure safe and efficient operation of pits. Laser scanning technology is one of the base methods of geospatial data collecting for building of man-made objects models. Laser scanning is widely used in mining when performing survey work, measurements, monitoring, and studying structural features on the outcroppings of the rock mass. The article describes the technological chain: the collection of geospatial data, the processing of the obtained data with the construction of a terrain model and the further use of the resulting model to solve practical tasks. The choice of optimal laser scanning parameters should be based on the technological features of a pit, the technical characteristics of used equipment and scanning density required to solve the tasks. The article demonstrates the use of the obtained model for determining the necessary geometric parameters of the structural features of the rock mass to conduct kinematic analysis of potential bench failures at the object of study. Based on the results of kinematic analysis, recommendations were developed for further mining operations and potential bench failures risks reducing. The proposed technology can be used and adapted for laser scanning, followed by the construction of a terrain model at various mineral deposits to solve a wide range of tasks and ensure the safety of open-pit mining. Due to the inclusion of laser scanners in the register of measuring instruments in Kazakhstan, high reliability of measurement accuracy is ensured. The technology allows both to obtain generalized data on the sides of the quarry, as well as detailed scans of individual ledges. A significant advantage is the automatic generation of a point cloud during scanning, which reduces in-house processing.

Keywords: laser scanning, geospatial data, digital terrain model, kinematic analysis, pit, rock mass structure.

Information about authors:

Yartseva Vera — *Phd Student, Senior Lecturer of the Department of Mine Surveying and Geodesy, Abylkas Saginov Karaganda Technical University, ave. Nursultan Nazarbayev, 56, 100027, Karaganda, Kazakhstan. Email: v.yartseva@ktu.edu; ORCID ID: https://orcid.org/0000-0003-3015-0280*

Ozhigin Dmitriy — *PhD, Senior Lecturer of the Department of Mine Surveying and Geodesy, Abylkas Saginov Karaganda Technical University, ave. Nursultan Nazarbayev, 56, 100027, Karaganda, Kazakhstan. Email: d.ozhigin@ktu.edu.kz; ORCID ID: https://orcid.org/0000-0002-2443-3068*

Dolgonosov Victor — *Doctor of Technical Sciences, Professor of the Department of Mine Surveying and Geodesy, Abylkas Saginov Karaganda Technical University, ave. Nursultan Nazarbayev, 56, 100027, Karaganda, Kazakhstan. Email: v.dolgonosov@ktu.edu.kz; ORCID ID: https://orcid.org/0000-0001-8110-2284*

Ozhigina Svetlana — *Candidate of Technical Sciences, Senior Lecturer, Department of Mine Surveying and Geodesy, Abylkas Saginov Karaganda Technical University, ave. Nursultan Nazarbayev, 56, 100027, Karaganda, Kazakhstan. Email: s.ozhigina@ktu.edu.kz; ORCID ID: https://orcid.org/0000-0001-7986-2858*

Ozhigin Sergey — *Doctor of Technical Sciences, Professor of the Department of Mine Surveying and Geodesy, Abylkas Saginov Karaganda Technical University, ave. Nursultan Nazarbayev, 56, 100027, Karaganda, Kazakhstan. Email: s.ozhigin@ktu.edu.kz; ORCID ID: https://orcid.org/0000-0003-2432-3851*

Introduction

Scientific and technological progress in the field of digital technologies has led to the improvement of methods for studying rock mass in the mining industry. This made it possible to take into account a larger number of parameters for constructing structural models that are as close as possible to the actual mining and geological situation of the studied field [[1], [2], [3]]. Using three-dimensional modeling of deposits has significantly influenced the entire mining process and the adoption of design decisions. The most important stage in creating models of a rock mass is the collection of initial data [[4], [5]]. Ground-based laser scanning is used for subsequent modeling of a pit and its individual elements. Pit

slopes are potentially dangerous objects. The use of laser scanning makes it possible to remotely obtain data on the structure of rock outcroppings on the surface of the open pit walls of pits, which ensures the safety of personnel conducting measurements. The efficiency of the work is an important advantage of this technology. Based on the constructed models, a wide range of applied mining tasks can be solved at a pit [[6], [7], [8]].

The problem of quickly performing three-dimensional surveys to account for mining, monitor the condition of rock slopes, and control reserves in mining requires a lot of effort and resources, placing special requirements on measuring instruments. Aerial photography and laser scanning technologies are suitable for the effective solution of these tasks. Ground-based laser scanning is superior to aerial photography in terms of accuracy and detail, especially in the study of complex geometric shapes and small cracks. However, aerial photography is more convenient for covering large areas and operational surveys, but is inferior in terms of measurement accuracy and detail of the resulting model [[9], [10]].

The article describes in stages the methodology of laser scanning for geospatial data collecting, subsequent processing of the obtained data with the construction of a digital terrain model, the study of structural features and their parameters. Kinematic analysis was also carried out to assess the probability of landslides.

The object of the study was the potentially dangerous section of the northern open pit wall of Chiganak pit of the barite deposit (Zhambyl region, Republic of Kazakhstan). The engineering and geological conditions of Chiganak deposit are classified as difficult. The geological structure of the deposit is characterized by a large tectonic disturbance (the presence of disjunctive and plicative disturbances) and the occurrence of rocky and semi-rocky dislocated fractured rocks with the presence of crushing and weathering zones.

Experimental part

The study of the elements of rock mass structure always begins with the selection of the scanning area where there are clearly visible structural elements on the outcroppings. To set and coordinate the position of the scanner, it is necessary to determine at least two solid points for cross-surveying the pit area under study and creating an overlap of scans.

The scanning density (scanning grid) is determined by the assigned tasks, the solution of which will be performed according to the resulting model. To achieve the stated density of the point cloud, even in blind spots, an increase in scanning density due to overlapping scans will not be taken into account. The initial data for calculating of the optimal parameters of the scanner installation are the size of the investigated section of the open pit wall of the pit, the required density of the point cloud, the technical characteristics and equipment of the scanner, as well as the technological features of the pit that affect the installation of the scanner.

To study the structural features of the potentially dangerous section of the northern open pit wall of Chiganak field pit, a minimum scanning density of 10*10 mm was adopted. Based on this, the optimal installation parameters of the Leica HDS 8800 3D scanner were determined. To obtain scans with an overlap of at least 80% and the scanning grid density of 10*10 mm, the distance between solid points was 35 meters, with the scanning range of about 30 m (Figure 1).

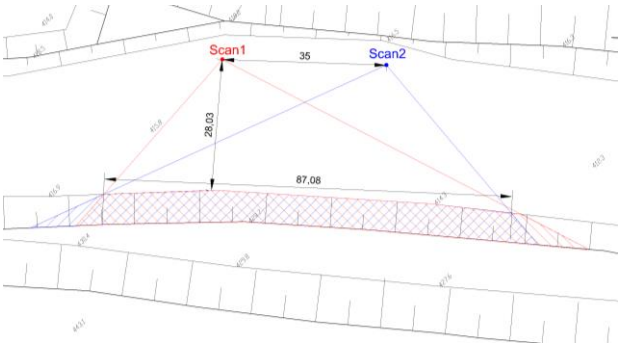

Figure 1 - Scheme of ground laser scanning of the studied section of the pit benches

The Leica HDS8800 scanner, which is a comprehensive laser scanning surveying system specially designed for use in the mining industry, was used to perform the study. The Leica HDS8800 has adaptive scan density and can scan in five modes. In scanning mode No. 16, a high level of detail of 21 mm is achieved at a distance of 100 mm, which can be increased by reducing the distance to the scanned object. The dependence of the scanning density on the selected mode and the scanning range from 14 to 30 meters is calculated (Table 1).

Table 1 - The dependence of the scanning density on the selected mode and the scanning range

Mode	Scanning range, m.								
	14	16	18	20	22	24	26	28	30
1	48.86	55.84	62.82	69.8	76.78	83.76	90.74	97.72	104.7
2	24.36	27.84	31.32	34.8	38.28	41.76	45.24	48.72	52.2
4	12.18	13.92	15.66	17.4	19.14	20.88	22.62	24.36	26.1
8	6.02	6.88	7.74	8.6	9.46	10.32	11.18	12.04	12.9
16	2.94	3.36	3.78	4.2	4.62	5.04	5.46	5.88	6.3

The creation of a survey justification begins with an analysis of the existing state geodetic networks (SGN) in the area of the studied object. Our analysis showed the presence of 11 SGN points, the coordinates of which were re-determined using GNSS (Global Navigation Satellite System) technologies. GNSS measurements by the receiver in static mode made it possible to re-obtain the coordinates of SGN points in the local coordinate system and perform a comparative analysis for a sample of points with high data reliability. The transformation of coordinates from the world system (WGS84) to the local system and network alignment were performed using the transformation file (transition key) of the Leica Infinity software, which is loaded into the GNSS receiver controller and makes it possible to immediately obtain coordinates in the local system.

GNSS technology was also used to determine the coordinates of solid points in static mode in conjunction with total station survey. The need to use a total station survey to create a planned altitude justification is dictated by the difficulty of satellite signal passing inside the pit, and as a result, the occurrence of measurement errors.

The result of ground-based laser scanning is a spatial model formed by a point cloud, each point of which is characterized by coordinates (X, Y, Z) and color. Subsequent desk processing of the resulting point cloud including the processes of combining scans and filtering them was performed using the Maptek I-Site Studio software.

When creating accurate three-dimensional models of objects, combining scans allows reducing the number of blind spots that are formed due to equipment limitations or geometric features of the object. Each scan is performed from different angles to maximize the coverage of the object's surface, then the results of several scans are combined into a single point cloud. This approach allows getting a detailed and complete model of the object.

The data filtering process is necessary to remove noise and unwanted elements to create an accurate and reliable model, as well as, if necessary, reduce the amount of data while preserving information about the geometry of the object. One of the main point cloud filtering methods based on measuring distances to neighboring points is to remove outliers that are far from the main surface of the object.

Coloring the points of the cloud in real colors allows decrypting the studied section of the pit using a three-dimensional model. The coordinates of the points, determined with an accuracy of 10 mm, make it possible to carry out the necessary measurements of the geometric parameters of cracks, rock boundaries and discontinuities with sufficient accuracy.

The geometric parameters of the structural features of the rock mass were also measured in the Maptek I-Site Studio software. The following geometric parameters of the structural elements are determined: the fall, the direction of the fall, the average distance between the cracks and the coordinate reference of the measurement sites (Figure 2).

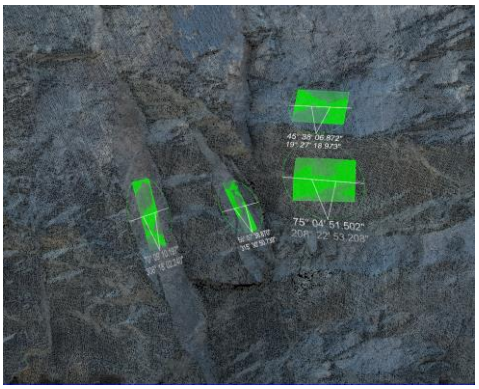

Figure 2 - Measuring process of structural elements geometric parameters

The obtained crack occurrence parameters are exported to Excel spreadsheet, the fragment of which is shown in Table 2.

Table 2 - Results of determining of cracks occurrence elements

No.	Y, m	X, m	Z, m	Fall, degree	Fall direction, degree
1	33437.581	19307.788	354.510	78.360	354.074
2	33437.631	19307.933	355.042	48.442	151.849
3	33435.970	19308.274	354.721	50.302	15.276
4	33436.087	19308.168	355.399	45.830	166.297
5	33438.774	19307.319	353.699	85.607	212.191
6	33446.847	19306.707	354.949	85.156	30.809
7	33447.120	19306.913	355.350	37.122	184.027
8	33447.620	19306.556	354.919	81.196	179.346
9	33457.285	19305.269	355.323	62.497	30.894
10	33457.465	19305.359	355.935	34.136	185.924
...					

Kinematic analysis based on rock jointing measurements.

The analysis of the condition of separate benches is based on the study of the properties of the rock formations composing them, structural elements and their features, the presence of weak rock contacts, faults, natural rock jointing, the degree of negative impact of drilling and blasting, weathering and oxidation processes. All of these factors, from the point of view of sustainability, have a negative impact to one degree or another. The task is to identify the dominant risk factors that can lead to local bench failure and deformations [[11], [12], [13], [14]].

The benches of the Chiganak deposit are composed of rocky and semi-rocky soil, broken by cracks of various orientations and intensities. Instability in such rock mass occurs by shifting along cracks or by overturning blocks. The possibility of such cases is determined by the spatial orientation of crack systems and man-made outcroppings of slopes. The complex of issues related to the study of the potential for crack stability violations with the fulfilment of the conditions of a special limit equilibrium is called kinematic analysis.

The Rocscience software package provides a special product named Dips for interactive analysis of geological data based on the orientation of crack systems to perform kinematic analysis and risk assessment of planar and wedge-shaped displacements (Figure 3).

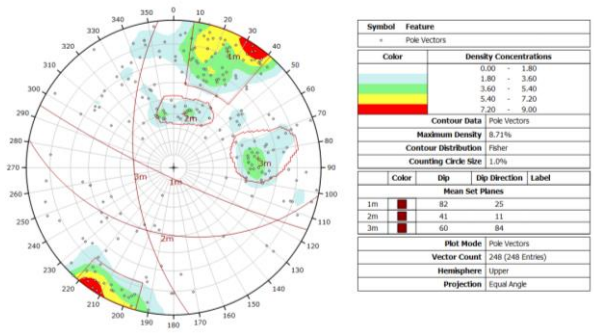

Figure 3 - The crack systems in Dips Rocscience software

The program uses stereographic projection and is a set of tools for various applications and analysis of geological data. The input data affecting the probability of bench failures are the orientation of the slope and crack systems, the slope angle of the bench and the angle of friction along the cracks. As a result of kinematic analysis, the probabilities of rock mass failure modes are determined in Dips [[15], [16], [17]].

There are three types of possible bench failures: Planar Sliding, Wedge Sliding, and Toppling [[16], [17]]:

1. Planar Sliding. A bench failure in the form of a flat slide is possible if the direction of fall of the crack system and the slope surface correspond to the developed space. In this case, the angle of incidence of the crack system is less than the angle of incidence of the slope surface, but exceeds the value of the angle of internal friction along the cracks. If these conditions are met, then the fragments of the bench limited by systems of cracks in the form of blocks have the potential to shift towards the developed space. The data and assessment of the possibility of flat sliding is shown in Figure 4.

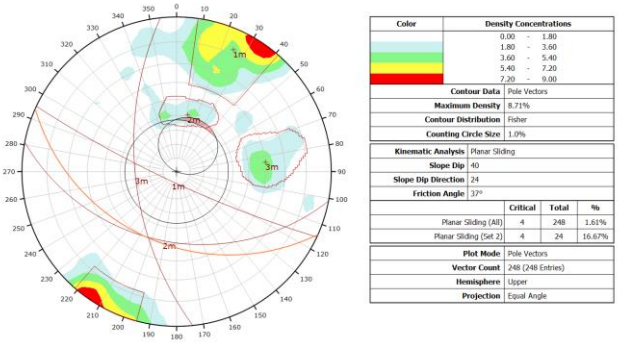

Figure 4 - Planar Sliding analysis

2. Wedge Sliding. This type of bench failure can occur in the open pit walls of pits, when two diagonal systems of cracks falling about the slope form a wedge, which is capable of shifting in the direction of the space left after mining. The condition for the possibility of such a displacement is the slope of the line of intersection of these planes towards the mining space, exceeding the value of the angle of internal friction along the cracks. Under these conditions, the displacement of the rock block in the form of a wedge occurs under the action of gravity. Kinematic analysis of wedge-shaped bench failure is an important tool for assessing the risks of bench failure in pits. It allows making preliminary calculations and identifying areas of increased risk of bench failure, which makes it possible to take appropriate measures to ensure the safety of mining operations. The data and assessment of the possibility of wedge sliding are shown in Figure 5.

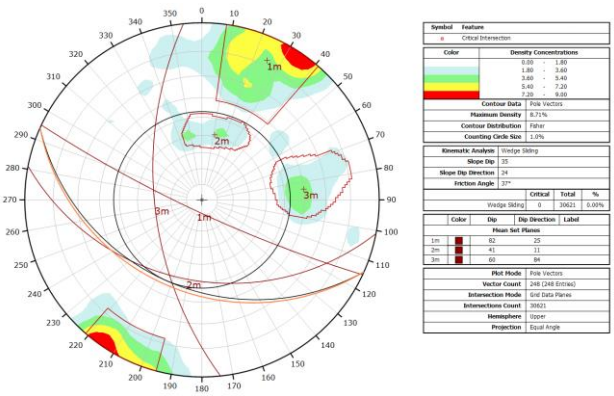

Figure 5 - Wedge Sliding analysis

3. Direct Toppling. This type of bench failure occurs when a rock mass fall along a vertical plane perpendicular to the slope surface. Direct toppling is often registered in pits where the slopes have a steep angle and the rocks have low strength. An important condition contributing to direct toppling is a decrease in the strength of the contour zone as a result of weathering, erosion, the influence of drilling and blasting, seismic activity and other factors. Direct toppling monitoring at a pit is essential to ensure the safety of workers and prevent devastating accidents. The data and assessment of the possibility of direct toppling are shown in Figure 6.

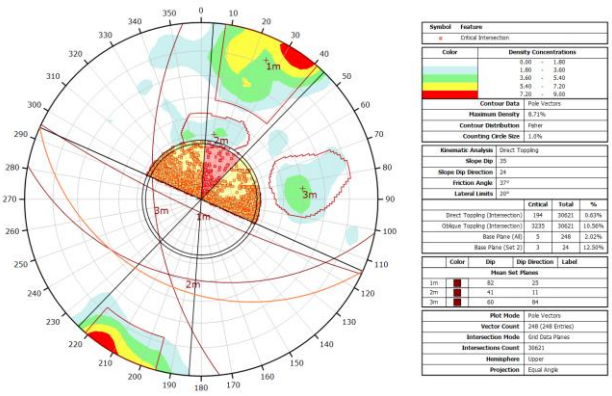

Figure 6 - Toppling analysis

The sensitive analysis of the «slope angle» parameter was realized to assess the actual condition of the benches of the open pit wall of the pit and make design decisions. The results of the analysis showed that a further increase in the slope angles is impossible due to a sharp increase in the risk of bench failure. The probability of direct toppling with the current slope angle parameters of 40 degrees already has a fairly high probability, and with an increase of 5 degrees, it doubles and has an extremely high value [[20], [21], [22], [23], [24]]. The potential risks for all types of bench failures with a further increase in the slope angle and the walls of the pit are shown in Table 3.

Table 3 - Impact of increasing slope angle on the degree of potential risk of failure

Slope angle, degree	*Planar sliding, %*	*Wedge sliding, %*	*Direct toppling, %*
40	16.7	1.28	29.17
45	37.5	5.43	58.33
50	58	9.72	70.83
55	66.67	12.71	75
60	66.67	15.63	75
65	66.67	20.29	75
70	66.67	27.82	75
75	66.67	35	75
80	66.67	41.4	75
85	66.67	50	75

Results and Discussion

Laser scanning of the pit slope section of the Chiganak barite deposit was carried out using a Leica HDS 8800 mining laser. The survey justification for this was created using GNSS technologies. The density of laser scanning throughout the entire area was 10 mm or higher. A representative volume of geospatial data on structural elements of the rock mass was collected in the form of an accurate three-dimensional model. Based on this model, measurements were made of the geometric parameters of structural elements necessary for conducting kinematic analysis: the dip, the direction of dip, the average distance between cracks, and the coordinate reference for measurement sites. A kinematic analysis was then performed using the Dips software package. The results showed the probability of all three types of potential bench failures at a current slope angle of 40 degrees. The highest potential risk of failure is in direct toppling, which amounts to 29.17%. To evaluate the design solutions for increasing the slope angles, a thorough analysis was conducted using the slope angle as a parameter, with an interval of 5 degrees. This analysis revealed that it is not possible to further increase the angle due to the high probability of direct toppling at the current angle of 40 degrees. With an increase of just 5 degrees, the probability of toppling becomes extremely high, doubling from the current value.

Laser scanning is an excellent data acquisition tool for building three-dimensional models of open

pits and their elements. The three-dimensional models obtained apply to solving a wide range of tasks, including studying the rock mass structural features, assessing the open pit slopes' stability and analyzing possible failures. Laser scanners are included in the register of measuring instruments of the Republic of Kazakhstan, which makes it possible to obtain measurements with the declared accuracy, guaranteed by device verification certificates. Laser scanning can be used as a method for generalized data obtaining on the condition of the pit wall section and detailed scans of individual sections of its benches. The use of laser scanning technology makes it possible to significantly reduce the stage of desk processing, since a point cloud is generated during the scanning process. The resulting point cloud, in which coordinates and color are assigned to each point, is immediately imported from the scanner's memory into the software for further processing. The resulting three-dimensional models apply to solving a wide range of tasks. The proposed technology for collecting geospatial data provides the construction of a digital three-dimensional model with a pixel size of 10 mm. The limitation of using this model is based solely on its pixel size.

Conclusions

The proposed technique for geospatial data collecting based on laser scanning and GNSS technologies can be used to obtain three-dimensional models that provide the required accuracy. Laser scanning has no restrictions and is applicable in pits for the extraction of any type of minerals. The speed of three-dimensional model obtaining and its accuracy make it possible to quickly solve topical issues arising during mining operations. It is planned to further develop data collection technology based on laser scanning to construct a more detailed digital three-dimensional model of open pit elements to study microcracks and their impact on the rock mass condition.

Conflicts of interest. No conflicts of interest

CRediT author statement: **V. Yartseva**: Conceptualization, Writing draft preparation; **D. Ozhigin**: Software, Data curation; **V. Dolgonosov**: Methodology. Visualization; **S. Ozhigina**: Investigation. **S. Ozhigin**: Validation, Supervision.

Cite this article as: Yartseva VF, Ozhigin DS, Dolgonosov VN, Ozhigina SB, Ozhigin SG. Study of rock mass structural features based on laser scanning results. Kompleksnoe Ispolzovanie Mineralnogo Syra = Complex Use of Mineral Resources. 2026; 338(3):72-80. https://doi.org/10.31643/2026/6445.30

Лазерлік сканерлеу негізінде тау массивінің құрылымдық ерекшеліктерін зерттеу

Ярцева В.Ф., Ожигин Д.С., Долгоносов В.Н., Ожигина С.Б., Ожигин С.Г.

Әбілқас Сағынов атындағы Қарағанды техникалық университеті, Қарағанды, Қазақстан

Мақала келді: *22 қаңтар 2025*
Сараптамадан өтті: *21 ақпан 2025*
Қабылданды: *29 сәуір 2025*

ТҮЙІНДЕМЕ

Тау-кен жұмыстарының қауіпсіздігі мәселесінде карьердің беткейлерінің тұрақтылығын бақылау маңызды рөл атқарады. Көлбеу тұрақтылықты бағалау және тәуекелдерді басқару карьерлерді қауіпсіз және тиімді пайдалануды қамтамасыз ету үшін міндетті болып табылады. Лазерлік сканерлеу технологиясы техногендік объектілердің модельдерін құру үшін геокеңістіктік деректерді жинаудың негізгі әдістерінің бірі. Тау-кен өндірісінде лазерлік сканерлеу түсірілім жұмыстарында, өлшеулерде, бақылауларда және тау жыныстарының беткейлерінің құрылымдық ерекшеліктерін зерттеуде кеңінен қолданылады. Мақалада қарастырылған технологиялық тізбек: геокеңістіктік деректерді жинау, алынған деректерді өңдеу арқылы жер бедерінің моделін құру және практикалық мәселелерді шешу үшін алынған модельді одан әрі пайдалану. Лазерлік сканерлеудің оңтайлы параметрлерін таңдау карьердің технологиялық ерекшеліктеріне, пайдаланылатын жабдықтың техникалық сипаттамаларына, қойылған міндеттерді шешу үшін қажетті сканерлеу тығыздығына негізделуі керек. Мақалада зерттеу объектісіндегі ықтимал опырылуларға кинематикалық талдау жүргізу мақсатында массивтің құрылымдық ерекшеліктерінің қажетті геометриялық параметрлерін анықтау үшін алынған модельді қолдану көрсетілген. Кинематикалық талдаудың алынған нәтижелері негізінде тау-кен жұмыстарын одан әрі жүргізу және ықтимал опырылу қаупін азайту бойынша ұсыныстар жасалды. Ұсынылған технология кең ауқымды мәселелерді шешу және ашық әдіспен өндірудің қауіпсіздігін қамтамасыз ету үшін

	әр түрлі пайдалы қазбалар кен орындарында кейіннен жер бедері үлгісін салу арқылы лазерлік сканерлеу үшін пайдаланылуы және бейімделуі мүмкін. Лазерлік сканерлерді Қазақстанның өлшеу аспаптарының тізіліміне енгізудің арқасында өлшеу дәлдігінің жоғары сенімділігі қамтамасыз етіледі. Технология карьер жақтары бойынша жалпылама деректерді алуға және жеке ойықтарды егжей-тегжейлі сканерлеуге мүмкіндік береді. Маңызды артықшылығы - сканерлеу кезінде нүктелердің бұлты автоматты түрде жасалады, бұл камералық өңдеуді азайтады.
	Түйін сөздер: лазерлік сканерлеу, геокеңістіктік деректер, рельефтің сандық моделі, кинематикалық талдау, карьер, тау массивінің құрылымы.
Ярцева Вера Фаридовна	***Авторлар туралы ақпарат:*** *PhD докторант, Маркшейдерлік іс және геодезия кафедрасының аға оқытушысы, Әбілқас Сағынов атындағы Қарағанды техникалық университеті, Н.Назарбаев 56, 100027, Қарағанды, Қазақстан. Email: v.yartseva@ktu.edu; ORCID ID: https://orcid.org/0000-0003-3015-0280*
Ожигин Дмитрий Сергеевич	*PhD, Маркшейдерлік іс және геодезия кафедрасының аға оқытушысы, Әбілқас Сағынов атындағы Қарағанды техникалық университеті, Н.Назарбаев 56, 100027, Қарағанды, Қазақстан. Email: d.ozhigin@ktu.edu.kz; ORCID ID: https://orcid.org/0000-0002-2443-3068*
Долгоносов Виктор Николаевич	*Т.ғ.д., Маркшейдерлік іс және геодезия кафедрасының профессоры, Әбілқас Сағынов атындағы Қарағанды техникалық университеті, Н.Назарбаев 56, 100027, Қарағанды, Қазақстан. Email: v.dolgonosov@ktu.edu.kz; ORCID ID: https://orcid.org/0000-0001-8110-2284*
Ожигина Светлана Борисовна	*Т.ғ.к., Маркшейдерлік іс және геодезия кафедрасының аға оқытушысы, Әбілқас Сағынов атындағы Қарағанды техникалық университеті, Н.Назарбаев 56, 100027, Қарағанды, Қазақстан. Email: s.ozhigina@ktu.edu.kz; ORCID ID: https://orcid.org/0000-0001-7986-2858*
Ожигин Сергей Георгиевич	*Т.ғ.д., Маркшейдерлік іс және геодезия кафедрасының профессоры, Әбілқас Сағынов атындағы Қарағанды техникалық университеті, Н.Назарбаев 56, 100027, Қарағанды, Қазақстан. Email: s.ozhigin@ktu.edu.kz; ORCID ID: https://orcid.org/0000-0003-2432-3851*

Исследование структурных особенностей горного массива на основе лазерного сканирования

Ярцева В.Ф., Ожигин Д.С., Долгоносов В.Н., Ожигина С.Б., Ожигин С.Г.

Карагандинский технический университет имени Абылкаса Сагинова, Караганда, Казахстан

Поступила: *22 января 2025*
Рецензирование: *21 февраля 2025*
Принята в печать: *29 апреля 2025*

АННОТАЦИЯ

Мониторинг устойчивости откосов уступов и бортов карьера играет важную роль в вопросе безопасности ведения горных работ. Оценка устойчивости откосов и управление рисками являются обязательными для обеспечения безопасной и эффективной эксплуатации карьеров. Технология лазерного сканирования является одним из основных методов сбора геопространственных данных для построения моделей техногенных объектов. Лазерное сканирование широко применяется в горном деле при выполнении маркшейдерских работ, измерений, мониторинга и изучения структурных особенностей на выходах горного массива. В статье рассмотрена технологическая цепочка: сбор геопространственных данных, обработка полученных данных с построением модели местности, и дальнейшее использование полученной модели для решения практических задач. Выбор оптимальных параметров лазерного сканирования должен основываться на технологических особенностях карьера, технических характеристиках используемого оборудования, на требуемой плотности сканирования, необходимой для решения поставленных задач. В статье показано использование полученной модели для определения необходимых геометрических параметров структурных особенностей массива с целью проведения кинематического анализа потенциальных обрушений на объекте исследования. На основе полученных результатов кинематического анализа были выработаны рекомендации по дальнейшему ведению горных работ и снижению рисков потенциальных обрушений. Предложенная технология может быть использована и адаптирована для проведения лазерного сканирования с последующим построением модели местности на различных месторождениях полезных ископаемых для решения широкого круга задач и обеспечения безопасности открытых горных работ. Благодаря включению лазерных сканеров в реестр измерительных приборов Казахстана, обеспечивается высокая достоверность точности измерений. Технология позволяет как получать обобщенные данные о бортах карьера, так и детализированные сканы отдельных уступов. Существенным преимуществом является автоматическая генерация облака точек во время сканирования, что сокращает камеральную обработку.

	Ключевые слова: лазерное сканирование, геопространственные данные, цифровая модель местности, кинематический анализ, карьер, структура горного массива.
Ярцева Вера Фаридовна	***Информация об авторах:*** *PhD докторант, старший преподаватель кафедры Маркшейдерского дела и геодезии, Карагандинский технический университет имени Абылкаса Сагинова, пр. Н.Назарбаева 56, 100027, Караганда, Казахстан. Email: v.yartseva@ktu.edu; ORCID ID: https://orcid.org/0000-0003-3015-0280*
Ожигин Дмитрий Сергеевич	*PhD, старший преподаватель кафедры Маркшейдерского дела и геодезии, Карагандинский технический университет имени Абылкаса Сагинова, пр. Н.Назарбаева 56, 100027, Караганда, Казахстан. Email: d.ozhigin@ktu.edu.kz; ORCID ID: https://orcid.org/0000-0002-2443-3068*
Долгоносов Виктор Николаевич	*Д.т.н., профессор кафедры Маркшейдерского дела и геодезии, Карагандинский технический университет имени Абылкаса Сагинова, пр. Н.Назарбаева 56, 100027, Караганда, Казахстан. Email: v.dolgonosov@ktu.edu.kz; ORCID ID: https://orcid.org/0000-0001-8110-2284*
Ожигина Светлана Борисовна	*К.т.н., старший преподаватель кафедры Маркшейдерского дела и геодезии, Карагандинский технический университет имени Абылкаса Сагинова, пр. Н.Назарбаева 56, 100027, Караганда, Казахстан. Email: s.ozhigina@ktu.edu.kz; ORCID ID: https://orcid.org/0000-0001-7986-2858*
Ожигин Сергей Георгиевич	*Д.т.н., профессор кафедры Маркшейдерского дела и геодезии, Карагандинский технический университет имени Абылкаса Сагинова, пр. Н.Назарбаева 56, 100027, Караганда, Казахстан. Email: s.ozhigin@ktu.edu.kz; ORCID ID: https://orcid.org/0000-0003-2432-3851*

References

[1] Kosarev N, Goldobin D, Sermiagin R, Kemerbayev N, Sholomitskii A. Evaluation of the high-degree global gravity field models in the territory of Kazakhstan. International Journal of Engineering and Geosciences. 2025; 10(1):14-21. https://doi.org/10.26833/ijeg.1485621

[2] Moser DV, Levin E, Satbergenova AK. The research study in the convergence of the results of processing radar images sentinel-1a with field observations of agricultural sites. Geodesy and cartography. 2019; 950(8):52–58. http://doi.org/10.22389/0016-7126-2019-950-8-52-58

[3] Alipbeki O, Grossul P, Rakhimov D, Kupidura P, Alipbekova C, Musaif G, Turekeldiyeva R, Augambaev K, Begaliyeva M. Ecosystem Health Assessment of the Zerendy District, Kazakhstan. Sustainability. 2025, 17(1):277. https://doi.org/10.3390/su17010277

[4] Alipbeki O, Alipbekova C, Mussaif G, Grossul P, Zhenshan D, Muzyka O, Turekeldiyeva R, Yelubayev D, Rakhimov D, Kupidura P, Aliken E. Analysis and Prediction of Land Use/Land Cover Changes in Korgalzhyn District, Kazakhstan. Agronomy. 2024; 14:268. https://doi.org/10.3390/agronomy14020268

[5] Renato Macciotta. Slope risk management in light of uncertainty and environmental variability-2021 Canadian Geotechnical Colloquium. Canadian Geotechnical Journal. 2023; 60(12):1777-1791. https://doi.org/10.1139/cgj-2022-0626

[6] Bilgehan Kekeç, Niyazi Bilim, Emre Karakaya, Dhikra Ghiloufi. Applications of Terrestrial Laser Scanning (TLS) in Mining: A Review. Turkey Lidar Journal. 2021; 3(1):31-38. https://doi.org/10.51946/melid.927270

[7] Sokalski D, Wojewoda J. Comparison of the consistency of structural measurements made using the traditional method and with the use of point cloud from terrestrial laser scanning in a selected site of Radków Bluff (Table Mountains, SW-Poland). Landform Analysis. 2023; 42:37-49. https://doi.org/10.12657/landfana-042-003

[8] Xu Z, Xu E, Wu L, Liu S, Mao Y. Registration of Terrestrial Laser Scanning Surveys Using Terrain-Invariant Regions for Measuring Exploitative Volumes over Open-Pit Mines, Remote sensing. 2019; 11(6):606. https://doi.org/10.3390/rs11060606

[9] Druz RA, Protasova AV, Ohunov ShR, Kshanovskaja AV. Comparison of airborn laser scanning and aerial survey using unmanned air vehicles. Mining Informational and Analytical Bulletin. 2023; 5:130-14. https://doi.org/10.25018/0236_1493_2023_5_0_130

[10] Tan Y, Liu X, Jin S, Wang Q, Wang D, Xie XA. Terrestrial Laser Scanning-Based Method for Indoor Geometric Quality Measurement. Remote Sensing. 2024; 16(1):59. https://doi.org/10.3390/rs16010059

[11] Nizametdinov FK, Baryshnikov VD, Zhanatuly E, Nagibin AA, Tuyakbai AS, Nizametdinov NF, Estaeva AR. Selection and Justification of Design Variables for Strength Properties of Rocks in Slope Stability Analysis for Open Pits. Journal of Mining Science. 2021; 57:386-392. https://doi.org/10.1134/S1062739121030042

[12] Bagaraja Sirait, Silti Salinita, Zulfahmi, Eko Pujianto. Assessing slope failure in coal mining using kinematic analysis, IOP Conference Series: Earth and Environmental Science. International Seminar on Mineral and Coal Technology, Bandung. 2021; 882:012060. https://doi.org/10.1088/1755-1315/882/1/012060

[13] Ozdogan MV, Deliormanli AH. Determination of possible failure surfaces in an open-pit slope caused by underground production. Bulletin of Geophysics and Oceanography. 2020; 61(2):199-218. https://doi.org/10.4430/bgta0305

[14] David Saiang. Back Analysis of Narrow Vein Open Stope Stability and Verification Using Kinematic and Empirical Methods. Proceedings of the Rocscience International Conference. 2023. https://doi.org/10.2991/978-94-6463-258-3_3

[15] Liu W, Sheng G, Kang X, Yang M, Li D, Wu S. Slope Stability Analysis of Open-Pit Mine Considering Weathering Effects. Applied Sciences. 2024; 14:8449. https://doi.org/10.3390/app14188449

[16] Xu S, Wang B, Wang D, Zhang J. A practical stability/instability chart analysis for slope large deformations using the material point method. Engineering Geology. 2024; 338:107611. https://doi.org/10.1016/j.enggeo.2024.107611

[17] Christian Obregon, Hani Mitri. Probabilistic approach for open pit bench slope stability analysis – A mine case study. International Journal of Mining Science and Technology. 2019; 29(4):629-640. https://doi.org/10.1016/j.ijmst.2019.06.017

[18] Duncan C. Wyllie, Christopher W. Mah. Rock slope engineering (4th Edition). Taylor & Francis e-Library. 2005.

[19] Hudson JA, Harrison JP. Engineering rock mechanics. An introduction to the principles. Elsevier Science. 2000.

[20] Agyei G, Ocran L, Buaba EM. Slope Angle Estimation Of Amoanda East Pit Of Abosso Gold Fields, Ghana. Nigerian Journal of Technology. 2019; 38(3):594-602. http://dx.doi.org/10.4314/njt.v38i3.8

[21] Yi He, Junyan Yu, Ran Yuan, Wenfa Wang, Nikolaos Nikitas. Stability and failure mechanisms in three-dimensional cracked slope: Static and dynamic analysis. Computers and Geotechnics. 2022; 144:104626. https://doi.org/10.1016/j.compgeo.2021.104626

[22] Lu Y, Chen X, Wang L. Research on Fracture Mechanism and Stability of Slope with Tensile Cracks. Applied Sciences. 2022; 12:12687. https://doi.org/10.3390/app122412687

[23] Yi He, Yan Liu, Yingbin Zhang, Ran Yuan. Stability assessment of three-dimensional slopes with cracks. Engineering Geology. 2019; 252:136-144. https://doi.org/10.1016/j.enggeo.2019.03.001

[24] Nizametdinov NF, Baryshnikov VD, Nagibin AA, Nizametdinov RF, Tuyakbay AS. Justification of Pitwall Parameters: A Case-Study of Koktaszhal Deposit, Kazakhstan. Journal of Mining Science. 2022; 58:527-533. https://doi.org/ 10.1134/S1062739122040019

Crossref

DOI: 10.31643/2026/6445.31
Earth sciences

Study of geochemical characteristics of the Bakyrchik ore zone

Kopobayeva A.N., Musabayeva M.K., *Amangeldikyzy A., Askarova N.S., Issatayeva F.M., Toleubek K.E., Mazakh B.

Abylkas Saginov Karaganda Technical University, Karaganda, Kazakhstan

** Corresponding author email: amangeldykyzy@inbox.ru*

Received: *February 24, 2025*
Peer-reviewed: *March 18, 2025*
Accepted: *April 30, 2025*

ABSTRACT

The article presents a study on the geochemical characteristics of the ore deposits in the Bakyrchik ore area (Bakyrchik, Glubokiy Log, Zagadka, Promezhutochnoe), which is located in the Zharminsk district of the Abay region in Eastern Kazakhstan.The aim of the study is to identify and describe the geochemical characteristics of the ore deposits in the Bakyrchik ore field, and to analyze the distribution and zonation of elements within ore bodies and areas of dispersed mineralization. The results of spectral analysis on 30 rock samples collected from various depths (550–700 meters) in the vertical mineralization profile of the Bakyrchik field. Samples were taken from core material from different wells in different areas of the field, including Bakyrchik, Glubokiy Log, Zagadka, and Promezhutochnoe, as well as from zones of ore bodies and other areas such as zones of fracture, mylonite, calcite, and sulfide mineralization, considering lithological features. Based on the results of geochemical studies conducted, the characteristics and differences in geochemical properties of large and small ore deposits have been identified, and the distribution of chemical elements within zones of dispersed mineralization has been described. The practical significance of this work lies in the fact that the revealed patterns of element distribution and geochemical zoning to predict the presence of new ore deposits, interpret chemical anomalies, estimate the level of erosion of mineralization, and optimize exploration and assessment efforts in other areas within the ore field.

Keywords: geochemical zonation, ore bodies, near-ore halos, Bakyrchik zone, gold-arsenic mineralization, diffuse mineralization.

Information about authors:

Kopobayeva Aiman Nygmetovna — *PhD, associate professor of the Geology and Exploration MD Department of Abylkas Saginov Karaganda Technical University, 100000, Karaganda, Kazakhstan. E-mail: kopobayeva@inbox.ru; ORCID ID: https://orcid.org/0000-0002-0601-9365*

Musabayeva Makpal Kalhamanovna — *Master's student at Geology and Exploration MD Department of Abylkas Saginov Karaganda Technical University, 100000, Karaganda, Kazakhstan. Email: makpal_m88@mail.ru; ORCID ID: https://orcid.org/0009-0009-9160-9500*

Amangeldikyzy Altynay — *PhD, acting associate professor of the Geology and Exploration MD Department of Abylkas Saginov Karaganda Technical University, 100000, Karaganda, Kazakhstan. E-mail: amangeldykyzy@inbox.ru; ORCID ID: https://orcid.org/0000-0002-6665-8804*

Askarova Nazym Srazhadinkyzy — *PhD, senior lecturer of Geology and ExplorationI MD department of Abylkas Saginov Karaganda Technical University, 100000, Karaganda, Kazakhstan. E-mail: srajadin-nazym@mail.ru; ORCID ID: https://orcid.org/0000-0002-2103-6198*

Issatayeva Farida Muratovna — *PhD, Head of the Geology and ExplorationI MD department of Abylkas Saginov Karaganda Technical University, 100000, Karaganda, Kazakhstan. E-mail: isataeva.farida@gmail.com; ORCID ID: https://orcid.org/0000-0001-6208-3292*

Toleubek Kymbat Esmakhaikyzy — *PhD student at Geology and Exploration MD Department of Abylkas Saginov Karaganda Technical University, 100000, Karaganda, Kazakhstan. E-mail: toleubek.94@mail.ru; ORCID ID: https://orcid.org/0000-0003-2126-8084*

Bakytzhan Mazakh — *PhD student at Geology and Exploration MD Department of Abylkas Saginov Karaganda Technical University, 100000, Karaganda, Kazakhstan. E-mail: 06.06.2005@mail.ru; ORCID ID: https://orcid.org/my-orcid?orcid=0000-0002-2378-320X*

Introduction

Kazakhstan occupies a leading position among countries with a rich mineral resource base, particularly in the field of gold mining. However, in recent decades, there has been a decline in easily accessible gold deposits, leading to the need for strategies to develop “blind” deposits – those hidden at considerable depths or covered by dense sedimentary rocks. With the increasing demand for gold in world markets and the dwindling supply of readily available raw materials, studying the geochemical characteristics of ore bodies becomes crucial.

The Bakyrchik ore zone is a strategically important gold mining facility due to its significant

reserves and unique geochemical zoning. The study of gold-antimony-arsenic and gold-tungsten zones in the Bakyrchyk ore field allows us to gain a deeper understanding of the patterns of ore formation in difficult tectonic conditions [[1], [2], [3]].

The aim of the study is to study the geochemical characteristics of ore objects in the Bakyrchik ore field, as well as to analyze the zoning and distribution of elements in ore bodies and areas of scattered mineralization. This will contribute to developing methods for predicting hidden deposits, which is particularly important for gold-bearing areas with dense sedimentary rock cover [[4], [5], [6]].

The practical significance of the study lies in the analysis of patterns of distribution of elements that can be used to predict new ore bodies and assess the level of erosion of mineralization. The results have the potential to optimize exploration activities both in Kazakhstan and other regions with similar geological features, which will strengthen Kazakhstan's position in the gold market and ensure the sustainable development of its mining industry.

The relevance of studying this ore field is in the fact that it provides an in-depth and detailed approach to studying geochemical patterns, which can improve the efficiency of exploration and assessment work. Unlike other studies, which often focus on individual elements or associations, this study looks at a complex geochemical zone with the identification of four distinct zones, each with unique geochemical characteristics. This method allows not only identifying new ore bodies but also more accurately predicting their size and composition.

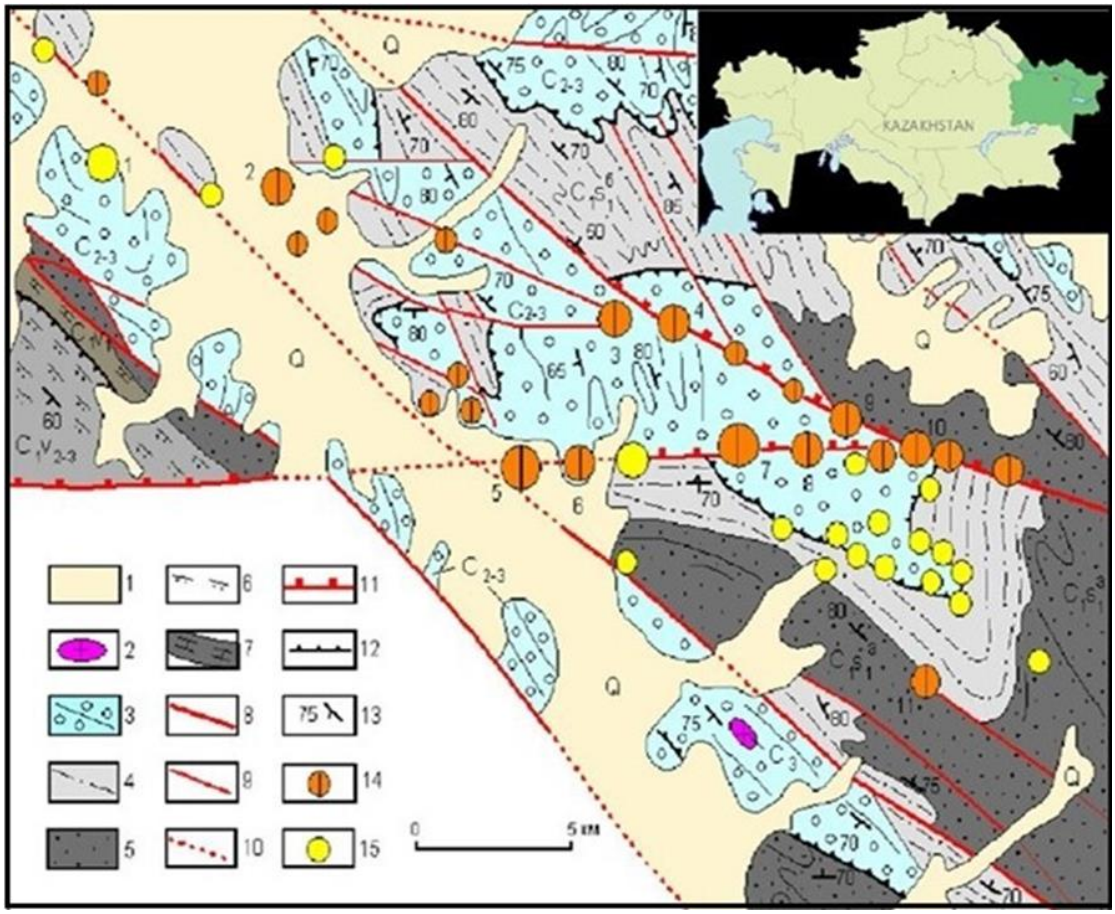

Figure 1 - Geological map of the Bakyrchik ore field (using materials by V.I. Tikhonenko)

1 – Quaternary deposits; 2 – 7 – geological formations: 2 – plagiogranite-granodiorite, C_3; 3 – Molasses limnic carbonaceous, C_{2-3}, 4 – grauvaccian silty-lithic sandstone, C_{1s} (4 – upper sandstone – siltstone and 5 – lower sandstone subformations), 6 – flyschoid carbonate-calcareous – terrigenous, C_{1v2-3}, 7 – limestone – sandstone – silty, C_{1v1}; 8 – 11 – discontinuous faults (8 – deep, 9 – shallow faults, 10 – under loose sediments, 11 – ore-controlling), 12 – thrust, 13 – elements of formation, 14 – 15 – ore formations (14 gold-arsenic – carbonate, 15 gold-quartz). Deposits: 1– Espe, 2 – Kostobe, 3– Dalny I, 4– Dalny, 5– Bolshevik, 6– Chelobai, 7 – Bakyrchik, 8 – Glubokiy log, 9 – Promezhutochnoe, 10 – Bizhan

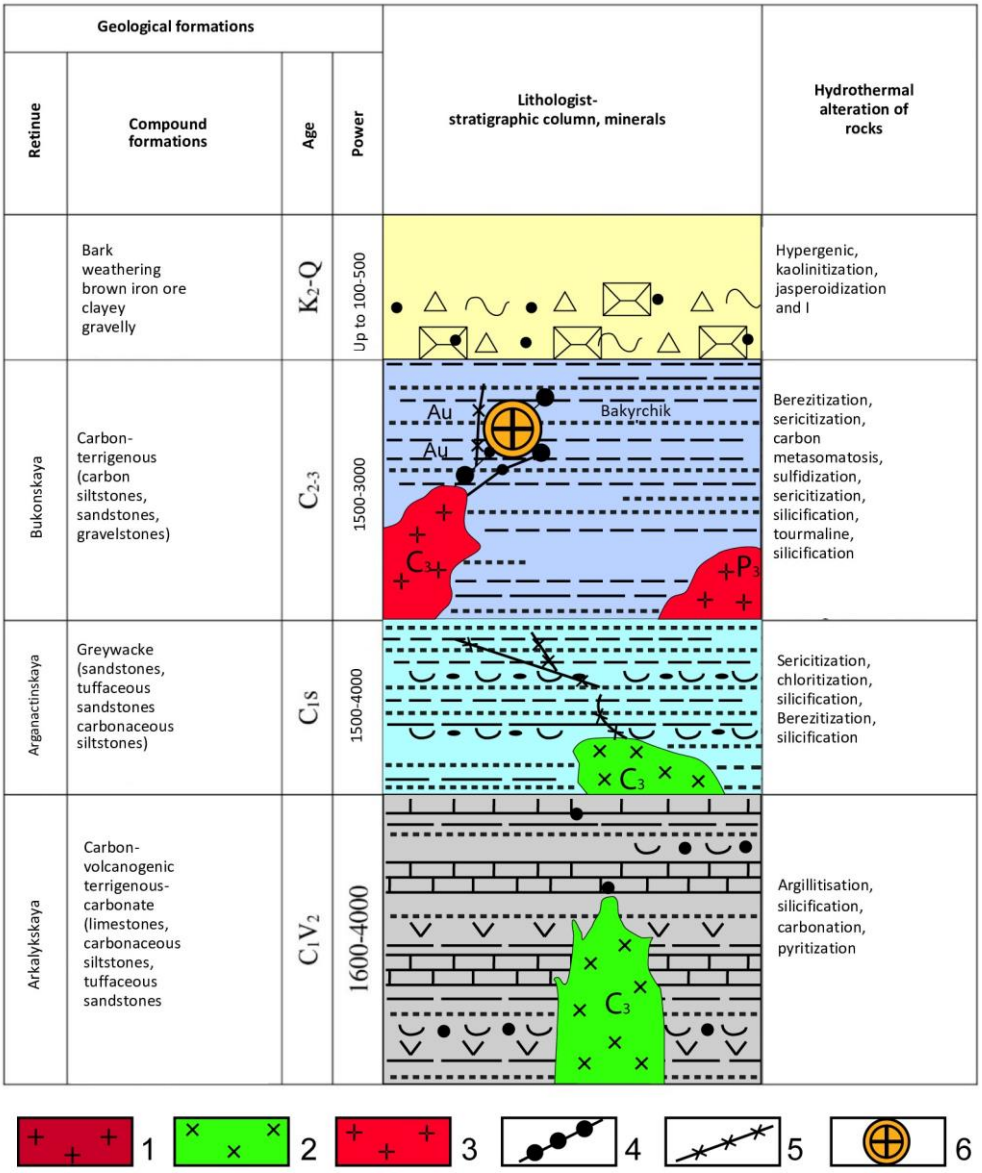

Figure 2 - Lithological and stratigraphic column of the area with metallogenic load (according to M. S. Rafailovich and B. A. Dyachkov)

1-5 – magmatic formations and sub-formations of the collision stage: 1 – leucogranite (the Delbegetey complex, P_2), 2 – gabbro-diorite-granodiorite granodiorite complex (Kunush complex, C_3) 3 – small intrusive plagioclase granites (Kunush complex. C_3), 4 – dikes of mottled composition, 5 – medium basic composition (Kunush complex and its analogs, C_3; geological and industrial minerals: 6 – giant Bakyrchik deposit

In addition, a significant difference of this study is the attention to zones of dispersed mineralization (ZDM), which are usually considered only as by-products in most world studies. In this case, these zones have been analyzed in detail, making it possible to identify promising areas more accurately and avoid mistakes when selecting objects for further work.

Knowledge of the features of zonation of ore bodies and halos helps increase the accuracy of predictive models and effective planning for exploration work.

The Bakyrchik ore field is an important gold mining facility in Kazakhstan. Its peculiarity lies in the unique geochemical zoning of the ore bodies, which makes it possible to deeply study the patterns of ore formation in a complex tectonic environment [[7], [8]].

The analysis of near-ore halos and zones of scattered mineralization at this facility contributes to the development of new methods for predicting

"blind" deposits. Successful development of these "blind" gold deposits within the Bakyrchik ore field would make it possible to apply the results obtained in other areas. This would strengthen Kazakhstan's position on the global gold market and ensure steady growth in the mining industry.

Geological settings. According to the traditional scheme of structural and formation zoning of the Zaisan fold region, the district is located in the central part of Kalba synclinorium, within the Kalba-Naryn structural and formation zone, extending in a narrow band along the West Kalba fault (Fig. 1) [[9], [10]].

The following stratigraphic units of the Paleozoic group are involved in the geological structure of the area (Fig. 2):

1. Arkalyk formation (C_{1ar});
2. Aganaktin formation (C_{1ag});
3. Bukon formation (C_{2bk}).

Formations of weathering crusts, of areal and linear morphological types, are conventionally attributed to the Mesozoic period. The weathering crust develops along Paleozoic rocks, sedimentary and igneous in origin, lies under a cover of Neogene-Quaternary sediments and, in places, comes to the surface on tops of hills and steep slopes [[11], [12]]. According to conditions of occurrence and the structure of the weathered crust within the area they are divided into two types: areal and linearly fractured. According to chemical properties they belong to sialite. Depending on the source rock, the weathering crusts are divided into kaolin and nontronite [13].

Cenozoic deposits (Neogene and Quaternary) are also widely distributed within the area. They form river valleys, intermountain depressions, and areas covered with foam, covering 20-30% of the territory with uneven coverage. Neogene deposits are products of crustal erosion, weathering, and sedimentation in lake-lagoon conditions. They are mainly developed in the valleys of the Kyzyl-Su and Kuely rivers. Quaternary sediments (clay, sandy loam, loam, sand, pebble) fill all lowered relief forms and form terraces in river valleys and outflow cones. The total thickness is 40-70 meters. The area is characterized by a weak magmatic activity in the form of intrusive bodies of serpentinite ultramafic rocks, several dike formations of varied composition, and small intrusions of gabbro and granite. The largest intrusions are part of the Char complex, located southwest outside the Contract Square.

Intrusive complexes are distinguished on the territory of the district – the ultrabasic (Charsky) complex (C1v), granodiorite-plagiogranite (C3-P), gabbro-monzocite-granite (T1) [[14], [15], [16]].

Discontinuous faults on the territory of the region manifest themselves in the form of large faults of the first order, which serve as boundaries of large tectonic blocks and have a north-western strike, intrablock faults of the same strike (of the second order), as well as near-latitude and latitudinal carboniferous faults [[17], [18], [19]].

Research methods

In this paper, the patterns of distribution of geochemical features of the Bakyrchik ore field objects are analyzed and characterized: Bakyrchik, Glubokiy Log, Zagadka, Promezhutochnoe.

Core testing of core drilling wells was carried out on ore bodies, crushing zones, mylonite, hardening, and sulfide mineralization, with lithology considered. 30 core samples were analyzed using the spectral method at the Central Laboratory of Bakyrchik Mining Enterprise, which is accredited and registered with the State System for Technical Regulation in Kazakhstan. To analyze the geochemical features of ore bodies, spectral analysis was performed initially for 17 elements: gold (Au), arsenic (As), antimony (Sb), copper (Cu), molybdenum (Mo), tungsten (W), cobalt (Co), vanadium (V), lead (Pb), zinc (Zn), nickel (Ni), chromium (Cr), manganese (Mn) , iron (Fe), calcium (Ca) and magnesium (Mg). However, only 6 elements were selected for further detailed study: gold (Au) arsenic (As) antimony (Sb) Copper (Cu), Molybdenum (Mo) and tungsten (W). This choice is due to the fact that some elements were not found in significant concentrations or were not geochemically interesting in the context of the research objectives. Selected elements play a key role in ore formation processes and reflect characteristic geochemical patterns in the Bakyrchik ore zone. Their analysis revealed the geochemical zonation, features of the mineralization distribution, and relationships between elements, which are crucial for predicting new ore deposits and optimizing exploration and evaluation efforts. Narrowing the set of analyzed elements ensured a focus on the most relevant data, increasing the efficiency of interpretation and application of results.

Sampling was carried out by cutting the core along the axis in a stone-cutting machine. After that, half was sent for testing, and the other half remained as a backup.

Results and Discussion

A comparative analysis of the geochemical features of zonation, including antimony enrichment, transition from antimony to gold mineralization, association of gold with arsenic and tungsten with gold mineralization revealed characteristic zones in the vertical range of the studied area:

1. Upper antimony – gold-arsenic zone; which are characterized by a sharp predominance of antimony over gold and arsenic;

2. The first intermediate – gold-arsenic-antimony zone (with or without weakly manifested tungsten mineralization);

3. The second intermediate zone is mainly a gold-arsenic zone (without antimony, often with weakly manifested tungsten mineralization). Sometimes there is an increase in concentrations of cobalt, vanadium, copper, and molybdenum.;

4. The root – gold-tungsten-arsenic zone (often with an abnormally high content of copper and molybdenum). The tungsten content reaches tenths of a percent, and tungsten is strongly correlated with copper. The zone can be represented as an area of combination of two clearly manifested geochemical associations: gold-arsenic and tungsten-copper (with molybdenum) [20].

An analysis of the geochemical distribution showed that the zonation of elements in the ore bodies of Bakyrchik's ore zone is formed by the vertical profile of mineralization. Figure 3 shows the distribution of main and associated elements, revealing a concentric zoning structure resembling a funnel-shaped beam.

The bundle-like development of ore bodies, accompanied by contrasting vertical differentiation of elements, can be used to interpret chemical anomalies, linking ore bodies and assessing the level of erosion in other parts of an ore field. Thus, two geochemical zones (gold-arsenic-antimony and gold-arsenic with tungsten) are distinguished at Zagadka site, corresponding to the first intermediate and second intermediate zones.

Antimony-gold-arsenic mineralization can be attributed to the upper ore erosion section.

The presence of a second independent ore body with tungsten-containing gold-arsenic ores at deep levels is justified by geochemical zoning, analogy with the vertical scale of mineralization, and data on erosion sections

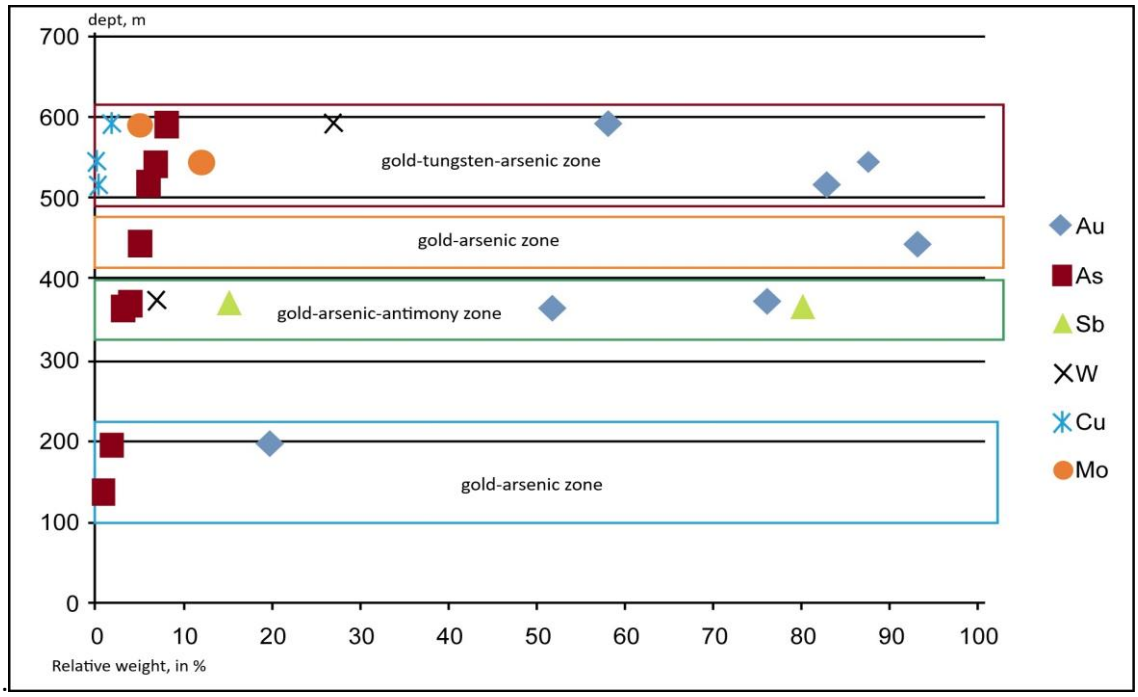

Figure 3 – Distribution of elements in ore bodies in the Bakyrchik ore zone

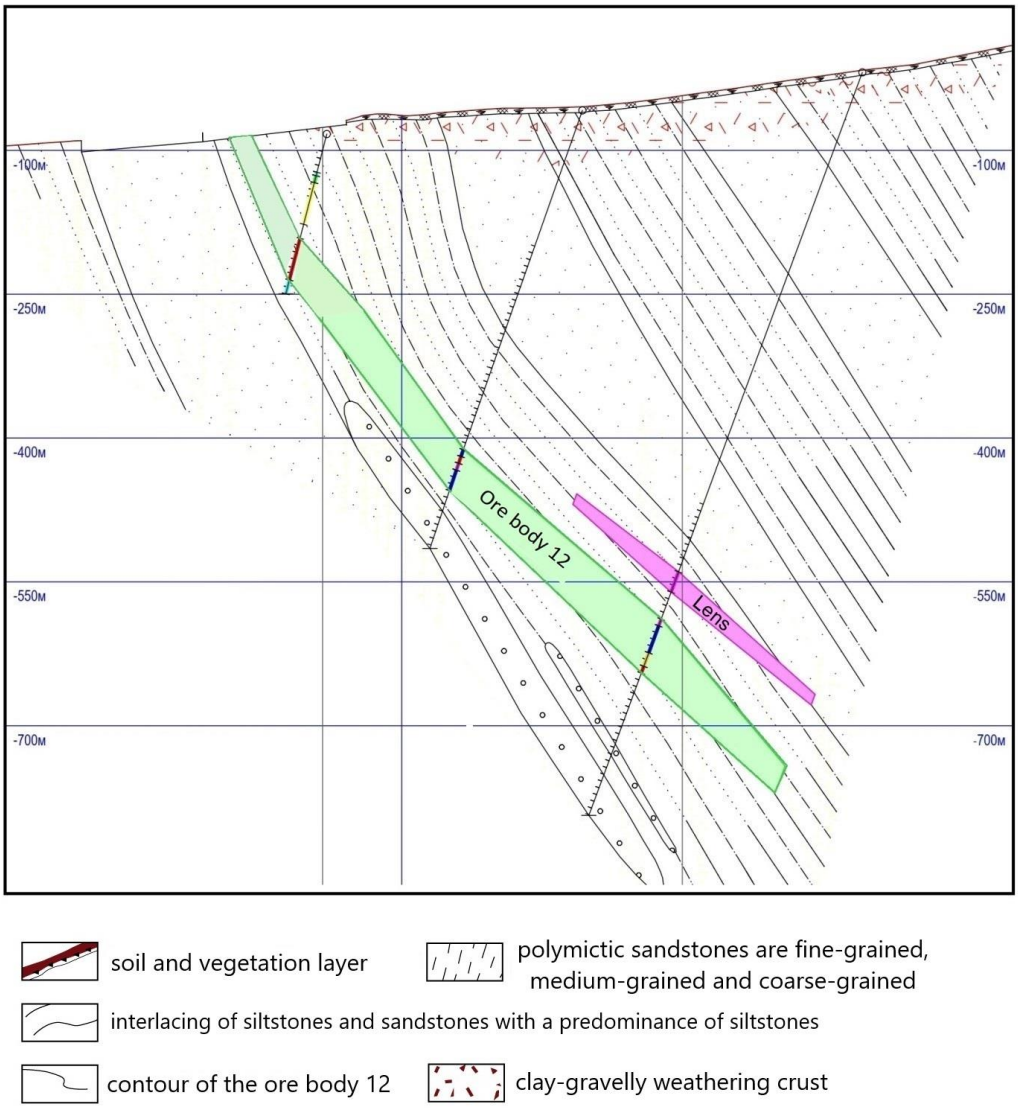

Figure 4 – Geological section of ore body 12

Geochemical features of ore bodies having various sizes

Ore bodies of different sizes vary significantly in their geochemical characteristics.

In the 12 ore body (Fig. 4, 5), the concentration of gold (Au) is unevenly distributed. This indicates local enrichment zones associated with hydrothermal activity. In small ore bodies, gold is distributed more evenly, which indicates their simplified structure and the absence of obvious zonation.

Arsenic (As) in the 12th ore body correlates closely with gold, reaching peaks in the range of 583-599 m, which is typical for arsenopyrite mineralization. In small ore bodies, the concentration of arsenic is low and practically does not change, indicating its lesser role in the formation of these bodies.

Copper (Cu) exhibits similar behavior in both types of ore bodies: its concentration increases at a depth of 702 m, which may be associated with the transition to deeper mineralization zones, where copper plays a major role.

The concentrations of tungsten (W) and molybdenum (Mo) in both types of ore bodies are extremely low, indicating a weak participation of these elements in the mineralization process.

In general, the 12th ore body is characterized by complex zonation and local enrichment zones, reflecting the multilayered nature of its formation. Small ore bodies, in contrast, demonstrate a homogeneous distribution of elements, indicating a more simplified process of formation. This difference highlights the geochemical complexity of large ore bodies compared to smaller ones.

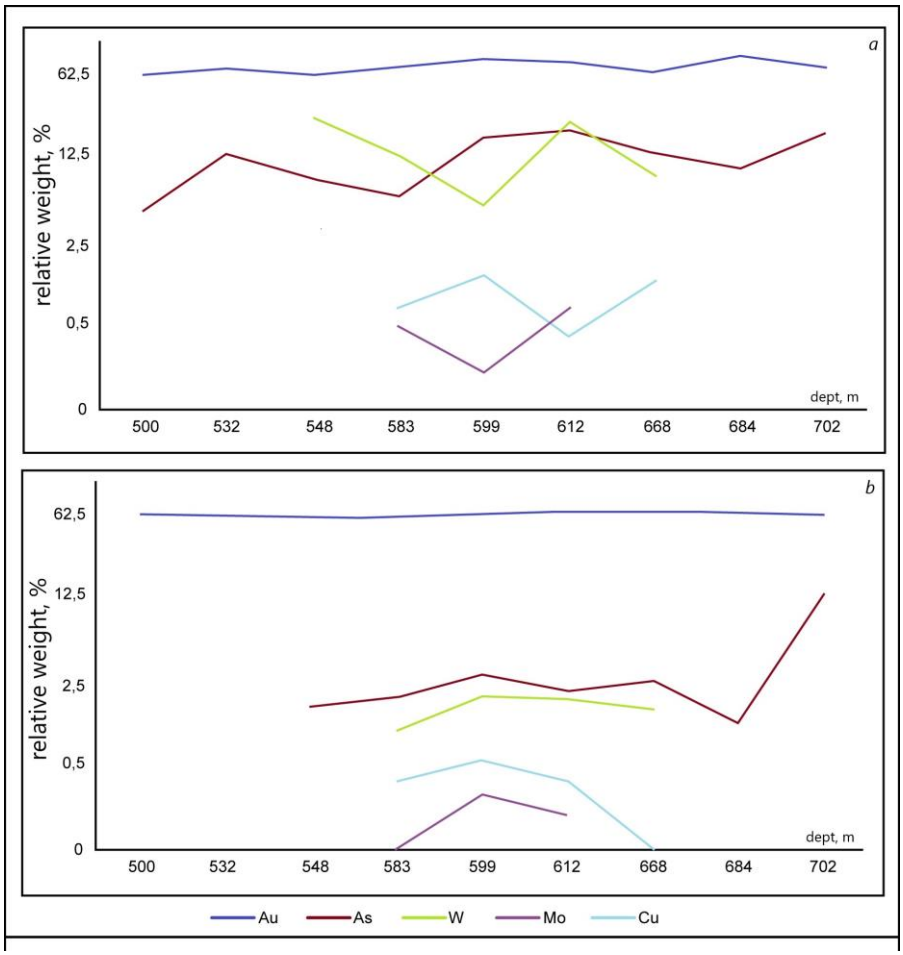

Figure 5 – Distribution of the main and associated components in the 12th ore body (a) and small ore bodies (b).

Geochemical features of zones of dispersed mineralization

In addition to concentrated ore deposits, there are numerous zones of gold-arsenic dispersed 7ineralization (ZDM) in ore fields that are of no practical interest. Due to their high content of gold and arsenic, they resemble near-ore haloes. Therefore, the problem of detecting and disassembling them is urgent. The geochemical features of several reference zones (Bakyrchik and Glubokiy Log) were studied [[21], [22], [23], [24]].

Based on the data obtained, a correlation matrix of near-ore haloes and zone of dispersed mineralization was constructed, which allowed us to assess the relationship between concentrations of various elements (Au, As, W, Cu, Mo) (Fig. 6).

Correlation between elements may indicate that minerals are found together under certain geological conditions. The positive correlation between gold (Au) and arsenic (As), for example, indicates that these elements often occur together in arsenopyrite zones. This is due to the fact that arsenic plays an important role in the formation of gold, suggesting that significant gold deposits may be located within these zones.

On the other hand, a negative correlation between gold and antimony (Sb) may indicate their mutual exclusion under geochemical conditions. This means that in places with high levels of antimony, gold content may be reduced. This information is important to consider when assessing the prospect of deposits.

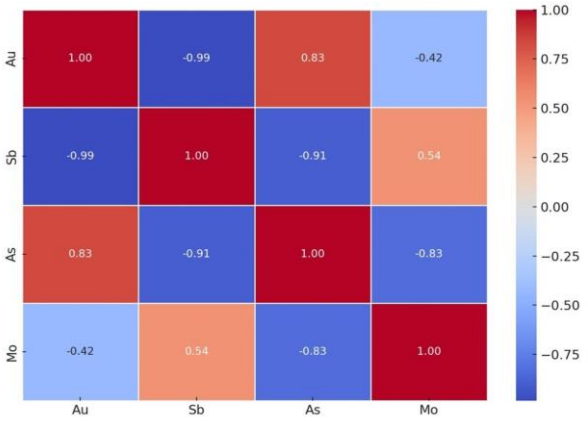

Figure 6 – Correlation matrix of elements near ore halos and zones of dispersed mineralization

The weak correlation of gold with arsenic, molybdenum (Mo) and tungsten (W) may indicate that they belong to different mineralogical associations formed under different conditions, and this knowledge can be useful to geologists and mining engineers in planning exploration and assessing potential deposits.

Based on the above, it can be concluded that the analysis of correlations between elements in areas of dispersed mineralization not only deepens our understanding of geochemical processes but also provides a basis for developing new methods for predicting and evaluating deposits.

Conclusions

The study confirmed the complexity of geochemical processes and emphasized the importance of considering geochemical and geological-structural features for forecasting and evaluating gold ore objects. As a result of this work four main geochemical zones were identified: the upper antimony-gold-arsenic zone, the intermediate gold-arsenics-antimony zone, and the gold-arsensic zone, as well as the root zone of gold, tungsten, and arsenic. These zones show vertical differentiation of elements that is manifested in beamlike structures, most prominent in the axial zones of ore bodies.

Significant differences between large and small ore bodies have been established. In large bodies, such as ore body 12, local gold enrichment zones are observed at depths of 583 meters and 684 meters, associated with a multilayer formation process. These zones are also associated with high correlation with arsenic, indicating the influence of arsenopyrite mineralization. On the other hand, small ore bodies are characterized by a more uniform distribution of elements, indicating a simpler process of their formation.

It has been established that zones of dispersed gold-arsenic mineralization have low concentrations of ore elements. This implies that these zones are not practical for practical use, and despite the presence of gold and arsenic, economic feasibility of developing such areas may be questionable since they do not contain enough minerals for efficient extraction. Therefore, for successful prediction and evaluation of gold ore bodies, it is essential to focus on ore bodies with higher levels of mineralization that are more concentrated.

Conflicts of interest. On behalf of all authors, the corresponding author states that there is no conflict of interest.

CrediT author statement: **A. Kopobayeva:** Conceptualization, Methodology, Investigation; **M. Musabayeva:** Investigation, Data curation, Writing draft preparation; **A. Amangeldikyzy:** Visualization, Editing, Writing - Reviewing; N. **Askarova**: Software; **F. Issatayeva:** Supervision.

Cite this article as: Kopobayeva AN, Musabayeva MK, Amangeldikyzy A, Askarova NS, Issatayeva FM, Toleubek KE, Mazakh B. Study of geochemical characteristics of the Bakyrchik ore zone. Kompleksnoe Ispolzovanie Mineralnogo Syra = Complex Use of Mineral Resources. 2026; 338(3):81-91. https://doi.org/10.31643/2026/6445.31

Бақыршық кен аймағының геохимиялық сипаттамаларын зерттеу

Копобаева А.Н., Мусабаева М.К., *Амангелдіқызы А., Асқарова Н.С., Исатаева Ф.М., Төлеубек К.Е., Мазах Б.

Әбілқас Сағынов атындағы Қарағанды техникалық университеті, Қарағанды, Қазақстан

Мақала келді: *24 ақпан 2025*
Сараптамадан өтті: *18 наурыз 2025*
Қабылданды: *30 сәуір 2025*

ТҮЙІНДЕМЕ

Мақалада Абай облысының Жарма ауданында орналасқан Бақыршық кен аймағының (Бақыршық, Терең сай, Жұмбақ, Аралық) кен денелерінің геохимиялық ерекшеліктерін зерттеу ұсынылған. Зерттеудің мақсаты – Бақыршық кен орнының кен объектілерінің геохимиялық ерекшеліктерін анықтау және сипаттау, сонымен қатар кен денелеріндегі және дисперсті минералдану аймақтарындағы элементтердің аймақтарға бөлінуін және таралуын талдау. Геохимиялық талдау үшін аккредиттелген зертханада зерттелген 30 жынысөзекті сынамалардың спектрлік талдауының нәтижелері пайдаланылды. Әртүрлі тереңдіктегі ұңғымалардың (550-700 м диапазонында) жынысөзегінен алынған сынамалар Бақыршық кен орнының әртүрлі учаскелеріндегі кенденудің вертикальдық профилі бойынша, атап айтқанда, келесі объектілерден: Бақыршық, Терең Сай, Жұмбақ, Аралық, кен денелерінің аймақтарында, сондай-ақ ұсақтау, милониттену, кварцтану және сульфидті минералдану аймақтарында литологиялық ерекшеліктерді ескере отырып талданады. Жүргізілген

	геохимиялық зерттеулердің нәтижелері бойынша ірі және ұсақ кенді денелердің геохимиялық сипаттамаларының ерекшеліктері мен айырмашылықтары анықталды, сондай-ақ шашыраңқы минералдану аймақтарында химиялық элементтердің таралу ерекшеліктері сипатталды. Жұмыстың практикалық маңыздылығы мынада: элементтердің таралу және геохимиялық аудандастырудың анықталған заңдылықтары жаңа кен денелерін болжау, химиялық аномалияларды түсіндіру, минералданудың эрозия деңгейін бағалау үшін қолданылады, сонымен қатар кен орнының басқа учаскелеріндегі барлау және бағалау жұмыстарын оңтайландыруға мүмкіндік береді.
	Түйін сөздер: геохимиялық аймақтылық, кен денелері, кен маңындағы ореолдар, Бақыршық аймағы, алтын-мышьяк минералдануы, шашыраңқы минералдануы.
Копобаева Айман Ныгметовна	***Авторлар туралы ақпарат:*** *PhD, Әбілқас Сағынов атындағы Қарағанды техникалық университетінің Геология және пайдалы қазбалар кен орындарын барлау кафедрасының қауымдастырылған профессоры, 100000, Қарағанды, Қазақстан. E-mail: kopobayeva@inbox.ru; ORCID ID: https://orcid.org/0000-0002-0601-9365*
Мусабаева Макпал Калхамановна	*Әбілқас Сағынов атындағы Қарағанды техникалық университетінің Геология және пайдалы қазбалар кен орындарын барлау кафедрасының магистранты, 100000, Қарағанды, Қазақстан. Email: makpal_m88@mail.ru; ORCID ID: https://orcid.org/0009-0009-9160-9500*
Амангелдіқызы Алтынай	*PhD, Әбілқас Сағынов атындағы Қарағанды техникалық университетінің Геология және пайдалы қазбалар кен орындарын барлау кафедрасының доцент м.а., 100000, Қарағанды, Қазақстан. E-mail: amangeldykyzy@inbox.ru; ORCID ID: https://orcid.org/0000-0002-6665-8804*
Асқарова Назым Сражадинқызы	*PhD, Әбілқас Сағынов атындағы Қарағанды техникалық университетінің Геология және пайдалы қазбалар кен орындарын барлау кафедрасының аға оқытушысы, 100000, Қарағанды, Қазақстан. E-mail: srajadin-nazym@mail.ru; ORCID ID: https://orcid.org/0000-0002-2103-6198*
Исатаева Фарида Муратовна	*PhD, Әбілқас Сағынов атындағы Қарағанды техникалық университетінің Геология және пайдалы қазбалар кен орындарын барлау кафедрасының меңгерушісі, 100000, Қарағанды, Қазақстан. E-mail: isataeva.farida@gmail.com; ORCID ID: https://orcid.org/0000-0001-6208-3292*
Төлеубек Қымбат Есмахайқызы	*Әбілқас Сағынов атындағы Қарағанды техникалық университетінің Геология және пайдалы қазбалар кен орындарын барлау кафедрасының докторанты, 100000, Қарағанды, Қазақстан. E-mail: toleubek.94@mail.ru; ORCID ID: https://orcid.org/0000-0003-2126-8084*
Мазах Бақытжан	*Әбілқас Сағынов атындағы Қарағанды техникалық университетінің Геология және пайдалы қазбалар кен орындарын барлау кафедрасының докторанты, 100000, Қарағанды, Қазақстан. E-mail: 06.06.2005@mail.ru; ORCID ID: https://orcid.org/my-orcid?orcid=0000-0002-2378-320X*

Изучение геохимических характеристик Бакырчикской рудной зоны

Копобаева А.Н., Мусабаева М.К., *Амангелдіқызы А., Асқарова Н.С., Исатаева Ф.М., Төлеубек К.Е., Мазах Б.

Карагандинский Технический Университет имени Абылкаса Сагинова, Карағанда, Казахстан

Поступила: *24 февраля 2025*
Рецензирование: *18 марта 2025*
Принята в печать: *30 апреля 2025*

АННОТАЦИЯ

В статье представлено исследование геохимических особенностей рудных тел Бакырчикской рудной зоны (Бакырчик, Глубокий Лог, Загадка, Промежуточное), расположенной в Жарминском районе Абайской области. Целью исследования является выявление и характеристика геохимических особенностей рудных объектов Бакырчикского рудного поля, а также анализ зональности и распределения элементов в рудных телах и зонах рассеянной минерализации. Для геохимического анализа использованы результаты спектрального анализа по 30 керновым пробам, исследованных в аккредитованной лаборатории. Пробы отобраные из керна скважин различных глубин (в диапазоне 550-700м), проанализированы в вертикальном профиле оруденения, на различных участках Бакырчикского рудного поля, в частности, с объектов: Бакырчик, Глубокий Лог, Загадка, Промежуточное, в зонах рудных тел, а также в зонах дробления, милонитизации, окварцевания и сульфидной минерализации, с учетом литологических особенностей. По результатам проведенных геохимических исследований установлены особенности и различия в геохимических характеристиках крупных и мелких рудных тел, а также описаны особенности распределения химических элементов в зонах рассеянной минерализации. Практическая значимость работы заключается в том, что выявленные закономерности распределения элементов и геохимической зональности могут быть использованы для прогнозирования новых рудных тел, интерпретации химических аномалий, оценки эрозионного уровня оруденения, а также позволяют оптимизировать поисковые и оценочные работы на других участках рудного поля.

	Ключевые слова: геохимическая зональность, рудные тела, околорудные ореолы, Бакырчикская зона, золотомышьяковая минерализация, рассеянная минерализация.
Копобаева Айман Ныгметовна	***Информация об авторах:*** *PhD, ассоциированный профессор кафедры Геология и разведка месторождений полезных ископаемых Карагандинского технического университета имени Абылкаса Сагинова, 100000, Караганда, Казахстан. E-mail: kopobayeva@inbox.ru; ORCID ID: https://orcid.org/0000-0002-0601-9365*
Мусабаева Макпал Калхамановна	*Магистрант кафедры Геология и разведка месторождений полезных ископаемых Карагандинского технического университета имени Абылкаса Сагинова, 100000, Караганда, Казахстан. Email: makpal_m88@mail.ru; ORCID ID: https://orcid.org/0009-0009-9160-9500*
Амангелдіқызы Алтынай	*PhD, и. о. доцента кафедры Геология и разведка месторождений полезных ископаемых Карагандинского технического университета имени Абылкаса Сагинова, 100000, Караганда, Казахстан. E-mail: amangeldykyzy@inbox.ru; ORCID ID: https://orcid.org/0000-0002-6665-8804*
Асқарова Назым Сражадинқызы	*PhD, старший преподаватель кафедры Геология и разведка месторождений полезных ископаемых Карагандинского технического университета имени Абылкаса Сагинова, 100000, Караганда, Казахстан. E-mail: srajadin-nazym@mail.ru; ORCID ID: https://orcid.org/0000-0002-2103-6198*
Исатаева Фарида Муратовна	*PhD, заведующий кафедрой Геология и разведка месторождений полезных ископаемых Карагандинского технического университета имени Абылкаса Сагинова, 100000, Караганда, Казахстан. E-mail: isataeva.farida@gmail.com; ORCID ID: https://orcid.org/0000-0001-6208-3292*
Толеубек Кымбат Есмахайкызы	*Докторант кафедры Геология и разведка месторождений полезных ископаемых Карагандинского технического университета имени Абылкаса Сагинова, 100000, Караганда, Казахстан. E-mail: toleubek.94@mail.ru; ORCID ID: https://orcid.org/0000-0003-2126-8084*
Мазах Бакытжан	*Докторант кафедры Геология и разведка месторождений полезных ископаемых Карагандинского технического университета имени Абылкаса Сагинова, 100000, Караганда, Казахстан. E-mail: 06.06.2005@mail.ru; ORCID ID: https://orcid.org/my-orcid?orcid=0000-0002-2378-320X*

References

[1] Soloviev SG, Kryazhev SG, Dvurechenskaya SS, Trushin SI. The large Bakyrchik orogenic gold deposit, eastern Kazakhstan: Geology, mineralization, fluid inclusion, and stable isotope characteristics. Ore Geology Reviews. 2020; 127:103863. https://doi.org/10.1016/j.oregeorev.2020.103863

[2] Kovalev K, Kalinin Yu, and etc. Relationship of antimony with gold mineralization in the ore districts of Eastern Kazakhstan. Russian Geology and Geophysics. 2014; 55:1170-1182. https://doi.org/10.1016/j.rgg.2014.09.003

[3] Mizernaya MA, Miroshnikova AP, Mizerny AI, Zikirova KT, Chernenko ZI. Geology, magmatism and specific features of mineralization of Bakyrchik ore field (Eastern Kazakhstan). Naukovyi Visnyk Natsionalnoho Hirnychoho Universytetu. 2023; 2. https://doi.org/10.33271/nvngu/2023-2/019

[4] Ludwig KR. SQUID 1.00, A User's Manual; Berkeley Geochronology Center Special Publication. 2000; 2:24-55.

[5] Serykh VI, Kopobayeva AN. Patterns of distribution of rare metal deposits in central Kazakhstan. News of the National Academy of Sciences of the Republic of Kazakhstan, Series of Geology and Technical Sciences. 2019; 1:143-150. https://doi.org/10.32014/2019.2518-170X.18

[6] Junussov M, Mohammad A, Longinos S. Geochemical analysis of organic matter associated with gold in ore deposits: A study of Kazakhstan and Hungary. Acta Geochim. https://doi.org/10.1007/s11631-024-00710-5

[7] Windley BF, Kroner A, Guo J, Qu G, Li Y, Chi Zhang. Neoproterozoic to Paleozoic geology of the Altai orogeny, NW China: new zircon age data and tectonic evolution. J. Geol. 2002; 110:719-737. https://doi.org/10.1086/342866

[8] Naumov E, Borisenko A, Kovalev K, Kalinin Y, Fedoseev G, Seltmann R. Gold deposits of Western Siberia and Eastern Kazakhstan: types and ages of mineralization, correlation with magmatic events. Proceedings of the 11th SGA Biennial Meeting Let's Talk Ore Deposits, Antofagasta, Chile. 2011: 82-84.

[9] Rafailovich MS. The geology of gold in Central Asia: the evolution of mineralization, metasomatic formations, explosive breccias, Almaty. 2013, 423.

[10] Dyachkov B, Mizernaya M, Kuzmina O, Zimanovskaya N, Oitseva T. Tectonics and metallogeny of East Kazakhstan. Intechopen. 2017. https://doi.org/10.5772/intechopen.72745

[11] Kuybida ML, Kruk NN, Paderin IP. Plagiogranite magmatizm of Ore Altay region, Russia. Granites and Earth Evolution: geodynamic position, petrogenesis and ore content of granitoid batholiths. First International Geological Conference. 26-29 August, Ulan-Ude, Russia. 2008, 234-257.

[12] Kirwin DJ, Forster CN, Kavaliers I, et.all. The Oyi Tolgoi copper-gold porphyry deposit, South Gobi, Mongolia. Geogynamics ang metallogeny of Mongolia with special emphasis on copper and gold deposits. London: CERCAMS. 2005, 155-168.

[13] Buslov MM, Fujiwara Y, Iwata K, Semakov NN. Late Paleozoic-Early Mesozoic Geodynamics of Central Asia. Geology and Geophysics. 2004; 7. https://doi.org/10.1016/S1342-937X(05)71064-9

[14] Xiao WJ, Windley BF, Huang BC, Han CM, Yuan C, Chen HL, Sun M, Sun S, Li L. End-Permian to mid-Triassic termination of the accretionary processes of the southern Altaids: implications for the geodynamic evolution, Phanerozoic continental growth, and metallogeny of Central Asia. Int. J. Earth Sci. 2009; 98:1189-1217. https://doi.org/10.1007/s00531-008-0407-z

[15] Kanaeva ZK, Kanaev AT, Semenchenko GV. Geological structure of the Bakyrchik gold-arsenic deposit in East Kazakhstan. K.I. Satpayev KSTU, Almaty, 2014.

[16] Soloviev SG, Kryazhev SG, Dvurechenskaya SS, Trushin SI. The large Bakyrchik orogenic gold deposit, eastern Kazakhstan: Geology, mineralization, fluid inclusion, and stable isotope characteristics. Ore Geology Reviews. 2020; 127(3):103863. https://doi.org/10.1016/j.oregeorev.2020.103863

[17] Baibatsha A. Geotectonics and Geodynamics of paleozoic structures from the perspective of plume tectonics: a case of Kazakhstan. International Journal of GEOMATE. 2020; 19(71):194-202. ISSN: 21862982 (P), 2186-2990, Japan. https://doi.org/10.21660/2020.71.31100

[18] Metallogeny of Central Asia from Kazakhstan to Xinjiang – Researchin Progress. CERCAMS-12 Workshop. London: Naturel History Museum. 2008.

[19] Umarbekova ZT, Dyusembaeva KSh. The characteristics and formation of black shale-hosted Bakyrchik-type gold mineralisation. Appl Earth Sci. 2019; 128(2):61-62. https://doi.org/10.1080/25726 838

[20] Dyachkov BA, Mizernaya MA, Maiorova N, Chernenko Z, Maiorov V, Kuzmina O. Geotectonic position and metallogeny of the greater altai geological structures in the system of the central asian Mobile Belt Boo: New Frontiers in Tectonic Research – General Problems sedimentary basins and island arcs. 2011. https://www.intechopen.com/chapters/17106

[21] Rafaylovich MS. The large gold-sulphide deposit of Bakyrchik in Kazakhstan: Geological structure prospecting model. Geology and Mineral Resources. 2009; 4:31-38.

[22] Kuibida ML, Kruk NN, Paderin IP. Plagiogranitic magmatism of the Rudny Altai. Granites and the evolution of the Earth: geodynamic position, petrogenesis and ore content of granitoid batholiths. Ulan-Ude: BSC SB RAS. 2008, 210-211.

[23] Dyachkov BA, Chernenko ZI, Mayorova NP, Mizernaya MA, Kuzmina ON. Geological conditions of formation and location of apocarbonate-type gold deposits in Eastern Kazakhstan. Ust-Kamenogorsk: EKSTU. 2011, 136.

Crossref
DOI: 10.31643/2026/6445.32
Earth Sciences

Acoustoemission of Graphite and Graphene

[1*]Zhangozin K.N., [2]Yurov V.M., [3]Kargin D.B.

[1]LLP Vostok, Astana, Kazakhstan
[2]LLP Vostok, Karaganda, Kazakhstan
[3]NAO L.N. Gumilyov Eurasian National University, Astana, Kazakhstan

**Corresponding author email 4kzh@mail.ru*

Received: *February 26, 2025*
Peer-reviewed: *April 15, 2025*
Accepted: *May 2, 2025*

ABSTRACT
In this paper, we propose a model of the acoustic emission mechanism of natural graphite and graphene. The thickness of the surface layer R(I) of graphite varies from 0.9 nm in the parallel to 2.46 nm in the perpendicular plane and contains three graphene monolayers. Corrugations on the surface of free graphene arise due to high internal stresses, leading to significant deformation energy. An estimate of the deformation energy associated with the reconstruction of the surface of graphite and graphene is proposed. We imagine a graphite nanolayer as a potential well with infinitely high walls, then the energy levels of the nanolayer are determined by one fundamental parameter - the lattice constant of the crystal. The lattice constant a changes in the R(I) layer due to size effects. As soon as the parameter a stops changing, the spectrum of quantum states passes into a continuous spectrum, where the classical Drude–Lorentz laws are fulfilled for graphite. Since the surface layer of graphite is a two-dimensional quantum medium, three quantum planes of graphite with a_1, a_2 and a_3 should be considered. The article considers one-, two- and three-layer graphene. The Fermi surface of graphene degenerates into the Dirac point, and the Fermi energy is zero. For two-layer graphene, the Fermi energy is E_F = 0.9 eV, and for three-layer graphene - E_F = 1.2 eV. Namely, all three quantum levels participate in the acoustic emission of graphite and graphene. In the article, it can be considered proven that in natural graphite (as well as in all solids), acoustic emission occurs due to the reconstruction of its surface, leading to the emergence of a surface layer R(I) and deformation energy E_d. The article proposes a thermoacoustics model that contains only experimentally determined parameters, and their accuracy is quite acceptable.

Keywords: acoustic emission, graphite, graphene, nanolayer, Fermi surface, crystal.

Information about authors:

Zhangozin Kanat Nakoshevich — *Director, Leading Researcher of TSK-Vostok LLP, Candidate of Physical and Mathematical Sciences, Associate Professor, Saryarka District, Republic Avenue, Building 3/2, Apartment 40, Astana, Kazakhstan. E-mail: 4kzh@mail.ru; ORCID ID: https://orcid.org/0000-0003-1234-0486*

Yurov Viktor Mikhailovich — *Leading researcher of TSK-Vostok LLP, candidate of physical and mathematical sciences, associate professor, Gogol street, house 51, apartment 55, Karaganda, Kazakhstan. E-mail: exciton@list.ru; ORCID ID: https://orcid.org/0000-0002-7918-9656*

Kargin Djumat Beisenbekovich — *Candidate of Physical and Mathematical Sciences, Associate Professor, Director of the Department of Technology Commercialization, L.N. Gumilyov Eurasian National University, Satpayev street building 2, Astana, Kazakhstan. E-mail: kargin_db@enu.kz; ORCID ID: https://orcid.org/0000-0002-1027-6428*

Introduction

Until the mid-20th century, graphite was used as pencils, electrodes, anodes, etc. Then it began to be used in metal production, in atomic and nuclear power engineering, in aviation and space technology [[1], [2], [3]]. The end of the 20th and the beginning of the 21st century were marked by the discovery of fullerenes (1985) [4], carbon nanotubes (1991) [5] and graphenes (2004) [6]. Carbon nanowalls, carbon sheets, nanocrystalline graphite, etc., have acquired a special role at present [7].

In Kazakhstan, Ushtogan LLP plans to mine graphite ores using an open pit method from the Sarytoganbai deposit in the Aktogai district of the Karaganda region. The subsoil user has already submitted a plan for developing the deposit for 2025-2049 on the Unified Ecological Portal of Kazakhstan. Studies have shown that the content of graphite from this deposit in the concentrate can be increased to 99.998%, and, importantly, without acid cleaning. The hydrometallurgical method is most suitable for enrichment.

We have developed a method for obtaining graphene from the graphite of this deposit by intercalating graphite with microcluster water. Further, the graphene additive is used to obtain concrete, which is very much needed for industrial enterprises in Kazakhstan. To obtain high-quality graphene concrete, it is necessary to use non-destructive testing [8], among which the acoustic emission method is of particular importance. However, to apply this method, it is necessary to know the structure of the graphite surface layer and the production of graphene from it, as well as their acoustic properties. The speed of acoustic waves in graphite is still being studied [9], but the mechanism of their occurrence, in addition to thermal vibrations, remains unknown to date.

The aim of this work is to clarify the mechanism of acoustic emission of natural graphite and graphene and their use to obtain graphene concrete.

Thickness of the surface layer of graphite

The thickness of the surface layer of a solid R(I) is given by the formula:

$$R(I) = \alpha \cdot \frac{\upsilon}{S}[m]. \qquad (1)$$

In equation (1): the molar volume of the element $\upsilon = M/\rho$ (M is the molar mass, ρ is its density), $\alpha = 0.17\ 10^{-9}$ mol, $S = 1\ m^2$.

A schematic representation of equation (1) is shown in Fig. 1.

For graphite and graphene, the thickness of the surface layer R(I) is given in Table 1.

The elastic parameters of graphene and graphite are presented in Table 2. In Table 2, the value W_a represents the adhesion energy, and E is the Young's modulus of elasticity.

In Table 1, the number in brackets represents the number of monolayers – n = R(I)/a (a is the lattice constant). The number of graphite monolayers is 3, which is confirmed experimentally (Fig. 2).

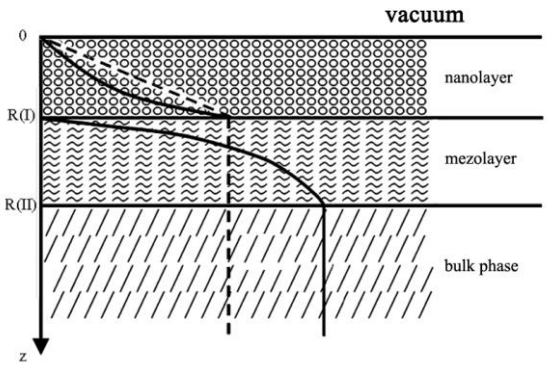

Figure 1 - Graphite diagram: nanolayer → mesolayer → bulk phase

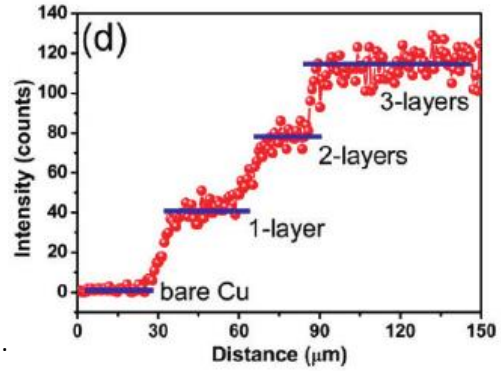

Figure 2 - Change in graphite parameters depending on the number of its monolayers [10].

We will calculate the estimate of the deformation energy associated with the reconstruction of the graphite surface using the formula:

$$E_d = \frac{1}{n} W_a \cdot R(I)^2. \qquad (2)$$

These data are shown in Table 3.

Table 1 - Surface layer thickness R(I) of graphite and graphene

Carbon	M, g/mol	ρ, g/sm^3	R(I)$_a$, nm	R(I)$_c$, nm	γ$_a$, mJ/m^2	γ$_c$, mJ/m^2
Graphite	12.0107	2.26	0.900 (3)	2.46 (3)	2195	130
Graphene	12.0107	2.26	0.246 (1)	0.14 (1)	2652	-

Table 2 - Elastic parameters of graphite and graphene

Carbon	W_{aa}, J/m^2	W_{ac}, J/m^2	σ_{isa}, GPa	σ_{isc}, GPa	E_a, GPa	E_c, GPa
Graphite	2.853	1.690	4.9	1.36	7.59	3.48
Graphene	3.448	-	118.4	-	1000	-

Table 3 - Deformation energy E_d of graphite and graphene

Carbon	E_{da}, eV	E_{dc}, eV
Graphite	2.27	1.42
Graphene	1.62	-

Figure 3 shows the corrugations on the graphene surface, which arise due to high internal stresses σis (Table 2), leading to significant deformation energy (Table 3).

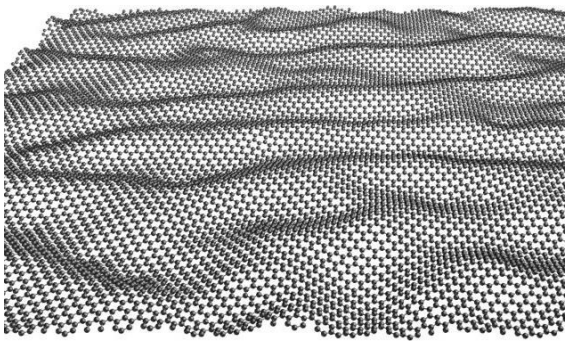

Figure 3 - Corrugated graphene

Figure 3 shows the occurrence of macrowaves on the graphene surface. We will represent a nanolayer with an area of S = 1 m^2 and a size of R(I) of graphite as a nonlinear capacitor - a varicond (due to the presence of size effects) on one of the plates of which large stresses σis develop, leading to significant deformation energy E_d (Table 3). This deformation energy first charges the capacitor, and then, under external influence (impact, friction, ultrasound, etc.), it is discharged (Fig. 4).

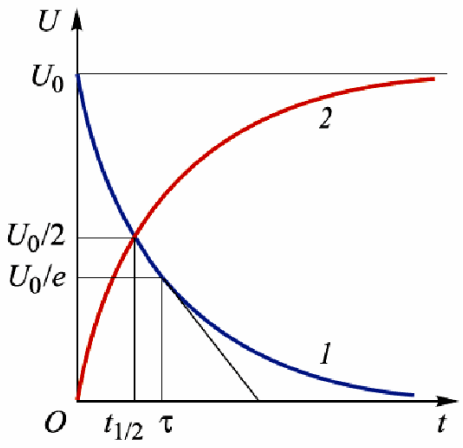

Figure 4 - Voltage change curves on the capacitor plates during its charging (1) and discharging (2)

The deformation energy E_d is spent on heat, acoustic emission (propagation of sound waves) (see below), exoemission (emission of slow electrons and ions) and luminescence.

Quantum structure of the surface layer of graphite

We will imagine the nanolayer in Fig. 1 as a potential well with infinitely high walls, then the energy levels $E_n(z)$ in it are equal to [11]:

$$Å_n(z) = \frac{\hbar^2\pi^2 n^2}{2m_e R(I)^2}, \qquad (3)$$

These levels are shown in Fig. 5a taking into account Table 1. The E_n level can be represented by Landau levels (Fig. 5b).

From equation (3) it follows that the energy levels E_n of the nanolayer are determined by one fundamental parameter – the crystal lattice constant **a** (this follows from n = R(I)/**a**):

$$Å_n(z) = \eta \cdot \frac{n^2}{à^2}, \qquad (4)$$

where η = const.

The lattice constant **a** changes in the R(I) layer due to the reconstruction of the graphite surface. This means that graphite monolayers can be represented as quantum planes with energy E_n. As soon as the parameter a stops changing, the spectrum of quantum states becomes a continuous spectrum, where the classical Drude–Lorentz laws are satisfied for graphite.

It follows from Fig. 5a that the energy level $E_n(\infty) = E_F$ is the Fermi energy level of graphite. In [12], the Fermi energy was calculated to be 1.5 eV for three-dimensional graphite and 2.0 eV for two-dimensional graphite. Since the surface layer of graphite is a two-dimensional medium, three quantum planes of graphite with $\mathbf{a_1}$, $\mathbf{a_2}$ and $\mathbf{a_3}$ should be considered. The first monolayer of graphite, graphene, determines unique physical and chemical properties [[13], [14]]. The motion of electrons in graphene is described by a two-component equation similar to the Dirac equation [13]. If we look for a solution to the Dirac equation in the form of a harmonic wave, we obtain the dispersion law for massless particles (Fig. 6) E = ± V_F k, and the solution itself has the form:

$$\tilde{N} = \frac{1}{\sqrt{2}} \cdot \begin{pmatrix} 1 \\ \pm e^{i\theta} \end{pmatrix} \cdot e^{ikr}, \theta = \mathrm{arctg}(k_y / k_x).$$

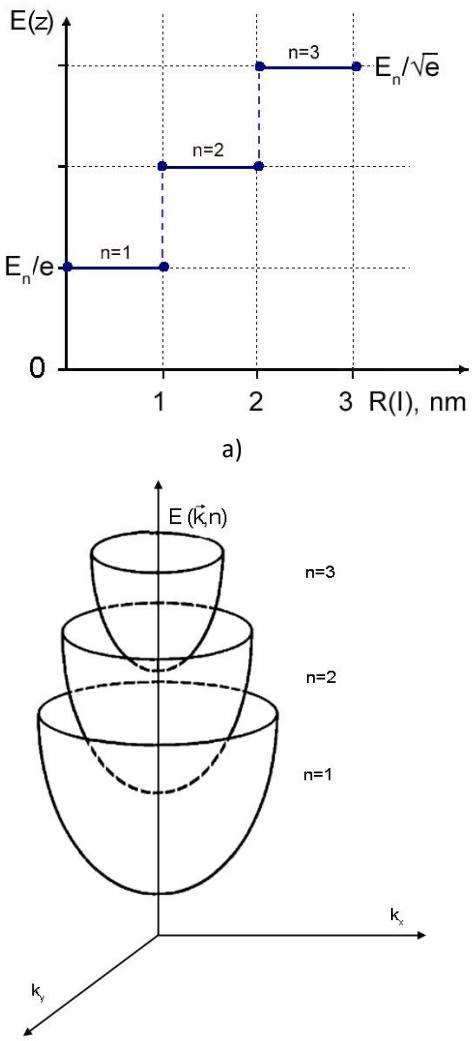

Figure 5 - Dependence of the energy level En in the nanolayer (a); quasi-discrete spectrum of electrons in the quantum well (b).

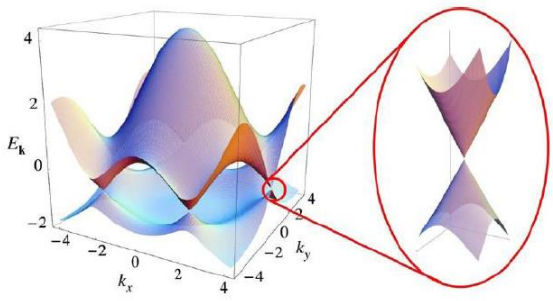

Figure 6 - Electronic structure of graphene [13].

The Fermi surface degenerates into the Dirac point (Fig. 6), and the Fermi energy is $E_F = 0$. Thus, graphene is a single-layer 2D Dirac material and is a quantum system at any temperature. The topological properties of graphene are due to the Dirac nature of the electron spectrum, which is similar to d-wave superconductors (cuprates, YBCO), which are also described by a massless Dirac Hamiltonian near the nodal points of the spectrum [15].

Bilayer graphene is different from monolayer graphene and graphite and exhibits improved physical, chemical, electronic and optical properties compared to graphene and bulk graphite materials [16]. Twisted bilayer graphene (tBLG) superlattice is formed when these layers are twisted at a small angle. The presence of disorder and interlayer interactions in tBLG improves several properties including optical and electrical properties. The studies of twisted bilayer graphene have been exciting and challenging so far, especially after the magic angle superconductivity was reported in tBLG [17]. Bilayer graphene can be considered as a “graphene + YBCO” system in the Landau–Zener model. We have shown that the superconducting transition temperature will be equal to:

$$\check{N}_{ń} = \frac{E_F}{k\ln(k\,\tau/2)} = \delta \cdot E_F, \qquad (5)$$

where δ = const, which is quite difficult to determine theoretically.

For us, the most important thing here is the dependence of the superconducting transition temperature on the Fermi energy E_F, which can be changed, for example, using magnetic or electric fields, or by changing the value of the magic angle. From Fig. 5a, taking into account the work [12], it follows that E_F for two-layer graphene is E_F=0.9 eV. In the work [18], for two-layer graphene, T_c = 1.7 K was obtained, which means that in (6) the value δ_1=1.9 K eV^{-1}.

Three-layer graphene differs from the latter two in mobility and conductivity [19]. A special feature of three-layer graphene is that after its magic-angle torsion, it develops superconductivity, which can withstand magnetic fields 2-3 times greater than the Pauli limit for spin-singlet pairing [20]. This case is similar to two-layer graphene, which can also be considered using the Landau–Zener Hamiltonian. From Fig. 5a, taking into account the work [12], it follows that the Fermi energy for three-layer graphene is E_F = 1.2 eV. In [21], it was obtained for three-layer graphene that T_c = 2.9 K, which means that in (6) the value δ_2 = 2.4 K eV^{-1}. Approximately, $\delta_1 = \delta_2 = 2$ = const is satisfied. The diagram of three-layer graphene is shown in Fig. 7.

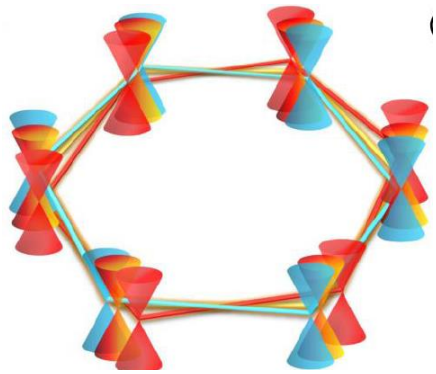

Figure 7 - Schematic Dirac cones of three graphene layers [22].

Acoustoemission of graphite and graphene

The essence of acoustoemission is the analysis of the parameters of extremely weak ultrasonic radiation accompanying any change in the structure of a solid, especially during its deformation (Fig. 8).

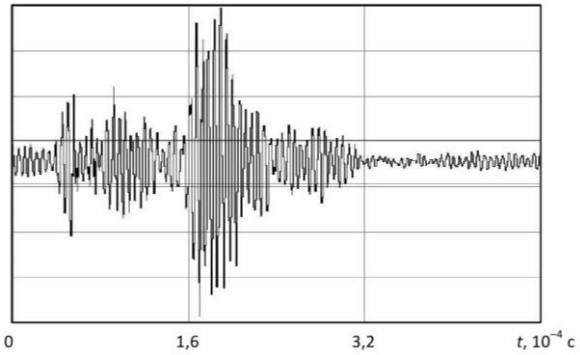

Figure 8 - Typical picture of the fine structure (oscillations) of acoustic emission signals recorded by a sensor on the surface of the body under study [23].

The total energy of the AE E_{AE} is equal to [23]

$$Ĺ_{ŕÝ} = \frac{\sigma_0^2 \cdot \lambda \cdot [R(I)]^2}{8\rho \cdot \upsilon^2}, \qquad (6)$$

where σ_0 is the maximum amplitude of elastic vibration stress; λ is the vibration wavelength; ρ is the density of the solid; υ is the speed of sound.

The maximum value of the wavelength λ propagating in a discrete chain of carbon along the z axis is equal to $R(I)_c$. The speed of sound in the surface layer of graphite is equal to υ = R(I)/τ, where τ is the relaxation time. For longitudinal modes, the relaxation time is τ_L = 0.2 10^{-12} s, for transverse modes – τ_T =2 10^{-12} s. For graphite, the speed of sound is shown in Table 4.

Table 4 - Speed of sound of longitudinal and transverse modes in graphite and graphene

Graphite	υ_L, m/s	υ_T, m/s
ρ = 2260, kg/m^3	4500	2380
ρ = 1986, kg/m^3 [24]	3505	1854
ρ = 1753, kg/m^3 [24]	2631	1591
Graphene	υ_L, м/с	υ_T, м/с
ρ = 0,77, mg/m^2 [[25], [26]]	19700	10700

In Table 4, lines 2 and 3 are taken from the work [24], where the values of the speed of sound in graphite were determined in samples of different densities. It is evident that the speed of sound increases with increasing crystal density.

On the contrary, the density of graphene is significantly lower than that of graphite [25], but the speed of sound in it is almost 5 times greater than that of graphite [26].

In equation (6), we take $\sigma_0 = \sigma_{is}$, then for the E_{AE} we obtain the values (Table 5).

Table 5 - AE energy

Carbon	E_{AEa}, eV	E_{AEc}, eV
Graphite	2.98	1.86
Graphene	2.13	-

Comparing Table 3 with Table 3, it is evident that the deformation energy E_d of graphite and graphene, arising due to the reconstruction of their surface, coincides within the experimental error with the acoustic emission energy E_{AE}, i.e. $E_d \approx E_{AE}$.

Thus, it can be considered proven that in natural graphite (as in all solids), acoustic emission arises due to the reconstruction of its surface, leading to the emergence of a surface layer R(I) and deformation energy E_d.

Let us transform formula (6). As a result, we obtain:

$$Ĺ_{ŕÝ} = \frac{4{,}6 \cdot T_m \cdot E \cdot R(I)}{M} \cdot (eV), \qquad (7)$$

where T_m is the melting point of the solid (K); E is the Young's modulus (GPa); M is the mass of the crystal (kg).

From formula (7) it follows that the value of the E_{AE} is proportional to the temperature, and this allows graphene to be used as a thermophone - a device in which thermoacoustics forces heat to be converted into sound [27]. Such a graphene

thermophone differs from speakers and piezoelectric transducers by the complete absence of mechanical moving elements (Fig. 9).

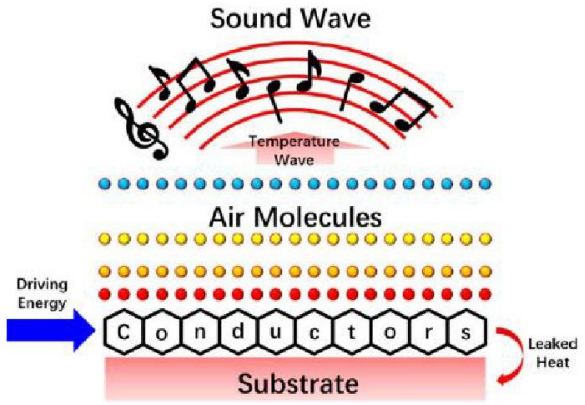

Figure 9 - Operating principle of the hydroacoustic transducer [27]

The first thermoacoustics model was proposed in 1917 and the last one in 2018 (see review in [27]), but only qualitative estimates were obtained.

Our model, represented by equation (7), contains only experimentally determined parameters and their accuracy is quite acceptable.

The value of the acoustic emission energy in formula (7) is proportional to R(I).

Cracks determine the performance of all existing structures and are studied by the acoustic emission method (see bibliography in [[28], [29]].

In 2019, the International Organization for Standardization (ISO) developed three new standards:

ISO 16836. Non-destructive testing. Acoustic emission testing. Method for measuring AE signals in concrete;

ISO 16837. Non-destructive testing. Acoustic emission testing. Method for qualifying damage assessment in reinforced concrete beams;

ISO 16838. Non-destructive testing. Acoustic emission testing. Method for classifying active cracks in concrete structures.

We have shown that the evolution of nanocracks occurs according to the law:

$$L_C = 10^2 L_{\mu m} = 10^4 L_{nm} = 0{,}17 \cdot 10^{-5} \frac{M}{\rho} \quad (8)$$

where L_{nm}, $L_{\mu m}$, L_C are the lengths of nanocracks, mesocracks and the critical length of cracks before the destruction of a solid.

Equation (8) shows: the number of cracks in concrete in the region of nanostructure I is 10^5, in mesoscopic II it is 10^7 and in the pre-destruction region III it is about 10^9.

Adding graphene to cement mortar significantly strengthens (by 4-5 times) standard concrete and reduces the number of nanocracks.

Conclusion

The energy of deformation is created during the reconstruction of graphite and all other solids, and even liquids, when they are finite and in contact with either a vacuum or the external environment. The energy of deformation is spent on heat, acoustic emission (propagation of sound waves), exoemission (emission of slow electrons and ions) and luminescence. This is the mechanism of graphite acoustic emission. In this case, the surface layer of graphite and graphene, which is obtained by splitting graphite, are responsible for acoustic emission.

Conflict of interest. On behalf of all the authors, the correspondent author declares that there is no conflict of interest.

CRediT author statement: **K.Zhangozin** Methodology. Data curation; **V.Yurov:** Calculations of parameters. Drawing up figures and tables; **D.Kargin :** Reviewing and editing.

Acknowledgements. This scientific article was published as part of the grant funding for 2024-2026 IRN No. AP32488258 "Development of an innovative technology for obtaining graphene by intercalating graphite with microcluster water and modifying HTSC ceramics with graphene" (the study is funded by the Science Committee of the Ministry of Science and Higher Education of the Republic of Kazakhstan).

Cite this article as: Zhangozin KN, Yurov VM, Kargin DB. Acoustoemission of Graphite and Graphene. Kompleksnoe Ispolzovanie Mineralnogo Syra = Complex Use of Mineral Resources. 2026; 338(3):92-100. https://doi.org/10.31643/2026/6445.32

Графит пен графеннің акустикалық эмиссиясы

[1*] Жангозин К.Н., [2] Юров В.М., [3] Каргин Д.Б.

[1] ТСК-Восток ЖШС, Астана, Қазақстан
[2] ТСК-Восток ЖШС, Қарағанды, Қазақстан
[3]Л.Н.Гумилев атындағы Еуразия ұлттық университеті, Астана, Қазақстан

Мақала келді: *26 ақпан 2025*
Сараптамадан өтті: *15 сәуір 2025*
Қабылданды: *2 мамыр 2025*

ТҮЙІНДЕМЕ

Мақалады табиғи графит пен графеннің акустикалық эмиссия механизмінің үлгісі ұсынылады. Графиттің беткі қабатының R (I) қалыңдығы параллель жазықтықта 0,9 нм-ден перпендикуляр жазықтықта 2,46 нм-ге дейін өзгереді және үш графен моноқабаттарын қамтиды. Еркін графеннің бетіндегі гофрлар айтарлықтай деформация энергиясына әкелетін жоғары ішкі кернеулерден туындайды. Графит пен графеннің бетін қалпына келтіруге байланысты деформация энергиясын бағалау ұсынылады. Біз графитті наноқабатты шексіз биік қабырғалары бар потенциалды ұңғыма ретінде елестетеміз, содан кейін наноқабаттың энергетикалық деңгейлері бір іргелі параметрмен – кристалдың кристалдық тор тұрақтысымен анықталады. Кристалдық тор константасы R(I) қабатында өлшемдік әсерлерге байланысты өзгереді. А параметрі өзгеруін тоқтатқаннан кейін кванттық күйлер спектрі үздіксіз спектрге айналады, мұнда графит үшін классикалық Друд-Лоренц заңдары орындалады. Графиттің беткі қабаты екі өлшемді кванттық орта болғандықтан, графиттің a_1, a_2, a_3 және болатын үш кванттық жазықтығы қарастырылуы керек. Мақалада бір, екі және үш қабатты графен қарастырылады. Графеннің Ферми беті Дирак нүктесіне айналады, ал Ферми энергиясы нөлге тең. Екі қабатты графен үшін Ферми энергиясы E_F = 0,9 эВ, ал үш қабатты графен үшін E_F = 1,2 эВ. Атап айтқанда, осы кванттық деңгейлердің үшеуі де графит пен графеннің акустикалық эмиссиясына қатысады. Мақалада табиғи графитте (барлық қатты денелердегі сияқты) акустикалық эмиссия оның бетінің қайта құрылуына байланысты пайда болып, беттік қабаттың R(I) түзілуіне әкелетіні және деформация энергиясы Ed болатыны дәлелденген деп санауға болады. Мақалада тек эксперименталды түрде анықталған параметрлерді қамтитын термоакустика моделі ұсынылған және олардың дәлдігі әбден қолайлы.

Түйін сөздер: акустикалық эмиссия, графит, графен, наноқабат, Ферми беті, кристалл.

Авторлар туралы мәліметтер:

Жангозин Канат Нәкешұлы — *ТСК-Восток ЖШС директоры, жетекші ғылыми қызметкер, физика-математика ғылымдарының кандидаты, доцент, Сарыарқа ауданы, Республика даңғылы, 3/2 корпус, 40-пәтер, Астана, Қазақстан. E-mail: 4kzh@mail.ru; ORCID ID: https://orcid.org/0000-0003-1234-0486*

Юров Виктор Михайлович — *ТСК-Восток ЖШС жетекші ғылыми қызметкері, физика-математика ғылымдарының кандидаты, доцент, Гоголь көшесі 51 пәтер 55, Қарағанды, Қазақстан. E-mail: exciton@list.ru; ORCID ID: https://orcid.org/0000-0002-7918-9656*

Қаргин Жұмат Бейсенбекұлы — *Л.Н. Гумилев атындағы Еуразия ұлттық университетінің физика-математика ғылымдарының кандидаты, доцент, ғылыми қызметкер, Сәтбаев көшесі, 2-ғимарат, Астана, Қазақстан. E-mail: kargin_db@enu.kz; ORCID ID: https://orcid.org/0000-0002-1027-6428*

Акустоэмиссия графита и графена

[1*]Жангозин К.Н., [2]Юров В.М., [3]Каргин Д.Б.

[1]ТОО ТСК-Восток, Астана, Казахстан
[2]ТОО ТСК-Восток, Караганда, Казахстан
[3]НАО Евразийский национальный университет имени Л.Н. Гумилева, Астана, Казахстан

Поступила: *26 февраля 2025*
Рецензирование: *15 апреля 2025*
Принята в печать: *2 мая 2025*

АННОТАЦИЯ

В настоящей статье предлагается модель механизма акустоэмиссии натурального графита и графена. Толщина поверхностного слоя R(I) графита изменяется от 0,9 нм в параллельной до 2,46 нм в перпендикулярной плоскости и содержит три графеновых монослоя. Гофры на поверхности свободного графена возникают за счет высоких внутренних напряжений, приводящих к значительной энергии деформации. Предложена оценка энергии деформации, связанной с реконструкцией поверхности графита и графена. Нанослой графита представим как потенциальную яму с бесконечно высокими стенками, тогда уровни энергии нанослоя определяются одним фундаментальным параметром – постоянной кристаллической решетки кристалла. Постоянная кристаллической решетки а изменяется в слое R(I) из-за размерных эффектов. Как только параметр а перестает

изменяться, спектр квантовых состояний переходит в непрерывный спектр, где для графита выполняются классические законы Друде–Лоренца. Поскольку поверхностный слой графита представляет собой двумерную квантовую среду, то следует рассматривать три квантовые плоскости графита с a_1, a_2 и a_3. В статье рассмотрен одно-двух-трехслойный графен. Поверхность Ферми у графена вырождается в точку Дирака, а энергия Ферми равна нулю. Для двухслойного графена энергия Ферми равна E_F = 0,9 эВ, а для трехслойного графена - E_F = 1,2 эВ. Именно, все эти три квантовых уровня участвуют в акустической эмиссии графита и графена. В статье можно считать доказанным, что в природном графите (как и всех твердых телах) акустическая эмиссия возникает из-за реконструкции его поверхности, приводящая к возникновению поверхностного слоя R(I) и энергии деформации E_d. В статье предложена модель термоакустики, которая содержит только экспериментально определяемые параметры и точность их довольно приемлема.

Ключевые слова: акустоэмиссия, графит, графен, нанослой, поверхность Ферми, кристалл.

Сведения об авторах:

Жангозин Канат Накошевич *Директор ТОО ТСК-Восток, ведущий научный сотрудник кандидат физико-математических наук, доцент, район Сарыарка, проспект Республика, дом 3/2, квартира 40, Астана, Казахстан. E-mail: 4kzh@mail.ru; ORCID ID: https://orcid.org/0000-0003-1234-0486*

Юров Виктор Михайлович *Ведущий научный сотрудник ТОО ТСК-Восток, кандидат физико-математических наук, доцент, улица Гоголя 51, квартира 55, Караганда, Казахстан. E-mail: exciton@list.ru; ORCID ID: https://orcid.org/0000-0002-7918-9656*

Каргин Джумат Бейсенбекович *Кандидат физико-математических наук, доцент, исследователь Евразийского национального университета им. Л.Н. Гумилева, улица Сатпаева, дом 2, Астана, Казахстан. E-mail: kargin_db@enu.kz; ORCID ID: https://orcid.org/0000-0002-1027-6428*

References

[1] Savvatimskii AI. Plavleniye grafita i zhidkogo ugleroda [Melting of graphite and liquid carbon]. Uspekhi Fizicheskikh Nauk [Advances in Physical Sciences]. 2003; 173(12):1371-1379. (in Russ.).

[2] Jmurikov EI, Bubnenkov IA, Dremov VV, Samarin SI, Pokrovskii AS, Harkov DV. Grafit v nauke i yadernoi tehnike [Graphite in science and nuclear engineering]. Novosibirsk. 2013, 193. (in Russ.).

[3] Panyukov SV, Subbotin AV, Arzhakov MV. Dimensional changes in bulk graphite caused by irradiation: Theory. Zhurnal Yadernykh Materilov. 2013; 439(1-3):72-83. https://doi.org/10.1016/j.jnucmat.2013.03.070

[4] Kroto HW, Heath JR, O'Brien SC, Curl RF, Smalley RE. C60: Buckminsterfullerene. Nature. 1985; 318:162-163. https://doi.org/10.1038/318162a0

[5] Iijima S. Helical microtubebules of graphitic carbon. Nature. 1991; 354(6348):56-58. https://doi.org/10.1038/354056a0

[6] Novoselov KS, Geim AK, Morozov SV, Jiang D, Zhang I, Dubonos SV, Grigorieva IV, Firsov AA. Electric field effect in atomically thin carbon films. Science. 2004; 306(5696):666-669. https://doi.org/10.1126/science.1102896

[7] Wu Y, Qiao P, Chong T, Shen Z. Carbon nanowalls grown by microwave plasma-enhanced chemical vapor deposition. Advanced Materials. 2002; 14(1):64-67.

[8] Panin VE, Sergeev VP, Panin AV. Nanostrukturirovanie poverhnostnih sloev konstrukcionnih materialov i nanesenie nanostrukturnih pokritii [Nanostructuring of surface layers of structural materials and application of nanostructured coatings]. Tomsk. Izd vo TPU. 2010, 254. (in Russ.).

[9] Muraveva OV, Blinova AV, Denisov LA, Bogdan OP. Osobennosti rasprostraneniya akusticheskih normalnih voln v tonkih poristih listah termorasshirennogo grafita [Features of Propagation of Acoustic Normal Waves in Ton-Porous Sheets of Thermally Expanded Graphite]. Pribori i metodi izmerenii. 2024; 15(3):213-230. (in Russ.).

[10] Abidi IH, Weng L-T, Wong KPJ, Tyagi A, Gan L, Ding Y, et al. A New Approach to Revealing Individual Atomic Layers of 2D Materials and Their Heterostructures. Chemistry of Materials. 2018; 30(5):1718-1728. https://doi.org/10.1021/acs.chemmater.7b05371

[11] Landau LD, Lifshic EM. Kurs teoreticheskoi fiziki. Kvantovaya mehanika _nerelyativistskaya teoriya [Course of Theoretical Physics. Quantum Mechanics (Nonrelativistic Theory)]. M.Fizmatlit. 2004; III:800. (in Russ.).

[12] Moliver SS. Oje_spektroskopicheskoe proyavlenie korrelyacii elektronov poverhnosti Fermi grafita [Auger Spectroscopic Manifestation of Electron Patterns on the Fermi Surface of Graphite]. Fizika tverdogo tela. 2004; 46(9):1537-1543. (in Russ.).

[13] Novoselov KS. Grafen_ materiali Flatlandii [Graphene: Materials of Flatland]. Uspehi fizicheskih nauk. 2011; 181(12):1299-1311. (in Russ.). https://doi.org/10.3367/UFNr.0181.201112f.1299

[14] Zhang T. Graphene. From Theory to Applications. Springer. 2022, 142.

[15] Ostrovskii PM. Elektronnie svoistva neuporyadochennogo grafena [Electronic Properties of Disordered Graphene]. Dissertaciya doktora fiz._mat. nauk_ Chernogolovka. 2019, 227. (in Russ.).

[16] Rozhkov AV, Sboychakov AO, Rakhmanov AL, Nori F. Electronic Properties of Graphene-Based Bilayer Systems. Physics Reports. 2016; 648:1-104. http://dx.doi.org/10.1016/j.physrep.2016.07.003

[17] Nimbalkar A, Kim H. Potential and Challenges of Twisted Bilayer Graphene: A Review. Nano-Micro Lett. 2020; 12(126):125-145. https://doi.org/10.1007/s40820-020-00464-8

[18] Sboychakov AO, Rozhkov AV, Rakhmanov AL. Magic radius of the quantum dot of bilayer AA graphene. Modern Electrodynamics. 2022; 1(1):6-13. https://doi.org/10.1103/PhysRevB.105.235415

[19] Codecido E, Wang QY, Koester R, Che S, Tian HD. Correlated insulating and superconducting states in twisted bilayer graphene below the magic one. Sci. Adv. 2019; 5(9):eaaw9770. https://doi.org/10.1126/sciadv.aaw9770

[20] Lu X, Stepanov P, Yang W, Xie M, Aamir MA, Das I, Urgell C, Watanabe K, Taniguchi T, Zhang G, Bachtold A, MacDonald AH, Efetov DK. Superconductors, orbital magnets, and correlated states in bilayer magic-angle graphene. Nature. 2019; 574(7780):653-657. https://doi.org/10.1038/s41586-019-1695-0

[21] Craciun MF, Russo S, Yamamoto M, Oostinga JB, Morpurgo AF, and Tarucha S. Trilayer graphene is a semimetal with a gate-tunable band overlap. Nature Nanotechnology. 2009; 4:383-388. https://doi.org/10.1103/PhysRevX.2.011004

[22] Devakul T, Ledwith PJ, Xia L-Q, Uri A, de la Barrera S, Jarillo-Herrero P, and Fu L. Magic-angle helical trilayer graphene. Science Advances. 2023; 9(36):eadi6063. https://doi.org/10.1126/sciadv.adi6063

[23] Builo SI. Fiziko_mehanicheskie_ statisticheskie i himicheskie aspekti akustiko_emissionnoi diagnostiki [Physicomechanical, statistical and chemical aspects of acoustic emission diagnostics]. Rostov_na_Donu; Taganrog_ Izdatelstvo Yujnogo federalnogo universiteta. 2017, 184. (in Russ.).

[24] Kuleev II, Kuleev IG, Baharev SM, Inyushkin AV. Vremena relaksacii i dlini svobodnogo probega fononov v rejime granichnogo rasseyaniya dlya monokristallov kremniya [Relaxation times and mean free paths of phonons in the boundary scattering regime for silicon single crystals]. Fizika tverdogo tela. 2013; 55(1):24-35. (in Russ.).

[25] Kokshaiskii AI, Shirgina NV, Korobov AI, Prohorov VM. Issledovanie akustouprugogo effekta v grafite [Study of the acoustoelastic effect in graphite]. Trudi shkoli_seminara Volni-2017. Akustika i akustooptika. 2017, 44-46. (in Russ.).

[26] Baimova YuA, Dmitriev SV, Savin AV, Kivshar YuS. Skorosti zvuka i plotnosti fononnih sostoyanii v odnorodno deformirovannom ploskom liste grafena [Sound velocities and phonon state densities in a uniformly deformed flat graphene sheet]. Fizika tverdogo tela. 2012; 54(4):813-820. (in Russ.).

[27] Boiko EV. Termoakustika grafenovih pokritii i vliyanie grafenovogo pokritiya na teplootdachu [Thermoacoustics of graphene coatings and the effect of graphene coating on heat transfer]. Dissertaciya kandidata fiz._mat. Nauk. Novosibirsk. 2024, 101. (in Russ.).

[28] Chernov DV. Razrabotka metodov diagnostiki ustalostnih treschin s pomoschyu akusticheskoi emissii [Development of methods for diagnosing fatigue cracks using acoustic emission]. Dissertaciya kandidata tehnicheskih nauk. Moskva. 2018, 148.

[29] Grigorev EV. Obosnovanie metoda kontrolya vliyaniya uprochnyayuschih obrabotok svarnih soedinenii na osnove rezultatov registracii signalov akusticheskoi emissii [Justification of the method for monitoring the influence of hardening treatments of welded joints based on the results of recording acoustic emission signals]. Dissertaciya kandidata tehnicheskih nauk. Sankt–Peterburg. 2024, 131. (in Russ.).

Crossref
DOI: 10.31643/2026/6445.33
Metallurgy

Study of Copper Leaching Technology from Copper Ores by Biochemical Method

Kenzhaliyev B., *Koizhanova A., Yerdenova M., Magomedov D., Bakraeva A., Abdyldayev N., Kassenova B.

Institute of Metallurgy and Ore Beneficiation JSC, Satbayev University, Almaty, Kazakhstan

**Corresponding author email: a.koizhanova@satbayev.university*

Received: *February 13, 2025*
Peer-reviewed: *March 19, 2025*
Accepted: *May 8, 2025*

ABSTRACT

The article presents the research results on the processing of dump ores of copper production from one of the deposits of Kazakhstan. The copper content in various rock formation samples and from different sampling points varies from 0.2 to 0.9%. On average, the calculated copper content on the southern side of the dump was 0.3%, and on the northern side, 0.28%. Phase analysis of the dump samples revealed that the bulk of the rock is represented by quartz, albite, muscovite, clinochlorite, and noticeable amounts of malachite and atacamite were noted from copper dumps in many areas. Detailed mineralogical analysis, in addition to oxidized forms of minerals, also recorded fragments of sulfide mineral formations such as pyrite, chalcopyrite, chalcosine, etc. For this type of deposit, the most effective method of processing will be the use of biohydrometallurgical heap leaching technology. According to percolation leaching, the use of trichloroisocyanuric acid (TCCA) as a chemical oxidant was considered, and an adapted culture of A.Ferrooxidans was also used as a biooxidant. According to percolation leaching, the use of trichloroisocyanuric acid (TCCA) as a chemical oxidant was considered, and an adapted culture of A.Ferrooxidans was also used as a biooxidant. Standard sulfuric acid leaching served as a control option. As a result of the application of the chemical oxidation method using TCCA, an increase in copper extraction into solution compared with other options was observed only during the first 7 cycles. The highest efficiency was observed in the variant of preliminary bacterial oxidation, 76.08% copper was extracted into the productive solution over 28 irrigation cycles. The resulting productive solutions of all variants were subjected to a full technological cycle of hydrometallurgical copper production. As a result of the extraction and re-extraction processes, electrolyte solutions were developed that fully correspond to the qualitative parameters necessary for electrolysis. At the electrolysis stage, 30.8 g of copper was deposited on the cathode from the accumulated electrolyte solutions, which gives a current recovery equal to 94.6%.

Keywords: copper-containing raw materials, biochemical method, leaching, AcidobacillusFerrooxidans, trichloroisocyanuric acid, extraction.

Information about authors:

Kenzhaliyev Bagdaulet Kenzhaliyevich — *Doctor of Technical Sciences, Professor, General Director-Chairman of the Management Board of the Institute of Metallurgy and Ore Beneficiation JSC, Satbayev University, Shevchenko str., 29/133, 050010, Almaty, Kazakhstan. Email: bagdaulet_k@satbayev.university; ORCID ID: https://orcid.org/0000-0003-1474-8354*

Koizhanova Aigul Kairgeldyevna — *Candidate of technical sciences, head of the laboratory of special methods of hydrometallurgy, Institute of Metallurgy and Ore Beneficiation JSC, Satbayev University, Shevchenko str., 29/133, 050010, Almaty, Kazakhstan. Email: a.koizhanova@satbayev.university; ORCID ID: https://orcid.org/0000-0001-9358-3193*

Yerdenova Mariya Beisenbekovna — *Researcher, Institute of Metallurgy and Ore Beneficiation JSC, Satbayev University, Shevchenko str., 29/133, 050010, Almaty, Kazakhstan. E-mail: m.erdenova@satbayev.university; ORCID ID: https://orcid.org/0000-0002-7496-5097*

Magomedov David Rasimovich — *Researcher, Institute of Metallurgy and Ore Beneficiation JSC, Satbayev University, Shevchenko str., 29/133, 050010, Almaty, Kazakhstan. E-mail: davidmag16@mail.ru; ORCID ID: https://orcid.org/0000-0001-7216-2349*

Bakraeva Akbota Nurdildakyzy — *Junior Research Fellow, Institute of Metallurgy and Ore Beneficiation JSC, Satbayev University, Shevchenko str., 29/133, 050010, Almaty, Kazakhstan. E-mail: bakraeva.akbota@mail.ru*

Abdyldayev Nurgali Nurlanovich — *Lead Engineer, Institute of Metallurgy and Ore Beneficiation JSC, Satbayev University, Shevchenko str., 29/133, 050010, Almaty, Kazakhstan. Email: n.abdyldaev@satbayev.university; ORCID ID: https://orcid.org/0000-0001-8145-5741*

Kassenova Batikha Akhaevna — *Candidate of Technical Sciences, Leading Researcher, Assoc. Prof., Institute of Metallurgy and Ore Beneficiation JSC, Satbayev University, Shevchenko str., 29/133, 050010, Almaty, Kazakhstan. Email: batiha@mail.ru; ORCID ID: https://orcid.org/0000-0002-4360-8687*

Introduction

A distinctive feature of most copper deposits in Kazakhstan is the depletion of high-grade ore reserves and the accumulation of off-balance stockpiles containing low copper grades (0.1–0.5%). The processing of such off-balance copper raw materials, predominantly composed of oxidized copper minerals, is typically carried out using conventional hydrometallurgical techniques. These include sulfuric acid leaching, followed by solvent extraction and electrowinning processes.

However, in addition to distinctly sulfide or oxidized copper ores, there exist numerous deposits characterized by complex mineral compositions. In such cases, copper is primarily found in oxidized mineral forms, but the ores also contain significant quantities of pyrite, arsenopyrite, and other iron- and sulfur-bearing compounds. Although oxidized copper minerals dissolve readily in sulfuric acid, the presence of ferrous iron and other sulfides in the ore (or in stockpiles) leads to a substantial increase in acid consumption during hydrometallurgical processing. Moreover, the presence of minerals containing various combinations of iron, calcium, carbonates, and silicates (such as tremolite, clinochlore, calcite, etc.) can also negatively affect the leaching process.

The modern standard technology for copper recovery through heap leaching and solvent extraction has been extensively studied and described by both domestic and international researchers [[1], [2], [3], [4], [5], [6], [7], [8]]. In recent years, increasing attention has been directed toward the use of microorganisms for copper extraction. The term "bacterial leaching" refers to an accelerated biological process for extracting metals from ores.

Numerous studies have demonstrated the economic feasibility of bioleaching. It has been shown that the preliminary bio-treatment of oxidized ores can significantly enhance copper recovery. Furthermore, the pre-adaptation of microorganisms has been found to improve the overall efficiency of the bioleaching process.

The role of *Thiobacillus ferrooxidans* bacteria in the bioleaching of sulfide ores is well established. During biogeotechnological processes, metals are converted from water-insoluble sulfides into water-soluble sulfates. *Thiobacillus ferrooxidans* is capable of oxidizing all metal sulfides. These bacteria obtain the carbon necessary for their growth from carbon dioxide. They thrive in acidic environments (within a pH range of 1.0–4.8) and at temperatures between 3°C and 40°C. The optimal conditions for their growth are a pH of 2–3 and a temperature of 28°C. *Thiobacillus ferrooxidans* can be found in aquatic environments, soils, sulfur deposits, and sulfide ore bodies, but their activity is only observed in the presence of oxygen.

In the biogeotechnological leaching process, sulfide-bearing ore or industrial waste is irrigated with sulfuric acid and ferric salt solutions, followed by the introduction of viable *Thiobacillus ferrooxidans* cultures. To intensify bacterial leaching, oxygen from the air is supplied. As the leaching solution percolates through the sulfide material, metals are transferred into a soluble state. Thus, heap leaching represents an effective method for processing off-balance oxidized copper ores from deposits in the Republic of Kazakhstan. The key parameters of the process are determined experimentally and depend on the chemical and phase composition of the ore.

Both domestic and international practices have demonstrated the use of bacterial cultures as oxidizing agents [[9], [10], [11], [12], [13]]. One of the main advantages of bacterial oxidation is the high efficiency in converting ferrous iron (Fe^{2+}) into ferric iron (Fe^{3+}), along with the relatively low cost of this technology [[14], [15], [16], [17]].

When developing bioleaching technologies, it is essential to consider the sharply continental climate conditions typical of Kazakhstan. Although this technology has been widely adopted in countries such as South Africa, Australia, and Latin American nations, the experience of Finland’s Talvivaara company also serves as a notable example. In particular, the implementation of biochemical technology at the Kolmisoppi deposit in 2009–2010 enabled the company to increase production by a factor of 2.7 [[18], [19], [20]].

The object of the study is the bulk ores of copper production at one deposit in Kazakhstan. The purpose of the study is to develop a unique technology that will allow recycling piles, where oxidation minerals are covered with significant inclusions of sulfide minerals and iron–calcium silicates. The use of bacteria as a catalyzing factor for oxidative processes makes it possible to significantly increase the level of transition of copper extraction to a productive solution. Conducting experiments on percolating leaching provides for laboratory simulations of pile leaching. In total, different technological samples were selected, which represent different components of the mound: a rock with significant inclusions of malachite; a sample consisting mainly of a conglomerate; a

sample consisting of siltstone; a sample of sandstone, which is more concentrated at the base of the mound.

Experimental Part

Before starting percolation, the main parameters of the leaching process were selected: the concentration of sulfuric acid in the leaching solution was set to 2.5%; the irrigation density was 10 L/m²·h. Additionally, before the main irrigation with sulfuric acid, the sample's moisture saturation and moisture capacity were calculated. The irrigation area is calculated using the following formula: $S = \pi R^2$. After calculating the irrigation surface area and knowing the given irrigation density (L/m²·h), the volume is then calculated.

The loading of ore samples from the waste heap into the percolators was done in the following mass proportions: malachite – 5%, conglomerate – 30%, aleurolite – 40%, sandstone – 25%. All rocks were pre-mixed before loading, and a composite sample was taken. The only exception was sandstone: 10% of the 25% was placed at the bottom of the percolator to simulate the base of the waste heap, and the remaining 15% was evenly mixed with the rest of the ore mass.

Each rock sample and the composite ore mass for loading were subjected to preliminary X-ray fluorescence analysis. The analysis results are presented in Table 1, where the composition of each individual sample and the composite average sample for the given mass proportions are shown. The theoretical composition of the composite sample was also calculated based on the mass ratios of the samples.

Table 1 – Elemental Composition of Heap Sample Types and Composite Sample for Given Mass Ratios, %

Element	Name of components, %				Mixed sample indicators, %	
	Malachite	Conglomerate	Aleurolite	Sandstone	Actual	Theoretical
O	53.64	50.979	54.209	52.471	50.339	52.777
Na	1.119	1.318	1.802	1.079	1.567	1.4419
Mg	1.246	0.642	1.368	1.331	1.103	1.13485
Al	5.806	3.485	6.789	6.975	4.867	5.79515
Si	22.022	27.846	27.843	25.795	25.708	27.041
P	0.054	0.048	0.062	0.068	0.053	0.0589
S	0.269	0.031	0.116	0.026	0.479	0.07565
Cl	0.012	0.015	0.013	0.015	0.026	0.01405
K	1.147	0.579	1.199	1.662	0.834	1.126
Ca	5.953	5.162	0.855	2.12	3.044	2.718
Ti	0.435	0.239	0.476	0.522	0.312	0.414
V	0.006	0.006	0.007	0.01	0	0.0074
Mn	0.178	0.132	0.066	0.163	0.123	0.116
Fe	2.921	1.38	2.676	3.797	2.289	2.579
Cu	0.448	0.103	0.178	0.028	0.15	0.1315
Zn	0.014	0.007	0.013	0.015	0.024	0.0117
Rb	0.009	0.003	0.007	0.012	0.005	0.00715
Sr	0.011	0.007	0.007	0.014	0.01	0.00895
Zr	0.01	0.006	0.011	0.013	0.01	0.00995
Ba	0	0	0.1	0	0.416	0.04
Pb	0.006	0	0	0.016	0.01	0.0043

The samples were taken from various points and studied using the OLYMPUS BX-51 microscope under reflected light by the mineralogical method. The main part of the sample is composed of gangue minerals. Among the ore minerals, very fine pyrite grains are distinguishable, ranging in size from 0.01–0.05 mm. Pyrite grains are mostly found in their free state, although occasionally they are integrated into the gangue mass. The fine sulfide material retains its characteristic angular and irregular shapes. Chalcopyrite is found in individual grains, with sizes up to 0.02 mm. The images of the sulfide fragments are shown in Figure 1.

After determining the elemental composition, the main phase components, represented by various mineral compounds, were identified in the copper heap samples using X-ray phase analysis. The analysis was carried out on a D8 Advance (BRUKER) diffractometer using Cu – Kα radiation. The results of the X-ray phase analysis are presented in Tables 2 and 3. According to the X-ray phase analysis data, The main part of the rock-forming material in the heap is represented by quartz, which is present in both the northern and southern parts of the heap. Albite, calcite, clinochlore, and muscovite are also found in significant amounts.

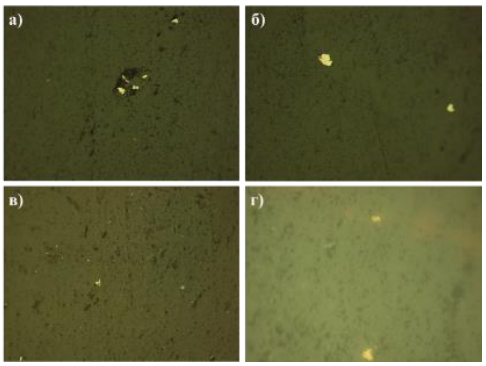

a) – Pyrite in gangue material; b) – Free pyrite grains; c) – Very fine pyrite grains;d) – Chalcopyrite grains

Figure 1 – Photographs of the mineralogical analysis of the sample at 400x magnification.

Table 2 – Phase composition results for the northern part of the heap

Name of components	Formula	Proportion in the sample,%		
		Point 1	Point 2	Point 3
Quartz (syn.)	SiO_2	61.5	42.6	63.1
Albit	$Na(AlSi_3O_8)$	18.1	32.5	24.7
Calcite/calcium carbonate	$CaCO_3$	12.2	-	4.4
Muscovite	$H_2KAl_3Si_3O_{12}$	4.9	5.2	3.7
Clinochlor-1MIIb	$(Mg,Fe)_6(Si,Al)_4O_{10}(OH)_8$	3.3	-	4.1
Atakamite	$Cu_2Cl(OH)_3$	-	10.1	-
Hydrosulphate of potassium	$K_3H(SO_4)_2$	-	5.5	-
Potassium sulphite hydrate	$K_2(S_3(SO_3)_2)(H_2O)_{1.5}$	-	4.2	-
hematite (syn)	Fe_2O_3			
thenardite (syn)	Na_2SO_4	-	-	-

Table 3 – Results of the phase composition of the southern side of the mound

Name of components	Formula	Proportion in the sample,%		
		Point 1	Point 2	Point 3
Кварц (syn)	SiO_2	73.9	74.3	64.7
Albit	$NaAl_{0,91}Si_3O_8$	10.2	11.7	14.8
Malachite (syn)	$Cu_2(OH)_2CO_3$	9.1	-	-
Clinochlor -1MIIb, (ferroan)	$(Mg,Fe)_6(Si,Al)_4O_{10}(OH)_8$	4.0	6.7	6.1
Muscovite	$H_4K_2(Al,Fe)_6Si_6O_{24}$	2.7	3.4	5.5
Calcite/calcium carbonate	$CaCO_3$		3.8	8.8

Discussion of Results

As a result, the composite copper ore from the heap was loaded into three percolators, and three percolation leaching variants were studied (Figure 2):

1) Standard sulfuric acid leaching without additional oxidation; 2) Leaching with preliminary bacterial oxidation; 3) Leaching with preliminary chemical oxidation.

Figure 2 – Loaded percolators for three leaching options

The mineral raw material was subjected to oxidation during the moisture conditioning stage. For the bacterial oxidation variant, the percolator was filled with a nutrient solution containing A. ferrooxidans strains, adapted to copper compounds. In the chemical oxidation variant, a 0.5% trichloroisocyanuric acid (TICA) solution was used. In the percolator where leaching was performed without prior oxidation, a 0.5% dilute sulfuric acid solution was used for the conditioning process.

In all three variants, the moisture level was maintained at 10%. After the moisture conditioning and oxidation treatments, the leaching process was initiated. A solution with a 25 g/L concentration of sulfuric acid was supplied via peristaltic pumps at a 10 L/m²·h irrigation rate, by the main leaching density.

After the ore material passed through the percolators, the volume of the resulting pregnant leach solutions was monitored, and the residual sulfuric acid content, along with the copper ion concentration, was analyzed.

The concentration of sulfuric acid in the pregnant solutions was adjusted up to 25 g/L, and their volume was brought to 2 liters, after which they were reused in subsequent leaching cycles.

The first copper extraction was carried out after 17 leaching cycles, at which point the copper concentration in the solution exceeded 3 g/L. Post-extraction leaching was performed using raffinate—the solution remaining after copper was recovered from the pregnant leach solution using an organic extractant.

The second stage of copper extraction occurred during the final phase of the percolation leaching process, specifically after 28 cycles.

The results of the percolation leaching, as well as the copper recovery dynamics from the pregnant leach solution using both conventional and oxidative methods, are presented in Table 4 and Figure 3.

Based on the analysis of the data table and the graphical results, it was found that during the initial stage of leaching (the first seven irrigation cycles), the copper recovery rates remained nearly identical across all systems. In the subsequent days, an increase in the amount of copper transferred into the solution was observed in the chemical oxidation system. However, over time, the efficiency of chemical oxidation began to decline, while the metal recovery rate continued to increase in the bacterial oxidation variant.

When the copper concentration in the solution reached 3–4 g/L, its transfer rate into the secondary pregnant leach solutions temporarily decreased. To restore the intensity of this process, additional experiments on copper extraction and re-extraction were conducted. These methods allowed for the selective separation of dissolved copper from the pregnant solutions and its transfer to the electrolyte phase.

The extraction was carried out using a 10% solution of the copper-selective extractant Lix 984 dissolved in the organic solvent Escaid. During the extraction, the ratio of aqueous to organic phases was 1:1, and during the re-extraction, it was 3:5. Phase separation and settling processes were performed in separatory funnels (Figure 4).

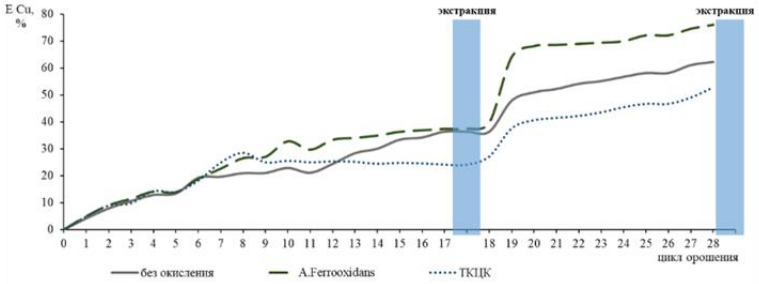

Figure 3 - Dynamics of product release into solution

In the first stage of extraction, 57.45% of the standard sulfuric acid leaching solution was.

From the bacterial oxidation leachate, 66.79% of copper was transferred to the electrolyte, while from the solution treated with the TCIC oxidizing agent (trichloroisocyanuric acid), the transfer reached 69.02%. In addition to the raffinate, a certain amount of copper also remained in the organic phase. This phenomenon is attributed to the one-time copper loss that occurs when freshly prepared organic-phase solutions are used. Such losses are due to the retention of a portion of copper by the organic phase during the extraction process, and this retained copper cannot be completely removed even during the washing stage.

However, no further accumulation of copper in the organic phase was observed – after complete re-extraction, its concentration typically stabilized at 0.2–0.5 g/L.

In the second stage of the extraction process, copper transfer to the electrolyte reached 84.04% for the standard sulfuric acid method, 84.4% for the bacterial oxidation method, and 78.06% for the chemical oxidation method using TCIC. The extraction performance of pregnant leach solutions obtained through different methods is presented in Table 5.

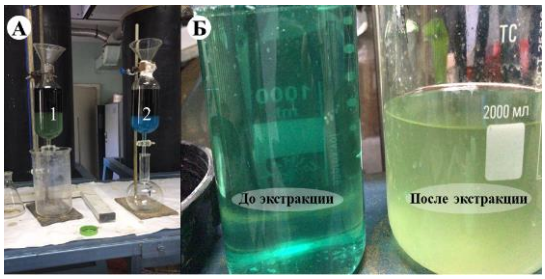

a) separation of aqueous and organic phases
b) in the separation pits:
1– extraction, 2 – re-extraction;
b) color change of the product solution.

Figure 4 - Extraction and re-extraction processes, sedimentation and separation in the funnel

Table 4 – Results of percolation leaching of copper-containing sample

Product solution parameters																				
Cu,g/l	H_2SO_4,g/l	Fe^{3+}, g/l	Fe^{2+}, g/l	V,l	H_2SO_4,ml	E Cu, %	Cu, g/l	H_2SO_4,g/l	Fe^{3+},g/l	Fe^{2+}, g/l	V,l	H_2SO_4, ml	E Cu, %	Cu, g/l	H_2SO_4, g/l	Fe^{3+}, g/l	Fe^{2+},g/l	V,l	H_2SO_4, ml	E Cu, %
1	2	3	4	5	6	7	8	9	10	11	12	13	14	15	16	17	18	19	20	21
Without oxidation, only H2SO4 25 g/l							A.Ferrooxidans + H2SO4 25 g/							TCCC + H2SO4 25 g/l						
0,5	5.1	1.1	0.2	2.0	22.1	4.17	0.63	3.70	2.3	0.1	2.0	23.67	4.94	0.66	0.00	1.40	0.10	2.0	27.8	4.89
0,94	5.4	1.2	0.2	2.0	21.8	7.83	1.15	5.88	2.5	0.15	2.0	21.24	9.02	1.20	1.08	1.50	0.10	2.0	26.6	8.89
1,41	11.3	1.8	0.2	1.8	16.5	10.58	1.62	11.3	2.7	0.15	1.8	16.48	11.44	1.65	6.80	1.50	0.10	1.6	21.7	9.78
1,54	9.8	2.2	0.2	2.0	16.9	12.83	1.80	10.8	3.3	0.15	2.0	15.78	14.12	1.92	7.35	1.70	0.10	2.0	19.6	14.22
1,78	10.3	2.5	0.3	1.8	17.5	13.35	1.96	12.25	3.3	0.2	1.8	15.53	13.84	2.10	10.10	2.10	0.10	1.8	17.7	14.00
2,3	12.0	2.5	0.3	2.0	14.4	19.17	2.4	16.0	3.3	0.2	2.0	10.00	18.82	2.45	10.80	2.40	0.10	2.0	15.8	18.15
2,35	12.7	2.7	0.3	2.0	13.7	19.58	2.88	14.7	3.5	0.2	2.0	11.44	22.59	3.36	11.20	2.40	0.15	2.0	15.3	24.89
2,51	11.76	3.2	0.3	2.0	14.7	20.92	3.38	13.72	3.5	0.2	2.0	12.53	26.51	3.85	8.82	2.40	0.15	2.0	18.0	28.52
2,65	11.5	3.4	0.3	1.3	19.5	14.35	4.12	16.4	3.6	0.2	1.6	13.20	25.85	3.41	9.80	2.50	0.15	0.8	23.4	10.10
2,74	5.0	3.4	0.3	2.0	22.2	22.83	4.18	12.3	3.6	0.2	2.0	14.11	32.78	3.45	5.00	2.50	0.15	2.0	22.2	25.56
2,81	12.3	3.4	0.3	1.8	15.5	21.08	4.20	13.5	3.6	0.2	1.8	14.28	29.65	3.50	9.00	2.80	0.20	1.3	21.3	16.85
2,92	15.92	3.6	0.3	2.0	10.1	24.33	4.25	17.4	3.8	0.2	2.0	8.44	33.33	3.42	17.60	2.80	0.20	2.0	8.2	25.33
3,4	20.09	3.8	0.3	2.0	5.5	28.33	4.34	19.6	4.3	0.2	2.0	6.00	34.04	3.40	10.29	3.00	0.20	2.0	16.3	25.19
3,6	15.4	4.0	0.3	2.0	10.7	30.0	4.45	16.9	4.3	0.2	2.0	9.00	34.90	3.30	18.40	3.00	0.20	2.0	7.3	24.44
4,0	16.4	4.0	0.3	2.0	9.6	33.33	4.63	15.7	4.5	0.23	2.0	10.33	36.31	3.35	17.40	3.20	0.25	2.0	8.4	24.81
4,1	14.1	4.2	0.3	2.0	12.1	34.17	4.70	16.0	4.5	0.23	2.0	10.00	36.86	3.32	14.50	3.20	0.25	2.0	11.7	24.59
4,36	13.47	4.2	0.33	2.0	12.8	36.33	4.77	16.66	4.5	0.23	2.0	9.27	37.41	3.26	13.72	3.20	0.28	2.0	12.5	24.15
Extraction: 10 % Lix984 / 90 % Escaid							Extraction: 10 % Lix984 / 90 % Escaid							Extraction: 10 % Lix984 / 90 % Escaid						
1,35	25.0	4.5	0.4	2.0	0.0	36.33	1.09	25.0	4.8	0.25	2.0	0.0	39.75	0.52	25.0	3.5	0.3	2.0	0.0	27.17
3,03	12.74	4.5	0.4	1.8	15.0	47.81	4.46	15.2	4.8	0.25	1.8	12.58	64.12	2.03	11.5	3.5	0.3	1.75	16.6	37.64
3,1	19.1	4.5	0.4	2.0	6.6	50.92	4.5	17.64	4.9	0.25	2.0	8.18	68.17	2.14	15.4	3.5	0.32	2.0	10.67	40.67
3.25	19.6	4.7	0.5	2.0	0.0	52.17	4.55	26.95	4.9	0.25	2.0	0.0	68.58	2.24	26.0	3.5	0.3	2.0	0.0	41.5
3.48	10.3	4.7	0.5	2.0	16.3	54.08	4.6	17.15	5.0	0.25	2.0	8.72	69.0	2.33	12.25	3.5	0.3	2.0	14.17	42.25
3.79	14.2	4.75	0.5	2.0	12.0	56.67	4.72	18.4	5.1	0.25	2.0	7.33	70.0	2.72	14.7	3.7	0.35	2.0	11.44	45.5
3.6	14.7	4.7	0.5	2.0	11.4	55.08	4.65	17.15	5.0	0.25	2.0	8.72	69.42	2.49	15.2	3.55	0.3	2.0	10.89	43.58
3.96	17.2	4.9	0.5	2.0	0.0	58.08	4.98	17.2	5.1	0.25	2.0	0.0	72.17	2.87	17.2	3.7	0.35	2.0	0.0	46.75
4.2	18.86	4.9	0.55	1.8	8.9	56.58	5.11	20.3	5.2	0.28	1.8	7.48	68.99	3.02	18.4	3.7	0.35	1.8	9.38	45.48
4.31	15.93	4.95	0.55	2.0	0.0	61.0	5.27	18.13	5.2	0.28	2.0	0.0	74.58	3.15	14.7	3.9	0.35	2.0	0.0	49.08
4.45	10.29	5.09	0.6	2.0	16.3	62.17	5.45	17.15	5.2	0.28	2.0	8.72	76.08	3.6	10.29	3.9	0.38	2.0	16.34	52.83

Table 5 – Copper balance during extraction and re-extraction process

Өнім атауы	Solution parameters								
	Without oxidation, only H2SO4 25 g/l			A.Ferrooxidans + H2SO4 25 g/			TCCC + H2SO4 25 g/l		
	Cu, g/l	V, l	%	Cu, g/l	V, l	%	Cu, g/l	V, l	%
Extraction 1									
PLS (productive solution)	4.36	2.0	100.00	4.77	2.0	100.00	3.26	2.0	100.00
Raf (mixed solution)	1.35	2.0	31.0	1.09	2.0	22.9	0.52	2.0	16.0
Organic	2.02	0.5	11.6	1.976	0.5	10.4	1.96	0.5	15.0
Electrolyte	16.7	0.3	57.45	21.24	0.3	66.79	15.0	0.3	69.02
Cu from circulation, g	6.02			7.36			5.48		
Extraction 2									
PLS (productive solution)	4.45	2.0	100.00	5.45	2.0	100.00	3.6	2.0	100.00
Raf (mixed solution)	0.6	2.0	13.5	0.8	2.0	14.7	0.7	2.0	19.4
Organic	0.44	0.5	2.5	0.2	0.5	0.9	0.36	0.5	2.5
Electrolyte	45.0	0.3	84.04	55.2	0.3	84.40	37.0	0.3	78.06
Cu from circulation,gr	13.72			16.66			11.28		

The copper concentration in the obtained electrolytes met the required parameters (at least 30 g/L, not exceeding 60 g/L). All produced electrolytes were used in the next technological stage – copper electrowinning in an electrolytic cell. For the deposition process, a copper cathode with an initial mass of 94.2 g was used, while insoluble lead plates served as anodes. The electrochemical equivalent of copper is A = 0.329 mg / (A·s). The electrolysis process lasted for 11 hours. The theoretical yield of metal during electrolysis was calculated using the following formula:

$$G = A \cdot I \cdot t \quad (1)$$

where:
G – the mass of the deposited substance,
I – electric current, A,
t – time, s.

$$G = 0.329\ mg/(A{\cdot}s) \times 2.5\ A \times 11 \times 60 \times 60 = 32{,}571\ mg = 32.571\ g \quad (2)$$

After the electrolysis process was completed, the cathode mass increased to 125 g (Figure 4). Thus, 30.8 g of copper was deposited on the cathode. The current efficiency of copper deposition was calculated as:

$$ECu = G\_actual / G\_theoretical \times 100\% = 30.8 / 32.571 \times 100\% = 94.6\%$$

Conclusion

Thus, the material composition of copper-bearing mineral raw materials was studied, and sampling from the heap was carried out. The bulk of the heap rock consists of conglomerates, siltstone, and sandstone, while the copper minerals identified include malachite, chalcopyrite, and atacamite. The copper content in various lithological samples and samples taken from different points of the heap ranged from 0.2% to 0.9%. On average, the estimated copper content was 0.3% in the southern part of the heap and 0.28% in the northern part.

Phase analysis of the heap samples showed that the primary mass of the rock is composed of quartz, albite, muscovite, and clinochlore. In certain zones, a significant presence of malachite and atacamite was found as copper-bearing minerals. Detailed mineralogical analysis revealed the presence of both oxidized copper minerals and sulfide mineral formations such as pyrite, chalcopyrite, chalcocite, and other compounds. Hence, the study of the chemical, phase, and mineralogical composition of copper-bearing materials from the heap revealed the heterogeneous distribution of copper in various

mineral forms, as well as the presence of associated impurity elements.

In the percolation leaching process, trichloroisocyanuric acid (TCCA) was used as a chemical oxidant, while an adapted culture of *A. ferrooxidans* bacteria was used as a bio-oxidant. The standard sulfuric acid leaching method served as a control. The use of the TCCA-based chemical oxidation method resulted in a higher copper recovery during the first seven leaching cycles compared to the other methods. However, over time, the effectiveness of chemical oxidation gradually declined, and by the end of 28 leaching cycles, the copper recovery reached 52.83%. During the same period, sulfuric acid leaching yielded 62.17% copper recovery. The highest efficiency was observed in the bio-oxidation method using bacteria, where 76.08% of copper was transferred to the pregnant leach solution after 28 irrigation cycles.

The pregnant leach solutions obtained from all three methods were subjected to the complete hydrometallurgical processing cycle. As a result of the extraction and re-extraction stages, electrolyte solutions that fully met the quality parameters required for electrowinning were obtained. During the electrolysis stage, 30.8 g of copper was deposited on the cathode from the electrolyte solution, corresponding to a current efficiency of 94.6%.

During the experiments, the optimal conditions for the growth of *A. ferrooxidans* bacterial culture, adapted to the chemical composition of copper-containing mineral raw materials, were determined. The results showed that for effective bio-oxidation of mineral raw materials, the initial bacterial solution used in the pretreatment should maintain a pH level not lower than 1.5. An increase in pulp acidity and a drop in pH below 1.2 negatively affect the viability of bacterial cells.

The optimal temperature range for the growth and development of *A. ferrooxidans* culture was found to be between 20–30 °C. Under the most favorable conditions (pH = 2.3, temperature = 20–30 °C), the concentration of bacterial cells increased from 0.1×10^6 cells/cm³ to 2.8×10^6 cells/cm³.

The catalytic mechanisms by which microorganisms influence the oxidation of sulfide minerals in copper-bearing raw materials were also identified. The presence of the bacterial culture as a catalytic factor significantly accelerates the decomposition rate of sulfide minerals, particularly those containing copper (e.g., chalcopyrite, chalcocite, etc.).

The best selectivity results were observed when using an extractant from the LIX984 series:

The highest copper extraction from solution was 94.0%; The lowest iron co-extraction was 0.83%.

Based on the evaluation of copper-loading capacity of the organic phase, the optimal flow ratio between the pregnant leach solution and the organic phase was determined to be O:A = 1:2. If the ratio exceeds O:A > 1:5, the viscosity of the organic phase increases due to oversaturation, which in some cases may lead to the formation of stable emulsions or phase separation issues.

Conflict of interest. On behalf of all the authors, the correspondent author declares that there is no conflict of interest.

CRediT author statement: **B. Kenzhaliyev**: Conceptualization, Methodology, Supervision; **A. Koizhanova**: Data curation, Writing - Original draft preparation; **D. Magomedov** and **M. Yerdenova:** Visualization, Investigation; **A. Bakrayeva**: Software; **N. Abdyldayev** and **B. Kassenova**: Validation.

Acknowledgement. This research has been/ was/is funded by the Science committee of thec with the Ministry of Science and Higher Education of the Republic of Kazakhstan (Grant BR24992757).

Cite this article as: Kenzhaliev B, Koizhanova A, Yerdenova M, Magomedov D, Bakraeva A, Abdyldayev N, Kassenova B. Study of Copper Leaching Technology from Copper Ores by Biochemical Method. Kompleksnoe Ispolzovanie Mineralnogo Syra = Complex Use of Mineral Resources. 2026; 338(3):101-111. https://doi.org/10.31643/2026/6445.33

Мыс кендерінен мысты биохимиялық әдіспен шаймалау технологиясын зерттеу

Кенжалиев Б.К, Койжанова А.К., Ерденова М.Б., Магомедов Д.Р., Бакраева А.Н., Абдылдаев Н.Н, Касенова Б.А.

Металлургия және кен байыту институты АҚ, Сәтбаев университеті, Алматы, Қазақстан

Мақала келді: *18 ақпан 2025*
Сараптамадан өтті: *19 наурыз 2025*
Қабылданды: *8 мамыр 2025*

ТҮЙІНДЕМЕ

Мақалада Қазақстанның бір кен орнында мыс өндірісінің үйінді кендерін қайта өңдеу бойынша зерттеу нәтижелері ұсынылған. Әртүрлі жыныстардан алынған сынамалардағы мыстың мөлшері 0,2-0,9 % аралығында өзгереді. Орташа есеппен үйіндінің оңтүстік жағында мыс мөлшері 0,3 %, солтүстік жағында – 0,28 % құрайды. Үйінді сынамаларын фазалық талдау жыныстың негізгі массасы кварц, альбит, мусковит, клинохлордан тұратынын көрсетті, ал кейбір учаскелерде мыс минералдары – малахит және атакамиттің айтарлықтай мөлшері анықталды. Минералогиялық зерттеу барысында тотығу түрлерімен қатар, сульфидті минералдардың (пирит, халькопирит, халькозин және т.б.) бөлшектері де табылды. Бұл кен орындары үшін ең тиімді қайта өңдеу әдісі ретінде үйінділік шаймалаудың биогидрометаллургиялық технологиясын қолдану ұсынылады. Перколяциялық шаймалау барысында химиялық тотықтырғыш ретінде трихлоризоцианур қышқылын (ТХЦҚ) қолдану мүмкіндігі зерттелді, ал биооксидант ретінде A. Ferrooxidans бейімделген дақылы пайдаланылды. Бақылау нұсқасы ретінде стандартты күкіртқышқылды шаймалау жүргізілді. ТХЦҚ негізінде химиялық тотықтыру әдісі қолданылған кезде, мыс алу көрсеткіші басқа нұсқалармен салыстырғанда тек алғашқы 7 цикл ішінде жоғары болды. Ең жақсы нәтиже алдын ала бактериялық тотықтыру кезінде байқалды, 28 сулау циклының ішінде өнімді ерітіндіге мыстың 76,08 %-ы өтті. Барлық нұсқалардың алынған өнімді ерітінділері мыс гидрометаллургиясының толық технологиялық циклынан өтті. Экстракция және реэкстракция процестері нәтижесінде электролиз жүргізуге қажетті сапалық параметрлерге толық сәйкес келетін электролит ерітінділері алынды. Электролиз сатысында алынған электролит ерітінділерінен катодта 30,8 г мыс тұндырылды, бұл ток бойынша бөліп алу дәрежесін 94,6 % жеткізді.

Түйін сөздер: құрамында мыс бар шикізат, биохимиялық әдіс, шаймалау, Acidobacillus Ferrooxidans, трихлоризоцианур қышқылы, экстракция.

Авторлар туралы ақпарат:

Кенжалиев Бағдаулет Кенжалиевич — *Техника ғылымдарының докторы, профессор, Металлургия және кен байыту институты АҚ-ның Бас директоры - Басқарма төрағасы, Сәтбаев Университеті, 050010, Шевченко к-сі, 29, Алматы, Қазақстан. Email: bagdaulet_k@satbayev.university; ORCID ID: https://orcid.org/0000-0003-1474-8354*

Қойжанова Айгүл Кайргельдыквна — *Техника ғылымдарының кандидаты, зертхана меңгерушісі, Металлургия және кен байыту институты АҚ, Сәтбаев Университеті, 050010, Шевченко к-сі, 29, Алматы, Қазақстан. Email: a.koizhanova@satbayev.university; ORCID ID: https://orcid.org/0000-0001-9358-3193*

Ерденова Мария Бейсенбековна — *Ғылыми қызметкер, Металлургия және кен байыту институты АҚ, Сәтбаев Университеті, 050010, Шевченко к-сі, 29, Алматы, Қазақстан. E-mail: m.erdenova@satbayev.university; ORCID ID: https://orcid.org/0000-0002-7496-5097*

Магомедов Давид Расимович — *Ғылыми қызметкер, Металлургия және кен байыту институты АҚ, Сәтбаев Университеті, 050010, Шевченко к-сі, 29, Алматы, Қазақстан. E-mail: davidmag16@mail.ru; ORCID ID: https://orcid.org/0000-0001-7216-2349*

Бакраева Ақбота Нұрділдақызы — *Кіші ғылыми қызметкер, магистр, Металлургия және кен байыту институты АҚ, Сәтбаев Университеті, 050010, Шевченко к-сі, 29, Алматы, Қазақстан. Email: bakraeva.akbota@mail.ru*

Абдылдаев Нургали Нурланович — *Жетекші инженер, Металлургия және кен байыту институты АҚ, Сәтбаев Университеті, 050010, Шевченко к-сі, 29, Алматы, Қазақстан. Email: n.abdyldaev@satbayev.university; ORCID ID: https://orcid.org/0000-0001-8145-5741*

Касенова Батиха Ахайевна — *Техника ғылымдарының кандидаты, қауымд. проф., жетекші ғылыми қызметкер, Металлургия және кен байыту институты АҚ, Сәтбаев Университеті, 050010, Шевченко к-сі, 29, Алматы, Қазақстан. Email: batiha@mail.ru; ORCID ID: https://orcid.org/0000-0002-4360-8687*

Исследование технологии выщелачивания меди из медных руд биохимическим методом

Кенжалиев Б.К., Койжанова А.К., Ерденова М.Б., Магомедов Д.Р.
Бакраева А.Н., Абдылдаев Н.Н., Касенова Б.А.

АО Институт металлургии и обогащения, Satbayev University, Алматы, Казахстан

АННОТАЦИЯ

В статье представлены результаты исследований по переработке отвальных руд медного производства одной из месторождений Казахстана. Содержание меди в пробах различного породообразования и взятых из разных точек отбора варьируется от 0,2 до 0,9 %. В среднем по южной стороне отвала расчетное содержание меди составило 0,3 %, по северной – 0,28

Поступила: *13 февраля 2025*
Рецензирование: *19 марта 2025*
Принята в печать: *8 мая 2025*

%. Фазовым анализом проб отвала установлено, что основная масса породы представлена кварцем, альбитом, мусковитом, клинохлором, из медных отвалов в ряде участков отмечены заметные количества малахита и атакамита. Подробным минералогическим анализом, помимо окисленных форм минералов, зафиксированы также фрагменты сульфидных минеральных образований, таких как пирит, халькопирит, халькозин и др. Для данного типа месторождений наиболее эффективным методом переработки будет использование биогидрометаллургической технологии кучного выщелачивания. По перколяционному выщелачиванию в качестве химического окислителя был рассмотрен вариант применения трихлоризоциануровой кислоты (ТХЦК), в качестве биоокислителя также использовалась адаптированная культура A.Ferrooxidans. По перколяционному выщелачиванию в качестве химического окислителя был рассмотрен вариант применения трихлоризоциануровой кислоты (ТХЦК), в качестве биоокислителя также использовалась адаптированная культура A.Ferrooxidans. Стандартное сернокислотное выщелачивание служило в качестве контрольного варианта. В результате применения химического метода окисления с использованием ТХЦК рост извлечения меди в раствор по сравнению с другими вариантами, наблюдался только в течение первых 7 циклов. Наибольшая результативность наблюдалась в варианте предварительного бактериального окисления, за 28 циклов орошения в продуктивный раствор было извлечено 76,08% меди. Полученные продуктивные растворы всех вариантов подвергались полному технологическому циклу гидрометаллургического производства меди. В результате процессов экстракции и реэкстракции были наработаны растворы электролитов, полностью соответствующие качественным параметрам необходимым для проведения электролиза. На стадии электролиза из наработанных растворов электролитов было осаждено на катоде 30,8 г меди, что дает извлечение по току равное 94,6 %.

Ключевые слова: медьсодержащее сырье, биохимический метод, выщелачивание, Acidobacillus Ferrooxidans, трихлоризоциануровая кислота, экстракция.

Информация об авторах:

Кенжалиев Багдаулет Кенжалиевич — *Д.т.н., профессор, Генеральный директор-Председатель Правления АО Институт металлургии и обогащения, Satbayev University, ул. Шевченко, 29/133, Алматы, Казахстан. Email: bagdaulet_k@satbayev.university; ORCID ID: https://orcid.org/0000-0003-1474-8354*

Койжанова Айгуль Каиргельдиевна — *Кандидат технических наук, заведующая лабораторией специальных методов гидрометаллургии, АО Институт металлургии и обогащения, Satbayev University, ул. Шевченко, 29/133, Алматы, Казахстан. Email: a.koizhanova@satbayev.university; ORCID ID: https://orcid.org/0000-0001-9358-3193*

Ерденова Мария Бейсенбековна — *Научный сотрудник , АО Институт металлургии и обогащения, Satbayev University, ул. Шевченко, 29/133, Алматы, Казахстан. E-mail: m.erdenova@satbayev.university; ORCID ID: https://orcid.org/0000-0002-7496-5097*

Магомедов Давид Расимович — *Научный сотрудник, АО Институт металлургии и обогащения, Satbayev University, ул. Шевченко, 29/133, Алматы, Казахстан. E-mail: davidmag16@mail.ru; ORCID ID: https://orcid.org/0000-0001-7216-2349*

Бакраева Ақбота Нұрділдақызы — *Младший научный сотрудник, АО Институт металлургии и обогащения, Satbayev University, ул. Шевченко, 29/133, Алматы, Казахстан. E-mail: bakraeva.akbota@mail.ru*

Абдылдаев Нургали Нурланович — *Ведущий инженер, АО Институт металлургии и обогащения, Satbayev University, ул. Шевченко, 29/133, Алматы, Казахстан. Email: n.abdyldaev@satbayev.university; ORCID ID: https://orcid.org/0000-0001-8145-5741*

Касенова Батиха Ахайевна — *К.т.н, ассоц. проф., ведущий научный сотрудник, АО Институт металлургии и обогащения, Satbayev University, ул. Шевченко, 29/133, Алматы, Казахстан. Email: batiha@mail.ru; ORCID ID: https://orcid.org/0000-0002-4360-8687*

References

[1] Godirilwe LL, Magwaneng RS, Sagami R, Haga K, Batnasan A, Aoki S, Kawasaki T, Matsuoka H, Mitsuhashi K, Kawata M, Shibayama A. Extraction of copper from complex carbonaceous sulfide ore by direct high-pressure leaching. Minerals Engineering. 2021; 173:107181. https://doi.org/10.1016/j.mineng.2021.107181

[2] Magwaneng RS, Haga K, Batnasan A, Shibayama A, Kosugi M, Kawarabuki R, Mitsuhashi K, Kawata M. Investigation of copper and iron recovery from copper ore by high pressure leaching. International Journal of the Society of Material Engineering for Resources.2018; 23(1):80-83. https://doi.org/10.5188/ijsmer.23.80

[3] David T Hopkins, Stephanie MacQuarrie, Kelly A Hawboldt. Removal of copper from sulfate solutions with the use of biochar derived from crab processing by-product Journal of Environmental Management. 2022; 303:114270. https://doi.org/10.1016/j.jenvman.2021.114270

[4] Sariev O, Dossekenov M, Kelamanov B, & Abdirashit A. High-carbon ferromanganese smelting on high-base slags. Kompleksnoe Ispolzovanie Mineralnogo Syra = Complex Use of Mineral Resources.2020; 315(4):63-73. https://doi.org/10.31643/2020/6445.38

[5] Santaolalla A, Gutierrez J, Gallastegui G, Barona A, Rojo N. Immobilization of Acidithiobacillus ferrooxidans in bacterial cellulose for a more sustainable bioleaching process. Journal of Environmental Chemical Engineering. 2021; 9(4). https://doi.org/10.1016/j.jece.2021.105283

[6] Lin M, Yang B, Lin H, Liu S, Wang J. Catalytic Effects of Red Mud and Acidithiobacillus ferrooxidans on Biodissolution of Pyrite IOP Conference Series: Earth and Environmental Science, 2021; 768(1):012019. https://doi.org/10.1088/1755-1315/768/1/012019

[7] Ignatiev MM, Magad E, Koyzhanova AK, Amanzholova LU, Atanova OV. Study of complexation during processing from the productive solutions of heap leaching copper by liquid extraction. Bulletin of KazNITU.2016; 1:153-161.

[8] Lv X, Zhao H, Zhang Y, Yan Z, Zhao Y, Zheng H, Liu W, Xie J, Qiu G. Active destruction of pyrite passivation by ozone oxidation of a biotic leaching system. Chemosphere. 2021; 277:130335. https://doi.org/10.1016/j.chemosphere.2021.130335

[9] Kenzhaliyev B, Ketegenov T, Mussapyrova L, Nadirov R. Ultrasound-Assisted Selective Leaching of Arsenic from Copper Smelting Flue Dust. Minerals. 2024; 14(6):532. https://doi.org/10.3390/min14060532

[10] Koizhanova AK, Magomedov DR, Tastanov EA, Kenzhaliyev BK, Sedelnikova GV, Berkinbayeva AN. Intensification of copper leaching from heaps with the use of biological oxidation. Metalurgija.2022; 61(3-4):789-792.). https://hrcak.srce.hr/274040

[11] Koizhanova A, Magomedov D, Abdyldayev N, Kamalov E, Yerdenova M, Bakrayeva A. Copper Extraction from Complex Waste Dumps by Biochemical Leaching Method. Journal of Ecological Engineering. 2022; 23(10):283-290. https://doi.org/10.12911/22998993/152342

[12] Meadows NE, Pollard DM. Oxidative lead chalkopyritein a chloridesulphate lixivant. Res. and Dev Met. Austral. Inst. Mining and Met. Adelaide Parkville. 1987, 109-114.

[13] LvX, ZhaoH, Zhang Y, Yan Z, Zhao Y, Zheng H, Liu W, Xie J, Qiu G. Active destruction of pyrite passivation by ozone oxidation of a biotic leaching system. Chemosphere.2021; 277:130335. https://doi.org/10.1016/j.chemosphere.2021.130335

[14] Santaolalla A, Gutierrez J, Gallastegui G, Barona A, Rojo N. Immobilization of Acidithiobacillus ferrooxidans in bacterial cellulose for a more sustainable bioleaching process. Journal of Environmental Chemical Engineering. 2021; 9(4):105283. https://doi.org/10.1016/j.jece.2021.105283

[15] Koizhanova A, Kenzhaliyev B, Magomedov D, Kamalov E, Yerdenova M, Bakrayeva A, Abdyldayev N. Study of Factors Affecting the Copper Ore Leaching Process. ChemEngineering. 2023; 7(3):54. https://doi.org/10.3390/chemengineering7030054

[16] Song C-I, Jo C-M, Ri H-G. Immobilization of Acidithiobacillus ferrooxidans-1333 on the waste ore particles for the continuous oxidation of ferrous iron. Iranian Journal of Biotechnology. 2020; 18(3):55-61. https://doi.org/10.30498/ijb.2020.125528.2224

[17] Dyussebekova M, Kenzhaliyev B, Kvyatkovskiy S, Kozhakhmetov S, Semenova A, Sukurov B. Study of the Effect of Fluxing Ability of Flux Ores on Minimizing of Copper Losses with Slags during Copper Concentrate Smelting. Metals. 2022; 12(8):1240. https://doi.org/10.3390/met12081240

[18] Wu S, et al. Effect of Bi(III) on flotation of copper sulfide from leaching residue of copper smelting dust. Minerals Engineering. 2025; 220:109092. https://doi.org/10.1016/j.mineng.2024.109092

[19] Sulphuric Acid Price Trend and Forecast. URL: https://www.chemanalyst.com/Pricing-data/sulphuric-acid-70[20]LME Copper. URL: https://www.lme.com/Metals/Non-ferrous/LME-Copper#Trading+day+summary

[20] Koizhanova A, Kenzhaliyev B, Magomedov D, Erdenova M, Bakrayeva A, & Abdyldaev N. Hydrometallurgical studies on the leaching of copper from man-made mineral formations. Kompleksnoe Ispolzovanie Mineralnogo Syra = Complex Use of Mineral Resources. 2024; 330(3):32-42. https://doi.org/10.31643/2024/6445.26

Crossref
DOI: 10.31643/2026/6445.34
Metallurgy

Research into the possibility of air separation of cake at the Pavlodar aluminum smelter

Abikenova G.K., Tverdokhlebov S.A., Dauletov D.D., *Danchenko I.S.

LLP Scientific and Research Engineering Center ERG, Pavlodar, Kazakhstan

** Corresponding author email: Irina.S.Danchenko@erg.kz*

Received: *November 1, 2024*
Peer-reviewed: *December 11, 2024*
Accepted: *May 14, 2025*

ABSTRACT

Air separation can play a key role in the sintering process of the charge material in the alumina production at the Pavlodar Aluminum Plant. During sintering, sinter dust is formed, which must be effectively separated from the bulk material, since its fine fraction is a source of formation of a solid phase carried away with the solution, which increases the number of secondary losses of valuable components. The use of air separation will solve this problem, providing a high degree of separation of the sinter product into coarse and fine fractions, thereby intensifying the further process of hydrochemical processing of the sinter from the sintering furnaces. The main goal of these studies was to reduce the loss of valuable components from the sinter, namely aluminum oxides and alkali, which are carried away with the solid phase of the tubular apparatus effluent. This paper considers the preliminary classification of sinter dust in air separators and its separate leaching. Extensive (pilot) laboratory tests determined the separation boundary of sinter classes (– 0.25 mm), which allows increasing alumina extraction by ~ 2% and suggests a reduction in the number of operating furnace lines by 0.26 units by reducing ballast flows, and the optimal indicator of air separation efficiency was determined to be ~ up to 97%. The results demonstrate the importance of air separation in ensuring the quality of the sinter product and improving the efficiency of alumina production technology as a whole.

Keywords: air separation, extraction of valuable components, alumina, sintering process, sinter.

Information about the authors:

Abikenova Gulnur Kanybekovna — *Candidate of Technical Sciences, General Director of LLP Scientific Research Center ERG, Kunaev Street, 2, 010000, Astana, Kazakhstan. Email: Gulnur.Abikenova@erg.kz*

Tverdokhlebov Sergey Andreevich — *Engineer – chemical technologist, LLP Scientific and Research Engineering Center ERG, Industrial zone East, Building 65, 140000, Pavlodar, Kazakhstan. Email: tatburgelo@mail.ru*

Dauletov Dauren Dauletovich — *Master's degree in the field of enrichment, Head of the laboratory LLP Scientific Research Center ERG, Pavlodar, Industrial zone East, Building 65, 140000, Pavlodar, Kazakhstan. Email: Dauren.Dauletov@erg.kz*

Danchenko Irina Sergeevna — *Engineer – chemical technologist, engineer – technologist LLP Scientific Research Center ERG, Industrial zone East, Building 65, 140000, Pavlodar, Kazakhstan. Email: Irina.S.Danchenko@erg.kz*

Introduction

Air separation is a technological process in which polydisperse systems are separated into fractions based on the settling velocity of particles of various sizes under the influence of centrifugal gravitational forces in a horizontal or upward flow. The overall function of a classifier is to separate particles into coarse and fine fractions [1]. The air separation process is widely used worldwide in various industries [2]. For example, in China, air separation is used for classifying coking coals, for separating and processing valuable components from spent lithium-ion batteries, and for separating fly ash [[3], [4], [5]]. In the existing process flow at the Pavlodar Aluminum Plant (PAP), the leaching of sinter from the sintering shop is carried out in tubular leaching units, from which a solid phase, the so-called “gray” sludge, is carried out along with the non-desiliconized aluminate solution [6]. Upon further residence in the aluminate solution during the autoclave desilication stage, the “gray” sludge becomes enriched with aluminum oxide and alkali, causing their loss from the aluminate solution.

To address the existing problem, a technical solution was proposed: separating the sinter dust through preliminary classification in air separators. This would enhance the efficiency of the sinter hydrochemical processing (Figure 1).

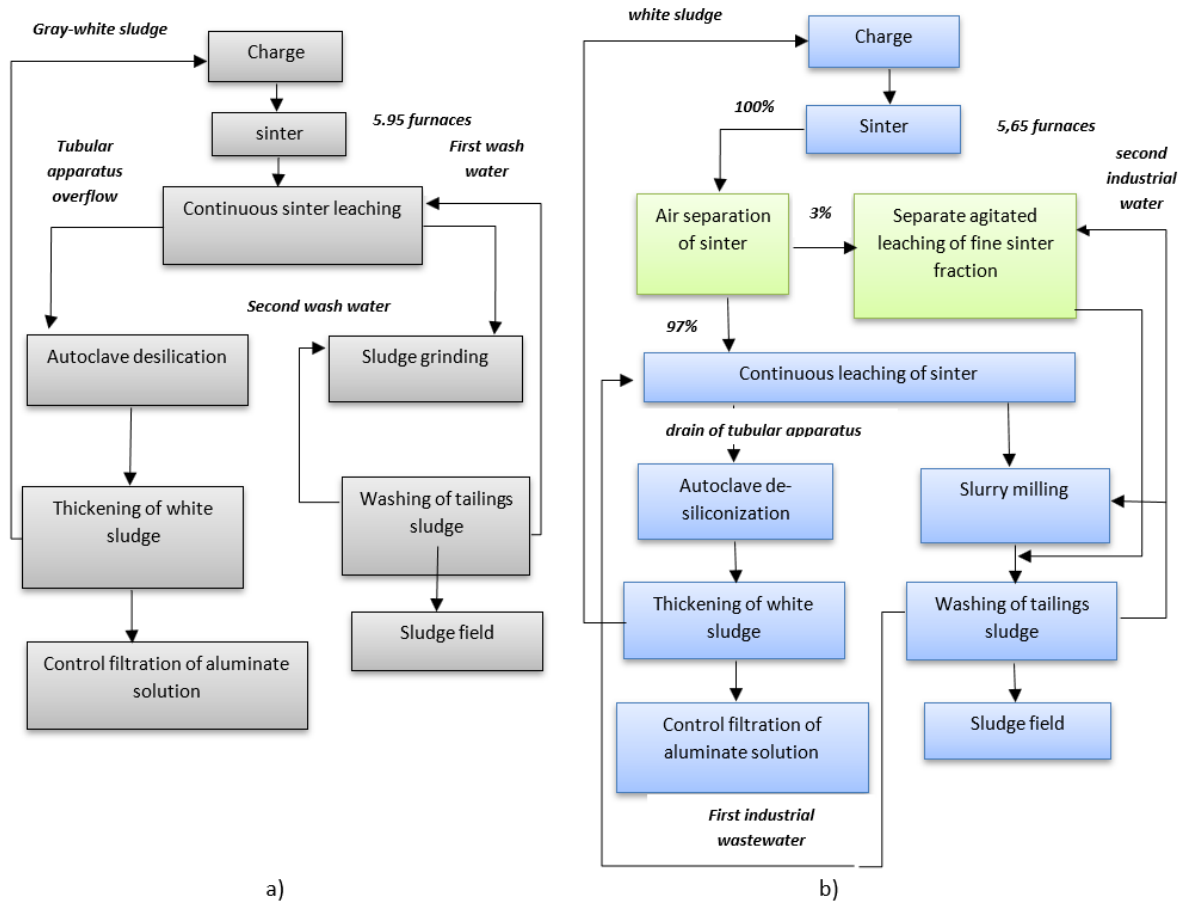

Figure 1 – a) Existing sinter leaching process at PAP;
b) Proposed process with preliminary sinter classification

There are several methods for eliminating the conditions for the formation of "gray sludge," which have been utilized in the production practice of PAP. One such method is leaching the sinter in a "Reacol" column-type apparatus [7].

According to this scheme, the sinter was first classified on separate drum screens with a mesh size of 5 mm (the usually used sizes are 10 and 8 mm), and then the separated sinter fraction was subjected to agitation leaching in a "Reacol" column-type apparatus with a pulsed supply of the leaching agent – water.

The use of a metal mesh with a rather large mesh size of 5 mm on the existing drum screens was technologically unjustified. With this technology, using a particle size of -5 mm, under-leaching of the sinter was observed, as well as losses of valuable components along with the sludge. The pulsed supply mode of the leaching agent in the "Reacol" type apparatus did not ensure complete extraction of valuable components from the sinter.

In addition, there was an inefficiency in the sinter separation and rapid mechanical wear of the classifying metal mesh, increased circulation flows of the sinter, which increased the energy costs at the crushing unit.

The next method involves separating the solid phase from the slurry discharge of the tubular leaching units using hydrocyclones [8]. A pilot-industrial installation of a battery of 10 hydrocyclones with a diameter of 150 mm was assembled for testing. The slurry discharge from one tubular leaching unit was subjected to classification.

This method also did not prove effective for the technological process of PAZ. Frequent cases of "sanding" of the hydrocyclones led to a high content of solid particles in the overflow, which was sent for autoclave desilication. As a result, the task of reducing the ballast flow to the sintering furnaces was only 50% solved.

The use of larger hydrocyclones with a diameter of 250 mm also did not solve the problem of the ballast flow and even reduced the efficiency of sludge removal to 30%.

The Boksitogorsk Alumina Plant of RUSAL employs a method of classifying and leaching sinter that is similar to our proposed method. Alumina-containing sinters are classified by a 0.5 mm fraction,

and the fraction finer than 0.5 mm is combined with aspirational sinter dust and mixed with under-sludge water, thus performing agitation leaching of the mixture, after which it is directed to co-washing with the sludge from leaching sinter fractions larger than 0.5 mm.

The technical solution implemented at the Boksitogorsk alumina plant was also applied at another RUSAL alumina plant - Achinsk. Testing of the proposed method was carried out with crushed sinter from an industrial stream. This method showed significant extraction of aluminum oxide from the fine fraction.

In the presented technology, implemented and tested at the RUSAL alumina plants, the preliminary separation of the fine part of the sinter is carried out by mechanical screening. The method of mechanical screening implies the use of capital-intensive structures, since conveyor routes and metal-intensive sorting units are required to move the bulk material (sinter). The optimal screening mode for powdered materials is operation within the 1-3 mm range. At smaller screening limits, energy consumption per 1 ton of product increases significantly, the dimensions of the equipment increase, and the need for frequent replacement of the screens arises [9]. For classifying materials with a particle size of less than 1 mm, it is advisable to use air classification. By regulating the speed and trajectory of the air flow, the size of the separated particles can be varied [[10], [11]].

Air separation is based on the ability of material particles, located in a vertical, horizontal or centrifugal air flow, to fall out of it under the influence of gravity, centrifugal inertial forces, or the combined effect of these forces under certain conditions [12].

For successful air separation, the air flow must have a homogeneous velocity field. For particles of a single size, called the separation boundary, dynamic equilibrium must be established throughout the entire separation zone. Particles of other sizes must be carried out of the separation zone in different directions: smaller than the separation boundary – in one direction, larger – in the other. The forces acting on a particle of any size must be adjustable within a wide range [10].

The design of air separators should provide the ability to regulate the air flow velocity and uniform distribution of the material being sorted, as well as the complete and timely removal of material particles separated by size from the separator. The separation boundary can be controlled by changing the operating mode of the classifier, for example, by changing the air flow velocity. It is known that the separation efficiency is determined by two factors: the concentration of the material and the design of the apparatus [13].

Review articles [[14], [15], [16]] provide a detailed examination of each type of equipment for particle separation.

In the article [17], the authors describe one of the novelties of air classifiers, which uses the inertial-gravitational design principle for separating solid particles.

Experimental part

According to the developed standards of the organization, Joint Stock Company Aluminum of Kazakhstan (JSC “AK”), the following research methods were carried out: sieve analysis of sinter, chemical analysis of liquid phases, and X-ray spectral analysis.

The following were used for testing:

- Laboratory separation unit from Lamel 777 (Minsk);
- Stand-mounted air gravity classifier from URAL-OMEGA (Magnitogorsk);
- Semi-industrial enrichment plant with a pneumatic separator of the “Sepair” type from GORMASHEXPORT (Novosibirsk).

Results and Discussion

The first stage of laboratory research aimed to determine the boundary particle size in the sinter that is carried away with the aluminate solution from the tubular apparatuses and is a source of formation of “gray” sludge.

By conducting numerous samplings of the overflows from all tubular apparatuses, it was established that the boundary size is the (-0.25) mm fraction. This dimensional fractional composition was to be removed, and separate leaching performed. It was also established that the average content of the (-0.25) mm fraction in the crushed sinter entering the tubular leaching units was approximately 3%.

In laboratory conditions, the sinter was classified into fractional compositions: (+0.25) mm and (-0.25) mm, and their separate leaching with liquid agents used in production conditions was carried out.

Table 1 presents the results of the separate leaching of the sinter.

Table 1 – Results of the separate leaching of the sinter

	Composition of Solid Phase					Extraction		Composition of Liquid Phase							
	%					%		g/L							
	Na_2O	Al_2O_3	SiO_2	CaO	Fe_2O_3	Na_2O	Al_2O_3	Al_2O_3	Na_2O total	Na_2O carbonate	Na_2O caustic	M caustic	% soda	SiO_2	M_{si}
	Initial sinter, including the fraction - 0.25 mm														
Sludge	**1.85**	**4.40**	19.5	40.7	24.3	**89.4**	**84.9**	107.5	84.3	2.6	81.7	1.3	3.1	2.28	49.0
	Sinter without the fraction -0.25 mm														
Sludge	**1.48**	**3.81**	19.3	40.3	24.0	**92.2**	**86.9**	110.2	87.3	2.3	85.0	1.3	2.7	2.25	49.0

Table 2 – Results of separate agitation leaching of the fine fraction of the sinter

Name	Состав жидких фаз						Состав твердых фаз				
	g/L						%				
	Al_2O_3	Na_2O total	Na_2O carbonate	Na_2O caustic	M caustic	% soda	Na_2O	Al_2O_3	SiO_2	CaO	Fe_2O_3
Original sinter							15.7	19.0	12.9	25.7	18.4
Weak leaching water	18.4	16.7	0.9	15.8	1.41	5.4					
Sludge							1.97	4.77	18.7	38.4	27.4
Liquid phase of the sludge	35.4	32.7	2.1	30.6	1.42	6.4					

Technological leaching of the isolated fine fraction of sinter (-0.25 mm) was carried out with weak wash water at a temperature of 75 °C and a leaching time of 3 minutes.

The coarse fraction of sinter (+0.25) mm was leached under production conditions used in tubular leaching units with strong wash water at a temperature of 85 °C and a time of 45 minutes. As can be seen from the data in Table 1, when removing the fine fraction (-0.25) mm from the sinter, the extraction of alumina and alkali from the coarse sinter increases by 2.0 and 2.8%, respectively.

The alumina content in the sludge after the separation of the fine fraction (-0.25) mm from the sinter with weak wash water, for a short leaching time (no more than 3 minutes), was approximately the same level as in the waste sludge - 4.77% (Table 2).

Table 2 presents the results of separate agitation leaching of the fine sinter fraction.

It was established that with separate leaching of the fine sinter fraction (-0.25) mm for a short time, 3 minutes, the fine sinter has time to leach without secondary losses. This indicates that the conditions for the formation of “gray” sludge are eliminated. Under production conditions, the fine fraction of sinter (-0.25) mm should also be leached with weak wash water.

The purpose of the second stage was to determine the conditions for thickening the sludge after separate leaching of the sinter fraction (-0.25) mm. According to the conditions of the designed production process, the dedusted coarse sinter fraction (+0.25) mm after leaching in a tubular leaching unit and grinding in a rod mill was mixed with the sludge from the leaching of the fine sinter fraction (-0.25) mm under conditions of re-pulping with weak wash water. Then, according to the scheme, the mixture of sludges after hydrocycloning was sent to the head washer of the washing line.

Planned mixtures of sludges from separate leaching of the sinter were prepared, with their further thickening in laboratory conditions using a flocculant. Based on the results of the laboratory work, satisfactory thickening of the sludge mixture after separate leaching of the sinter was determined.

Based on the data from the studies, it was hypothesized that, under production conditions, the sludge after the separate leaching of the fine sinter

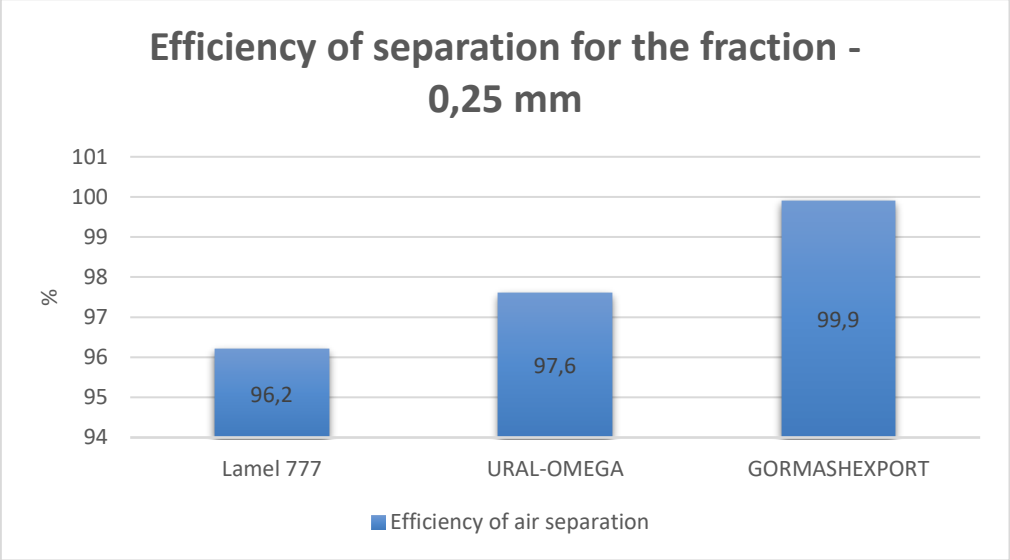

Graph 1 – Indicators of pilot tests for air separation of sinter.

fraction (-0.25 mm) would satisfactorily settle in a mixture with the rod mill sludge and not be carried away with the overflow (with strong wash water) from the head washers.

To confirm the results of the laboratory tests on the classification of the fine part of the sinter, a pool of companies producing shelf-type air classifiers and pneumatic separation devices with nozzle air supply was identified. Companies such as Lamel 777, URAL-OMEGA, and GORMASHEXPORT were selected [[18], [19], [20]].

The graph below shows the efficiency of air separation of sinter, as implemented by the above-mentioned companies, which allows for an assessment of the comparative results of their work.

Based on the conducted tests from all three companies, the possibility of air separation of sinter was confirmed. An air separation efficiency indicator of ~ up to 97.0% was determined for the declared boundary fraction of sinter (-0.25) mm.

The highest contamination - up to 40% of the sifted fine fraction with sinter of the neighbouring larger (+0.25) mm fraction - is present on the Lamel 777 classifier. Less contamination with the (+0.25) mm fraction, from 12 to 24%, is present on the GORMASHEXPORT classifier (using SEPAIR technology) [21]. The minimum contamination with the (+0.25) mm fraction, from 10 to 15%, is present on the URAL-OMEGA classifier.

According to the results of the sinter separation pilot tests, in terms of technical equipment and completeness, as well as the possibility of integration into the technological scheme in the existing production facility, the most suitable is the classifying installation of the company URAL-OMEGA from Magnitogorsk (Figure 2).

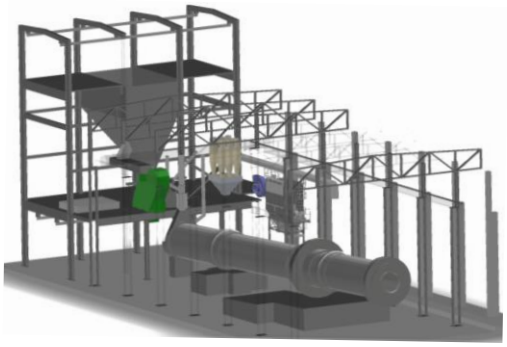

Figure 2 - Classifying the unit of the URAL-OMEGA company on a tubular leaching unit.

Conclusions

Based on extensive laboratory research, it has been established that removing the fine part of the sinter, 0.25 mm, with subsequent separate leaching allows increasing alumina extraction by ~ 2% without worsening the sludge settling performance during washing.

The possibility of air separation of sinter at the PAZ sintering stage has also been confirmed, and the optimal air separation efficiency indicator has been determined to be ~ up to 97.0%.

The classifying unit of the URAL-Omega company showed the most suitable test results for air separation of sinter for the technological process of the PAZ sintering stage.

The result of the technical solution of preliminary air separation of sinter will be an increase in the overall alumina extraction by 2% and

a reduction in the number of operating furnace strands by 0.26 units due to a decrease in ballast flows, respectively, a decrease in losses of useful components (alumina and alkali), as well as a positive impact of the scheme on the environmental situation of the shop.

Conflicts of interest. On behalf of all authors, the corresponding author declares that there is no conflict of interest.

CRediT author statement: **G.Abikenova:** Management, conceptualization, data curation; **D.Dauletov, S.Tverdokhlebov:** Author's supervision, reviewing and editing; **I.Danchenko:** Research, writing - original draft preparation.

Acknowledgments. This research did not receive any specific grant from funding agencies in the public, commercial, or non-profit sectors.

Cite this article as: Abikenova GK, Tverdokhlebov SA, Dauletov DD, Danchenko IS. Research into the possibility of air separation of cake at the Pavlodar aluminum smelter. Kompleksnoe Ispolzovanie Mineralnogo Syra = Complex Use of Mineral Resources. 2026; 338(3):112-119. https://doi.org/10.31643/2026/6445.34

Павлодар алюминий зауытында күйежентекті ауда ажырату зерттеу мүмкіндіктері

Әбікенова Г.Қ., Твердохлебов С.А., Дәулетов Д.Д., Данченко И.С.

ЖШС ERG ғылыми-зерттеу инженерлік орталығы, Павлодар, Қазақстан

Мақала келді: *1 қараша 2024*
Сараптамадан өтті: *11 желтоқсан 2024*
Қабылданды: *14 мамыр 2025*

ТҮЙІНДЕМЕ

Әуе сепарациясы Павлодар алюминий зауытының глинозем өндірісіндегі шихтаны күйдіру процессінде аса маңызды рөл атқаруы мүмкін. Күйдіру кезінде күйдіру шаңы түзіледі, оны негізгі материалдан тиімді түрде бөлу қажет, себебі оның ұсақ фракциясы қатты фазаның қалыптасуының көзі болып табылады, бұл пайдалы компоненттердің екінші жағындағы жоғалту мөлшерін арттырады. Әуе сепарациясын пайдалану осы тапсырманы шешуге мүмкіндік береді, күйдіру өнімін ірі және ұсақ фракцияларға жоғары дәрежеде бөлу арқылы, осылайша күйдіру пештерінің спекасын гидрохимиялық қайта өңдеу процесін интенсификациялайды. Бұл зерттеулердің негізгі мақсаты спецификациядан пайдалы компоненттердің, атап айтқанда, алюминий оксидтері мен сілтілердің, қатты фаза бойынша түтікше аппаратының ағысымен бірге ұшып кетуін азайту болды. Бұл жұмыста ауа сепараторларында спекалық шаңның алдын ала жіктелу процесі және оны жеке шаймалау қарастырылады. Кеңейтілген зертханалық сынақтар спеканың кластарын бөлу шегін (– 0,25 мм) анықтады, бұл глиноземді ~ 2%-ға көбейтуге мүмкіндік береді және балласттық ағындарды төмендету арқылы жұмыс істейтін пештік жіптердің санын 0,26 бірлікке қысқартуды жорамалдайды. Ауа сепарациясының тиімділік көрсеткіштері ~ 97% деп анықталды. Алынған нәтижелер спекалық өнімнің сапасын қамтамасыз ету және глинозем өндірісінің технологиясының тиімділігін арттыру үшін ауа сепарациясының маңыздылығын көрсетеді.

Түйін сөздер: ауаны бөлу, жіктеу, пайдалы компоненттерді алу, глинозем, спекание үдерісі, спек.

Авторлар туралы ақпарат:

Әбікенова Гүлнұр Қаныбекқызы *Техника ғылымдарының кандидаты, ЖШС ERG ғылыми-зерттеу инженерлік орталығы бас директордың м.а., Қонаева 2 үй, 010000, Астана, Қазақстан. Email: Gulnur.Abikenova@erg.kz*

Твердохлебов Сергей Андреевич *Инжер – химик технолог, ЖШС ERG ғылыми-зерттеу инженерлік орталығы, Шығыс өнеркәсіптік аймағы, құрылыс 65, 140000, Павлодар, Қазақстан. Email: tatburgelo@mail.ru*

Дәулетов Дәурен Дәулетұлы *Байыту бағыты бойынша магистр, зертхана бастығы, ЖШС ERG ғылыми-зерттеу инженерлік орталығы, Шығыс өнеркәсіптік аймағы, құрылыс 65, 140000, Павлодар, Қазақстан. Email: Dauren.Dauletov@erg.kz*

Данченко Ирина Сергеевна *Инженер – химик технолог, инженер – технолог, ЖШС ERG ғылыми-зерттеу инженерлік орталығы, Шығыс өнеркәсіптік аймағы, құрылыс 65, 140000, Павлодар, Қазақстан. Email: Irina.S.Danchenko@erg.kz*

Исследование возможности воздушной сепарации спека на Павлодарском алюминиевом заводе

Абикеноа Г.К., Твердохлебов С.А., Даулетов Д.Д., Данченко И.С.

ТОО Научно – исследовательский инжиниринговый центр ERG, Павлодар, Казахстан

Поступила: *1 ноября 2024*
Рецензирование: *11 декабря 2024*
Принята в печать: *14 мая 2025*

АННОТАЦИЯ

Воздушная сепарация может сыграть ключевую роль в процессе спекания шихты в глиноземном производстве Павлодарского алюминиевого завода. Во время спекания образуется спековая пыль, которую необходимо эффективно отделять от основного материала, т.к. ее мелкая фракция является источником образования твердой фазы, выносимой с раствором, что увеличивает величину вторичных потерь полезных компонентов. Использование воздушной сепарации позволит решить эту задачу, обеспечивая высокую степень разделения спекового продукта на крупную и мелкую фракции, тем самым интенсифицируя дальнейший процесс гидрохимической переработки спека печей спекания. Основной целью данных исследований являлось снижение потерь полезных компонентов из спека, а именно оксидов алюминия и щелочи, которые уносятся вместе с твердой фазой слива трубчатого аппарата. В данной работе рассматривается процесс предварительной классификации спековой пыли в воздушных сепараторах и ее раздельное выщелачивание. Расширенными лабораторными испытаниями была определена граница разделения классов спека (– 0,25 мм), что позволяет увеличить извлечение глинозема ~ на 2% и предполагает сокращение количества работающих печных ниток на 0,26 ед. за счет снижения балластных потоков, определен оптимальный показатель эффективности воздушной сепарации ~ до 97%. Полученные результаты демонстрируют важность воздушной сепарации для обеспечения качества спекового продукта и повышения эффективности технологии глиноземного производства в целом.

Ключевые слова: воздушная сепарация, классификация, извлечение полезных компонентов, глинозем, процесс спекания, спек.

Информация об авторах:

Абикенова Гульнур Каныбековна — *Кандидат технических наук, и.о. Генерального директора ТОО Научно – исследовательский инжиниринговый центр ERG, Кунаева, дом 2, 010000, Астана, Казахстан. Email: Gulnur.Abikenova@erg.kz*

Твердохлебов Сергей Андреевич — *Инженер – химик технолог, инженер – технолог, ТОО Научно – исследовательский инжиниринговый центр ERG, Промышленная зона Восточная, строение 65, 140000, Павлодар, Казахстан. Email: tatburgelo@mail.ru*

Даулетов Даурен Даулетович — *Магистр по направлению обогащения, начальник лаборатории, ТОО Научно – исследовательский инжиниринговый центр ERG, Промышленная зона Восточная, строение 65, 140000, Павлодар, Казахстан. Email: Dauren.Dauletov@erg.kz*

Данченко Ирина Сергеевна — *Инженер – химик технолог, инженер – технолог, ТОО Научно – исследовательский инжиниринговый центр ERG, Промышленная зона Восточная, строение 65, 140000, Павлодар, Казахстан. Email: Irina.S.Danchenko@erg.kz*

References

[1] Michael Betz, Marco Gleiss, Hermann Nirschl. Effects of Flow Baffles on Flow Profile, Pressure Drop and Classification Performance in Classifiers. A review. 2021; 9(7):1213. https://doi.org/10.3390/pr9071213

[2] Gal'perin VI. Air classification of bulk materials materials. Part 1. Basic definitions and technological indicators. (Electronic resource). 2005. https://www.elibrary.ru/download/elibrary_15201561_35666482.pdf

[3] Xueshuai Zhu, Chenyu Zhang, Ping Feng, Xizu Yang, Xiaojuan Yang. A novel pulsated pneumatic separation with variable-diameter structure and its application in the recycling spent lithium-ion batteries. A review. 2021; 131:20-30. https://doi.org/10.1016/j.wasman.2021.05.027

[4] Лун Хуан, Рунью Лю, Цюхуа Мяо, Жуйпин Цзоу, Хайшэнь Цзян, Чэньлун Дуань, Шибо Куанг. Dynamic characteristics of the flow field of the disrupted structures of the air classifier and application for effective separation of fly ash. A review. 2024; 12(6):114706. https://doi.org/10.1016/j.jece.2024.114706

[5] Arjun Kumar Pukkella, Jan J. Cilliers, Kathryn Hadler. A comprehensive review and recent advances in dry mineral classification. 2023; 201:108208. https://doi.org/10.1016/j.mineng.2023.108208

[6] Ibragimov AT, Budon S V. Razvitiye tekhnologii proizvodstva glinozema iz boksitov Kazakhstana [Development of technology for the production of alumina from bauxite in Kazakhstan]. Pavlodar: House of Printing LLP. 2010, 215. (in Russ).

[7] Pat. 10773 KZ. Sposob gidrokhimicheskoy pererabotki tverdogo veshchestva i reaktor dlya ego osushchestvleniya [Method for hydrochemical processing of solid matter and a reactor for its implementation]. Tverdokhlebov SA, Glukhov IA, Podnebesnyy GP, Synkova LN. 15.10.2001. (in Russ).

[8] Pat. 1667. Sposob gidrokhimicheskoy pererabotki speak [Method of hydrochemical processing of sinter]. Pechenkin MN, Yanin SV, Sabitov AR, Rakhiyanov MA, Tverdokhlebov SA, Ponezha AI. 15.09.2016. (in Russ).

[9] Ponomarev VB. Pererabotka metallurgicheskih shlakov metodom pnevmaticheskoj separacii. [Processing of metallurgical slags by pneumatic separation]. Zhurnal stal = Intermet Inzhiniring. 2015; 2:82-83. (In Rus.). https://www.elibrary.ru/download/elibrary_24219851_45466287.pdf

[10] Air sorting. https://studref.com/362206/tehnika/vozdushnaya_sortirovka#aftercont (Electronic resource). 2024 (date of access: 30.10.2024)

[11] Installations for air separation of materials. https://forpsk.ru/index.php/stati/oborudovanie/232-ustanovki-dlya-vozdushnoj-separatsii-materialov. 2012 (Electronic resource) (date of access: 14.02.2025)

[12] Smyshlyaev GH. Vozdushnaya klassifikaciya v tehnologii pererabotki poleznyh iskopaemyh [Aerial classification in technology recycling useful fossils]. Moskva: Izdatel'stvo nedra. 1969, 108. (in Russ).

[13] Ponomarev VB. Raschet i proektirovanie oborudovaniya dlya vozdushnoj separacii sypuchih materialov [Calculation and design of equipment for air separation of bulk materials]. Uchebnoe posobie. Ekaterinburg: Izdatel'stvo Ural'skogo universiteta. 2017, 90. (in Russ).

[14] Arjun Kumar Pukkella, Jan Cilliers, Kathryn Hadler. Design of parabolic conic gas cyclones for coarse particle classification: A CFD study with Response Surface Methodology. 2024; 433:119217. https://doi.org/10.1016/j.powtec.2023.119217

[15] Mohammad Barimani, Sheldon Green, Steven Rogak. Particulate concentration distribution in centrifugal air classifiers. A review. 2018; 126:44-51. https://doi.org/10.1016/j.mineng.2018.06.007

[16] Qi Chen, Junhao Hu, Haiping Yang, Daqian Wang, Huihui Liu, Xianhua Wang, Hanping Chen. Experiment and simulation of the pneumatic classification and drying of coking coal in a fluidized bed dryer. A review. 2020; 214:115364. https://doi.org/10.1016/j.ces.2019.115364

[17] Ashkan Bagherzadeh, Masoud Darbandi, Mohammad Bagher Barezban. Numerical simulation of particle separation in a two-phase flow passing through a vortex-based air classifier using Eulerian–Lagrangian DDPM approach. A review. 2024; 445:120036. https://doi.org/10.1016/j.powtec.2024.120036

[18] Multi-product cascade-gravity classifiers. URL: https://www.lamel777.ru/ikk_i_pereabotka_otsevov/kgk/ (Electronic resource) (date of access: 30.10.2024)

[19] Classifiers. https://uralomega.ru/equipments/separators (Electronic resource) (date of access: 30.10.2024)

[20] Dry enrichment - pneumatic separation complex SEPAIR. URL: https://gmexp.ru/equipment/type/grav/sepair.html (Electronic resource) (date of access: 30.10.2024)

[21] Peter V Polyakov, Nataliya V Oleinikova, Vladimir A Makarov. Prakticheskiye rezul'taty i perspektivy sukhogo obogashcheniya nekonditsionnykh rud i tekhnogennykh otkhodov metodom pnevmoseparatsii. XII Kongress Tsvetnyye metally i mineraly [Practical results and perspectives for dry beneficiation of substandard ores and technogenic wastes by pneumatic separation method. XII Congress Non-ferrous metals and minerals], September 9-13; Krasnoyarsk, Russia. (Issue XII), 2024, 96 -98. https://doi.org/10.12731/978-5-907608-43-6

МАЗМҰНЫ
СОДЕРЖАНИЕ
CONTENTS

ENGINEERING AND TECHNOLOGY

EARTH SCIENCES

METALLURGY

Техникалық редакторлар:
Г.К. Қасымова, Н.М.Айтжанова, Т.И. Қожахметов

Компьютердегі макет:
Г.К. Қасымова

Дизайнер:
Г.К. Қасымова, Н.М.Айтжанова

“Металлургия және кен байыту институты” АҚ
050010, Қазақстан Республикасы, Алматы қаласы, Шевченко к-сі, 29/133

Жариялауға 15.05.2025 жылы қол қойылды

Технические редакторы:
Г.К. Касымова, Н.М. Айтжанова, Т.И. Кожахметов

Верстка на компьютере:
Г.К. Касымова

Дизайнер:
Г.К. Касымова, Н.М.Айтжанова

АО “Институт металлургии и обогащения”
050010, г. Алматы, Республика Казахстан. ул. Шевченко, 29/133

Подписано в печать 15.05.2025 г.

Technical editors:
G.K. Kassymova, N.M. Aitzhanova, T.I. Kozhakhmetov

The layout on a computer:
G.K. Kassymova

Designer:
G.K. Kassymova, N.M. Aitzhanova

“Institute of Metallurgy and Ore Beneficiation” JSC
050010, Almaty city, the Republic of Kazakhstan. Shevchenko str., 29/133

Signed for publication on 15.05.2025